LONDON'S GLOBAL UNIVERSITY

Investigating the mechanisms of the heat shock response impairment in Huntington's disease mouse models

A thesis submitted

for the degree of Doctor of Philosophy

Casandra Gomez Paredes

UCL Queen Square Institute of Neurology

University College London

October 2021

Abstract

Huntington's disease (HD) is a neurodegenerative disease caused by the expansion of a CAG repeat within exon 1 of the huntingtin (*HTT*) gene. This produces a mutant HTT protein with an abnormally long polyglutamine stretch, which is prone to misfold and form aggregates, as detected in HD patients and mouse models, and which have aberrant interactions with members of key cellular pathways that become disrupted.

The heat shock response is a cytoprotective mechanism that aims to prevent and reduce aggregation and maintain proteome integrity. It is regulated by heat shock factor 1 (HSF1) which, under stress conditions, activates the transcription of the heat shock genes.

In this thesis, a comprehensive analysis of the heat shock response has been described for HD mouse models R6/2 and zQ175, after *in vivo* pharmacological induction with the compound NVP-HSP990. The expression of *Hsf1* and nine heat shock genes was measured from mouse tissue lysates by a QuantiGene multiplex assay, developed and validated for this purpose. Evidence of an impairment of the heat shock response was found in brain hemispheres, tibialis anterior and striatum of both models, with less consistent evidence in the cortex. As a potential cause of this dysregulation, HSF1 levels were analysed in brain and muscle, however, a decrease in HSF1 was not detected in either tissue.

SIRT1 can deacetylate HSF1 and maintain it in a competent state, bound to heat shock gene promoters. SIRT1 levels decline with disease progression in HD mouse models, therefore, whether a decreased SIRT1 activity could be responsible for the impaired heat shock response was investigated. The analysis of the heat shock gene expression with QuantiGene revealed that *Sirt1* overexpression on R6/2 mice did not significantly improve the heat shock response impairment in brain or tibialis anterior.

Impact statement

Huntington´s disease (HD) is a devastating neurodegenerative disorder that manifests in an adult or juvenile form with a myriad of motor, cognitive and psychiatric symptoms. In the adult disease, the symptoms generally appear in mid-life (around 40 years of age) and the onset in the juvenile HD cases is when individuals are younger than 20 years of age. HD patients will progressively deteriorate over the course of 15 - 20 years, leading to their eventual death. HD is autosomal dominantly inherited and is transmitted from an affected parent to offspring with a 50 % probability. A higher incidence of HD cases is found in Western and European populations and in the UK alone, approximately 12 / 100,000 individuals are affected by the disease. Currently, no disease-modifying treatments are available.

The genetic cause of HD is an expanded CAG repeat in exon 1 of the huntingtin (*HTT*) gene, which leads to the production of a mutant HTT protein that contains an abnormally long polyglutamine tract. This mutant HTT protein is prone to form misfolded and aggregated structures, as observed in HD patients and mouse models, which could destabilise crucial cellular pathways such as energy metabolism, transcriptional regulation, protein homeostasis or synaptic transmission.

The development of therapeutic interventions aimed at preventing aggregate formation or enhancing the activity of cellular disaggregation machineries is a rational approach for HD. To that end, increasing our understanding of protein homeostasis mechanisms, and how they are disrupted by mutant HTT, is highly relevant in HD research.

The heat shock response is a conserved cellular mechanism of defence against proteotoxic insults such as the presence of HTT aggregates. The induction of the heat shock response is regulated by HSF1, which activates the transcription of the heat shock genes to encode the heat shock proteins, the main effectors of the response. Previous studies in our group identified an impairment in the heat shock response in HD mice as disease progressed.

In this thesis, a comprehensive characterisation of the heat shock response impairment in brain and muscle tissues from two HD mouse models, zQ175 and R6/2, after pharmacological activation of the heat shock response with NVP-HSP990 compound, is provided.

The levels of HSF1 were analysed in all tissues, and the overexpression of SIRT1, a deacetylase that could prolong transcriptional activation of heat shock genes via deacetylation of HSF1, was tested as an approach to restore the heat shock response impairment. A novel QuantiGene multiplex assay was designed and validated to simultaneously analyse the expression of nine heat shock genes and the regulators *Hsf1* and *Sirt1*, directly from tissue lysates.

The methodologies developed and optimised in this thesis have been published and will aid in the detailed analysis of the heat shock response by other groups. The mechanistic studies have contributed to our understanding of the heat shock response impairment in HD and will help to inform therapeutic strategies targeting the heat shock response and proteostasis. These results may be applicable in the design of therapeutic approaches not only in HD, but also in other disorders characterised by the presence of aggregates, such as amyotrophic lateral sclerosis, Alzheimer's disease, Parkinson's disease or spinocerebellar ataxias.

Acknowledgements

First and foremost, I wish to express my sincere gratitude to my supervisor, Professor Gillian Bates, for giving me this wonderful opportunity and trusting in me with this project, thank you very much for the constant guidance, support and feedback throughout the whole PhD journey. I would like to add a special thanks to my secondary supervisor, Dr Bernadett Kalmar, for all her encouragement and kindness.

I feel privileged to have had the chance to do this PhD in the Bates lab and Huntington's disease centre, I am grateful to each one of the lab members for their motivation and helpful contributions. I wish to acknowledge a few people in particular that have made a significant impact on me for the culmination of this PhD: my fellow PhD student Michael Mason, for his friendship, continuous collaboration and support all the way, I could not have had a better companion to share this PhD experience with; Marie Bondulich, for her great energy, reliability and her typical efficiency in absolutely everything; Aikaterini Papadopoulou, for her insights, sharing her knowledge and technical suggestions; Sandra Fienko, for her enthusiasm, analytical thinking and all the laughs; Kirupa Sathasivam for all her expertise and technical advice; and the *in vivo* team, past and current members, for all their assistance when needed. Thank you all very much, I really appreciate it.

Last, but definitely not least, I am very grateful to Nacho and Michi, for putting up with me and my moments of struggle and stress during this time and for their immense love and care. Finally, I would like to dedicate this to my eternally supportive parents, Carmen and Pedro; this would not have been possible without their endless love and faith in me.

Declaration of authorship

I, Casandra Gomez Paredes, confirm that the work presented in this thesis is my own. Where information has been derived from other sources, I confirm that this has been indicated in the thesis.

Publications

- As first author:

Gomez-Paredes, C., Mason, M., Taxy, B., Papadopoulou, A., Paganetti, P., & Bates, G. (2021). The heat shock response, determined by QuantiGene multiplex, is impaired in HD mouse models and not caused by HSF1 reduction. *Scientific Reports, 11*(1), 9117

Part of the data presented in Chapters 3 and 4 of this thesis were included in this publication.

Poster presentations

- "Investigating the mechanisms of the heat shock response impairment in Huntington's disease". Casandra Gomez-Paredes, Michael A. Mason, Aikaterini S. Papadopoulou, Gillian P. Bates.
  Poster presented at the European Huntington's disease network (EHDN) Plenary Meeting in Vienna, Austria, 2018.

- "Investigating the mechanisms of the heat shock response impairment in Huntington's disease". C. Gomez-Paredes, M. A. Mason, A. S. Papadopoulou, G. P. Bates.
  Poster presented at the Society for Neuroscience (SfN) conference in Chicago, USA, 2019.

Table of contents

List of Figures

List of Tables

Abbreviations

AAV	Adeno-associated virus
AceCS2	Acetyl CoA synthetase 2
Actb	Actin beta
AD	Alzheimer's disease
ADP	Adenosine diphosphate
ALS	Amyotrophic lateral sclerosis
AMPK	Adenosine monophosphate-activated protein kinase
ANOVA	Analysis of variance
APS	Ammonium persulfate
AROS	Active regulator of SIRT1
ARRIVE	Animal research: reporting of *in vivo* experiments
ASO	Antisense oligonucleotide
ATP	Adenosine triphosphate
Atp5b	ATP synthase subunit beta
ATTECs	Autophagosome-tethering compounds
AVG	Average
BAC	Bacterial artificial chromosome
BDNF	Brain-derived neurotrophic factor
bp	base pairs
BSA	Bovine serum albumin
BubR1	mitotic spindle checkpoint protein BUBR1
Ca^{++}	Calcium
CAG	Cytosine adenine guanine
Canx	Calnexin
Cas9	CRISPR associated protein 9
cDNA	Complementary DNA
CK2	Casein kinase 2
CMA	Chaperone-mediated autophagy
CPS1	Carbamoyl phosphate synthase 1
CRISPR	Clustered regularly interspaced short palindromic repeats
CSF	Cerebrospinal fluid
CV	Coefficient of variation
DBC1	Deleted in breast cancer 1
DBD	DNA binding domain
DNA	Deoxyribonucleic acid
Dnaja1	DnaJ, member A1, HSP40
Dnaja3	DnaJ, member A3, HSP40
Dnajb1	DnaJ, member B1, HSP40

Dnajb5	DnaJ, member B5, HSP40
DNase	Deoxyribonuclease
dNTP	Deoxyribonucleotide triphosphate
DRPLA	Dentatorubropallidoluysian atrophy
DTT	Dithiothreitol
ECL	Enhanced chemiluminescence
EDTA	Ethylenediaminetetraacetic acid
Eif4a2	Eukaryotic translation initiation factor 4A2
ERAD	Endoplasmic reticulum associated protein degradation
ESCs	Embryonic stem cells
FAN1	Fanconi-associated nuclease 1
FELASA	Federation of European Laboratory Animal Science Association
FFPE	Formalin-fixed, paraffin-embeded
FOXO	Forkhead box O transcription factor
GAPDH	Glyceraldehyde 3-phosphate dehydrogenase
GCN5	General control non-repressed 5
GDH	Glutamate dehydrogenase
GeM-HD	Genetic modifiers of Huntington's disease
GeoMean	Geometric mean
GOI	Gene of interest
GWAS	Genome-wide association study
HAT	Histone acetyl transferase
HCl	Hydrochloric acid
HD	Huntington's disease
HDAC	Histone deacetylase
HEAT	Huntingtin, Elongation factor 3, protein phosphatase 2A, TOR1
HEPES	4-(2-hydroxyethyl)-1-piperazineethanesulfonic acid
HIF-1α	Hypoxia-inducible factor 1-alpha
HK	Housekeeping
HR	Heptad repeat
HSC70	Heat shock cognate 70
HSE	Heat shock element
HSF1	Heat shock factor 1
HSP	Heat shock protein
Hsp90aa1	Heat shock protein 90, member A1; HSP90
Hsp90ab1	Heat shock protein 90, member B1; HSP90
Hspa1a/b	Heat shock protein 1A/B, HSP70
Hspa9	Heat shock protein A9, HSP70
Hspb1	Heat shock protein 1, HSP25
Hspb6	Heat shock protein B6, α-crystallin-related, HSP20

Hspd1	Heat shock protein 1 (chaperonin), HSP60
Hspe1	Heat shock protein 1 (chaperonin), HSP10
Hsph1	Heat shock protein 105/110 kDa; HSP110
HSR	Heat shock response
HTT	Huntingtin
ICDH2	Isocitrate dehydrogenase
iPSCs	Induced pluripotent stem cells
IVC	Individually ventilated cage
JNK1	c-Jun N-terminal kinase
JOHD	Juvenile onset Huntington's disease
Kb	Kilobase
KCl	Potassium chloride
kDa	Kilodalton
LXR	Liver X receptor
Lys	Lysine
MCD	Malonyl CoA decarboxylase
MEFs	Mouse embryonic fibroblasts
MFI	Median fluorescence intensity
miRNA	MicroRNA
MLH1	MutL homolog 1
MnSOD	Manganese superoxide dismutase
MSH2	MutS homolog 2
MSH3	MutS homolog 3
mTOR	Mammalian target of rapamycin
N17	N-terminal with 17 amino acids
NaCl	Sodium chloride
NAD	Nicotinamide adenine dinucleotide
NaF	Sodium fluoride
NAM	Nicotinamide
NaOH	Sodium hydroxide
NBD	Nucleotide binding domain
NEF	Nucleotide exchange factor
NFL	Neurofilament light chain
NK-κB	Nuclear factor kappa enhancer binding protein
NSAID	Non-steroidal anti-inflammatory drug
NVP-HSP990	2-amino-7, 8-dihydro-6H-pyrido [4, 3-d] pyrimidin-5-one
PAF53	RNA polymerase associated factor 53
PARP1	Poly ADP ribose polymerase 1
PCR	Polymerase chain reaction
PD	Parkinson's disease

PDH	Pyruvate dehydrogenase
PGC-1α	PPAR-γ coactivator 1 alpha
PMSF	Phenylmethanesulfonyl fluoride
PolyQ	Polyglutamine
PPAR-γ	Peroxisome proliferator-activated receptor-gamma
PRD	Proline-rich domain
PROTACs	Proteolysis-targeting chimeras
PrP	Prion promoter
PTM	Post-translational modification
PVDF	Polyvinylidene fluoride
RD	Regulatory domain
RIPA	Radioimmunoprecipitation assay
RISC	RNA-induced silencing complex
RNA	Ribonucleic acid
RNase H	Ribonuclease H
ROS	Reactive oxygen species
Rpl13a	Ribosomal protein L13a
RT	Room temperature
RT-qPCR	Real-time quantitative polymerase chain reaction
SAPE	Streptavidin-conjugated R-phycoerythrin
SBD	Substrate binding domain
SBMA	Spinal and bulbar muscular atrophy
SCA	Spinocerebellar ataxia
SD	Standard deviation
Sdha	Succinate dehydrogenase complex flavoprotein subunit A
SDS	Sodium dodecyl sulphate
SDS-PAGE	Sodium dodecyl sulphate-polyacrylamide gel electrophoresis
SEM	Standard error of the mean
Ser	Serine
Sir2	Silent Information Regulator 2
siRNA	Small interfering RNA
SIRT	Sirtuin
SOD1	Superoxide dismutase 1
STACs	Sirtuin activating compounds
TAD	Transactivation domain
TAE	Tris acetate EDTA
TALENs	Transcription activator-like effector nucleases
TBS	Tris-buffered saline
TCA	Tricarboxylic acid
TDP-43	TAR-DNA binding protein 43

TE	Tris EDTA
TEMED	Tetramethylethylenediamine
Tg	Transgenic
TGS	Tris glycine SDS
TMS	Total motor score
U3-55k	U3 small nucleolar RNA protein specific component
Ubc	Ubiquitin C
UCP2	Uncoupling protein 2
UHDRS	Unified Huntington's disease rating scale
UPR	Unfolded protein response
UPS	Ubiquitin proteosome system
WAT	White adipose tissue
WT	Wild-type
YAC	Yeast artificial chromosome
ZFP	Zinc finger protein

Chapter 1. Introduction

1.1 History and epidemiology of Huntington's disease

Huntington's disease (HD) is a monogenic neurodegenerative disease of autosomal dominant inheritance. Individuals affected usually present an onset of symptoms during mid-life (adult onset, 40 years of age on average), but the symptoms can also manifest during childhood in the juvenile form of the disease (onset before 20 years of age); with a disease progression of approximately 15 – 20 years. Symptoms of the disease include motor impairment, cognitive decline and psychiatric disturbances (Bates *et al.,* 2015; Tabrizi *et al*., 2020; Ghosh and Tabrizi, 2018).

HD is present in all populations; however, it is more common in populations of European descent. HD is estimated to affect approximately 4 - 10 / 100,000 people in Western and European countries (Kay *et al*., 2017) with significantly lower incidence in Asian and African populations. In the UK, 11.2 – 13.5 / 100,000 people are estimated to suffer from HD (Evans *et al*., 2013). Some Venezuelan communities, such as the Maracaibo region, are among the areas with highest prevalence in the world (Wexler *et al*., 2004).

The clinical features of the adult-onset form and pattern of inheritance were initially described in 1872 by George Huntington. The juvenile form of the disease was described by J. Hoffman. Later in the 1970s and early 1980s, HD gene mapping projects were carried out, including expeditions by Nancy Wexler to several regions of Venezuela, where a high incidence of HD cases had been reported, to obtain resources. This all led to the mapping of HD gene in 1983 by Gusella and colleagues to the short arm of chromosome 4 (Gusella *et al*., 1983) and its later gene isolation in 1993 (The Huntington's disease collaborative research group, 1993). The presence of a CAG trinucleotide repeat (encoding glutamine [Q]), that was abnormally expanded only on the HD chromosomes, was identified as the causative mutation.

1.2 Clinical features and diagnosis of Huntington's disease

HD belongs to the group of trinucleotide repeat expansion disorders and, specifically, those referred to as polyglutamine diseases because of the expanded CAG trinucleotide that encodes a polyglutamine tract. There are nine neurodegenerative diseases caused by expansion of CAG trinucleotide: Huntington's disease, spinal and bulbar muscular atrophy (SBMA), dentatorubropallidoluysian atrophy (DRPLA) and the spinocerebellar ataxias (SCAs) with six forms (SCA1, 2, 3, 6, 7 and 17). Although they all share the characteristic of polyglutamine expansion, they have differences in the causative genetic component or CAG range (Lieberman *et al*., 2019).

The clinical features of HD are characterised by motor, cognitive and psychiatric disturbances. The disease, according to the presentation and development of symptoms, could be divided in two phases. There is a "premanifest" or prodromal phase, in patients who are carriers of the HD gene mutation but are not showing motor impairment or only very subtle signs; however, during this phase they may suffer from some psychiatric or cognitive symptoms, and this is accompanied by striatal atrophy and loss of corticostriatal connectivity (Tabrizi *et al*., 2013). In the "manifest" phase, which is considered the official disease onset, there is a definite presence of motor symptoms, including chorea or bradykinesia (Ghosh and Tabrizi, 2018). The timing and prevalence of these symptoms have recently been analysed by McAllister *et al*., (2021).

As tools for clinical diagnosis and monitoring, the Unified Huntington's disease rating scale (UHDRS), with motor, cognitive, behavioural, emotional and functional capacity components, and the total motor score (TMS) subscale are commonly used to assign a score and diagnose the disease onset as well as to assess disease progression (Ghosh and Tabrizi, 2018). Due to the inherited pattern of genetic transmission, genetic testing is available to predict and diagnose, as well as to determine the CAG repeat length in patients who might be showing symptoms suspected as HD. Patients with a family history have a 50 % chance of having inherited the mutation from an

affected parent and mutation carriers would have a 50 % chance of transmitting it to the next generation.

1.2.1 Motor symptoms

The most common feature of the motor symptoms is chorea, which consists of short and involuntary movements with a variable pattern, more usually in the extremities and face. Other motor symptoms include dystonia (prolonged muscle contraction and abnormal posture), bradykinesia (slowness of movements) and muscle rigidity, which also affect the voluntary movements, especially as the disease progresses. All these symptoms cause an impairment and progressive deterioration of the normal posture, gait and reflexes (Ghosh and Tabrizi, 2018).

1.2.2 Cognitive and psychiatric symptoms

Several cognitive features have been described to be dysfunctional in HD: deficits in learning, memory and attention as well as sensory perception and processing, impaired executive functioning (difficulties in organisational skills and development of actions) and, in advanced stages of the disease, severe dementia. The most common neuropsychiatric disturbances described in HD are depression and anxiety (with the highest incidence), increased apathy over disease progression and irritability. Occasionally, patients also present obsessive-compulsive behaviours and psychosis, communication difficulties, swallowing/feeding problems and sleeping and circadian rhythm disturbances (Ghosh and Tabrizi, 2018). Both cognitive and psychiatric symptoms have often been detected in the premanifest stage of HD, long before the defined disease onset.

Neuropathology characteristics include brain atrophy in striatal regions (caudate nucleus and putamen) and cell loss of medium spiny neurons, especially, with a high vulnerability to HD pathogenesis (Vonsattel and DiFiglia, 1998). However, HD is considered a disease of not only the brain but the whole body.

Additional to the symptoms observed in the nervous system, there are some peripheral characteristics of the disease, including weight loss, muscle atrophy, endocrine dysregulation and heart failure, among others (Ghosh and Tabrizi, 2018; Lakra *et al*., 2019; Zielonka *et al*., 2014).

1.3 Genetics of Huntington's disease and effect of CAG repeat length

As identified by the Huntington's disease collaborative research group in 1993, the causative genetic mutation in HD is an expanded CAG trinucleotide repeat within exon 1 of the 67-exon huntingtin (*HTT*) gene, located in chromosome 4p16.3. This encodes a mutant version of the huntingtin (HTT) protein that contains an abnormally long polyglutamine (polyQ) stretch at the N-terminus.

Because of its autosomal-dominant pattern of inheritance, the presence of this mutation in a single allele of the gene is sufficient to cause the disease. Healthy, non-affected individuals carry between 10 to 35 CAGs. The presence of 36 – 40 CAGs results in a reduced penetrance form of HD which may or may not lead to the development of symptoms. Individuals who would become symptomatic have a full penetrance of the mutation, with 40 or more CAGs in the affected allele(s) (Figure 1.1). Those individuals with 27 – 35 CAGs (intermediate-length allele) are generally asymptomatic. However, because of the unstable nature of the expanded repeat, there is a possibility of CAG repeat expansion during meiosis (Zühlke *et al*., 1993; Telenius *et al*., 1993) which may lead to >35 CAGs to be passed down to the subsequent generations, therefore with an increased risk of disease manifestation. This meiotic expansion accounts for the genetic anticipation, whereby there are progressively earlier disease onsets or appearance of first symptoms with disease transmission through generations. Juvenile HD cases, generally inherited via paternal transmission (which more commonly undergo large expansions in the CAG repeat size), contain > 55 CAGs (Telenius *et al*., 1993; Schultz *et al*., 2020).

1.3.1 Correlation between CAG repeat length and age of onset

There is an inverse correlation between CAG repeat length and age of onset (Langbehn *et al*., 2010; Lee *et al*., 2012). Generally, longer CAG repeat length determines an earlier age of onset, however, great variability has been detected in the age of onset in the range of 40 – 50 CAG repeats (Figure 1.1).

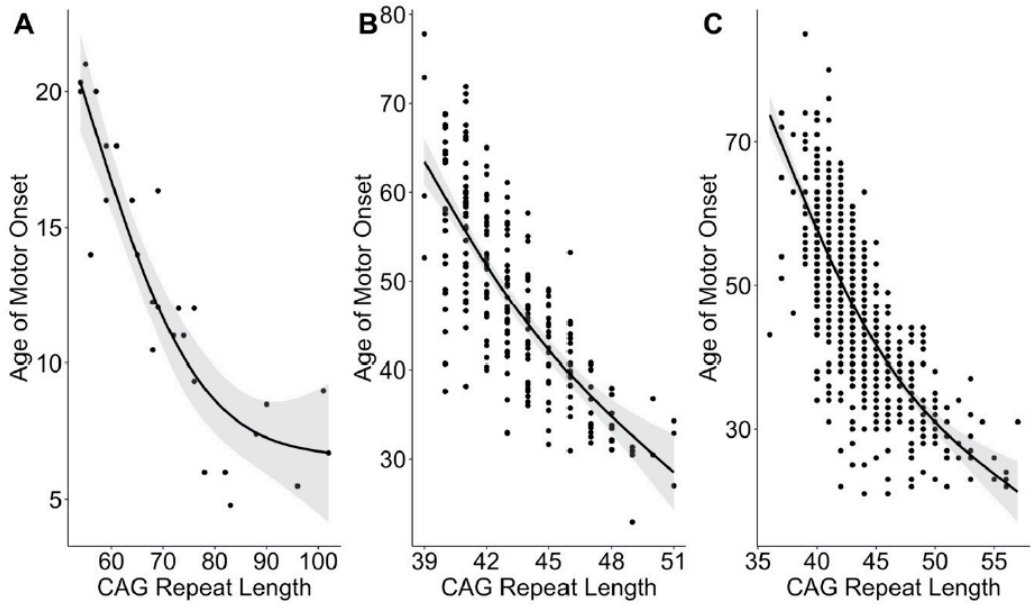

Figure 1.1. Association between the CAG repeat length and age of motor onset in adult and juvenile cases of HD from different studies.
The CAG repeat length is associated with the age of motor onset. Datasets are from (A) Kids-JOHD study in juvenile cases of HD (Schulz et al., 2020), (B) Predict-HD study in adults (Paulsen et al., 2014), (C) Enroll-HD study in adults (Landwehrmeyer et al., 2016). Image taken from Schultz et al., (2020) and reproduced with permission (open access).

1.3.2 Genetic modifiers of Huntington's disease

Approximately, 50 - 70 % of variation in the age of onset and progression of disease is determined by CAG repeat length (Ghosh and Tabrizi, 2018). The rest of the variability is associated with genetic modifiers and genomic differences that may be inherited and influence HD course (Kaltenbach *et al*, 2007; GeM-HD consortium, 2015, 2019; Holmans *et al*., 2017; Gusella *et al*., 2014).

Currently, many studies have generated a lot of interest on the DNA repair machinery enzymes and factors associated with the incomplete splicing of *HTT* gene as important modifiers of HD pathogenesis, age of disease onset and somatic expansion of the CAG repeat (GeM-HD consortium, 2019; Bettencourt *et al*., 2016; Hensman-Moss *et al*., 2017).

1.4 Somatic instability and expansion of the CAG repeat

The CAG repeat length that is inherited in HD exhibit both meiotic (Zühlke *et al*., 1993) and somatic expansion capacities. The somatic expansion of the CAG repeat length during an affected individual's lifetime is considered a prominent modifier of HD (Aronin *et al*., 1995; Swami *et al*., 2009). Somatic expansion has been described to occur in post-mortem brain and peripheral tissues from HD patients (Pinto *et al*., 2020) as well as in HD mouse models (Lee *et al*., 2011; Dragileva *et al*., 2009; Wheeler *et al*., 1999; Gonitel *et al*., 2008; Mangiarini *et al*., 1997).

Somatic expansion of the CAG repeat length is likely to be caused by DNA damage and repair processes. In line with this, recent genome-wide association studies (GWAS) in HD patients (GeM-HD, 2015, 2019) have been carried out that identified genes involved in the DNA repair machinery to be significantly correlated with HD haplotypes and polymorphisms that are associated with a delayed or earlier disease onset; these include the mismatch repair pathway proteins MSH3 (Flower *et al*., 2019; Hensman-Moss *et al*., 2017; Tomé *et al*., 2013), MSH2 (Wheeler *et al*., 2003; Kovalenko *et al*., 2012) or MLH1 (Pinto *et al*., 2013) and the DNA interstrand cross-link repair nuclease FAN1 (Kim *et al*., 2020; Goold *et al*., 2021). The effects on the disease, either slowing or accelerating it, are thought to occur via somatic expansion of the CAG repeat (Wheeler and Dion, 2021).

1.5 Incomplete splicing of the *HTT* gene

The *HTT* gene with a CAG repeat expansion may undergo abnormal RNA processing during transcription, in a process known as incomplete splicing. As discussed later, this mechanism is responsible for the generation of one of the highly pathogenic short N-terminal HTT fragments (Gipson *et al*., 2013).

The presence of an expanded CAG repeat in the *HTT* gene may prevent *HTT* mRNA from splicing from exon 1 to exon 2, instead leading to a premature termination of transcription in intron 1 and the generation of a small polyadenylated transcript called *HTT1a*. This *HTT1a* transcript, that contains exon 1 and the 5' end of intron 1, is then translated to produce the exon 1 HTT protein (Figure 1.2). The incomplete splicing and the *HTT1a* transcript have been detected in HD knock-in mouse models (Sathasivam *et al*., 2013) as well as in fibroblasts and post-mortem brains from HD patients (Neueder *et al*., 2017). Although the incomplete splicing is confirmed to occur in HD, the mechanisms underlying this process are still unknown.

The exon 1 HTT protein resulting from incomplete splicing has been shown to be highly pathogenic. The HD mouse models expressing a genomic *HTT* fragment containing exon 1, such as the transgenic R6/2 mice (Mangiarini *et al*., 1996), encode a short N-terminal HTT fragment and develop a rapidly progressing HD phenotype with a short lifespan.

The higher expression of the truncated *HTT1a* transcript in post-mortem tissues from juvenile cases of HD (over 55 CAGs) suggests that incomplete splicing is a CAG repeat length-dependent process in patients (Neueder *et al*., 2017). Somatic expansion of the CAG repeat may further exacerbate incomplete splicing and lead to an increased *HTT1a* expression and exon 1 HTT production.

1.6 The toxicity and aggregation of mutant huntingtin

The HTT protein, with a molecular weight of 350 kDa (The Huntington's disease collaborative research group, 1993; Hoogeveen *et al*., 1993) is a conserved and ubiquitously expressed protein (Li *et al*., 1993) that may shuttle between nucleus and cytoplasm (Truant *et al*., 2007). The normal functions of wild-type HTT are not completely understood. HTT is believed to have a scaffolding function and play an important role in neural development, BDNF production and transport (Zuccato *et al*., 2007; Saudou and Humbert, 2016). Lack of HTT expression has been demonstrated to be embryonically lethal (Zeitlin *et al*., 1995).

The HTT protein is organised in multiple alpha-helical domains of HEAT (Huntingtin, Elongation factor 3, protein phosphatase 2A, TOR1) repeats, as demonstrated recently (Guo *et al*., 2018). In between these HEAT repeats, there are disordered regions known to undergo post-translational modifications (PTMs) (Ratovitski *et al*., 2017; Steffan *et al*., 2004; Kratter *et al*., 2016). Particularly, the proteolytic cleavage of HTT by caspases or other proteases has been described to occur in these regions resulting in the generation of diverse mutant HTT cleaved products (Figure 1.2; Lunkes *et al*., 2002; Juenemann *et al*., 2011).

An array of mutant HTT fragments can be produced by proteolysis, all of them containing an N-terminal segment of 17 amino acids (known as N17) followed by the polyQ region starting in residue 18 (of variable length according to the CAG repeats) and then a proline-rich domain (PRD). The N17 and PRD regions flanking polyQ may also modulate the aggregation process, as detected *in vitro* (Shen *et al*., 2016). The N17 region is a subject of post-translational modifications (Steffan *et al*., 2004) and may be involved in triggering the aggregation process (Thakur *et al*., 2009; Vieweg *et al*., 2021).

The smallest N-terminal fragment is the exon 1 HTT fragment as generated by incomplete splicing (Sathasivam *et al*., 2013; Figure 1.2). This fragment has the ability to form aggregated structures and is considered a key pathogenic form in the disease (Landles *et al*., 2010). Its expression is sufficient to cause the HD pathological phenotype in mice (Mangiarini *et al*., 1996).

The generation of HTT fragments by either proteolysis or incomplete splicing of the *HTT* gene, eventually gives rise to the appearance of intranuclear inclusions and cytoplasmic aggregates (Figure 1.2), the main pathological markers of the disease, as detected in the brains and periphery of HD patients (DiFiglia *et al*., 1997; Gutekunst *et al*., 1999) and mouse models (Davies *et al*., 1997; Landles *et al*., 2010; Schilling *et al*., 1999; Sathasivam *et al*., 1999). The HTT aggregates may assemble progressively in different conformations in intermediate oligomeric species, amyloid-like fibrillar structures and inclusions as observed in the nucleus and cytoplasm (Scherzinger *et al*., 1997, 1999; Sathasivam *et al*., 2010).

It is yet to be clearly determined whether the formation of intracellular aggregates may be the driver of neuronal dysfunction or, on the contrary, they could provide some beneficial or protective effects. On one side, some studies identify these nuclear and cytoplasmic aggregates as primary pathogenic contributors and responsible for neuronal dysfunction, mainly through the sequestration of essential cellular components that would lead to disruption of normal cellular mechanisms (Davies *et al*., 1997; Woerner *et al*., 2016; Shirasaki *et al*., 2012; Kim *et al*., 2016). On the other hand, alternative reports hypothesise that the formation of aggregates/inclusions may work as a cellular protective mechanism as they can contain the smaller and more cytotoxic oligomeric species of mutant HTT and mitigate apoptosis (Arrasate *et al*., 2004; Ramdzan *et al*., 2017; Kuemmerle *et al*., 1999; Miller *et al*., 2011, Takahashi *et al*., 2008).

The specific pathogenic contribution of these aggregates is still under debate; it might be possible that they exert a dual protective/pathogenic role in the cell, depending on the stages of the disease as well as cellular and tissue localisations of these aggregates (Arrasate and Finkbeiner, 2012; Bates, 2003).

Additionally, post-translational modifications on mutant HTT, influenced by the CAG repeat length (Lakhani *et al.*, 2010), may have the capacity to modulate its aggregation and toxicity (Arbez *et al*, 2017), affecting mainly its interactions with other proteins (Ehrnhoefer *et al*., 2011). Examples of this are: phosphorylation at Ser421 that reduced neurodegeneration by promoting mutant HTT clearance in mice (Kratter *et al*., 2016) or the phosphorylation at Ser13 and Ser16, which played significant roles in the misfolding and formation of aggregates *in vitro* and HD mice (Gu *et al*., 2009).

The polyQ tract expansion confers new and toxic properties to HTT protein, resulting in a major contributor to HD pathogenesis and, therefore, identifying HD as a toxic gain-of-function disease.

1.6.1 Downstream cellular processes affected by mutant huntingtin protein

The accumulation of misfolded HTT fragments into aggregates within the cells results in aberrant interactions with an extensive array of proteins (Shirasaki *et al*., 2012; Kim *et al*., 2016). Moreover, it is established that multiple components of relevant cellular pathways involved in protein homeostasis, cell cycle regulation, transcriptional regulation and energy metabolism are sequestered within the aggregates (Yang and Hu, 2016). The sequestration of these components along with the abnormal interactions between mutant HTT and other proteins leads to the disruption of essential cellular processes (Labbadia and Morimoto 2013; Bates *et al*., 2015; Wanker *et al*., 2019; Hughes and Jones, 2014; Figure 1.2) such as:

- Mitochondrial and energy metabolism dysfunction (Johri *et al*., 2013; Orr *et al*., 2008; Franco-Iborra *et al*., 2020).
- Synaptic dysregulation and excitotoxicity: alterations in neuronal circuitry and axonal transport (Trushina *et al*., 2004; Milnerwood *et al*., 2010).
- Transcriptional dysregulation (Hodges *et al*., 2006; Langfelder *et al*., 2016).
- Proteostasis impairment and clearance of mutant HTT: a detailed review on this can be found in the next section.
- Inflammation (activation of reactive microglia and astrocytes) (Palpagama *et al*., 2019).
- Impaired vesicular trafficking and nucleocytoplasmic transport (Gasset-Rosa *et al*., 2017; Woerner *et al*., 2016; Zhou *et al*., 2021).

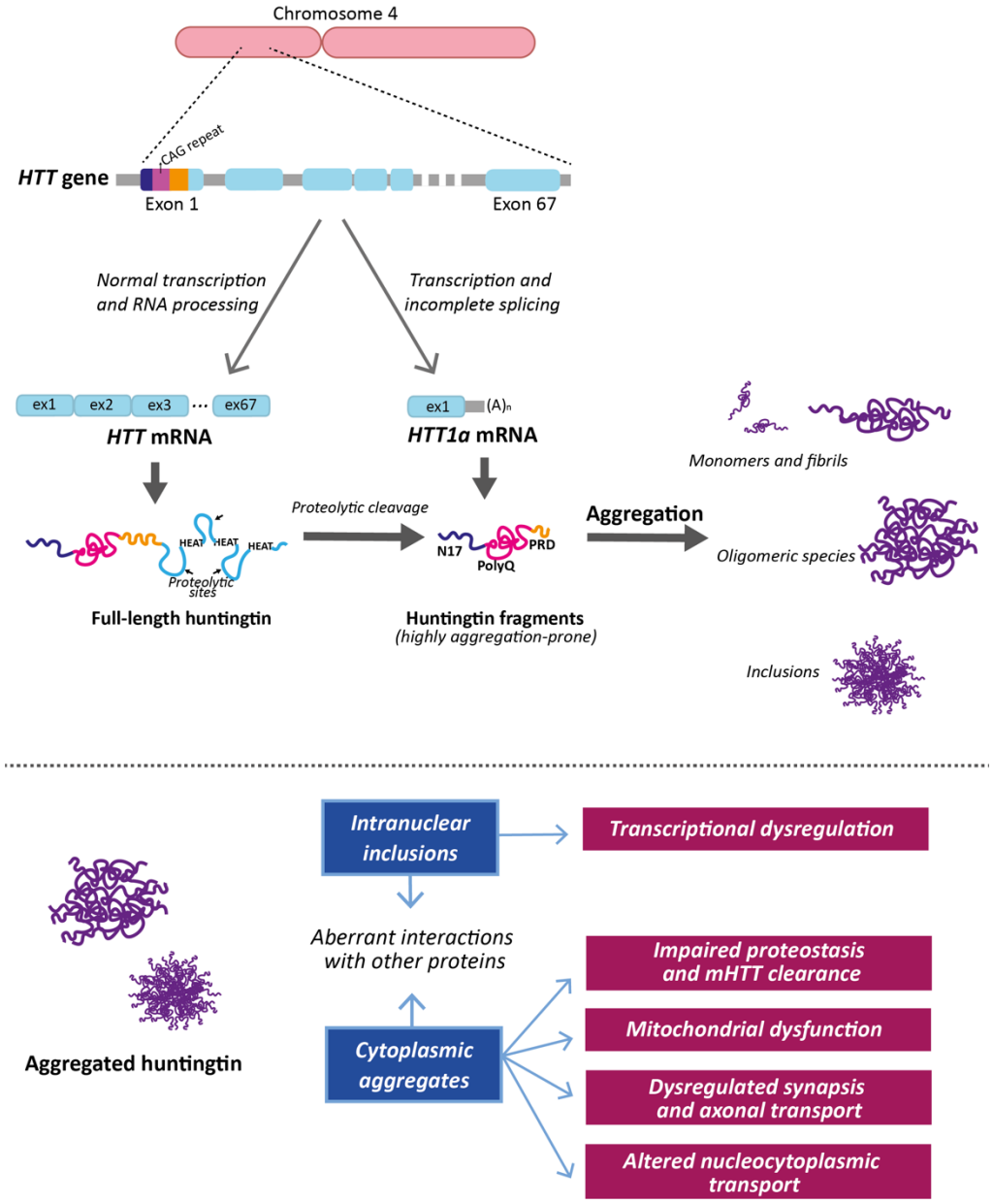

Figure 1.2. Huntingtin processing, from HTT RNA transcription to formation of aggregates species and their effects on cellular processes.

HTT gene, with an expanded CAG repeat and 67 exons on chromosome 4, may be normally processed to a full-length transcript and generate a full-length HTT *protein. But it can also undergo a process of incomplete splicing whereby it generates a HTT1a transcript to encode an exon 1* HTT *protein. This exon 1* HTT *fragment along with other fragments generated by proteolytic cleavage of the full-length* HTT *are prone to aggregate and form fibrils, oligomers and inclusions within cells.* HTT *aggregates, in either nucleus or cytoplasm, engage in aberrant interactions with other proteins and significantly affect essential cellular processes, as indicated. HEAT: Huntingtin, Elongation factor 3, protein phosphatase 2A, TOR1; N17: N-terminal with 17 amino acids; polyQ: polyglutamine; PRD: proline-rich domain.*

1.7 Protein homeostasis and its dysregulation in Huntington's disease

1.7.1 The proteostasis network

Cells have developed a system for protein quality control that is defined as the proteostasis or protein homeostasis network. This network, comprised of numerous factors and signalling pathways, aims to maintain the functional integrity and structural stability of the entire cellular proteome during the processes of protein synthesis, folding, trafficking/transport, post-translational modifications and/or clearance (Powers *et al*., 2009; Labbadia and Morimoto., 2015; Jayaraj *et al*., 2019). The molecular chaperones, described as helpers in the conformational native assembly of another protein without being part of its final conformation, are an essential part of this network and are present at all stages of the protein homeostasis. These are some key signalling pathways comprising the proteostasis network that work in a timely and coordinated manner (represented in Figure 1.3):

- Heat shock response (Morimoto, 2011; Lindquist, 1986): the main effectors of this response are the stress-activated chaperones, heat shock proteins.
- Unfolded protein response (in mitochondria and endoplasmic reticulum): (Karagöz *et al*., 2019; Melber and Haynes, 2018).
- Autophagy-lysosome and ubiquitin proteasome (UPS) systems: primary pathways that act in combination for the degradation and clearance of damaged/misfolded proteins (Dikic, 2017; Hershsko and Ciechanover, 1998). The autophagy-lysosome system can be further divided into:
    - Microautophagy: direct engulfment of material to degrade by lysosomes in the cytoplasm.
    - Chaperone-mediated autophagy (CMA) (Kaushik and Cuervo, 2012).
    - Macroautophagy, generally referred to as autophagy, involves cargo recognition and is usually implicated in the removal of oligomeric species or aggregated forms of proteins.

  Initially, the UPS is the first mechanism of protection for the degradation of short-lived unfolded/misfolded proteins by selectively tagging these proteins

with ubiquitin and promoting its cleavage into small peptides. The UPS degradation requires the unfolding of the protein substrate by 26S proteasome complex (Prakash and Matouschek, 2004). Chaperone-mediated autophagy acts by chaperone HSC70 recognising specific exposed KFERQ hydrophobic sequences (which in the native states are buried internally) on the substrates (Kiffin *et al*., 2004) and transferring them into the lysosomes for degradation. If misfolded or aggregated proteins elude these first mechanisms of defence, they are recognised and directed to macroautophagy by autophagic adaptors like p62 (Matsumoto *et al*., 2011; Rogov *et al*., 2014). The misfolded proteins are then engulfed into autophagosomes and digested by hydrolases after the fusion with lysosomes (autophagolysosomes) (Ciechanover and Kwon, 2015).

- Other pathways integrated in the proteostasis network: pathways involved in the regulation of oxidative stress defence, epigenetic chromatin regulation, inflammation or Ca^{++} regulation (Powers *et al*., 2009; Jayaraj *et al*., 2019).

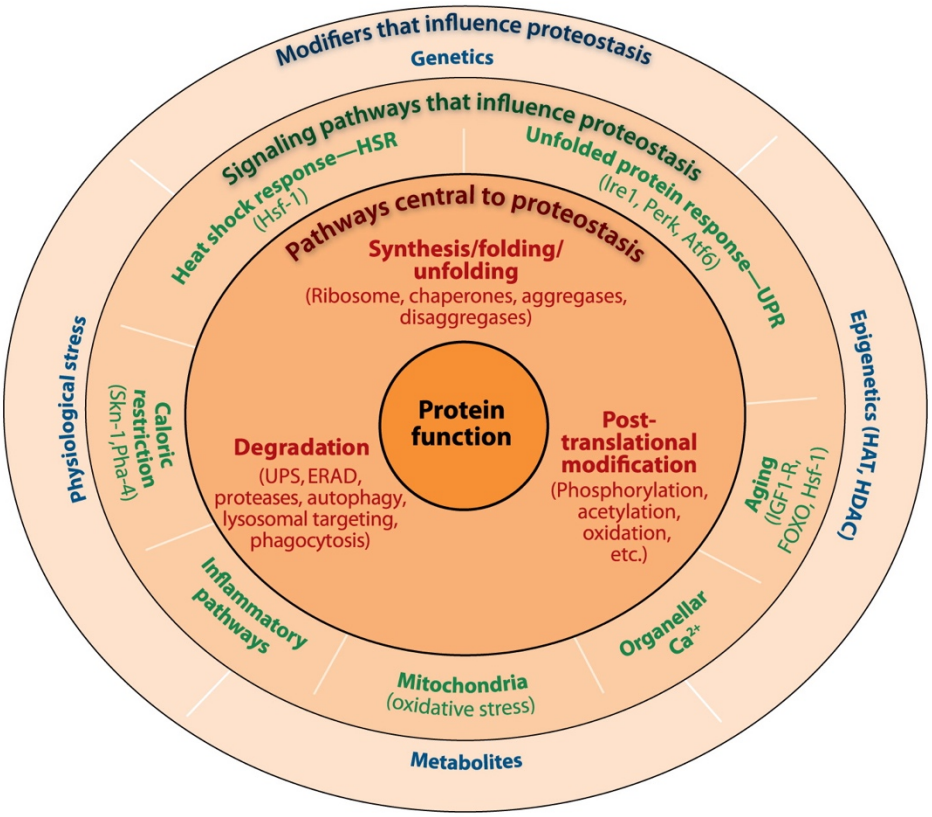

Powers ET, et al. 2009.
Annu. Rev. Biochem. 78:959–91

Figure 1.3. Pathways and modifiers that form the proteostasis network.
The protein processes that are regulated by the proteostasis network and the components/actions involved in them are indicated in red font in the center. The signalling pathways that mainly influence protein homeostasis are marked in green font. The outer layer in blue font indicates other modifiers (epigenetics, stress, genetics…) that can significantly alter protein homeostasis. Image is from publication by Powers et al., (2009), reproduced with permission. HSR: heat shock response; UPR: unfolded protein response; UPS: ubiquitin proteosome system; ERAD: endoplasmic reticulum associated protein degradation; HAT: histone acetyl transferases; HDAC: histone deacetylases.

1.7.2 The heat shock response: induction and regulation

Among the central signalling pathways of the proteostasis network, the focus of this thesis is on the heat shock response. It is a highly conserved cellular response with a protective nature, that is promptly induced by environmental or physiological stress such as elevated temperatures, altered pH, presence of toxins, bacteria or viruses or oxidative stress (Lindquist, 1986; Morimoto, 2011). During aging or in neurodegeneration, proteostasis in general, and the heat shock response, can be highly compromised (Hipp *et al*., 2019). The appearance of mutations caused by errors during the DNA replication, exacerbated by aging or by pathological conditions (e.g., CAG repeat expansion in HD or cell proliferation in cancer) may lead to a vulnerable state in the cells, with unstable peptides that are more likely to misfold or form protein aggregates or intermediate oligomeric species.

The main regulator of the heat shock response is the heat shock factor 1 (HSF1) (Vihervaara and Sistonen, 2014; Joutsen and Sistonen, 2019). This is the best characterised member of the highly conserved HSF1 family, which contains six members in mammals: HSF1, HSF2, HSF3, HSF4, HSFX and HSFY (Joutsen and Sistonen, 2019). It can shuttle between nucleus and cytoplasm under physiological conditions (during absence of stress) but locates mainly in the nucleus during heat shock (Mercier *et al*., 1999; Vujanac *et al.,* 2005).

HSF1 is kept in the cytoplasm or nuclear compartments in a monomeric form and inactivated by the inhibitory action of chaperones HSP90, HSP70 and HSP40. Upon exposure to stress conditions, HSF1 dissociates from the inhibitory complex with HSP90 and other chaperones and trimerises. HSF1 accumulates or translocates to the nucleus where it undergoes extensive post-translational modifications (especially hyperphosphorylation) that contribute to the high-affinity binding to the heat shock elements (HSE) located in the promoter regions of the heat shock genes (Baler *et al*., 1993). The heat shock genes encode the heat shock proteins, which are the primary effectors of the folding, re-assembly or degradation of misfolded/aggregated proteins. After that, the heat shock response is attenuated, promoted by the

acetylation of HSF1 which will significantly reduce the binding and residence of HSF1 on the promoter sites of the heat shock genes. This leads to the eventual dissociation of HSF1 from the promoters and its ubiquitin-dependent degradation (Kim *et al*., 2016), although there is limited evidence on the specific mechanisms of clearance and/or disassembly of HSF1 in the cytoplasm (Figure 1.4; Akerfelt *et al*., 2010; Gomez-Pastor *et al*., 2018; Anckar and Sistonen, 2011).

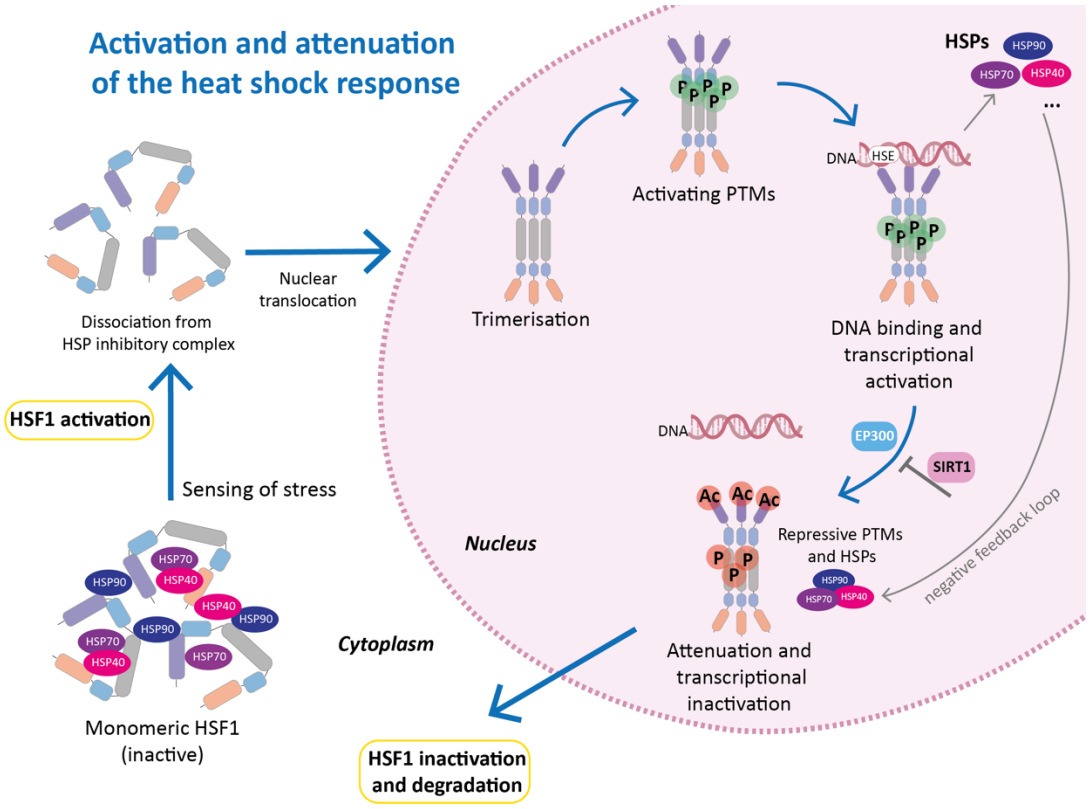

Figure 1.4. Schematic of the activation and attenuation of the heat shock response.
Under absence of stress, HSF1 *is monomeric and inactivated by* HSP90/HSP70/HSP40*. Under stress-sensing conditions,* HSF1 *is dissociated from the inhibitory complex and undergoes trimerisation and multiple activating post-translational modifications in the nucleus. Then,* HSF1 *binds to the HSE in the promoters of the heat shock genes to activate transcription and production of heat shock proteins. During attenuation of the heat shock response, the repressive action from the negative feedback loop by heat shock proteins and other inhibitory post-translational modifications (such as acetylation by* EP300*; reversed by* SIRT1*) lead to the inactivation and degradation of* HSF1*. HSP: heat shock protein; HSE: heat shock element; P: phosphorylation; Ac: acetylation; PTMs: post-translational modifications.*

The heat shock proteins can be classified into families, according to their molecular weights, which is also used in the nomenclature of these proteins (Smith *et al*., 2015; Kampinga *et al*., 2009; Kim *et al*., 2013; Frydman, 2001). These are the main groups:

- HSP70 family (encoded by *HSPA* genes in humans): these 70 kDa chaperones act by recognising the hydrophobic residues of newly synthesised, unfolded or misfolded proteins to assist in their folding or promote their degradation. Their structure is formed by a N-terminal ATPase nucleotide binding domain (NBD) and a C-terminal substrate binding domain (SBD) with intermediate domains. Their ATP-regulated activity is dependent on interactions with HSP40 and nucleotide exchange factor (NEF) chaperones (Rosenzweig *et al*., 2019; Mayer and Gierasch, 2019; Kampinga and Craig, 2010).
- HSP90 family (encoded by *HSPC* genes in humans): it contains 90 kDa members and is one of the most abundant in cells. These ATP-dependent homodimer chaperones have numerous and diverse types of client proteins including protein kinases, cell cycle regulators or hormone receptors, with which they usually interact and stabilise in the late stages of folding (Karagöz and Rüdiger, 2015; Biebl and Buchner, 2019).
- HSP110 family (encoded by *HSPH* genes in humans): also known as nucleotide exchange factors (NEF) with 100 - 110 kDa in molecular weight. They regulate and stabilise HSP70 and assist in the dissociation of amyloid-like deposits (Shorter, 2011; Bracher and Verghese, 2015).
- DNAJ or HSP40 family (encoded by *DNAJA, DNAJB, DNAJC* genes in humans). A 40 kDa family of chaperones, all containing a J-domain, and act mainly as co-chaperones of HSP70 by stimulating ATP activity (Zarouchlioti *et al*., 2017; Kampinga *et al*., 2019). They are divided in three classes (DNAJA, DNAJB, DNAJC) depending on their domain composition (Cheetham and Caplan, 1998).
- HSP60/HSP10 family or chaperonins (encoded by *HSPD*, *HSPE* and *CCT* genes in humans): these ATP-dependent, double-ring chaperones of ~10 kDa or ~60 kDa form a complex with an internal cavity to fold the substrate polypeptides.

They are further classified in two groups (I and II) (Bukau and Horwich, 1998; Horwich *et al*., 2007). Some of the described members are GroEL (group I) or TRiC (group II).

- HSPB family or small heat shock proteins (encoded by *HSPB* genes in humans): these chaperones are ATP-independent and range from 12 to 42 kDa in molecular weight. They can mediate and prevent the aggregation of unfolded/misfolded proteins until they are assisted by HSP90 or HSP70 chaperones (Mogk *et al*., 2019, Janowska *et al*., 2019).

1.7.2.1 Modulation of HSF1 activity

The HSF1 protein is comprised of several structural and functional domains that are maintained across different species (schematic representation in Figure 1.5):

- a DNA-binding domain (DBD) at the N-terminus. The helix loop structure present in this domain facilitates and stabilises the interaction with DNA and other factors (Littlefield and Nelson, 1999; Ahn *et al*., 2001; Neudegger *et al*., 2016).
- a regulatory domain (RD) in the central region, involved in the sensing of stress and regulation of HSF1 during the absence of stress (Newton *et al*., 1996). It is flanked by two leucine-zipper-like hydrophobic modules with heptad repeats (HR-A and HR-B next to the DBD and HR-C following the RD) that form the oligomerisation domain that mediates (HR-A and HR-B) or represses (HR-C) the trimerisation of HSF1 (Rabindran *et al*., 1993; Liu and Thiele, 1999).
- a transactivation domain (TAD) at the C-terminus formed by two modules, which is involved in the transcriptional activation of the targeted heat shock genes (Green *et al*., 1995).

As mentioned, throughout the activation and attenuation of the heat shock response, HSF1 is tightly regulated by the action of chaperones as well as by post-translational modifications (Anckar and Sistonen, 2011; Neef *et al*., 2011; Gomez-Pastor *et al*., 2018; Joutsen and Sistonen, 2019).

During activation of the heat shock response, HSP90 exerts its repressive action by binding to the regulatory domain of HSF1, affecting its trimerisation, and HSP40/HSP70 associate with the transactivation domain, impeding the transcriptional activation (Zou *et al*., 1998; Guo *et al*., 2001; Abravaya *et al*., 1992; Shi *et al*., 1998). After the attenuation of the response, the newly synthesised chaperones re-associate with the corresponding HSF1 domains in a negative feedback manner to control the duration and magnitude of the heat shock response (Baler *et al*., 1992; Kmiecik *et al*., 2020).

Among the post-translational modifications, phosphorylation is the most common in HSF1. A series of serine (Ser) sites have been identified in the HSF1 domains that are subjected to phosphorylation (Guettouche *et al*., 2005). Specifically, Ser230, Ser320 and Ser326 are some of the residues that, when phosphorylated, enhance HSF1 transcriptional activity (Holmberg *et al*., 2001; Guettouche *et al*., 2005; Figure 1.5). On the other hand, Ser303 and Ser307 are among the residues that have a repressive effect on HSF1 when they are phosphorylated during the attenuation phase of the heat shock response (Kline and Morimoto, 1997; Figure 1.5).

Other post-translational modifications include: the Ser303 phosphorylation-dependent sumoylation of residue Lys298, with unclear mechanism and effect on HSF1 activation (Hietakangas *et al*., 2003; Kmiecik *et al*., 2021), and the acetylation of lysine (Lys) residues (Westerheide *et al*., 2009; Zelin and Freeman, 2015) which correlates with the attenuation of the heat shock response (Figure 1.5). The acetylation of Lys80 in HSF1 DNA binding domain (a residue which is in direct contact with DNA) by the acetyltransferase EP300 (Raychaudhuri *et al*., 2014) is key in the attenuation phase of the heat shock response. Lys80 acetylation can be reversed by the histone deacetylase SIRT1 (Westerheide *et al*., 2009).

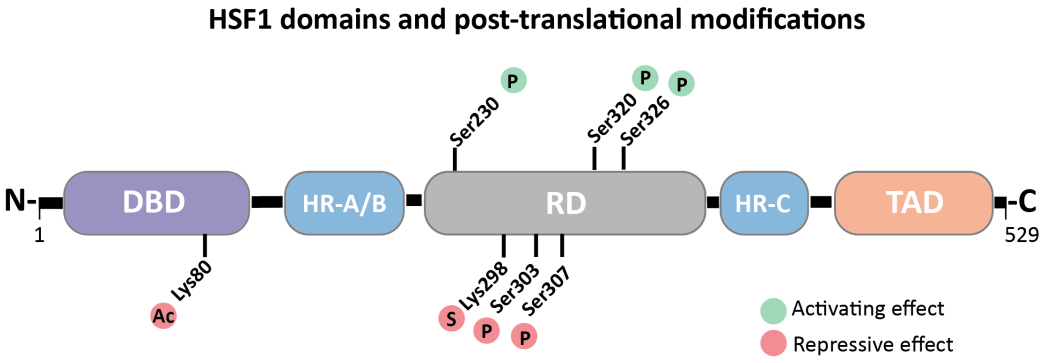

Figure 1.5. HSF1 *domains and main post-translational modifications affecting its activity.*
The organisation of HSF1 *domains is highly conserved across species. The* HSF1 *protein contains 529 amino acids in humans. At the N-terminus, the DBD domain is involved in the interaction with the promoters of the heat shock genes; at the central region, the RD domain, where most of the post-translational modifications occur, is flanked by two HR domains, that facilitate* HSF1 *trimerisation; at the C-terminus, the TAD domain that promotes the transcriptional activation of the targeted heat shock genes. Several residues in these domains are highlighted, as they undergo post-translational modifications (phosphorylation, sumoylation or acetylation) that have relevance in either activating (green) or repressing (red)* HSF1*, as indicated. DBD: DNA binding domain; HR: heptad repeats; RD: regulatory domain; TAD: activation domain; Ser: serine; Lys: lysine; Ac: acetylation; S: sumoylation; P: phosphorylation.*

1.7.2.2 Pharmacological induction of the heat shock response

The design and development of compounds that could promote the heat shock response, by activating HSF1 or prolonging its transactivation activity has been a subject of great interest to restore proteostasis in protein conformational diseases (Westerheide and Morimoto, 2005; Calamini and Morimoto, 2012; Pratt *et al.*, 2015; Luo *et al.*, 2010; Wang *et al.*, 2013). Several approaches have been taken to activate HSF1:

- Compounds targeting and inhibiting HSP90:

This the most widely studied and promising approach. These compounds selectively target and bind to HSP90 to disrupt its interaction with HSF1 and subsequently lead to HSF1 activation; additionally, a non-canonical role for HSP90 in the modulation of HSF1 activity and the heat shock response has been proposed, mediated by HSP90 involvement in the removal of HSF1 trimers from the heat shock elements in DNA (Kijima *et al*., 2018). Among the HSP90 inhibitors, geldanamycin and its derivatives (such as 17-AAG or 17-DMAG), celastrol (Westerheide *et al*., 2004) or radicicol are some of the most studied, with potent activation of the heat shock response. Because of the implications of HSP90 client proteins in the activation of tumorigenic signalling pathways and cell proliferation, some of these HSP90 inhibitors have been taken further into pre-clinical or clinical development stages for cancer therapies (Neckers and Workman, 2012; Serwetnyk and Blagg, 2021).

However, some disadvantages have been reported for these compounds such as toxicity in liver, difficulty in the synthesis and formulation, low bioavailability or inefficient cross of the blood brain barrier, which have negatively affected further clinical evaluation of these compounds in humans (Neckers and Workman, 2012; Serwetnyk and Blagg, 2021). Additionally, some of these HSP90 inhibitors require routes of administration, e.g., intravenous, which may make its application difficult *in vivo*.

In this thesis, the HSP90 inhibitor NVP-HSP990 (2-amino-7,8-dihydro-6H-pyrido[4,3-D]pyrimidin-5-1), was administered *in vivo* to mice to pharmacologically induce the heat shock response. This compound, supplied by Novartis Pharma, is administered orally, well-tolerated and penetrates the blood brain barrier (Menezes *et al*., 2012; McBride *et al*., 2014). NVP-HSP990 binds to the N-terminal domain of HSP90 that modulates its ATPase activity. By hindering its ATPase activity, HSP90 capacity to interact with proteins is disrupted. After NVP-HSP990 administration, HSP90 therefore dissociates from the inhibitory complex formed with HSF1. As a consequence, HSF1 is released and the heat shock response is initiated. NVP-HSP990

has been approved for the treatment of cancer patients as a potent antiproliferative drug (Menezes *et al*., 2012; Spreafico *et al*., 2015). The NVP-HSP990 compound has been previously employed in our group to pharmacologically activate the heat shock response in mice (Carnemolla *et al*., 2014; Carnemolla *et al*., 2015; Labbadia *et al*., 2011; Neueder *et al*., 2014; Neueder *et al*., 2017).

- Compounds modulating HSP70 function:

Some compounds have been described that target either the HSP70 substrate binding domain (e.g., 15-deoxyspergualin or geranylgeranylacetone) or the nucleotide binding domain (e.g., SW02, methylene blue or MKT-077) to enhance (Hirakawa *et al*., 1996; Katsuno *et al*., 2005) or inhibit HSP70 activity through different mechanisms of action (Nadler *et al*., 1992; Wang *et al*., 2010).

- Other approaches:

Non-steroidal anti-inflammatory drugs (NSAIDS) like sodium salicylate or prostaglandins have been reported to activate HSF1 (Jurivich *et al*., 1992; Amici *et al*., 1992). The small molecule HSF1A was also identified to activate HSF1 and induce chaperones by interaction with TRiC chaperone (Neef *et al*., 2010; Neef *et al*., 2014). A screening in a cell-based assay identified several hundred small molecules with potential to induce HSP70 expression through different mechanisms (Calamini *et al*., 2012).

Other compounds like the hydroxylamine derivative arimoclomol and riluzole are not well-characterised and the mechanisms of action are not completely understood, although they are believed to prolong the duration of HSF1 binding to heat shock elements or increase the levels of HSF1 via chaperone-mediated autophagy inhibition (Yang *et al*., 2008). Arimoclomol has been reported to provide beneficial effects in the context of amyotrophic lateral sclerosis (ALS), in mouse models of the disease (Kalmar *et al*., 2008); it was in clinical trials for the treatment of ALS patients (Kalmar *et al*., 2014; Lanka *et al*., 2009) but its approval was recently denied.

1.7.3 The heat shock response as a therapeutic target in neurodegeneration and Huntington's disease: rationale and previous work

The presence of damaged or misfolded proteins in cells triggers the activation of the heat shock response. This can be a consequence of environmental or physiological stress, but it is also caused and further exacerbated by mutations that are associated with protein conformational disorders such as Alzheimer's disease (AD), Parkinson's disease (PD), amyotrophic lateral sclerosis (ALS), HD and spinocerebellar ataxias (SCA) or prion disorders (Sinnige *et al*., 2020). A hallmark of these neurodegenerative diseases is the accumulation of cellular aggregates (amyloid-β and tau, α-synuclein, SOD1 and TDP-43, polyglutamine tracts and prion proteins, respectively). These aggregates may engage in aberrant interactions, resulting in the collapse of cellular physiology (Olzscha *et al*., 2011), and the ability to respond to situations of proteotoxic stress becomes diminished or is deregulated in the context of these disorders and exacerbated with aging (Gidalevitz *et al*., 2006; Hipp *et al*., 2014, 2019; Boland *et al*., 2018; Labbadia and Morimoto, 2015).

The enhancement of the protein-folding capacity and clearance mechanisms in cells by increasing the expression of chaperones has been a promising avenue to explore as a therapeutic strategy in the protein conformational diseases, including HD (Calamini and Morimoto, 2012; Bose and Cho, 2017; Lindquist and Kelly, 2011; Boland *et al*., 2018; Ciechanover and Kwon, 2015; Muchowski and Wacker, 2005).

For HD, interactome studies have indicated that members of the chaperone families interact with HTT or are contained within HTT aggregates such as HSP90 (Baldo *et al*., 2012; Shirasaki *et al*., 2012) and members of HSP40, HSP70 families (Jana *et al*., 2000; Lotz *et al*., 2010; Guzhova *et al*., 2011; Monsellier *et al*., 2015). This may lead to the progressive reduction of chaperone members that has been observed in the brain of HD R6/2 model (Hay *et al*., 2004; Neueder *et al*., 2017; Yamanaka *et al*., 2008).

The modulation of chaperones, either genetically or pharmacologically, has been an important approach pursued in HD (Reis *et al*., 2017). The individual or combined genetic manipulation of mostly HSP70 or HSP40 or other chaperones has led to

modest improvements in HD mice (Hansson *et al*., 2003), and reduction of aggregation in cultured cells (Rujano *et al*., 2007; Hageman *et al*., 2010; Gillis *et al*., 2013; Muchowski *et al*., 2000). The overexpression of chaperone HSJ1a (DNAJ) in HD R6/2 mice significantly reduced the level of aggregation of mutant HTT in brain and improved some HD phenotypes (Labbadia *et al*., 2012). And recently, Scior *et al*. (2018) showed an efficient suppression of formation and disaggregation of amyloid fibrils by a trimeric chaperone complex *in vitro* and in *C. elegans* models of HD.

Other small heat shock proteins have also been investigated as potential suppressors of polyQ toxicity and aggregation, such as HSPB7, in a *Drosophila* and cellular polyQ model, and that its N-terminus was required for both interaction and suppressing activity (Vos *et al*., 2010; Wu *et al*., 2019).

The coordinated upregulation of chaperones by pharmacological induction, either by activating HSF1 directly of by HSP90 inhibition could be a more beneficial manner to increase the protein folding capacity in HD and polyglutamine disorders. It has shown efficient induction of the heat shock response and positive outcomes in: organotypic slice cultures derived from HD R6/2 mice, with delayed aggregation formation after treatment with radicicol/geldanamycin (Hay *et al.,* 2004); inhibition of mutant HTT aggregation in HD cellular model (Sittler *et al*., 2001); reduction of aggregation *in vivo* in a *Drosophila* model of SCA (Fujikake *et al*., 2008) and mouse models of SBMA (Katsuno *et al*., 2005; Waza *et al*., 2005). Labbadia *et al*. (2011), in our group, demonstrated the amelioration of some HD phenotypes and reduced level of aggregation in two mouse models of HD after pulsed treatment with HSP90 inhibitor NVP-HSP990. However, these beneficial effects were transient as, with the disease progression, the ability to induce the heat shock response became impaired.

The following Table 1.1 summarises previous studies involving heat shock proteins in HD, as well as the genetic and pharmacological approaches taken as therapeutic strategies.

Table 1.1. Heat shock proteins / genes previously studied in HD and summary of strategies and outcomes.

Interaction with HTT, expression analysis and effects of chaperones on modulating HTT aggregation

HSP family	*Heat shock gene / protein*	*Reference*	*Model*	*Method*	*Study outcomes*
HSP70	HSC70	Monsellier *et al.,* 2015	Purified HTT polypeptides with varying polyQ lengths and synthetic Nt17 peptides	Electron microscopy, FTIR spectroscopy, circular dichroism, mass spectrometry, seeding assays…	HSC70 (together with HSP40 co-chaperones HDJ1, HDJ2) bound to N-terminal HTT exon 1 fragment and affected its aggregation in a polyQ tract-independent manner. The surface interface of the interaction was mapped by mass spectrometry.
	HSC70, HSP70	Hay *et al.,* 2004	Mice (R6/2)	Western blotting; IHC; confocal microscopy	HSP70 levels were decreased in R6/2 brains by 12 weeks of age. HSC70 colocalised with nuclear HTT aggregates in R6/2 cortex, striatum (8 weeks), hippocampus (4 weeks).
	HSP70	Yamanaka *et al.,* 2008	Cells (Neuro2a transfected to express HTT with 18Q or 150Q and cortical neurons) Mice (R6/2)	IHC, fluorescence microscopy; EMSA; IP, Western blotting; RT-PCR	HSP70 mRNA and protein expression was reduced in mouse brain from 8 weeks, as the transcription factor NF-Y was found to be sequestered in mutant HTT aggregates (NF-Y binding to HSP70 promoter was reduced). Reduction of HDJ1 was also observed.
HSP40 and HSP70	HDJ-1, HDJ-2 (HSP40), HSC70, HSP70	Jana *et al.,* 2000	Cells (Neuro2a with N-terminal htt-EGFP-16Q, 60Q, 150Q) Mice (R6/1, R6/2)	CoIP, immunoblotting, IHC, fluorescence microscopy	In cells, HSP40 (HDJ-1, HDJ-2), HSC70, HSP70 interacted with polyQ-expanded HTT (coimmunoprecipitated with soluble HTT; HDJ-2 and HSC70 co-localised in cytoplasmic HTT aggregates). In HD mouse brains, HDJ-2 and HSC70 co-localised in nuclear inclusions.
	DNAJB1 (HSP40), HSP70	Lotz *et al.,* 2010	Cells (PC12, Q103); purified GST-HD53Q, GST-HD20Q	SEC, atomic force microscopy, dot-blot, filter trap assay, Western blotting	HSP70 was associated with HTT oligomers, this was dependent on (DNAJB1) HSP40 and ATP.

HSP40 and HSP70	DnaJ, Ydj1 (HSP40), DnaK (HSP70)	Muchowski *et al.,* 2000	Yeast (20Q, 53Q); GST fusion proteins (HD20Q, HD53Q) expressed in *E. coli* and purified	Electron microscopy; coIP; immunofluorescence; filter trap assays	Purified DnaK (HSP70) and DnaJ (HSP40) interacted with regions of HTT in GST-HS20Q or 53Q. Coprecipitation of HSP70 and Ydj1 (HSP40) with exon 1 HTT segment in yeast HD53Q.
HSP40	HSJ-2/HSDJ (HSP70 co-chaperone)	Wyttenbach *et al.,* 2000	Cells (COS-7, PC12, SH-SY5Y; transfected with part of HTT exon 1 with 23Q - 74Q)	IHC Western blotting	HSP40, HSP70 and 20S proteasome co-localised with HTT inclusions.
	HDJ1, HDJ2	Hay *et al.,* 2004	Mice (R6/2)	Western blotting RT-qPCR IHC Confocal microscopy	HDJ1 and HDJ2 colocalised with mutant HTT aggregates in cortex, striatum (8 weeks), hippocampus (4 weeks). Levels of HD1, HDJ2 were decreased in R6/2 brains by 12 weeks of age. HDJ1 mRNA levels did not change in R6/2 so HDJ1 may be sequestered into aggregates.
	DNAJB6, DNAJB8	Gillis *et al.,* 2013	Cells (HeLa; co-transfected, Q99)	Confocal and FRET-FLIM microscopy	DNAJB6, DNAJB8 interacted directly with polyQ tract of polyQ proteins and HTT exon1 fragments
	DNAJB6	Mansson *et al.,* 2014	Purified polyQ peptides and constructs with *Htt* exon1	Purification of peptides Thioflavin T binding (fibrillation assay) Electron microscopy, size exclusion chromatography	Purified DNAJB6 efficient at suppressing the aggregation of polyQ peptides *in vitro*, in a mechanism independent of ATP and HSPA1 (HSP70) and based on a direct interaction with polyQ peptides.
HSP90	HSP90	Baldo *et al.,* 2012	Cells (*Hdh*Q150 ES and neurons, HN10)	CoIP	Physical interaction between mutant and WT HTT with HSP90 (HTT as HSP90 client protein)
	HSP90	He *et al.,* 2017	Cells (HEK293; transfected, Q18 and Q100)	Supernatant/pellet fractionation; GST pull-down assays; NMR spectroscopy, SEC	HSP90 recognised N-terminus of HTT and regulated HTT aggregation by USP19 (deubiquitinating enzyme), that interacted with HSP90
HSPB (small heat shock proteins)	HSPB7	Vos *et al.,* 2010	Cells (HEK293 and NG-108 cells; mutant *Htt* exon 1 Q74 co-expressed with HSPB7)	FLIM and confocal microscopy; FRET; immunostaining	HSPB7 found to interact with polyQ proteins (staining in inclusion periphery).

HSPB (small heat shock proteins)	HSPB7	Wu *et al*., 2019	Cells (HEK293)	Aggregation assays; gene cloning; Western blotting; Immunofluorescence	Explains mechanism by which HSPB7 prevented aggregation of poly Q proteins, dependent on its N-terminal domain to associate with aggregates
Chaperonins	TRiC	Shahmoradian *et al.*, 2013	*In vitro* (purified HTT constructs (Q51) and TRiC)	Cryo-electron microscopy and tomography; 3D mapping to resolve structural interaction; GST aggregation assay	TRiC inhibited mutant HTT exon 1 (with 51 CAGs) aggregation *in vitro* by interacting with mutant HTT fibrils and encapsulating smaller oligomers
	TRiC (and subunits)	Tam *et al.,* 2006	Yeast (*S. cerevisiae)* cell extracts Purified GST-Htt-exon1 (Q18, Q51)	Fluorescence microscopy; aggregation assay; GST pull downs	TRiC interacted with polyQ HTT (normal and pathogenic forms) and inhibited aggregation
HSP70 co-chaperones	BAG-1	Jana and Nukina, 2005	Cells (HD15Q, HD150Q)	Immunofluorescence, IP, Western blotting, cell viability assay	BAG-1 associated with polyQ-expanded HTT aggregates through interaction with HSP70/HSC70.
	CHIP	Jana *et al.,* 2005	Cells (mouse Neuro2a; 16Q, 150Q; transfected)	CoIP, immunoblotting Immunofluorescence Degradation assays	CHIP was recruited into HTT aggregates and interacted with polyQ-expanded N-terminal region (co-immunoprecipitated).

Genome-wide screens / Proteomic interactome studies

Heat shock genes / proteins identified	***Reference***	***Model***	***Method***	***Study outcomes***
HSP40 members (DNAJA2, DNAJB1, DNAJC7, DNAJA1), HSP70, HSP110, HSP90, TRiC subunits	Kim *et al.,* 2016	Cells (Neuro2a expressing HttEx1-eGFP with Q18, Q64, Q150)	Combined in-cell single fluorescence spectroscopy and quantitative proteomics; SILAC-MS	Soluble polyQ-expanded HttEx1 oligomers found to interact with up to 875 proteins. Several members of the HSP40 family (DNAJA2, DNAJB1, DNAJC7, DNAJA1) as well as HSP70, HSP110, HSP90 and TRiC subunits were identified.
HSP90, HSP110, HSP70, HSC70, HSPB8, HSP60, TCP1, CCT8…	Shirasaki *et al.,* 2012	Mouse (BACHD) *Drosophila* HD model (Q128)	Affinity-purification mass spectrometry WGCNA analysis	747 proteins found to associate with full-length HTT in HD and WT mouse brains. A module was enriched in proteostasis proteins. Some were validated as HTT interactors and genetic modifiers in *Drosophila*.
CG6603 (HSP110)*; hsp83* (HSP90)*; hsc70-5* (HSP70)*; dhdj1* (HSP40)*; T-cp1* (chaperonin), *hsf*	Zhang *et al*., 2010	*Drosophila* (expressing GFP-tagged HTT with different polyQ lengths; HD93 model)	Genome-wide RNAi screen Cell-based quantitative assay to measure aggregates Microscopy	Screen identified 126 genes involved in regulating mutant HTT protein aggregation. The activities of two hits (*hsp110* and *tra1*) were modulated *in vivo*. Depletion of *CG6603* (HSP110) resulted in aggregate formation in cells; in HD93 flies, it caused accelerated eye degeneration.
cct-1, cct-2, cct-4, cct-5, cct-6, cct-7 (chaperonins), *hsp-6, hsp-1* (HSP70), *rme-8* (DNAJ)	Nollen *et al.,* 2004	*C. elegans* (with YFP and Q0, Q24, Q33, Q35, Q40)	Genome-wide RNAi screens Fluorescence microscopy and FRAP Immunoblotting	Screen to identify genes that resulted in appearance of aggregates when suppressed; 186 genes identified. Members of chaperonins, HSP70, HSP40 were identified as genetic modifiers of protein aggregation

Genetic manipulation of chaperones

Genetic approach	*Heat shock genes/proteins*	*Reference*	*Model*	*Method*	*Study outcomes*
Overexpression	**HSP40, HSC70 (HSP70), HSP110**	Scior *et al.,* 2018	Cells (HD patient-derived iPSCs with 44Q, HEK293 Htt exon1 Q97) *C.elegans* (with Q35-Q128)	FRET assays, electron and fluorescence microscopy, sedimentation analysis, filter retardation, Western blotting	The trimeric chaperone complex suppressed amyloid fibril formation *in vivo* and *in vitro* and disaggregated HTT fibrils. The J-protein (HSP40) was the limiting factor. Their genetic depletion in *C. elegans* increased HTT aggregates.
Overexpression HSP70 and HSP40	**HSP40 and HSP70**	Lotz *et al.,* 2010	Cells (PC12, Q103); purified GST-HD53Q, GST-HD20Q	SEC, atomic force microscopy, dot-blot, filter trap assay, Western blotting	Overexpression of HSP70 and HSP40 in cells reduced levels of insoluble HTT; they targeted specific oligomers of HTT and decreased their levels and toxicity.
	Ydj1 (HSP40), HSP70	Muchowski *et al*., 2000	Yeast (20Q, 53Q); GST fusion proteins (HD20Q, HD53Q) purified	Electron microscopy; coIP; immunofluorescence; filter trap assays	Overexpression of Ydj1 (HSP40) or HSP70 inhibited formation of insoluble inclusions in HD53Q yeast.
	HDJ-1 (HSP40) and HSP70	Sittler *et al.,* 2001	Cells (COS1 with 51Q)	Immunoblotting, filter retardation assay, fluorescence microscopy	Single HSP40 or HSP70 overexpression reduced aggregation of insoluble exon1 HTT protein by 30-40% and by 60-80% when both overexpressed.
	HDJ-1 (HSP40), HSC70 (HSP70)	Jana *et al.,* 2000	Cells (Neuro2a with N-terminal htt-EGFP-150Q)	Immunofluorescence and quantitation of aggregate formation and cell death	Overexpression of HDJ-1 or HSC70 suppressed formation of HTT aggregates and reduced cell death (higher efficiency with co-expression)
	HspA1A (HSP70), DnaJB1 (HSP40)	Rujano *et al.,* 2007	Cells (O23, N2A transfected to express EGFP-HDQ23, Q43, Q53, Q74)	Confocal microscopy and time-lapse imaging, Western blotting, filter trap assays	HspA1A (HSP70) overexpression alone did not suppress formation of inclusions; DnaJB1 (HSP40) overexpression reduced inclusion formation and was dependent on interaction with HSP70/HSC70 and enhanced when HspA1A was also overexpressed.

Overexpression	**CHIP and CHIP + HSC70**	Jana *et al.,* 2005	Cells (mouse Neuro2a; 16Q, 150Q; transfected)	CoIP, immunoblotting Immunofluorescence Degradation assays	CHIP overexpression enhanced the ubiquitination of polyQ -expanded HTT and promoted degradation; reduced HTT aggregation.
Overexpression HSP70		Guzhova *et al*., 2011	Cells (SK-N-SH tranfected; Q25 or Q103)	Confocal microscopy, IP, Western blotting, filter trap assays	Pure recombinant HSP70 protein addition or overexpression inhibited the formation of polyQ HTT aggregates by binding to GAPDH and polyQ. HSP70 bound to polyQ region in a mechanism dependent on ATP.
		Hay *et al.,* 2004	Mice (R6/2 crossed to mice overexpressing HSP70) and organotypic hippocampal slice culture assay	Phenotype assessment (body weight, Rotarod, grip strength) IHC; confocal microscopy	HSP70 overexpression delayed aggregation by one week in hippocampal slices; transient inhibitory effect HSP70 overexpression did not improve weight loss, Rotarod or grip strength performance in R6/2
		Hansson *et al*., 2003	Mice (R6/2 crossed with transgenic mice overexpressing human HSP70)	IHC, stereology optical fractionator technique, Western blotting, paw clasping measurement	R6/2 mice overexpressing HSP70 had a delayed body weight loss (not in brain weight); but the number and size of inclusions, striatal volume, paw clasping phenotype or survival were not affected and were similar as in R6/2 mice.
Deletion	**HSP70**	Wacker *et al*., 2009	Mice (R6/2 crossed with *Hsp70.1/3* KO mice)	Phenotype assessment (survival, Rotarod, body weight, activity, paw clasping); Western blotting, IHC	In R6/2 mice with deletion of *Hsp70.1/3:* phenotype was exacerbated, enhanced severity, survival was decreased, motor deficits worsened; increased size and number of mutant HTT inclusions in brains.
Overexpression	**HSJ-1a (HSP40)**	Labbadia *et al.,* 2012	Mice (R6/2 crossed with human HSJ1a overexpressing mice) Cells (SK-N-SH, transfected)	Behavioural assessment Western blotting, IP, coIP, AGERA, Seprion, RT-qPCR, IHC, filter trap assays…	HSJ1a overexpression reduced mutant HTT aggregation and aggregates size and enhanced its solubility in R6/2 mice; HSJ1a acted on high MW HTT complexes, and this was dependent on HSP70 co-operation. Mice showed a modest improvement on motor performance (Rotarod, grip strength, open field) but no effect on brain or body weight.
Overexpression	**HSJ-2/HSDJ (HSP40)**	Wyttenbach *et al.,* 2000	Cells (COS-7, PC12, SH-SY5Y; transfected with HTT ex1 and 23Q - 74Q)	IHC; Western blotting	Overexpression of HSJ-2 did not change inclusion formation in PC12 and SH-SY5Y cells, but it did in COS-7 cells.

Overexpression / siRNA downregulation	**DNAJB6, DNAJB8 (HSP40)**	Hageman *et al.,* 2010	Cells (N2A, SH-SY5Y, HEK93, transfected to express HDQ74-EYFP, HDQ119-EYFP and chaperones), *Xenopus laevis* tadpoles (Q74, Q119)	Filter trap assay, Western blotting, FLIM microscopy, mass spectrometry, siRNA downregulation	Screen of members of HSPA (HSP70), HSPH (HSP110) and DNAJ (HSP40) families. DNAJB subfamily members DNAJB6, DNAJB8 were the most potent suppressors of aggregation, independent of HSP70 and dependent on C-terminal Ser-rich region. Downregulation of DNJB6b by siRNA in cells enhanced aggregation HDACs interacted with DNAJB members and HDAC4 inhibition reduced anti-aggregation activities.
Overexpression	**DNAJB6 (HSP40)**	Kakkar *et al.,* 2016	Cells (HEK293, NG108; Q23, Q74) Mice (R6/2 crossed with DNAJB6 overexpressing mice)	Filter trap assays; Western blotting, IP; Thioflavin analysis for fibril formation; IHC; behavioural assessment	In cells: inhibitory effect on fibril formation (Q74) In R6/2 overexpressing DNAJB6: Reduced HTT aggregation and number of inclusions in brain; delayed motor dysfunction (Rotarod, grip strength and clasping); 20 % extension of lifespan
Overexpression	**DNAJB6, DNAJB8 (HSP40)**	Gillis *et al.,* 2013	Cells (HEK293, Mel Juso, HeLa; co-transfected, Q104)	Confocal and FRET-FLIM microscopy; filter trap assay, immunoblotting	DNAJB6, DNAJB8 reduced HTT exon 1 aggregation and improved their clearance. This was dependent on the Ser-rich region of DNAJB6, DNAJB8.
Deletion	**DNAJB6, DNAJA1, DNAJB1 (HSP40)**	Rodriguez-Gonzalez *et al*., 2020	Cells (HEK293 with polyQ74Htt)	CRISPR/Cas9 (to KO DNAJA1, DNAJB1, DNAJB6); Western blotting; fluorescence microscopy; filter trap assay; trypan blue	DNAJB6 KO increased HTT aggregation and cell death; DNAJA1 KO decreased HTT aggregation; DNAJB1 KO did not change aggregation propensity. Experiments rescuing their expression confirmed their conclusions.
Overexpression	**HSP27 (human)**	Zourlidou *et al.,* 2007	Mice (R6/2 crossed to HSP27 transgenic mice)	Behavioural assessment Aconitase assays Immunoblotting, IHC	HSP27 overexpression did not reduce oxidative stress in R6/2 brains and did not modify phenotype. HSP27 suggested to remain inactive in R6/2 brains (differential activation)
Overexpression	**HSP27**	Wyttenbach *et al*., 2002	Cells (COS-7; SK-N-SH; httEx1-EGFP with 23 - 103Q)	IHC, Western blotting, estimation of ROS production, polyQ aggregates, cell death	HSP27 overexpression reduced ROS and oxidative stress (regulated by HSP27 phosphorylation) and suppressed cell death in HD cells but not HTT aggregation.

Overexpression	**HSPB7**	Vos *et al.,* 2010	Cells (HEK293 and NG-108 cells; mutant *Htt* exon 1 Q74 co-expressed with HSPB members) *Drosophila* (Q78; SCA3 model)	Filter trap assay; FLIM and confocal microscopy; FRET; immunostaining	Comparison of anti-aggregation abilities of members of HSPB family in HD and SCA3. HSPB7 was the most potent suppressor of aggregation in cells and reduced polyQ-associated toxicity in cells and eye degeneration in *Drosophila*.
Overexpression	**hsp104 (yeast)**	Vacher *et al*., 2005	Mice (N171-82Q crossed with transgenic mice overexpressing yeast hsp104)	Western blotting, IHC Behavioural assessment	Hsp104 overexpression reduced aggregate formation and number of aggregates in cortex, and increased survival by 20 %. The motor phenotype or weight loss was not improved.
Overexpression	**HSP104, HSP27**	Perrin *et al.,* 2007	Rat (injected with lentiviral vectors expressing htt171-19Q, 82Q, hsp104, hsp27) Cells (rat striatal primary cultures, 82Q)	IHC Confocal microscopy; analysis of aggregate distribution	Overexpression of hsp104, hsp27 reduced polyQ HTT toxicity in rats and cells, reduced cell death in striatal neurons (the DARPP-32 expression was rescued, decreased number and reduced size of nuclear HTT aggregates)
Overexpression **BAG1 (HSP70 co-chaperone)**		Orr *et al.,* 2008	Mice (N171-82Q crossed with BAG1 transgenic mice) Cells (PC12 transfected; BAG1 siRNA)	Immunoblotting, IHC Phenotype assessment (Rotarod, limb clasping, body weight, survival) Synaptosome fractionation	BAG1 overexpression did not alter the levels of mutant HTT in mice. Improved motor performance (Rotarod) in male N171-82Q mice overexpressing BAG1. Level of mutant HTT in synaptosomes of BAG1 overexpressing male mice was decreased
		Jana and Nukina, 2005	Cells (HD15Q, HD150Q)	Immunofluorescence, IP, Western blotting, cell viability assay	BAG-1 overexpression reduced cell death but did not reduce aggregate formation.
Overexpression	**TRiC / CCT**	Zhao *et al.,* 2016	BACHD cortical and striatal neurons, PC12 cells (Q97, Q25)	Microfluidic chambers co-cultures, somal size analysis, imaging	Expression of CCT subunits enhanced degradation of mutant HTT via UPS; rescued BDNF expression
Deletion / Overexpression	**TRiC /CCT**	Tam *et al.,* 2006	Yeast (*S. cerevisiae;* Q103- or Q25-GFP) Cells (N2A, Q150; HeLa) Purified GST-Htt-exon1 (Q18, Q51)	Fluorescence microscopy; aggregation assays; GST pull downs;	Depletion of TRiC subunits enhanced aggregation in yeast and mammalian cells. Overexpression of TRiC subunit (CCT1) remodeled aggregate morphology *in vivo* and *in vitro* and reduced toxicity.

Pharmacological modulation of chaperones

Approach	*Compound*	*Reference*	*Model*	*Method*	*Study outcomes*
HSP90 inhibition	Geldanamycin (GA)	Sittler *et al.,* 2001	Cells (COS1, with 72Q)	Immunoblotting, filter retardation assay, fluorescence microscopy	GA increased expression of HSP40, HSP70 and HSP90 (HSR activated) and inhibited exon 1 HTT aggregation in a concentration-dependent manner. HSP40 and HSP70 colocalised with mutant HTT exon 1 in treated cells.
	Geldanamycin (GA), radicicol (RA), pyrollidine dithiocarbamate (PDTC)	Hay *et al.,* 2004	Mice (R6/2) (organotypic hippocampal slice culture assay)	Compounds added to medium at several concentrations (constant or pulsed dosing); Western blotting, IHC	PDTC failed to induce the expression of HDJ1 or HSP70 GA and RA induced the expression of HDJ1 (4 to 5-fold increase) and HSP70 Treatment with RA or GA decreased aggregate load but transiently
	NVP-AUY992	Baldo *et al.,* 2012	Cells (*Hdh*Q150 mouse ES and neurons, HN10, HEK93)	Compound added to cultures; Western blotting; ubiquitination assays; TR-FRET	NVP-AUY992 treatment reduced soluble full-length mutant HTT levels and increased mutant and WT HTT degradation via UPS by inhibiting the physical interaction HTT-HSP90
	NVP-HSP990	Labbadia *et al.,* 2012	Mice (R6/2, *Hdh*Q150)	RT-qPCR, Western blot, Seprion ligand ELISA Behavioural assessment	Increased protein levels of HSP Reduced mutant HTT aggregate load Improvement in Rotarod performance
	Geldanamycin (GA), radicicol (RA), 17-AAG, celastrol (CL), geranyl geranylacetone (GGA), sodium butyrate (SB)	Fujikake *et al.,* 2008	SCA3 *Drosophila* model (UAS-MJDtr-Q78, Q27), HD *Drosophila* model (UAS-Htt-Q128)	IHD, fluorescence microscopy, survival analysis, Western blotting, RT-PCR	17-AAG, GA and RA were effective at suppressing eye degeneration in flies in a dose-dependent manner. 17-AAG also increased survival and suppressed inclusion body formation of polyQ proteins.
	17-DMAG, 17-AAG, geldanamycin (GA)	Herbst and Wanker, 2007	Cells (COS1; EGFP-HD72Q)	RT-PCR, Western blot, filter retardation assay, fluorescence microscopy	Treatment of cells with 17-DMAG induced expression of HSP40, HSP70 and HSP105 and inhibited mutant HTT aggregation more efficiently than 17-AAG or GA

HSF1 activation	HSF1A	Neef *et al.,* 2010	Yeast strains for the screen; cells (HeLa, PC12 expressing httQ74-GFP); SCA3 *Drosophila* model (UAS-MJDtr-Q78)	HSF1A-biotin-asscociated assays; immunoblotting; fluorescence microscopy, aggregation and cytoxocity assays…	Yeast-based pharmacological screen to identify small molecule HSF1 activators found HSF1A, which was able to activate HSF1 and increase chaperone levels in cells and flies. HSF1A, by interaction with TRiC/CCT complex, reduced toxicity in flies and improved protein misfolding, reduced cell death in polyQ-expressing cells.
	F1	Calamini *et al*., 2012	Cells (HeLa transfected with heat shock inducible reporter with HSP70 promoter; *Hsf1*$^{-/-}$ MEFs; PC12 with HttQ74) *C. elegans* (Q35)	EMSA RT-PCR Western blotting, IP	Two high-throughput screening and characterisation of new proteostasis regulators that activate HSF1 (903,587 compounds) in HeLa cells identified 263 hits and 14 compounds were tested. F1 regulator was found to induce multiple stress response pathways with restorative effect on protein folding and suppressing aggregation in polyQ models.
	F1, celastrol	Bersuker *et al.,* 2013	Cells (U2OS Tet-on, HEK293 with HSE:GFP)	Flow cytometry; EMSA; fluorescence microscopy	Activation of HSR by HSF1 overexpression or treatment with celastrol or F1 exacerbated inclusion body formation
HSP70 activation	SW02 (stimulates ATPase activity)	Chafekar *et al.,* 2012	Yeast (Q46, Q25); cells (PC12, Q103)	Fluorescence microscopy; Western blotting; growth and ATPase activity assay; SDD-AGE, filter retardation assay	Reduced aggregation but increased polyQ toxicity in the Q46 yeast model (no effect on Q25). No effect on polyQ toxicity in cells. SW02 did not elicit a stress response in yeast or cells.
	YM-1 (mimics HSP70 co-chaperone Hip and accumulates HSP70)	Pinho *et al.,* 2021	Cells (U2OS transfected to express EGFP-HttEx1Q23 or Q74; PC12 with Q23, Q145)	IP, Western blotting, fluorescent microscopy	YM-1 treatment reduced N-terminal and full-length HTT aggregation (both interacted with HSP70) by increasing their proteasomal degradation.
HSP70 inhibition	CE12	Chafekar *et al*., 2012	Yeast (Q46, Q25), cells (PC12, Q103)	Fluorescence microscopy; Western blotting, growth assay, ATPase activity assay; SDD-AGE, filter retardation assay	Increased aggregation but reduced toxicity in Q46 yeast model. Improved survival in cells. CE12 did not elicit a stress response in yeast or cells.

Abbreviations Table 1.1.: AGERA = agarose gel electrophoresis for resolving aggregates; Co-IP = co-immunoprecipitation; ELISA = enzyme-linked immunosorbent assay; EMSA = electrophoretic gel mobility shift assay; FLIM = fluorescence lifetime microscopy; FRAP = fluorescence recovery after photobleaching; FRET = fluorescence resonance energy transfer; GFP = green fluorescent protein; GST = glutathione S transferase; HSE = heat shock element; HSP = heat shock protein; IHC = immunohistochemistry; IP = immunoprecipitation; MEF = mouse embryonic fibroblasts; MW = molecular weight; NMR = nuclear magnetic resonance; RNAi = RNA interference ; ROS = reactive oxygen species; RT-qPCR = real time quantitative PCR; SDD-AGE = semi-denaturating detergent agarose gel electrophoresis; SEC = size exclusion chromatography; SILAC-MS: stable isotope labelling by amino acids in cell culture based mass spectrometry; YFP = yellow fluorescent protein.

1.7.4 Clearance and degradation of mutant and aggregated huntingtin

Multiple studies have reported that proteostasis in general, and particularly protein clearance mechanisms, are compromised in HD (Waelter *et al*., 2001, Margulis and Finkbeiner, 2014; Soares *et al*., 2019; Harding and Tong, 2018). There is little evidence reported on the mechanisms by which mutant HTT is cleared from the cells (Jeong *et al*., 2009; Qi *et al*., 2012; Juenemann *et al*., 2013). It has been reported that mutant HTT can be initially tagged with ubiquitin for degradation (DiFiglia *et al*., 1997, Sieradzan *et al*., 1999; Juenemann *et al*., 2015) but the clearance machineries are disrupted by the sequestration of essential components of protein homeostasis into the aggregates (Shibata *et al*., 2006) or by inhibition of these processes by mutant HTT (Hipp *et al*., 2012; Martinez-Vicente *et al*., 2010).

The UPS system is dysfunctional in HD and poly-ubiquitinated chains are found in the aggregated HTT proteins in HD cellular models (Verhoef *et al*., 2002) as well as animal models and patients (Bennett *et al*, 2007; Ortega and Lucas, 2014).

The presence of mutant HTT also impairs the autophagic-lysosomal pathway (Martinez-Vicente *et al*., 2010; Menzies *et al*., 2017; Martin *et al*., 2014). Members or regulators of the autophagic-lysosomal pathway like mTOR or p62 were found to be contained in the aggregates of HD mice (Ravikumar *et al*., 2004) or *in vitro* (Bjorkoy *et al*., 2005). Mutant HTT can be targeted or processed by the autophagy system (Ravikumar *et al*., 2002, Qin *et al*., 2003) and the modulation of autophagy factors such as p62 has provided some contrasting results in HD. On one hand, the depletion of p62 was neuroprotective and decreased the levels of nuclear mutant HTT aggregates (Kurosawa *et al*., 2015), whereas other studies have reported that loss of p62 enhanced the mutant HTT toxicity (Bjorkoy *et al*., 2005; Saitoh *et al*., 2015). The stimulation of autophagy via inducers like rapamycin has also been studied in HD with positive results (Ehrnhoefer *et al*., 2018; Ravikumar *et al*., 2004; Berger *et al.,* 2006; Sarkar *et al*., 2009).

1.8 Sirtuins in neurodegeneration and HD

1.8.1 Characteristics and main functions of the sirtuin family

The sirtuins, named after the Silent Information Regulator 2 (Sir2) described in yeast as a transcriptional repressor (Kaeberlein *et al*., 1999; Imai *et al*., 2000), are an evolutionary conserved group of enzymes that belong to the class III of histone deacetylases (HDAC).

The sirtuin family is composed of seven members in mammalian cells which share a catalytic domain: SIRT1 to SIRT7, which can be localised in different subcellular compartments, sometimes determined by the cellular physiological conditions (Haigis and Sinclair, 2010; Frye, 2000). SIRT1, SIRT6 and SIRT7 are predominantly located in nuclear compartments (SIRT6 is associated with chromatin, SIRT7 within the nucleolus and SIRT1 can also shuttle to the cytoplasm to exert some functions [Tanno *et al*., 2007]); SIRT3, SIRT4 and SIRT5 are mitochondrial and SIRT2 is mainly cytoplasmic but has also been detected in the nucleus during mitosis (North and Verdin, 2007). Some reports have also debated the possibility of SIRT3 being translocated from nucleus to mitochondria under cellular stress conditions (Scher *et al*., 2007).

Even though they are referred to as histone deacetylases, histones and deacetylation are not the exclusive target and enzymatic activity, respectively, of sirtuins. These are the most studied enzymatic activities in the sirtuin family:

- Deacetylation: the most common enzymatic reaction, present in all sirtuins but with variable levels.
- ADP-ribosylation: observed in SIRT3, SIRT4, SIRT6 (Nogueiras *et al*., 2012; Haigis *et al*., 2006; Michishita *et al*., 2008).
- Demalonylation, desuccinylation: reported in SIRT5 and SIRT7 (Du *et al*., 2011; Li *et al*., 2016).
- Decrotonylation: reported in histones by SIRT1, SIRT2 and SIRT3 (Bao *et al*., 2014).

All of these enzymatic activities are dependent on the oxidised nicotinamide adenine dinucleotide (NAD^+) (Imai *et al*., 2000), unlike the rest of the histone deacetylases (classes I, II and IV), whose activity is regulated by Zinc (Milazzo *et al*., 2020). The most common enzymatic reaction of deacetylation on specific lysine residues releases nicotinamide (NAM) and O-acetyl-ADP-ribose along with the deacetylated substrate (Imai *et al*., 2000; Tanner *et al*., 2000). The metabolic status of the cells heavily influences the activity of sirtuins. Under conditions of oxidative stress or nutrient deprivation, the ratio NAD^+/NADH is high, which increases the presence of sirtuins and activates them (Xia *et al*., 2021). On the contrary, high concentrations of NAM inhibit the sirtuin reactions in a feedback regulation manner (Sauve *et al*., 2005, 2006; Bitterman *et al*., 2002).

As substrates, sirtuins interact with and modulate the functions of a myriad of proteins such as transcription factors, protein kinases or histones, that are involved in processes like cell signalling and survival, transcription, circadian rhythms or metabolic regulation.

SIRT2 is distributed ubiquitously, in relevant tissues like liver, adipose tissue, muscle or brain. Along with its first reported role at deacetylating tubulin in the cytoplasm (Inoue *et al*., 2007a; North *et al*., 2003), SIRT2 is considered to function as a cell cycle regulator, especially during mitosis (North and Verdin, 2007; Inoue *et al*., 2007a,b) when it targets histones (H4 Lys16) or the mitotic checkpoint kinase BubR1 (North *et al*., 2014). In metabolism, SIRT2 appears to be involved in various aspects of lipid and glucose metabolism, targeting factors like PGC-α or FOXO1 (Gomes *et al*., 2015). Other pathways where SIRT2 exerts deacetylation are related to inflammation or oxidative stress, with targets like NF-κB p65 (Rothgiesser *et al*., 2010).

The mitochondrial sirtuins (SIRT3, SIRT4, SIRT5) are implicated in the regulation of mitochondrial processes such as biogenesis, fusion/fission, mitophagy or mitochondrial respiratory machinery, therefore influencing the energy metabolism and the production of reactive oxygen species (ROS) and antioxidants. They are also thought to be associated with the regulation of cholesterol and fatty acid synthesis.

(Nogueiras *et al.*, 2012; Shi *et al*., 2005; Min *et al*., 2019; Kumar and Lombard, 2018; Haigis *et al*., 2006). SIRT3 targets key enzymes of all these metabolic pathways like acetyl CoA synthetase 2 (AceCS2), isocitrate dehydrogenase 2 (ICDH2) or manganese superoxide dismutase (MnSOD) (Nogueiras *et al*., 2012). SIRT4 main target is glutamate dehydrogenase (GDH) in pancreatic cells (Haigis *et al*., 2006), as well as others like malonyl-CoA decarboxylase (MCD) or pyruvate dehydrogenase (PDH), involved in fatty acid biosynthesis and glycolysis, respectively (Betsinger and Cristea, 2019). Glucose metabolism enzymes, like pyruvate dehydrogenase (PDH), GAPDH, or others like carbamoyl phosphate synthetase 1 (CPS1) involved in the urea cycle, are targeted by SIRT5 (Kumar and Lombard, 2018).

Studies on SIRT6 have revealed roles in DNA repair under oxidative stress as an ADP-ribosyltransferase and, mainly, as a histone deacetylase to modulate chromatin condensation and transcription, with effects on cellular processes like glycolysis (Liszt *et al*., 2005; Michishita *et al*., 2008; Chang *et al*., 2020).

SIRT7, in the nucleolus, is implicated in genome stability, transcriptional activation, ribosome biogenesis and RNA processing, via interaction with substrates like RNA polymerase I, histones and transcription factors (Ford *et al*., 2006; Blank and Grummt, 2017).

A more detailed description of SIRT1 is given in the next section.

Sirtuins are considered to be implicated in an array of pathologies such as cancer, inflammation, diabetes, cardiovascular and neurodegenerative diseases and, therefore, are a therapeutic target of interest (Chalkiadaki and Guarente, 2015; Donmez and Outeiro, 2013).

Table 1.1 summarises the intracellular localisations, main enzymatic reactions and targets of the sirtuin family members.

Table 1.2. Members of the sirtuin family, their intracellular location, main enzymatic activities, targets and cellular processes where they are implicated.

Member	*Intracellular localisation*	*Enzymatic activities*	*Main targets*	*Cellular processes*
SIRT1	**Nucleus / cytoplasmic** (shuttling)	**Deacetylation** Decrotonylation	P53, FOXO-3a, NFκB-p65, PGC-1α, PPAR-γ, UCP2, LXR, Histones (H1K27; H3 [K9, K14, K18, K56] H4 [K12, K6]), Ku70…	Cell survival; calorie restriction; glucose, fatty acid and energy metabolism; protein stress response…
SIRT2	**Cytoplasm** (may shuttle to nucleus)	**Deacetylation** Decrotonylation	BubR1 (mitotic kinase), tubulin, Histone H4K16; FOXO1, NF-κB p65…	Cell cycle regulation; lipid / glucose metabolism, oxidative stress
SIRT3	**Mitochondria**	**Deacetylation** Decrotonylation ADP-ribosylation	FOXO-3a, MnSOD, AceCS2, ICDH2, Ku70…	Mitochondrial processes, energy metabolism, TCA cycle…
SIRT4	**Mitochondria**	**ADP-ribosylation** Deacetylation Lipoamidase	GDH, MCD, PDH…	TCA cycle, fatty acid synthesis, glycolysis…
SIRT5	**Mitochondria,** cytoplasm	**Deacetylation Demalonylation Desuccinylation**	CPS1, PDH, GAPDH…	Lipid metabolism, urea cycle, TCA cycle, glycolysis…
SIRT6	**Nucleus** (associated to chromatin)	**Deacetylation ADP-ribosylation**	PARP-1; histones (H3K9, H3K56); DNA repair enzymes; HIF1α, GCN5…	DNA repair, chromatin regulation, glucose metabolism…
SIRT7	**Nucleus** (nucleolus)	**Deacetylation Desuccinylation**	RNA polymerase I, U3-55k, PAF53, histone H3…	rDNA transcription, RNA processing, genome stability…

TCA = tricarboxylic acid cycle; FOXO = forkhead box O transcription factor; NF-κB = nuclear factor kappa enhancer binding protein; PGC-1α = peroxisome proliferator-activated receptor-gamma coactivator 1 alpha ; PPAR-γ = peroxisome proliferator-activated receptor gamma; UCP2 = uncoupling protein 2; LXR = liver X receptor; BubR1 = mitotic spindle checkpoint protein BUBR1; MnSOD = manganese superoxide dismutase; AceCS2 = Acetyl CoA synthetase 2; ICDH2 = isocitrate dehydrogenase; GDH = glutamate dehydrogenase; MCD = malonyl CoA decarboxylase; PDH = pyruvate dehydrogenase; CPS1 = Carbamoyl phosphate synthase 1; GAPDH = glyceraldehyde 3-phosphate dehydrogenase; PARP-1 = poly ADP ribose polymerase 1 ; HIF1α = hypoxia-inducible factor 1-alpha; GCN5 = general control non-repressed 5; PAF53 = RNA polymerase associated factor 53; U3-55k = U3 small nucleolar RNA protein specific component.

1.8.2 SIRT1: characteristics, implications in cellular processes and main targets

Specifically, the focus of this thesis relies upon SIRT1. Among all the sirtuins, SIRT1 is the most extensively studied. It is mainly a nuclear protein, however, depending on its activity, it may shuttle to the cytoplasm thanks to its nuclear export signals (Tanno *et al.,* 2007). It is expressed ubiquitously across the majority of mammalian tissues, including liver, heart, muscle, pancreas, adipose tissue and brain.

SIRT1, through its primary enzymatic reaction (lysine deacetylation), interacts and modifies the functions of a wide spectrum of substrates, which, consequently, will affect significant physiological processes as diverse as energy metabolism, cell survival, inflammation or protein homeostasis (Herskovits and Guarente, 2014; Stünkel and Campbell, 2011; Nogueiras *et al*., 2012).

SIRT1 has roles in the modulation of DNA repair, epigenetic regulation and chromatin changes via deacetylation of histones (H1, H3 and H4) or proteins involved in the DNA damage response and cell survival such as Ku70, FOXO3a or p53 (Vaquero *et al.*, 2004; Brunet *et al*., 2004). The deacetylation of histones regulates chromatin condensation and, therefore, transcriptional activity. The deacetylation of p53 decreases its transcription level and, along with regulation of FOXO3a factor, has a pro-survival and anti-apoptotic effect, important in cell cycle regulation and also linked to tumorigenesis and aging (Brunet *et al*., 2004; Luo *et al*., 2001; Vaziri *et al*., 2001; Langley *et al*., 2002).

SIRT1 functions in energy metabolism, fatty acid oxidation and glucose homeostasis are facilitated by its interaction with important factors like PGC-1α, UCP2, FOXO transcription factors (FOXO3a, FOXO1 and FOXO4) and PPAR-γ, mainly in tissues like liver, white adipose tissue, pancreas and skeletal muscle. The deacetylation of these substrates stimulates gluconeogenesis during fasting or low glucose environment and decreases glycolysis (Rodgers *et al*., 2005, 2007). In line with this, SIRT1 role in mediating calorie restriction has been extensively investigated as a mechanism to promote cell survival and extend lifespan. Numerous reports indicated that the

activation or overexpression of SIRT1 in mice decreased cholesterol levels (by targeting LXR receptors that regulate cholesterol homeostasis [Li et al., 2007]) and increased fat mobilisation (by deacetylating PPAR-γ) (Bordone *et al*., 2007; Picard *et al*., 2004; Cohen *et al*., 2004; Chen *et al*., 2008).

The role of SIRT1 in protein homeostasis is focused on HSF1 regulation during the heat shock response. Direct regulation of HSF1 by SIRT1 (Westerheide *et al*., 2009) prolongs HSF1 binding to the promoters of heat shock genes, as covered in section 1.7.2.1. The link between SIRT1 and proteostasis is also supported by studies on the detrimental heat shock response and collapse of proteostasis observed in aging (Liu *et al*., 2014; Tomita *et al*., 2015; Raynes *et al*., 2013).

1.8.2.1 Regulation of SIRT1

Small molecules to pharmacologically modulate SIRT1 activity have been synthesised and investigated (Dai *et al*., 2018). Among the inhibitors, sirtinol, EX-527 or NAM are included. As activator compounds, or so-called STACs (Sirtuin Activating Compounds) resveratrol, SRT1720 or quercetin have been identified (Kaeberlein *et al*., 2005; Ajami *et al*., 2017). Particularly, resveratrol, a natural polyphenol extracted from wine, has been widely studied and shown to have effects of lifespan extension and neuroprotection (Howitz *et al*., 2003; Albani *et al*., 2010).

Some endogenous regulators of SIRT1 have also been described: AROS (active regulator of SIRT1) which activates SIRT1 function (Lakshminarasimhan *et al*., 2013), or DBC1 (deleted in breast cancer 1) which inhibits SIRT1 production (Escande *et al*., 2010; Kim *et al*., 2008). Both interact with SIRT1 by binding to the N-terminus, with opposite effects. Additionally, SIRT1 can also be regulated by phosphorylation (Sasaki *et al*., 2008) by protein kinases such as AMPK (Lau *et al*., 2014), JNK1 (Nasrin *et al*., 2009) or CK2 (Choi *et al*., 2017).

Figure 1.6 illustrates the main physiological roles where SIRT1 is involved, highlighting some of the main targets as well as regulators of its activity.

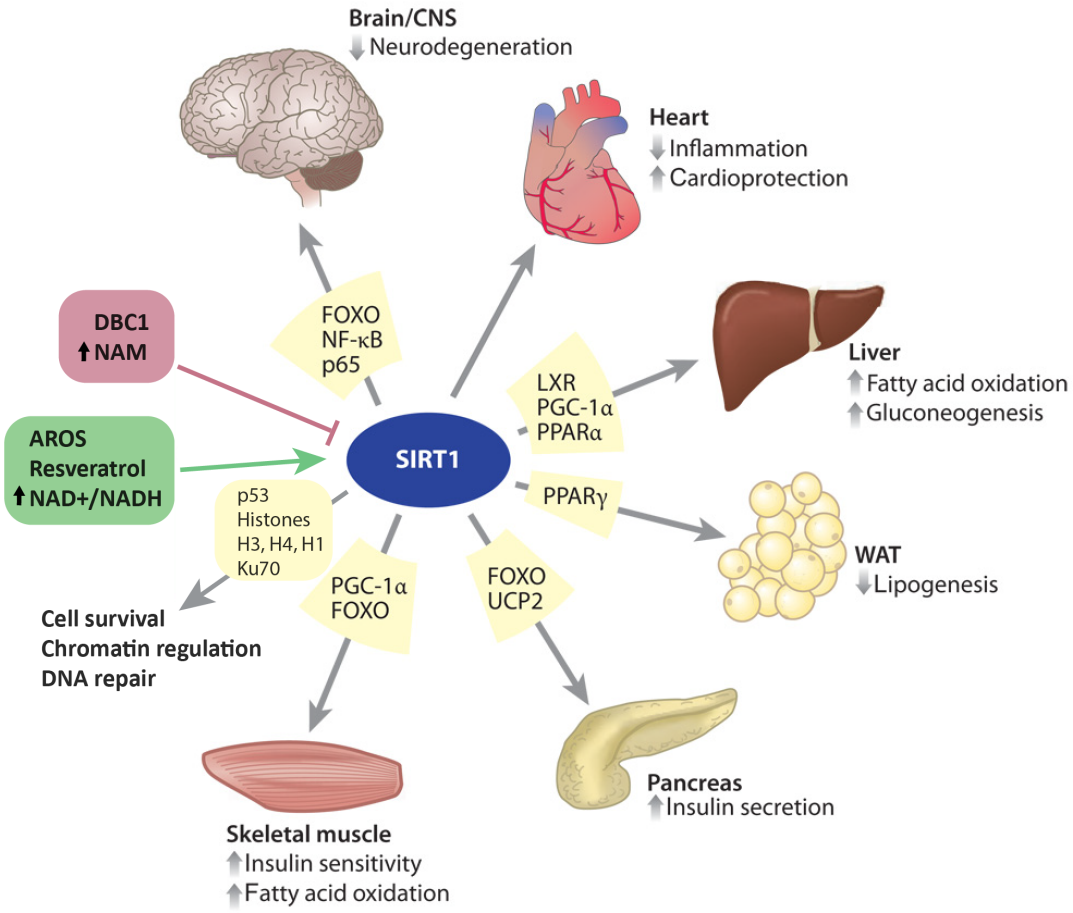

Figure 1.6. SIRT1 *main substrates, roles in physiology and regulators of its activity.* SIRT1 *plays important roles in cellular processes that affect a variety of tissues, through deacetylation of targets (in yellow boxes) that are implicated in these processes, as indicated.* SIRT1 *can be regulated through the levels of NAD+/NADH/NAM, activated by resveratrol or* AROS *and repressed by* DBC1*. Image adapted from a figure in Haigis and Sinclair, (2010); reproduced with permission.* DBC1*: deleted in breast cancer 1;* AROS*: active regulator of* SIRT1*; NAD+/NADH: nucleotide adenine dinucleotide (oxidised/reduced); NAM: nicotinamide; CNS: central nervous system; WAT: white adipose tissue.*

1.8.3 SIRT1 as a therapeutic target in neurodegeneration and Huntington's disease

SIRT1 has been investigated as target of interest in neurodegenerative diseases such as AD, PD, ALS and HD (Herskovits and Guarente, 2013; Langley and Sauve, 2013). Specifically in HD, SIRT1 has been evaluated as a potential factor to slow down the disease progression, with contrasting results (Duan, 2013; Naia and Rego, 2015; Neo and Tang, 2018). Some studies have reported a neuroprotective effect of SIRT1

overexpression or enhancement by resveratrol treatment in HD: rescue of dysfunctional phenotype in nematodes and reduced apoptosis in neurons derived from *Hdh*Q111 knock-in HD mouse models (Parker *et al*., 2005), improved motor function and reduction of brain atrophy in HD mouse model N171-82Q (Jiang *et al*., 2012) and extended survival and lower aggregation level in HD R6/2 mice (Jeong *et al*., 2012). On the contrary, another study by Pallos *et al*. (2008) reported that in *Drosophila* models of HD, the reduction of SIRT1 led to an amelioration of HD phenotype. Similar results were obtained by Smith *et al*. (2014) in *Drosophila* and *in vitro* models, and in HD R6/2 mice that, after administration of a SIRT1 inhibitor, showed alleviation of symptoms and prolonged survival. In other studies, such as the study by Ho *et al*. (2010) in the N171-82Q model of HD, the outcome was inconclusive as SIRT1 activation did not prolong survival but led to improved motor deficits.

Jiang *et al*. (2012) also revealed that mutant HTT interacts with SIRT1 and inhibits its deacetylating function and pro-survival effect due to hyperacetylation of substrates like FOXO3a. Recently in our group, Tulino *et al*. (2016) reported a regulatory mechanism of SIRT1 induction that is impaired in two mouse models of HD, R6/2 and *Hdh*Q150. These mice show a downregulated SIRT1 activity caused by the presence of mutant HTT, that alters the phosphorylation levels of SIRT1.

1.9 Modelling Huntington's disease for research

Numerous cellular and animal models of HD have been generated as tools to understand HD pathology as well as to screen and test novel therapeutic compounds. The development of a variety of HD models has been facilitated by the monogenic nature and dominant pattern of inheritance of the HD mutation.

1.9.1 Cellular models of HD

Patients-derived fibroblasts or stem cells (induced pluripotent stem cells [iPSCs] or embryonic stem cells [ESCs]), or different cell types derived from rodents (e.g., mouse embryonic fibroblasts [MEFs], neurons) (Geater *et al*., 2018).

1.9.2 Non-mammalian models of HD

Caenorhabditis elegans nematodes, zebra fish, *Drosophila melanogaster* flies or *Saccharomyces cerevisiae* yeast have been genetically engineered to express HTT with a polyQ expanded tract (Chongtham *et al*., 2018).

1.9.3 Rodent models of HD

These are by far the most extensively used models in HD research. Although there are some rat models of HD (BACHD or Tg51 [Yu-Taeger *et al*., 2012; Von Hörsten *et al*., 2003]), there are many more mouse models that have been widely applied to understand the basis of HD pathogenic mechanisms *in vivo* and to assess potential therapeutic compounds. The genomic similarities between mice and humans, the reliable and relatively easy methods of genetic manipulation and reduced costs are some of the benefits associated with these. Diverse strategies have been followed to obtain genetic mouse models of the disease (Farshim and Bates, 2018).

1.9.3.1 Transgenic mouse models

These models carry a transgene of the human *HTT* gene; either a 5' region that would produce N-terminal fragments of HTT (N-terminal fragment models), or the whole *HTT* gene with the expanded CAG repeat to generate a mutant version of the full-length HTT (full-length models). A non-exhaustive list of the most used models of both types can be found in Table 1.3.

Table 1.3. Transgenic mouse models of HD.

Model	Promoter	Genetic construct	CAG repeat length	Background	Phenotype	References
Transgenic N-terminal fragment models						
N171-82Q	Prion promoter (mouse)	cDNA with first 171 amino acids of human *HTT* plus 82 CAGs	82	B6C3H	Lifespan: ~6 months Presence of aggregates, loss of coordination, tremor, clasping	Schilling *et al.*, 1999 Luthi-Carter *et al.*, 2000
R6/1	*HTT* (human)	Exon 1 of human *HTT*	115	mixed	Weight loss, motor impairment, presence of inclusions…	Mangiarini *et al.*, 1996 Rattray *et al.*, 2013 Naver *et al.*, 2003
R6/2			~141-157	B6CBAF1 mixed	End-stage: 14-15 weeks Motor impairment (5-6 weeks) Weight loss	Mangiarini *et al.*, 1996 Carter *et al.*, 1999 Luthi-Carter *et al.*, 2000 Davies *et al.*, 1997 Li *et al.*, 1999
			~200	B6CBAF1	End-stage: 14 weeks Motor deficits (8 weeks) Brain atrophy (8 weeks) Weight loss	Mangiarini *et al.*, 1996 Rattray *et al.*, 2013 Landles *et al.*, 2020 Sathasivam *et al.*, 2010 Ribchester *et al.*, 2004
			~90	B6CBAF1	End-stage: 24 weeks Motor deficits (12 weeks)	Mangiarini *et al.*, 1996 Landles *et al.*, 2020
Transgenic full-length models						
YAC128	Full-length human *HTT* gene (with *HTT* promoter) inserted by YAC		~125 (with interrupting CAACAG sequences)	FVB/N C57BL/6	Brain atrophy (9 months) Motor deficits (6 months) Increased body weight	Slow *et al.*, 2003 Van Raamsdonk *et al.*, 2005 Pouladi *et al.*, 2012
BACHD	Full-length human *HTT* gene (with *HTT* promoter) inserted by BAC		~97 (mixed CAA-CAG)	FVB/N C57BL/6	Motor deficits, brain atrophy Increased body weight	Gray *et al.*, 2008 Pouladi *et al.*, 2012
BAC-CAG			~120 (plus CAA near 3')		In development	

- Transgenic N-terminal fragment models:

This category includes models from the R6 line, R6/1 and R6/2, and N171-82Q. N171-82Q mice were generated by inserting a cDNA that expresses the first 171 amino acids of human HTT with 82 CAGs, under the control of the mouse prion promoter (Schilling *et al*., 1999). Their phenotype is similar to the R6/2 model and lifespan is around 6 months. R6/1 and R6/2 are the most widely used mouse models of HD. They contain a copy of a human *HTT* fragment, with a *HTT* promoter and exon 1 and 200 bp of intron 1 (Mangiarini *et al*., 1996) which is translated to produce an exon 1 HTT protein; the R6/1 and R6/2 initially carried 115 and 150 CAGs, but this number increased through gametic transmission via males and there is a variety of CAG repeat lengths. R6/2 is the best characterised model; they present a rapidly progressing phenotype, with aggregate pathology (Li *et al*., 1999; Davies *et al*., 1997) and a short lifespan. A recent comparative study by Landles *et al*. (2020), described differences between two R6/2 lines with either 90 or 200 CAGs. R6/2$(CAG)_{200}$ end-stage is reached at around 14 weeks of age whereas R6/2$(CAG)_{90}$ reach end-stage by 24 weeks of age. Behavioural analysis indicated the start of motor impairment by 12 weeks of age in R6/2$(CAG)_{90}$ and 8 weeks in R6/2$(CAG)_{200}$ (Landles *et al*., 2020), which is correlated with brain volume changes (Rattray *et al.,* 2013), and as early as 5 - 6 weeks for some behavioural tests in R6/2 carrying 141-157 CAGs (Carter *et al*., 1999). Aggregation in the nucleus appears by 4 weeks of age in R6/2$(CAG)_{90}$, which correlates with the start of transcriptional dysregulation, whereas in R6/2$(CAG)_{200}$ the aggregation is more cytoplasmic and correlates with the progression of behavioural deficits (Landles *et al*., 2020). Alterations in synaptic plasticity or peripheral abnormalities have also been described in this model (Murphy *et al*., 2000; Ribchester *et al*., 2004). Both R6/1 and R6/2 lines show CAG repeat instability (Gonitel *et al*., 2008). The differences observed in R6/2$(CAG)_{200}$ and R6/2$(CAG)_{90}$ are related to the CAG repeat length, which is associated with a progressively less severe phenotype as it expands beyond 200 CAGs (Morton *et al*., 2009). As discussed before, the R6/1 and R6/2 models are representative of the incomplete splicing between exon 1 and 2 of *HTT* gene, that occurs in *Hdh* knock-in mice, YAC128 mice (Sathasivam *et al*., 2013) and HD patients (Neueder *et al*., 2017).

- Transgenic full-length models

These mice contain the entire CAG-expanded *HTT* gene that has been inserted via yeast artificial (YAC) or bacterial artificial (BAC) chromosome. The YAC128 mouse (Slow *et al*., 2003) contains several copies of the *HTT* gene and a CAG repeat, that contains two interrupting $(CAA)_3CAGCAA$ sequences at positions 24 and 109, encodes 125 glutamines. These mice display cortical and striatal atrophy by 9 - 12 months of age, striatal loss, motor and cognitive impairments by 6 - 8 months of age, presence of aggregates in brain (by 18 months of age) and increased body weight (Slow *et al*., 2003; Van Raamsdonk *et al*., 2005a, 2005b; Brooks *et al*., 2012; Bayram-Weston *et al*., 2012). BACHD mice were generated by Gray *et al*. (2008); they contain a modified version of the human mutant *HTT* with 97 mixed CAA-CAG repeats in exon 1.

The presence of CAGCAA sequences within the CAG repeats in both YAC128 and BACHD make them stable to CAG expansion, both somatically and during meiotic transmission. For this reason, they cannot be used in studies involving somatic instability. In line with this, a novel mouse model, BAC-CAG, has been generated that might be useful in this type of studies; it contains a tract of 120 CAGs, which is unstable, a CAA interruption followed by another 10 CAGs. This line is currently under characterisation.

1.9.3.2 Knock-in mouse models

These mice were obtained by inserting a CAG repeat expansion of variable sizes into the endogenous mouse *Htt* gene.

Lin *et al*. (2001) generated a *Hdh*Q150 mouse in which the mouse $(CAG)_2CAA(CAG)_4$ sequence was replaced with 150 CAGs. The lifespan for homozygous *Hdh*Q150 mice is about 22 months of age, when they display similar phenotypes to late-stage R6/2 mice (Woodman *et al*., 2007; Sathasivam *et al*., 2010). Studies have shown motor deficits in homozygous *Hdh*Q150 mice (starting by 36 weeks of age), cognitive dysfunction by 94 weeks of age and brain volume differences by 15 weeks of age

(Woodman *et al*., 2007; Rattray *et al*., 2017). The presence of aggregates is evident by 5 - 6 months of age (Bayram-Weston *et al*., 2012; Woodman *et al*., 2007; Landles *et al*., 2010).

Another strategy used to obtain knock-in mice was to replace exon 1 of the mouse *Htt* gene with human exon 1 *HTT* containing variable CAG repeat sizes. Two allelic series have been described with this approach: one was developed by Wheeler *et al*. (1999, 2000) whose genetic construct additionally contained 268 bp of human intron 1 instead of the 124 bp of mouse intron 1. *Hdh*Q92 and *Hdh*Q111 were reported to have nuclear deposits and are commonly used in studies of somatic instability (Wheeler *et al*., 1999, 2000). The CAG140 line was also developed, in which, in addition to human exon 1 *HTT*, 94 bp of mouse intron 1 was replaced with 10 bp of human intron 1, and a neo cassette was inserted upstream from the *Htt* gene (Menalled *et al*., 2003). The expansion of the CAG repeat in these mice led to the generation of the zQ175 line (Heikkinen *et al*., 2012; Menalled *et al*., 2012), which was later modified to obtain the zQ175 Delta Neo mouse line (Franich *et al*., 2019), lacking the neo cassette. zQ175 knock-in mice have been widely used and aggregates can be detected in the striatum and cortex from 4 months of age, brain atrophy by 3 - 4 months of age, behavioural deficits from 4.5 months of age and synaptic and neurotransmission impairment (Carty *et al*., 2015; Heikkinen *et al*., 2012; Menalled *et al*., 2012; Peng *et al*., 2016; Smith *et al*., 2014).

Table 1.4 summarises the details on the main knock-in HD mouse models.

Table 1.4. Knock-in mouse models of HD.

Model	*Promoter*	*Genetic construct*	*CAG repeat length*	*Background*	*Phenotype*	*References*
CAG140	Mouse *Htt*	Chimeric; human *HTT* exon 1 / mouse *Htt*	140-150	C57BL/6	End-stage: ~20 months Aggregates (4 months) Brain atrophy Cognitive/motor deficits (4-5 months)	Menalled *et al*., 2003
zQ175	Mouse *Htt*		180-200	C57BL/6		Heikkinen *et al*., 2012 Menalled *et al*., 2012 Smith *et al*., 2014 Carty *et al*., 2015 Peng *et al*., 2016
zQ175DN	Mouse *Htt*	zQ175 with 5' Neo cassette removed	180-200	C57BL/6		Franich *et al*., 2019
*Hdh*Q150	Mouse *Htt*	CAG expansion into exon 1 of mouse *Htt*	150	C57BL/6 CBA/Ca	End-stage: 22 months Aggregates (5-6 months) Brain atrophy Motor/cognitive dysfunction	Lin *et al*., 2001 Woodman *et al*., 2007 Bayram-Weston *et al*., 2012 Rattray *et al*., 2017 Sathasivam *et al*., 2013 Sathasivam *et al*., 2010
*Hdh*Q92 *Hdh*Q111 (Part of allelic series*)*	Mouse *Htt*	Chimeric; human/mouse exon 1	92 111	C57BL/6	Somatic instability	Wheeler *et al*., 2000 Wheeler *et al*., 1999

1.9.4 Large animal models of HD: sheep, minipigs, non-human primates

The need for models of HD in higher species other than rodents is correlated with the low success in translation from research in rodents to preclinical or clinical stages in humans, especially when it comes to therapeutic compounds. There may be aspects of metabolism or blood-brain barrier penetrance in rodents, as well as differences in brain size and organisation between the two species, that may be poorly representative of the human context. The short lifespan in rodents (approximately 2 - 2.5 years) also restricts the extension of studies. These limitations may be overcome using larger species that have longer lifespans and more anatomical and genetic similarities with humans, which can make research more translatable to humans (Morton and Howland, 2013; Howland *et al*., 2020). A list of these large models of HD can be found in Table 1.5.

1.9.4.1 Sheep model

The transgenic sheep model of HD, called OVT73, was generated by microinjection of a cDNA to express the full-length human *HTT* gene carrying 73 CAGs, under the control of human *HTT* promoter (Jacobsen *et al*., 2010). Their larger brain size makes them interesting for HD research involving MRI or drug delivery into the brain, to assess the biodistribution of compounds. A collaborative project to study their phenotype reported that the presence of HTT aggregates was evident in cortical brain by 18 months of age (Reid *et al*., 2013). They also showed metabolic dysregulation by 5 years of age, (Handley *et al*., 2016) and circadian rhythm and sleep pattern abnormalities were detected by 18 months and worsening with age (Morton *et al*., 2014).

1.9.4.2 Minipig models

The viable transgenic HD minipigs were obtained by lentiviral transduction of porcine embryos with a vector containing the human *HTT* cDNA to encode for the first 548 amino acids of HTT protein with a CAGCAA repeat encoding 145 glutamines, under the control of human *HTT* promoter (Baxa *et al*., 2013). Follow-up studies revealed

motor, cognitive and behavioural deficits from 4 - 5.9 years of age (Baxa *et al*., 2019), accumulation of mutant HTT aggregates at 48-month-old minipigs and cell loss at caudate nucleus, putamen and cortex by 60 - 70 months of age (Ardan *et al*., 2019). Yan *et al*. (2018) also generated a knock-in pig model via CRISPR (clustered regularly interspaced short palindromic repeats)/Cas9 technology, by replacing the endogenous pig *Htt* exon 1 with the human *HTT* exon 1 with 150 CAGs. These pigs have an unstable CAG repeat, presence of aggregates, reduced brain size and motor impairment observed by 5 months of age, with severe respiratory difficulties (Yan *et al.,* 2018).

1.9.4.3 Non-human primate models

Non-human primates such as monkeys (*Rhesus macaque*) have similar genomes and brain sizes and complexity as humans. Although they may be advantageous for some aspects of HD research, for instance, investigating cognitive symptoms or behaviour, the ethical issues and expensive costs on the generation and maintenance of these HD monkey models make their use very limited. There are some HD monkey models expressing a human *HTT* fragment, inserted through a lentivirus approach: one model was obtained via direct injection of the *HTT*171-82Q fragment into the striatum, and was showing aggregates and motor symptoms of the disease (Palfi *et al*., 2007); another transgenic model was generated via microinjection of a fragment with 84Q into the oocytes and brain sections analyses indicated the presence of HTT inclusions (Yang *et al*., 2008). A review of these and more recent developments can be found in Aron Badin, (2018).

Table 1.5. Large animal models of HD.

Model	Genetic construct	CAG repeat length	Phenotype	References
Sheep OVT73 (transgenic)	Full-length *HTT* with 73 CAGs under control of human *HTT* promoter	73	Lifespan: 10 - 15 years Aggregates by 18 months of age Metabolic dysregulation Sleep/circadian abnormalities	Jacobsen *et al*., 2010 Reid *et al*., 2013 Morton *et al*., 2014 Handley *et al*., 2016
Minipigs	First 548 amino acids of human HTT with 145 CAGCAA repeats (Transgenic)	145 (mixed CAGCAA)	Lifespan: 12 - 15 years Motor, cognitive and behavioural impairment (4 - 5.9 years) Aggregates in brain (60 - 70 months)	Baxa *et al*., 2013 Baxa *et al*., 2019 Ardan *et al*., 2019
	Human *HTT* exon 1 with 150 CAGs (Knock-in)	150 (CAG repeat is unstable)	Loss of medium spiny neurons Motor impairment Reduced brain size (5 months)	Yan *et al*., 2018
Non-human primates	Exon 1 of *HTT* plus 82-84 CAG repeats under control of ubiquitination promoter	82 - 84	Lifespan: ~6 months Presence of inclusions in brain, dystonia, chorea	Palfi *et al*., 2007 Yang *et al*., 2008

1.9.5 Considerations and selection criteria of the HD models

It is important to realise that no specific model of HD will be fully representative of the human condition or could be applied in all the scientific contexts. As HD models will be able to recapitulate only certain characteristics of the disease, the election of an appropriate model is essential when designing a research experiment. The selection criteria will be guided by the specifications of the research as well as the molecular and phenotypic characteristics of each HD model (Pouladi *et al*., 2013).

1.10 Therapeutics in Huntington's disease

So far, there are no disease-modifying therapies for HD and the treatments available focus on the relief of motor and psychiatric symptoms. Currently, the main therapeutic strategies under investigation aim to lower HTT expression (targeting either DNA, RNA or protein) through different approaches. A significant effort is also directed towards the exploration of biomarkers to assess novel therapies.

1.10.1 Huntingtin lowering

Given that pathology of HD is greatly associated with the toxic gain of functions conferred by the mutant HTT protein, therapeutic strategies have been and are currently being pursued to target CAG-expanded *HTT* and reduce the mutant HTT production (Wild and Tabrizi, 2017; Tabrizi *et al*., 2019) or enhance mutant HTT clearance (Barker *et al*., 2020). The different strategies are represented in Figure 1.7.

1.10.1.1 DNA and RNA targeting approaches to reduce HTT expression

- DNA-targeting strategies: Zinc finger proteins (ZFPs) and CRISPR/Cas9 system directly interact with *HTT* DNA.

  ZFPs (Klug, 2010), intracranially delivered via a viral vector, act on DNA by modulating gene expression through nucleases (ZFNs, transcription activator-like effector nucleases [TALENs]) or transcription factors. They can bind to specific DNA sequences of interest, such as the CAG tract, and have provided positive results in animal (Zeitler *et al*., 2019) or cell (Garriga-Canut *et al*., 2012) models of HD.

  The application of CRISPR/Cas9 system in HD is still in early development (Vachey and Déglon, 2018). The Cas9 RNA-guided nuclease cleaves DNA in specific sites. For *HTT* gene editing, it has been tested to excise the CAG repeat tract to correct the mutation or inactivate the mutant *HTT* allele in HD patient fibroblasts (Dabrowska *et al*., 2018; Shin *et al*., 2016) or BACHD mouse model (Yang *et al*., 2017). These approaches potentially could be applied to all HD gene mutation carriers with long-term effects from a single administration,

however, the invasive administration methods, irreversibility and the possibility of targeting other genes with CAG repeats are some of the concerns.

- RNA-targeting strategies: there are non-selective (targeting both wild-type and mutant HTT) and selective approaches that only target mutant *HTT.* They include antisense oligonucleotides (ASO), small interference RNAs (siRNAs) or artificial microRNAs (miRNA). All these approaches aim to degrade *HTT* RNA or suppress HTT translation by targeting *HTT* RNA (mRNA or pre-mRNA) by sequence complementarity.

  siRNAs and miRNAs target *HTT* mRNA when it is mature and spliced. As they do not cross the blood-brain barrier, they would be delivered via adenovirus-associated (AAV) viral vectors or liposomes, among others. Studies on mouse models (Harper *et al*., 2005; Wang *et al*., 2005; DiFiglia *et al*., 2007), cells (Chen *et al*., 2005) and minipigs (Evers *et al*., 2018) using these approaches gave evidence on significant and widespread reductions of mutant *HTT* mRNA levels.

  ASOs (Bennett *et al*., 2019) are short oligonucleotides that bind to *HTT* pre-mRNA; after ASO binding, the complex formed by ASO and *HTT* pre-mRNA would be degraded by ribonuclease H1 (RNase H1). Some studies on animal models indicated amelioration of symptoms with a sustained effect (Stanek *et al*., 2013; Kordasiewicz *et al*., 2012).

  The first HTT lowering clinical trial run in HD patients, used an ASO drug, IONIS-HTT_{Rx} or RG6042, developed by Ionis Pharmaceuticals. It was administered to 46 HD patients at early stages of the diseases, by intrathecal administration into the cerebrospinal fluid (CSF) via lumbar puncture. The outcomes of the phase I/IIa clinical trial were encouraging and showed high levels of safety and tolerability with dose-dependent HTT reductions in CSF samples (Tabrizi *et al*., 2019). The trial continued to phase III, sponsored by Roche; however, unfortunately, due to potential benefit/risk issues, it was

terminated early in March 2021. Other trials with similar approach are currently in development (Rodrigues and Wild, 2020).

Some disadvantages are associated with lowering wild-type HTT. As previous studies suggested, HTT is important during development as well as other cellular functions (Saudou and Humbert, 2016). Also, the deletion of HTT is embryonically lethal in mice (Nasir *et al*., 1995; Zeitlin *et al*., 1995) and, therefore, the consequences of reducing wild-type HTT are unknown (Liu and Zeitlin, 2017). Considering this, the approaches to selectively lower mutant HTT seem to be a safer strategy. On the other hand, HTT ablation is not deleterious in adult mice (Wang *et al*., 2016). Therefore, a high level of HTT reduction (over 50 %) may not be detrimental either in adult patients, as suggested by studies in humanised mouse models expressing the human *HTT* gene (Southwell *et al*., 2018). It is possible that a partial knockdown rather than complete suppression of *HTT* may have more beneficial effects, as wild-type HTT would continue to be sufficiently available to exert its cellular functions. This non-selective, partial reduction of HTT has also been shown to be safe and have beneficial effects in mice (McBride *et al*., 2008) and non-human primates (McBride *et al*., 2011).

1.10.1.2 Modulation of autophagy and UPS to promote HTT degradation

At the protein level, some strategies have been developed to promote mutant HTT degradation via autophagy or the UPS system (Barker *et al*., 2020; Figure 1.7). As seen earlier, HTT protein may be targeted for autophagy (Ravikumar *et al*., 2002) and recently, some compounds, called autophagosome-tethering compounds or ATTECs, have been developed that can facilitate interaction between mutant HTT and autophagosome component LC3 and enhance its clearance via autophagy (Li *et al*., 2019). Some of their advantages include efficient blood-brain barrier penetration and selective degradation of mutant HTT but not wild-type HTT.

Another approach is the application of proteolysis-targeting chimeras or PROTACs to promote the artificial ubiquitination of targets and the subsequent degradation by UPS system (Gu *et al*., 2018). PROTAC molecules are formed by a ligand that recruits

E3 ubiquitin ligase, a chemical linker and then, another ligand that binds to the target protein, in this case, mutant HTT. Evidence of success has been reported in HD patient fibroblasts (Tomoshige *et al*., 2017).

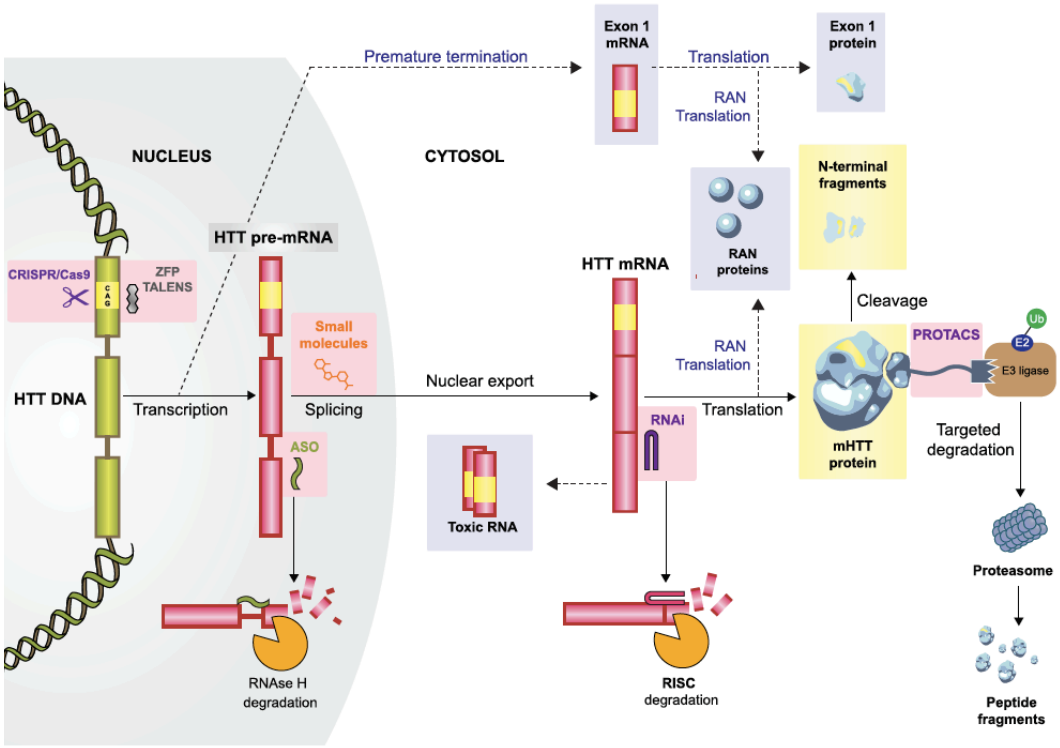

Figure 1.7. Huntingtin lowering strategies.
There are diverse therapeutic approaches to lower HTT, each one represented in pink boxes. The expanded CAG repeat/polyQ that is targeted is represented by yellow boxes. Image from Tabrizi et al., (2019), reproduced with permission. ZFP: zinc finger protein; TALENs: transcription activator-life effector nuclease; RNAse H: ribonuclease H; ASO: antisense oligonucleotide; RNAi: interference RNA; RISC: RNA-induced silencing complex; RAN: repeat associated non-ATG; PROTACS: proteolysis-targeting chimera.

1.10.2 Biofluid biomarkers

Biomarkers can be defined as those molecules that can be accurately measured and correlated with the disease progression, to indicate its clinical severity as well as an indicator of efficiency of a therapeutic compound after treatment. In HD, several biomarkers have been investigated. Mutant HTT can be quantified in the cerebrospinal fluid (CSF) samples from HD patients and has been validated to correlate with disease severity (Wild *et al*., 2015; Byrne *et al*., 2018). Its quantification in CSF in the mutant HTT lowering clinical trials (Tabrizi *et al*., 2019) has indicated the effectiveness of the lowering approach, as mutant HTT decreased in a dose-dependent manner.

Another two biomarkers generating great interest in recent years are neurofilament light protein (NFL) and tau protein. The concentrations of both NFL and tau were found to be increased in CSF of HD patients as compared to controls and even predicted their clinical progression (Byrne *et al*., 2017, 2018; Rodrigues *et al*., 2016). The levels of NFL in plasma from HD patients were also strongly correlated with clinical progression and brain atrophy (Byrne *et al*., 2017). The recent and ongoing work on the discovery and validation of biomarkers in HD will continue to be of valuable use in the evaluation of new therapeutic compounds for HD treatment.

1.11 Research aims of this thesis

The project of this thesis is focused on two parts:

- Characterisation of the heat shock response impairment in brain and muscle tissues of HD mouse model zQ175 over the course of the disease, in a comparative analysis with that in R6/2 model, after *in vivo* pharmacological induction of the heat shock response by NVP-HSP990. Previous to this, some preparatory steps will be taken:
    - Assess the efficacy and kinetics of the pharmacological induction of the heat shock response by compound NVP-HSP990.
    - Design and optimisation of a QuantiGene multiplex assay to simultaneously detect the gene expression of a large set of heat shock genes and validation of this methodology by comparison with established RT-qPCR assays.
- Investigation of potential mechanisms that may be causing the impairment of the heat shock response in HD mice. This will include:
    - Analysis of HSF1 levels in zQ175 brain and muscle tissues at late-symptomatic stages of the disease, as HSF1 has been reported to be abnormally degraded in HD (Gomez-Pastor *et al*., 2017).
    - Examine whether a decreased SIRT1 activity in HD models (Tulino *et al*., 2016) is behind the dysregulation of the heat shock response. To that end, *Sirt1* overexpressing mice will be crossed with R6/2 mice and allocated at early and late symptomatic stages for dosing with NVP-HSP990. Brain and muscle tissues will be collected at several time points after dosing and analysed by QuantiGene, to detect if the deficient levels of expression of the heat shock genes (Labbadia *et al*., 2011) had been restored by SIRT1 overexpression.

Chapter 2. Materials and methods

2.1 Materials

2.1.1 Mouse lines

zQ175 knock-in mice were generated by replacing mouse *Htt* exon 1 with human *HTT* exon 1, carrying approximately ~ 175 CAGs (Heikkinen *et al.,* 2012; Menalled *et al.,* 2012). The neomycin selectable marker was removed to generate the zQ175 Delta Neo mice (Franich *et al.,* 2019). R6/2 transgenic mice (Mangiarini *et al.,* 1996) were created by introducing a genomic fragment (containing human *HTT* promoter and exon 1 sequences) that encodes the exon 1 HTT protein with an expanded polyQ tract of ~ 200 CAGs. *Hsf1* $^{+/-}$ heterozygous mice (McMillan *et al.,* 1998) were generated by replacing a 1.8 kb genomic fragment that corresponded to six exons with a neomycin resistance expression cassette. The genomic fragment that was replaced contained sequences encoding part of the DNA binding domain and the oligomerisation domain of the HSF1 protein. *Sirt1* transgenic mice (Satoh *et al.,* 2010) were generated at Washington University (St. Louis, Missouri, USA) by inserting a 2.3 kb fragment of the mouse *Sirt1* cDNA into a vector carrying the mouse PrP promoter, then microinjected into C57BL/6J x CBA hybrid blastocysts to establish the line and then backcrossed to C57BL/6J mice.

2.1.2 Primers and sequences for genotyping and CAG repeat sizing

Table 2.1. Primers used for genotyping and CAG repeat sizing of the mouse lines used in the study

PCR	Primer name	Primer sequence (from 5' to 3')
zQ175 genotyping	**19Fhum**	*AGGAGCCGCTGCACCGA*
	431R2	*CTCTTCACAACAGTCATGTGCG*
R6/2 genotyping	**Hdac4#1**	*CTTGTTGAGAACAAACTCCTGCAGCT*
	Hdac4#2	*AGCCCTACACTAGTGTGTGTTACACA*
	33727	*CGCAGGCTAGGGCTGTCAATCATGCT*
	32253	*TCATCAGCTTTTCCAGGGTCGCCAT*
Sirt1 tg genotyping	**Sirt1 forward**	*CTTCAGATCAAGAGACGGTATCTATGCTCGCC*
	Sirt1 Reverse	*AGACGGCTGGAACTGTCCGGGATATATTTC*
	Fab Forward	*CCTCCGGAGAGCAGCGATTAAAAGTGTCAG*
	Fab Reverse	*TAGAGCTTTGCCACATCACAGGTCATTCAG*
Hsf1 genotyping	**Hsf1KO1**	*AGACCTGTCCTGTGTGCCTAGC*
	Hsf1KO2	*CAGGTCAACTGCCTACACAGACC*
	Neo3#3	*AGGACATAGCGTTGGCTACCCGT*
	Neo3#4	*GCCTGCTATTGTCTTCCCAATCC*
R6/2 and zQ175 CAG repeat sizing	**HD3 – 6-FAM-labelled Forward**	*CCTTCGAGTCCCTCAAGTCCTT*
	HD5 Reverse	*CGGCTGAGGCAGCAGCGGCTGT*

All primers were supplied by Eurofins.

2.1.3 Primers and probes sequences for RT-qPCR assays

Table 2.2. Primers, probes and sequences for the RT-qPCR assays used in the study

The following primers/probes were purchased from Thermo Fisher Scientific:

Type	*Gene Symbol*	*Protein name*	*Accession Number*	*TaqMan assay ID*
HK	*Canx*	Calnexin	NM_007597	Mm00500330_m1
HK	*Rpl13a*	Ribosomal Protein L13a	NM_009438	Mm01612987_g1
HK	*Atp5b*	ATP synthase subunit ß	NM_016774	Mm00443967_g1
HK	*Eif4a2*	Eukaryotic translation initiation factor 4A2	NM_013506	Mm01730183_gH
GOI	*Hspa1a/b*	Heat shock protein 1A/B, HSP70	NM_010479	Mm01159846_s1
GOI	*Hspb1*	Heat shock protein 1, HSP25	NM_013560	Mm00834384_g1
GOI	*Dnajb1*	DnaJ, member B1, HSP40	NM_018808	Mm00444519_m1
GOI	*Sirt1*	Sirtuin 1	NM_019812	Mm01168521_m1

The following primers/probes were designed in-house:

Type	*Gene Symbol*	*Protein name*	*ID*	*Sequence (5' - 3')*
GOI	*Hsf1*	Heat shock factor 1	**Forward primer**	*CGAGTGGGAACAGCTTCCA*
			Reverse primer	*ACTTGGGCAGCACCTCCTT*
			Probe	*TTTGACCAGGGCCAGTT*

GOI = Gene of interest; HK = Housekeeping gene

2.1.4 Probe regions and sequences for QuantiGene multiplex assays

Table 2.3. Probe regions and sequences for the QuantiGene 10-plex assay

Type	Gene Symbol	Protein name	Accession Number	Probe set region
HK	*Canx*	Calnexin	NM_007597	76 - 727
HK	*Rpl13a*	Ribosomal Protein L13a	NM_009438	2 - 467
HK	*Atp5b*	ATP synthase subunit β	NM_016774	22 - 409
HK	*Eif4a2*	Eukaryotic translation initiation factor 4A2	NM_013506	710 - 1271
HK	*Ubc*	Ubiquitin C	NM_019639	113 - 676
GOI	*Hsf1*	Heat shock factor 1	NM_008296	1712 - 2263
GOI	*Hspa1a/b*	Heat shock protein 1A/B, HSP70	NM_010479	2186 - 2721
GOI	*Hspb1*	Heat shock protein 1, HSP25	NM_013560	103 - 555
GOI	*Dnajb1*	DnaJ, member B1, HSP40	NM_018808	569 - 1125
GOI	*Sirt1*	Sirtuin 1	NM_019812	609 - 1219

GOI = Gene of interest; HK = Housekeeping gene

Table 2. 4. Probe regions and sequences for the QuantiGene 20-plex assay

Type	Gene Symbol	Protein name	Accession Number	Probe set region
HK	*Canx*	Calnexin	NM_007597	1195 - 1720
HK	*Rpl13a*	Ribosomal Protein L13a	NM_009438	2 - 467
HK	*Atp5b*	ATP synthase subunit β	NM_016774	22 - 409
HK	*Eif4a2*	Eukaryotic translation initiation factor 4A2	NM_013506	710 - 1271
HK	*Ubc*	Ubiquitin C	NM_019639	113 - 676
GOI	*Dnaja3*	DnaJ, member A3, HSP40	NM_023646	411 - 867
GOI	*Hspb6*	Heat shock protein B6, α-crystallin-related, HSP20	NM_001012401	35 - 438
GOI	*Hspa9*	Heat shock protein A9, HSP70	NM_010481	908 - 1395
GOI	*Dnajb5*	DnaJ, member B5, HSP40	NM_019874	687 - 1112
GOI	*Hsf1*	Heat shock factor 1	NM_008296	1712 - 2263
GOI	*Hspa1a/b*	Heat shock protein 1A/B, HSP70	NM_010479	2186 - 2721
GOI	*Hspb1*	Heat shock protein 1, HSP25	NM_013560	103 - 555
GOI	*Dnaja1*	DnaJ, member A1, HSP40	NM_008298	474 - 1101
GOI	*Dnajb1*	DnaJ, member B1, HSP40	NM_018808	569 - 1125
GOI	*Hspd1*	Heat shock protein 1 (chaperonin), HSP60	NM_010477	1732 - 2170
GOI	*Hspe1*	Heat shock protein 1 (chaperonin), HSP10	NM_008303	259 - 657
GOI	*Hsph1*	Heat shock protein 105/110 kDa; HSP110	NM_013559	1985 - 2430
GOI	*Hsp90aa1*	Heat shock protein 90, member A1; HSP90	NM_010480	245 - 989
GOI	*Hsp90ab1*	Heat shock protein 90, member B1; HSP90	NM_008302	1039 - 1542
GOI	*Sirt1*	Sirtuin 1	NM_019812	609 - 1219

GOI = Gene of interest; HK = Housekeeping gene

Table 2.5. Probe regions and sequences for the QuantiGene 18-plex assay

Type	Gene Symbol	Protein name	Accession Number	Probe set region
HK	*Canx*	Calnexin	NM_007597	1195 - 1720
HK	*Rpl13a*	Ribosomal Protein L13a	NM_009438	2 - 467
HK	*Atp5b*	ATP synthase subunit β	NM_016774	22 - 409
HK	*Eif4a2*	Eukaryotic translation initiation factor 4A2	NM_013506	710 - 1271
HK	*Sdha*	Succinate dehydrogenase complex flavoprotein subunit A	NM_023281	76 - 727
HK	*Gapdh*	Glyceraldehyde 3-phosphate dehydrogenase	NM_001001303	735 - 1001
HK	*Ubc*	Ubiquitin C	NM_019639	113 - 676
GOI	*Hsf1*	Heat shock factor 1	NM_008296	1712 - 2263
GOI	*Hspa1a/b*	Heat shock protein 1A/B, HSP70	NM_010479	2186 - 2721
GOI	*Hspb1*	Heat shock protein 1, HSP25	NM_013560	103 - 555
GOI	*Dnaja1*	DnaJ, member A1, HSP40	NM_008298	474 - 1101
GOI	*Dnajb1*	DnaJ, member B1, HSP40	NM_018808	569 - 1125
GOI	*Hspd1*	Heat shock protein 1 (chaperonin), HSP60	NM_010477	1732 - 2170
GOI	*Hspe1*	Heat shock protein 1 (chaperonin), HSP10	NM_008303	259 - 657
GOI	*Hsph1*	Heat shock protein 105/110 kDa; HSP110	NM_013559	1985 - 2430
GOI	*Hsp90aa1*	Heat shock protein 90, member A1; HSP90	NM_010480	245 - 989
GOI	*Hsp90ab1*	Heat shock protein 90, member B1; HSP90	NM_008302	1039 - 1542
GOI	*Sirt1*	Sirtuin 1	NM_019812	609 - 1219

GOI = Gene of interest; HK = Housekeeping gene

2.1.5 Buffers and reagents used in DNA extraction, genotyping and CAG repeat sizing

Lysis buffer for DNA extraction:

- 50 mM Tris-HCl (pH 8.0) (Roche)
- 100 mM EDTA (100938B, VWR)
- 0.5 % SDS (BP1311-200, Fisher Scientific)
- 1 mg / mL Proteinase K (P2308, SIGMA)

Agarose gel preparation and loading reagents:

- 50X TAE buffer:
  - 10 M Tris Base (BP152-1, Fisher Scientific)
  - 5.71 % (v / v) Acetic acid (695092, SIGMA)
  - 10 % (v / v) 0.5 M EDTA (pH 8.0) (100938B, VWR)
- Agarose (16500-500, Invitrogen)
- SYBR Safe DNA gel stain (S33102, Thermo Fisher Scientific)
- 100 bp DNA ladder (N3231L, New England Biolabs)

2.1.6 Reagents and lysis buffers used in SDS-PAGE and western blotting

KCl lysis buffer:

- 50 mM Tris HCl (pH 8.0) (Roche)
- 10 % Glycerol (G/0650/17, Fisher Scientific)
- 5 mM EDTA (100938B, AnalaR, BDH)
- 150 mM KCl (METTLER TOLEDO)

RIPA lysis buffer:

- 150 mM NaCl (S/3160/65, Fisher Scientific)
- 1 % NP40/IGEPAL CO-630 (542334-100G-A, SIGMA)
- 0.5 % Sodium deoxycholate (D6750-100G, SIGMA)
- 0.1 % SDS (BP1311-200, Fisher BioReagents)
- 50 mM Tris-HCl (pH 8.0) (Roche)

HEPES lysis buffer:

- 50 mM HEPES (pH 7.0) – (H3375-100G, SIGMA)
- 150 mM NaCl (S/3160/65, Fisher Scientific)
- 10 mM EDTA (100938B, AnalaR, BDH)
- 10 % NP40/IGEPAL CO-630 (542334-100G-A, SIGMA)
- 0.5 % Sodium deoxycholate (D6750-100G, SIGMA)
- 0.1 % SDS (BP1311-200, Fisher BioReagents)

Triton lysis buffer:

- 150 mM NaCl (S/3160/65, Fisher Scientific)
- 10 % Glycerol (G/0650/17, Fisher Scientific)
- 1 % Triton X-100 (H5141, Promega)
- 10 mM EDTA (100938B, AnalaR, BDH)
- 50 mM Tris-HCl (pH 8.0) (Roche)

Lysis buffers were supplemented with:

- Protease inhibitor cocktail tablets – cOmplete (04693132001, Roche) – 1 mini tablet added per 10 mL lysis buffer
- Phosphatase inhibitors:
    - PhosSTOP – (04906837001, Roche) – 1 tablet per 10 mL buffer
    - Halt Phosphatase cocktail (#1862495, Thermo Fisher Scientific)
    - 1 mM Sodium orthovanadate (S6508, SIGMA-ALDRICH)
    - 50 mM NaF (Sodium Fluoride) (P0759S, New England BioLabs)
- 1 mM DTT (Dithiothreitol) - (D9779-10G, SIGMA)
- 1 mM PMSF (Phenylmethanesulfonyl fluoride solution) – (93482, SIGMA)

Laemmli buffer (loading buffer):

- 250 mM Tris-HCl pH (6.8) (Roche)
- 4 % SDS (BP1311-200, Fisher BioReagents)
- 0.06 % Bromophenol blue (B0126, SIGMA)
- 40 % Glycerol (G/0650/17, Fisher Scientific)
- 10 % ß-Mercaptoethanol (M3148, SIGMA)

1X TGS Buffer: containing 25 mM Tris, 192 mM Glycine, 0.1 % (w / v) SDS, pH 8.3; from 10X TGS buffer stock (161-0772, Bio-Rad).

Transfer buffer

- 25 mM Tris Base
- 192 mM Glycine
- 20 % (v / v) Methanol

SDS-PAGE gels formulated to use with the Mini-Protean Tetra-Cell system (Bio-Rad):

8 % Resolving gel (volume of components for two gels, total of 10 mL):

- ProtoGel 30 % – (EC-890, National Diagnostics) – 2.67 mL
- 4X ProtoGel Resolving buffer – (EC-892, National Diagnostics) – 2.6 mL
- 10 % (w / v) APS (ammonium persulfate) – 100 µL
- TEMED – 10 µL
- Distilled H_2O – 4.62 mL

4 % Stacking gel (volume of components for two gels, total of 5 mL):

- ProtoGel 30 % – (EC-890, National Diagnostics) – 0.65 mL
- ProtoGel Stacking buffer – (EC-893, National Diagnostics) – 1.25 mL
- 10 % (w / v) APS (ammonium persulfate) – 50 µL
- TEMED – 10 µL
- Distilled H_2O – 3.05 mL

2.1.7 Antibodies

Table 2.6. Suppliers, catalogue numbers and dilutions for the primary antibodies used in the study

Supplier	*Antibody*	*Catalogue number*	*Dilution / concentration used*	*Other dilutions tested*	*Host species*
Bethyl Laboratories	HSF1	A303-176A	0.16 μg/mL	-	Rabbit polyclonal
Proteintech	HSF1	51034-1-AP	0.16 μg/mL (brain) 0.1 μg/mL (tibialis anterior)	-	Rabbit polyclonal
Santa Cruz	HSF1 (10H8)	sc-13516	-	1:200 - 1:500	Rat monoclonal
Cell Signalling Technology	HSF1	#4356T	-	1:1,000	Rabbit polyclonal
Invitrogen	HSF1	PA3-017	-	1:1,000 - 1:2,000	Rabbit polyclonal
Santa Cruz	HSF1 (E-4)	sc-17757	-	1:500 - 1:1,000	Mouse monoclonal
Abcam	HSF1 (10H8)	ab61382	-	1:1,000 - 1:2,000	Rat monoclonal
Abcam	HSF1	ab2923	-	1:500	Rabbit polyclonal
Bethyl Laboratories	HSF1	A303-174AT	-	1:2,000 - 1:3,000	Rabbit polyclonal
Bethyl Laboratories	HSF1	A303-175AT	-	1:1,000	Rabbit polyclonal
Enzo Life Sciences	HSF1	ADI-SPA-901-F	-	1:1,000 - 1:2,000	Rabbit polyclonal
Enzo Life Sciences	HSF1 (10H8)	ADI-SPA-950-F	-	1:1,000 - 1:2,000	Rat monoclonal
Abcam	ATP5B	ab14730	1:50,000	-	Mouse monoclonal

Table 2.7. Suppliers, catalogue numbers and dilutions for the secondary antibodies used in the study

Supplier	*Antibody*	*Catalogue number*	*Dilution used*	*Other dilutions tested*	*Host species*
Abcam	Anti-rat IgG H&L (HRP)	ab6734	1:2,000	-	Rabbit polyclonal
Agilent Dako	Anti-mouse IgG/HRP	P 0447	1:2,000	-	Goat polyclonal
Agilent Dako	Anti-rabbit IgG/HRP	P 0448	1:5,000	-	Goat polyclonal

IgG = immunoglobulin G; H + L = heavy and light chains; HRP = horseradish peroxidase

2.2 Methods

2.2.1 Ethics approval and compliance to ARRIVE guidelines

All the experimental procedures that involved the use of mice were carried out under the UK Home Office project license 70/9097 as well as a personal license and UCL establishment licence. The experiments were designed and conducted in agreement with the Animals (Scientific Procedures) Act 1986, in compliance with the ARRIVE guidelines and approved by the University College London Ethical Review Process Committee. Personal protective equipment was worn at all times during the procedures and included coveralls, face masks, disposable hairnets, overshoes and gloves provided by the animal facility.

2.2.2 Mouse husbandry, breeding and maintenance

Wild-type animals used in the initial optimisation and QuantiGene validation and kinetics experiments (Chapter 3 in the thesis) were (CBA/Ca x C57BL/6J)F1 mice (B6CBAF1/OlaHsd) from ENVIGO laboratories (The Netherlands). zQ175 Delta Neo mice were generated either on-site by backcross breeding between zQ175 males to C57BL/6J females (Charles River, UK) or obtained from the CHDI colony at Jackson Laboratory (Bar Harbor, Maine, USA) on the same background. R6/2 mice were always bred in-house by backcrossing R6/2 males to (CBA/Ca x C57BL/6J)F1 females (B6CBAF1/OlaHsd, ENVIGO laboratories, The Netherlands). *Hsf1* $^{+/-}$ heterozygous mice were obtained from the Jackson laboratory (Bar Harbor, Maine, USA) with stock number 010543; C;129-*Hsf1*^{tm1ljb}/J. *Hsf1* $^{+/-}$ heterozygous males were bred to B6CBAF1/OlaHsd females to maintain the colony and the intercross breeding between heterozygous males and females produced the *Hsf1* knockout mice. *Sirt1* transgenic mice were supplied by David Holzman's laboratory at Washington University in Missouri (USA). They were maintained in-house by backcrossing *Sirt1* transgenic males to C57BL/6J females (Charles River, UK). The intercross *Sirt1* transgenic x R6/2 colony was generated by breeding R6/2 males with *Sirt1* transgenic females.

Animals within each colony were always housed in individually ventilated cages (IVC) containing Aspen Chips 4 Premium bedding (Datesand) and environmental enrichment including chew sticks and play tunnels (Datesand). Dependent on gender, mice were grouped with up to five mice per cage and with genetically altered and wild-type mice combined. They had unlimited access to water and food (Teklad global 18 % protein diet, ENVIGO). Animals were kept under a 12-hour light / 12-hour dark cycle conditions and at a 21 °C ± 1 °C regulated temperature. Regular non-sacrificial FELASA screenings in the animal facility provided no evidence of pathogens.

2.2.3 DNA extraction and preparation

DNA was isolated from mouse ear biopsies that were collected at 10 days of age. The biopsy samples were lysed in 450 µL of DNA extraction lysis buffer with 25 – 50 µL of proteinase K (1 mg / mL; P2308, SIGMA), depending on the size of the biopsy sample, and incubated overnight at 55 °C. The following day, 300 µL of saturated NaCL (5 M; S/3160/65, Fisher Scientific) was added to the lysates and mixed thoroughly. Then, samples were centrifuged at 16,000 x *g* for 30 min. After centrifugation, the supernatant was transferred onto a fresh tube containing 600 µL of 100 % ethanol (VWR), vortexed and centrifuged again at 16,000 x *g* for 20 min. Then, after this centrifugation, the supernatant was discarded and 300 µL of 70 % ethanol was added to the pellet. After a gentle mix, the samples were subjected to a final centrifugation at 16,000 x *g* for 15 min, the supernatant was removed, and the pellets were left to air dry at room temperature (RT). After 2 - 3 h, the pellets were resuspended in 5 mM Tris-HCl solution. DNA concentration from the samples was quantified using a Nanodrop One (Thermo Fisher Scientific). Samples were diluted in 5 mM Tris-HCl as needed to the required concentration.

2.2.4 Genotyping and CAG repeat sizing

DNA samples were genotyped by polymerase chain reaction (PCR) using T100 thermal cyclers from Bio-Rad. The GoTaq G2 Flexi DNA polymerase system (M7848, Promega) was employed for the zQ175 Delta Neo, *Sirt1* transgenic and *Hsf1* lines and the DreamTaq Hot Start Green PCR Master Mix system (K9022, Thermo Fisher

Scientific) for the R6/2 line. The primers added and their sequences are detailed in Table 2.1, section 2.1.2.

For zQ175 Delta Neo genotyping, a 20 µL reaction contained 10 – 15 ng DNA, 1x GoTaq Flexi buffer, 2.5 mM $MgCl_2$, 0.2 mM dNTPs (Thermo Fisher Scientific), 1 µM forward and reverse primers and 1 U/ µL GoTaq2 polymerase. The amplification cycling conditions were 30 s at 98 °C for 1 cycle, (15 s at 98 °C, 15 s at 64 °C and 30 s at 72 °C) for 34 cycles and finally 5 min at 72 °C for 1 cycle. *Sirt1* transgenic genotyping involved a 20 µL reaction including 20 – 50 ng DNA, 1x GoTaq Flexi buffer, 2.5 mM $MgCl_2$, 0.2 mM dNTPs (Thermo Fisher Scientific), 1 µM *Sirt1* forward and reverse primers, 0.12 µM Fab forward and reverse primers and 0.05 U / µL GoTaq2 polymerase. The thermal cycling program was 1 min at 93 °C and 30 x (20 s at 93 °C, 3 min at 68 °C). For *Hsf1* genotyping, 20 – 50 ng DNA, 1x Go Taq Flexi buffer, 2 mM $MgCl_2$, 0.2 mM dNTP, 0.5 µM for each primer and 0.025 U / µL GoTaq2 polymerase were added into a 25 µL total reaction. The cycling program was 4 min at 95 °C, 35 x (25 s at 95 °C, 20 s at 60 °C, 45 s at 72 °C) and 1 min at 72 °C. R6/2 mice were genotyped by preparing a 10 µL reaction containing 50 – 100 ng DNA, 1x DreamTaq Master Mix and 1 µM for each primer. The cycling conditions were 3 min at 95 °C, 34 x (30 s at 95 °C, 30 s at 60 °C, 1 min at 72 °C) and 15 min at 72 °C. PCR products along with 5 µL of 100 bp DNA ladder (New England Biolabs) were loaded in a 2 – 3 % agarose gel (2 – 3 % agarose (w / v) in 1X TAE buffer) and electrophoresed at 140 V for 30 min to 1 hour until enough resolution was achieved to determine the genotypes. Gels were exposed for image detection using a ChemiDoc MP Imaging system (Bio-Rad).

CAG repeat sizing reaction for both R6/2 and zQ175 Delta Neo mice was as follows: a 13 µL reaction included 50 ng DNA for R6/2 and 10 ng for zQ175, 1x AmpliTaq Gold 360 Master mix (4398787, Applied Biosystems), 1.25 µL 360 GC enhancer (4398799, Applied Biosystems), 0.2 µM of each forward and reverse primers. The amplification program using T100 thermal cyclers (Bio-Rad) was: 10 min at 95 °C, 34 x (30 s at 95 °C, 30 s at 63 °C, 90 s at 72 °C) and 7 min at 72 °C. After amplification, 8 µL of a mix

containing Hi-Di formamide (4311320, Applied Biosystems) and 0.08 µL internal size standard MapMarker ROX100 (BioVentures Inc.) were added to a new plate along with 3 µL of PCR product. The plate containing the mix was sealed and denatured at 95 °C for 5 min and then immediately stored in - 20 °C freezer for at least 5 min. After brief centrifugation, the plate was processed in an ABI3730xl sequence analyser for capillary electrophoresis. Data were analysed using the software GeneMarker (SoftGenetics) to calculate CAG repeat sizes. The mean CAG repeat sizes ± SD for R6/2 and zQ175 Delta Neo mice used in the study are provided in Table 2.8 below.

Table 2.8. CAG repeat sizing information of the mice used in the study.

Mouse line	*Thesis chapter*	*Mean CAG repeat size ± SD*
zQ175	Chapter 4	198.18 ± 6.45
R6/2	Chapter 4	187 ± 1.67
Sirt1 tg x R6/2	Chapter 5	185.69 ± 2.98 (9 weeks) 184.69 ± 2.71 (14 weeks)

2.2.5 Formulation of NVP-HSP990 and dosing

The NVP-HSP990 (2-amino-7, 8-dihydro-6H-pyrido [4, 3-d] pyrimidin-5-one) compound was provided by Novartis Pharma AG. The compound was always formulated at a 12 mg / kg concentration, forming a suspension in 2 % methylcellulose (M0262, SIGMA) that was diluted in 0.9 % saline solution (20-9800-10, Severn Biotech). Both the NVP-HSP990 and vehicle (2 % methylcellulose in 0.9 % saline solution) were freshly prepared for each experiment on the day before the dosing procedures. The suspension was sonicated several times in an ultrasonic bath (XB3, Grant) to reduce the size of the particles. An adequate single dose of NVP-HSP990 or vehicle was administered via oral gavage to each mouse after weighing. To ensure an even suspension during the whole dosing procedure, thorough mixing in a magnetic stirrer was carried out between doses. Mice assigned for the dosing

experiments were randomised from their litters of origin and age matched as closely as possible. After dosing, mice were sacrificed at the corresponding time-points by cervical dislocation, the tissues of interest were harvested, snap-frozen in liquid nitrogen and then stored at - 80 °C until use.

2.2.6 RNA extraction, cDNA synthesis and RT-qPCR

Mouse brain hemispheres and muscle tissues were lysed in Qiazol lysis reagent (79306, Qiagen) and RNA extracted using the reagents and materials from the Qiagen RNeasy mini kit (74106, Qiagen), following the manufacturer's protocol. Brain hemispheres were homogenised in Qiazol reagent using a polytron homogeniser probe, washing the probe with distilled H_2O and ethanol between each homogenisation. Muscle tissues were lysed in Qiazol using the Ribolyser FastPrep-24 (MP Biomedicals) at 4 °C, at 6.5 m / s for 1 min for three times. When extracting RNA from QuantiGene homogenates, 500 µL of these homogenates were mixed with the same volume of Qiazol reagent using 1 mL hypodermic syringes and 23G and 26G needles (BD Microlance). The Qiazol homogenates were left for 5 min to promote dissociation of the nucleoprotein complexes and then transferred to a fresh tube. Chloroform (VWR) was then added in a 1:5 ratio to the initial Qiazol volume, samples were left at RT for 3 min, and vortexed thoroughly followed by a centrifugation at 16,000 x *g* for 15 min at RT. The upper aqueous phase of each sample was transferred to a new tube without disturbing the middle layer. A volume of 70 % ethanol equal to the volume transferred was added and mixed thoroughly. The mixed solution for each sample was then put into a RNeasy mini spin column in a 2 mL collection tube, then centrifuged for 15 s at 16,000 x *g*. The flow-through was discarded and 350 µL of RW1 buffer added to each RNeasy mini spin column, then centrifuged for 15 s at 16,000 x *g* and flow-through again discarded. Following this, 80 µL of DNaseI (diluted 1:8 in RDD buffer) (RNase-free DNase kit, 79256, Qiagen) was dispensed to each RNeasy mini spin column membrane for DNase treatment. Samples were then incubated at RT for 15 min. 350 µL of RW1 buffer were then added to the RNeasy mini spin column for each sample and they were centrifuged for 15 s at 16,000 x *g;* the flow-through was discarded. 500 µL of RPE buffer (with 100 % ethanol included

as per manufacturer's instructions) was added to the RNeasy mini spin column and centrifuged for 15 s at 16,000 x *g*, discarding the flow-through afterwards. Finally, the RNeasy mini spin column for each sample was placed into a new 2 mL collection tube and centrifuged at 16,000 x *g* for 2 min. The extracted RNA was eluted by transferring the RNeasy mini spin column into a new 1.5 mL collection tube, adding a volume of RNase-free H_2O (appropriate to the initial tissue size) directly onto the membrane and incubating at RT for 2 min, before centrifugation for 1 min at 16,000 x *g*. RNA concentration was quantified using a Nanodrop One (Thermo Fisher Scientific). Mouse brain tissue RNA samples were diluted to 1 µg in RNase-free H_2O in a 10 µL total volume. The reverse transcription of the RNA to obtain cDNA was performed using the M-MLV reverse transcriptase kit (28025-013, Invitrogen), in two parts: firstly, by adding 1 mM dNTP mix and 1 µL of random hexamers (100 ng / ul, Eurofins) to each 10 µL RNA sample. After mixing, the RNA samples were incubated for 5 min at 65 °C. Secondly, a pre-mix was prepared containing: 1x First-Strand buffer, 0.01 M DTT, 2 U / µL RNasin Plus RNase inhibitor (N2615, Promega) and 10 U / µL M-MLV reverse transcriptase in a total of 8 µL that was added to each previous reaction. The reverse transcription was then carried out as follows: 10 min at 25 °C, 50 min at 37 °C and 15 min at 70 °C.

A 1:6 dilution was prepared for each of the muscle cDNA samples, 1:50 for the brain cDNA samples and 1:30 for the ones extracted from QuantiGene homogenates. For RT-qPCR, 15 µL reactions were prepared in each well of 96-well thin wall Hard-Shell PCR plates (Bio-Rad) and in triplicates, containing each 3 µL of cDNA, 1x TaqMan Fast Advanced Master Mix (4444557, Applied Biosystems), 1x of the probe/primer assays purchased from Thermo Fisher Scientific or 0.3 µM of each forward and reverse primers and 0.2 µM of probes designed in-house (commercial and designed in-house assays are indicated in Table 2.2, section 2.1.3). Then, the plate was covered with Microseal "B" sealing adhesive film (MSB1001, Bio-Rad) and centrifuged at 800 x *g* for 30 s, before amplification was carried out in a CFX96 Real-time system C1000 thermal cycler (Bio-Rad) as follows: 95 °C for 40 s, 40 x (95 °C for 7 s and 60 °C for 20 s). The data analysis followed the $2^{-\Delta\Delta Ct}$ method (Livak and Schmittgen., 2001). The

GeoMean of the Ct values of *Atp5b, Canx, Rpl13a, Eif4a2, Sdha*, *Actb*, *Gapdh* was used to normalise the expression of the genes of interest (ΔCt) and further to the lowest expressor (highest ΔCt value) for each gene.

2.2.7 Tissue homogenisation and QuantiGene gene expression assays

Three QuantiGene multiplex assays were designed and used in this study: 10-plex, 20-plex and 18-plex (see Tables 2.3, 2.4, 2.5 in section 2.1.4); containing capture beads and probes designed for the specific targets of interest. All the reagents and materials used in these experiments were purchased from Thermo Fisher Scientific and applied according to manufacturer's recommendations.

The mouse tissues used in these experiments were initially weighed and homogenised by adding 300 µL of homogenising solution and 3 µL of proteinase K (in a 50 µg / µL concentration) per every 10 mg of tissue. Brain tissues (brain hemispheres, cortex and striatum) were homogenised with a Polytron homogeniser probe or motorised pestle. Tibialis anterior samples were homogenised using liquid nitrogen and a pre-chilled pestle and mortar that was sitting on dry ice. A small volume of liquid nitrogen was added to the mortar to which the frozen tibialis anterior samples were added. After becoming a powder, the samples were transferred into a fresh tube to which the working homogenisation solution (containing proteinase K) corresponding to their tissue weight was added. All homogenates were then lysed overnight in an incubator at 50 - 55 °C. If the samples were not fully lysed, 1 mL syringes with either 23G or 26G hypodermic needles (BD Microlance) were used to shear the remaining fragments. The following day, the samples were centrifuged at 3,000 x *g* for 15 min to pellet any debris and the supernatant was transferred to a fresh tube. The tissue homogenates were appropriately diluted in QuantiGene homogenising solution. Following the manufacturer's recommendations for fresh, frozen or formalin-fixed, paraffin-embedded (FFPE) tissues, on day 1, homogenates were pre-warmed (37 °C or RT) for at least 30 min. Then, 20 µL of the sample homogenates were added in duplicates or triplicates (two or three technical replicates) into each well of the hybridisation

plates. If processing a plate for the optimisation of sample input, a pool of samples from the same genotype or treatment group at equal tissue mass / volume, based on wet tissue weight solubilised (10 mg / 300 µL), was prepared. This undiluted pool of samples was then diluted in 2-fold or 3-fold serial dilutions using homogenising solution. If processing a plate for analysis of gene expression, the sample homogenates were diluted in homogenising solution according to the optimal dilution chosen in the previous optimisation experiment.

A working mix solution was then prepared by adding (in this order) nuclease-free water (HyClone water, 10307052, Fisher Scientific), lysis mixture, blocking reagent, proteinase K (50 µg / µL), capture beads and probe set from the corresponding multiplex assay, in accordance with the number of samples in the experiment. 30 µL of working solution were added into each well of the hybridisation plates. The plate was sealed with a pressure seal cover and incubated for 18 – 22 h at 54 °C in a VorTemp incubator shaking at 600 rpm. After incubation, on day 2, the plate was taken out of the incubator, centrifuged at 240 x *g* for 1 min and placed into a magnetic plate washer. The plate was washed with QuantiGene wash buffer four times. Pre-warmed (37 °C or RT) pre-amplifier solution was dispensed to the wells and the plate was incubated in the VorTemp shaker for 1 h at 50 °C and 600 rpm. The same protocol of washing and incubation was followed for the additional signal amplification reagents amplifier and label probe solutions. Lastly, SAPE solution (containing fluorescent Streptavidin-conjugated R-Phycoerythrin in SAPE diluent) was added, the plate was incubated for 30 min at 50 °C and 600 rpm, followed by the final four washes and resuspension in SAPE wash buffer. A MAGPIX instrument (Luminex Corporation) was employed to measure the median fluorescent intensity (MFI) of each sample in the plate using the xPonent software. For the analysis, the background MFI signal was always subtracted from each MFI value. For the optimisation of the sample input, the limit of detection, limit of quantification and accuracy of the fold change was calculated. For a gene expression experiment, the MFI data for each sample was normalised to the GeoMean of the housekeeping

genes. The average of the MFI in the sample replicates was calculated and normalised to the wild-type vehicle samples to determine the fold change of expression.

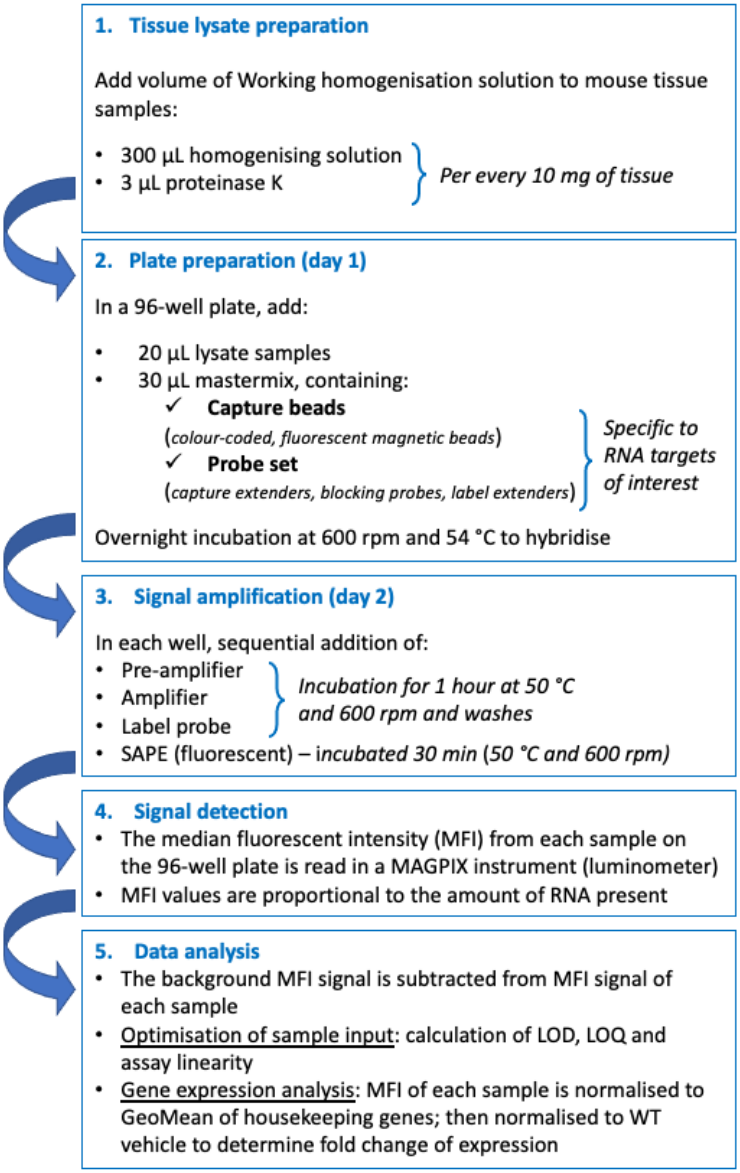

Figure 2.1. Flow chart of the QuantiGene methodology protocol.
The QuantiGene protocol that was followed for the experiments of gene expression analysis or optimisation of sample input using mouse tissue samples is summarised in the figure; starting with (1) the preparation of lysates from frozen mouse tissues, (2) the preparation of plates and addition of relevant reagents to hybridise with the RNA targets of interest, (3) amplification of the fluorescent signals, (4) signal detection as MFI values in a MAGPIX instrument and (5) analysis of the data obtained, depending on the purpose of the experiment. SAPE = Streptavidin-conjugated R-Phycoerythrin; MFI = median fluorescent intensity; LOD = limit of detection; LOQ = limit of quantification.

2.2.8 SDS-PAGE and western blotting

Mouse tissues were lysed in ice-cold buffers, either RIPA, KCl, HEPES or Triton buffer, prepared as indicated in section 2.1.8. These buffers were supplemented in all cases with cOmplete protease inhibitors, 1 mM PMSF and 1 mM DTT, and, where needed, with PhosSTOP phosphatase inhibitors (Roche), Halt phosphatase inhibitors cocktail (Thermo Fisher Scientific) or 50 mM NaF and 1 mM Na orthovanadate (New England Biolabs). Brain tissues (cortex, striatum or brain hemispheres) were homogenised with a Polytron probe homogeniser or a motorised pestle. Muscle tissues were homogenised using a Ribolyser FastPrep-24 (MP Biomedicals) at 4 °C at 6.5 m / s for 1 min for four times, leaving a 10 min break between each ribolysation. After homogenisation, samples were sonicated in a Q125 QSonica sonicator at 4 °C and 40 % amplitude, during 10 s for three times with 10 s intervals, then centrifuged twice at 13,000 x *g* at 4 °C for 10 min. The supernatant was collected and protein concentration estimated using the Pierce BCA protein assay (23223 for Reagent A, 23224 for Reagent B, Thermo Fisher Scientific) and albumin standard (23209, Thermo Fisher Scientific) following the supplier's instructions. 40 µg of protein was mixed with Laemmli loading buffer and denatured at 90 °C for 5 min.

Samples were loaded onto 10 % Criterion TGX Precast gels (Bio-Rad) along with 7 µL protein ladder (Precision Plus Protein Kaleidoscope Prestained protein standard, 1610375, Bio-Rad) and subjected to electrophoresis at 100 V until bands were sufficiently separated. Proteins were then transferred to a 0.45 µm nitrocellulose membrane (1620115, Bio-Rad) or 0.45 µm PVDF membranes (88518, Thermo Fisher Scientific) submerged in transfer buffer at 100 V. In some experiments, the polyacrylamide gels were made in-house using the Mini-Protean Tetra-Cell system (Bio-Rad). In these cases, the resolving and stacking gels were made using National Diagnostics reagents, as indicated in section 2.1.6. After transfer, membranes were blocked in either non-fat dried milk (Marvel) or BSA (A7906, SIGMA) in TBS buffer (94158, SIGMA) at 0.5 % to 5 % concentrations, for a minimum of 1 h at RT, before an overnight incubation at 4 °C with the primary antibodies at the selected concentrations / dilutions, as indicated in Tables 2.6 and 2.7 in section 2.1.7. During

optimisation, different combinations of buffers, phosphatase inhibitors, blocking solutions at concentrations from 0.5 % to 5 % and antibody dilutions were tested. The conditions are indicated in the figures in Chapter 4 that correspond to the characterisation of HSF1 antibodies. The optimised experimental conditions for the antibodies Proteintech 51034-1-AP and Bethyl A303-176A for HSF1 detection as shown in Chapter 4 were as follows: tissues were homogenised in ice-cold RIPA buffer containing cOmplete protease inhibitor (Roche), PhosSTOP phosphatase inhibitors (Roche), 1 mM PMSF and 1 mM DTT. Nitrocellulose membranes were blocked for at least 1 h in 0.5 % non-fat dried milk (Marvel) in TBS and primary antibodies were added at 1 µg in 6 mL (for brain tissues) or in 10 mL (for tibialis anterior) 0.5 % non-fat dried dried milk in TBS, then incubated overnight at 4 °C.

As a loading control, the ATP5B primary antibody (ab14730, Abcam) was used at a 1:50,000 dilution in 0.5 % non-fat dried milk in TBS and incubated with the membranes for 2 – 3 h at RT. After primary antibody incubations, membranes were washed 3 – 4 times for 10 min per wash in 0.02 % Tween – TBS (TBS-T). The corresponding secondary antibodies diluted in 0.02 % TBS-T were incubated with the blots at RT for 1 h. After the washes, Clarity Western ECL Substrate or Clarity Max Western ECL Substrate (Bio-Rad) was added to the blots to expose them using a ChemiDoc MP Imaging system (Bio-Rad). The blots were quantified with Image Lab software (Bio-Rad). The uncropped blots can be found in the Appendix.

2.2.9 Statistical analysis

All data obtained were screened for outliers through a ROUT test using GraphPad Prism software (version 7). Then, data were analysed with SPSS software (version 26) using either one-way ANOVA (factor: treatment), two-way ANOVA (factors: genotype and treatment) or independent samples *t*-test (unpaired Student's *t*-test). *Post-hoc* analyses with Bonferroni correction for multiple comparisons were applied where appropriate as indicated in the corresponding figure legends. *P*-values below 0.05 were considered as statistically significant. Graphs and figures were prepared using GraphPad Prism and Adobe Illustrator (version 24) software.

Chapter 3. Optimisation of methodologies and experimental conditions for the study of the heat shock response in Huntington's disease mouse models

3.1 Introduction

Previous studies of the heat shock response at the transcriptional level in HD, and other neurodegeneration models, have generally involved the administration of a pharmacological substance that would elicit the heat shock response and the use of a quantitative gene expression method such as real-time quantitative PCR (RT-qPCR) to measure the expression of major heat shock genes (Hay *et al*., 2004; Waza *et al*., 2005; Fujikake *et al*., 2008; Labbadia *et al*., 2011; Carnemolla *et al*., 2014; Neueder *et al*., 2017).

In this thesis, the NVP-HSP990 compound was administered to mice as the inducer of the heat shock response. NVP-HSP990 is a HSP90 inhibitor which acts by interacting with the ATP-binding domain of HSP90, affecting its ATPase activity (Menezes *et al.,* 2012). This prevents HSP90 from binding HSF1 and thereby the inhibitory effect that is exerted to maintain HSF1 in an inactivated state (Zou *et al*., 1998). As a consequence of releasing HSF1 from this HSP90 inhibitory complex, the heat shock response is activated, leading to the enhanced expression of the heat shock genes. The study by Labbadia *et al.* (2011) provided initial evidence of the potent but transient activation of the heat shock response in mice, including HD mouse models, at different ages, after oral administration of this NVP-HSP990 compound, without signs of toxicity.

The QuantiGene multiplex assay is an alternative approach for gene expression analysis to RT-qPCR. It offers some interesting characteristics that could be advantageous to this study and, also, it may overcome some of the limitations associated with RT-qPCR. The examination of this methodology for the transcriptional analysis of a broad range of heat shock genes after pharmacological induction of the heat shock response may facilitate the validation of therapeutic strategies that target the protein folding capacity.

To address these points and set up the experimental approaches to assess the heat shock response at the transcriptional level, some initial experiments were performed in a wild-type mouse context that would then be transferred to apply to HD models. These are the research aims covered in this chapter:

1. Test the efficacy of pharmacological induction of the heat shock response by two different batches of the NVP-HSP990 compound.
2. Validate the QuantiGene methodology for analysis of heat shock gene expression by comparison to RT-qPCR.
3. Understand the kinetics of pharmacological induction of the heat shock response by NVP-HSP990.
4. Design and optimise a QuantiGene multiplex assay to analyse the expression of an extensive set of heat shock genes of interest.

3.2 Efficacy of pharmacological induction of the heat shock response with separate batches of NVP-HSP990

The NVP-HSP990 compound has been previously applied by our laboratory to pharmacologically induce the heat shock response (Labbadia *et al.*, 2011; Carnemolla *et al.,* 2014; Neueder *et al*., 2014; Neueder *et al*., 2017). Due to these previous studies, two separate batches of NVP-HSP990 (batch 1 and batch 2), were available. To corroborate the efficacy of the compound as well as to ensure no differences were found between batches, a small-scale dosing experiment was conducted.

Wild-type mice in a (CBA/Ca x C57BL/6J)F1 background at 9 weeks of age (*n* = 6 mice per treatment group), were allocated to be administered with a single acute dose of either vehicle (2 % methylcellulose in 0.9 % saline solution), NVP-HSP990 batch 1 or NVP-HSP990 batch 2 (at 12 mg / kg). Brain hemispheres and tibialis anterior muscle tissues were harvested 4 hours after dosing for analysis.

The gene expression levels of three major heat shock genes *Hspa1a/b* (HSP70), *Hspb1* (HSP25), *Dnajb1* (HSP40) as well as the master regulator *Hsf1* were measured by RT-

qPCR in order to analyse the efficacy of pharmacological induction of the heat shock response by each of the NVP-HSP990 batches.

As illustrated in Figure 3.1, the treatment with NVP-HSP990 provoked a clear and significant induction in the expression levels of *Hspa1a/b*, *Hspb1* and *Dnajb1*, as compared to vehicle, in both brain hemispheres and tibialis anterior. Interestingly, the levels of induced expression in tibialis anterior were found to be much more elevated than in brain. This is consistent with previous data (Neueder *et al*., 2017) and it is likely to be attributed to a higher proteostasis capacity in muscle as compared to brain regions. Both batches of NVP-HSP990 led to a similar degree of induction in both brain or muscle, and no significant differences were observed between them. Therefore, NVP-HSP990 is efficacious at inducing the heat shock response in mouse brain and muscle tissues and either of the two available batches of NVP-HSP990 could be used in the subsequent dosing trials.

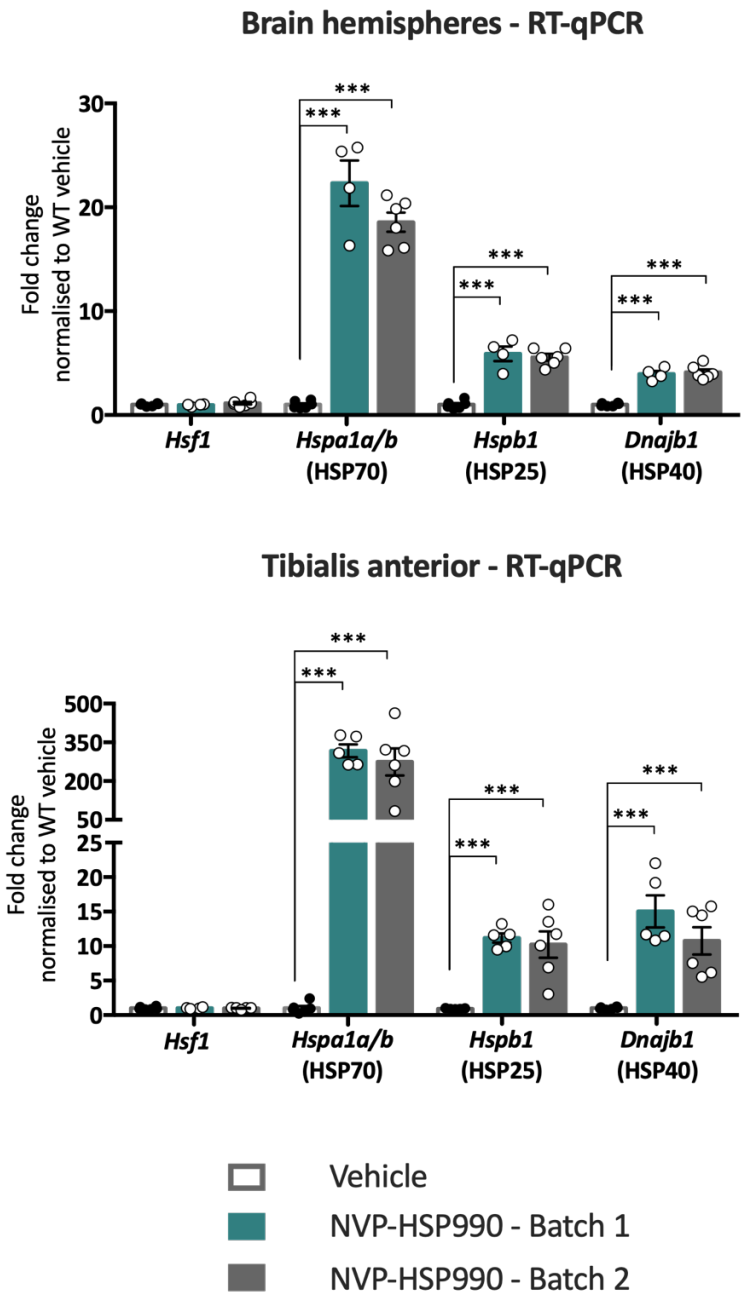

Figure 3.1. Expression levels of three major heat shock genes and Hsf1 in brain hemisphere and tibialis anterior of wild-type mice after induction of the heat shock response by two separate batches of NVP-HSP990.

The expression of heat shock genes Hspa1a/b (HSP70), *Hspb1* (HSP25) *and Dnajb1* (HSP40), *as well as regulator Hsf1, was analysed by RT-qPCR in wild-type mice after treatment with vehicle or NVP-HSP990. Expression was normalised to reference genes Atp5b, Canx, Rpl13a and Eif4a2. Statistical analysis was by one-way ANOVA and Bonferroni correction for multiple comparisons. N = 5 - 6 mice per treatment group. Mean ± SEM. *** p value ≤ 0.001.*

3.3 Design and optimisation of a QuantiGene 10-plex assay

QuantiGene is a methodology for the analysis of gene expression, based on branched DNA technology (Canales *et al*., 2006; Flagella *et al*., 2006), that allows the simultaneous detection of multiple targets (up to eighty genes of interest) directly from any tissue lysate. According to this, magnetic capture beads and probes are designed specifically for the detection of genes of interest or particular regions within them. These capture beads and probes hybridise to the targeted regions of the RNA molecules during incubation. Then, the sequential additions of pre-amplifier, amplifier, label probe reagents and, especially, the SAPE reagent, which contains fluorescent streptavidin-conjugated R-phycoerythrin, amplifies the luminescent signal that is detected and quantified on a MAGPIX instrument (Luminex). This signal is translated as a value of the median fluorescence intensity (MFI) for each sample and target that would be proportional to the amount of target RNA of interest that is present. A schematic workflow of this methodology can be found in the following Figure 3.2.

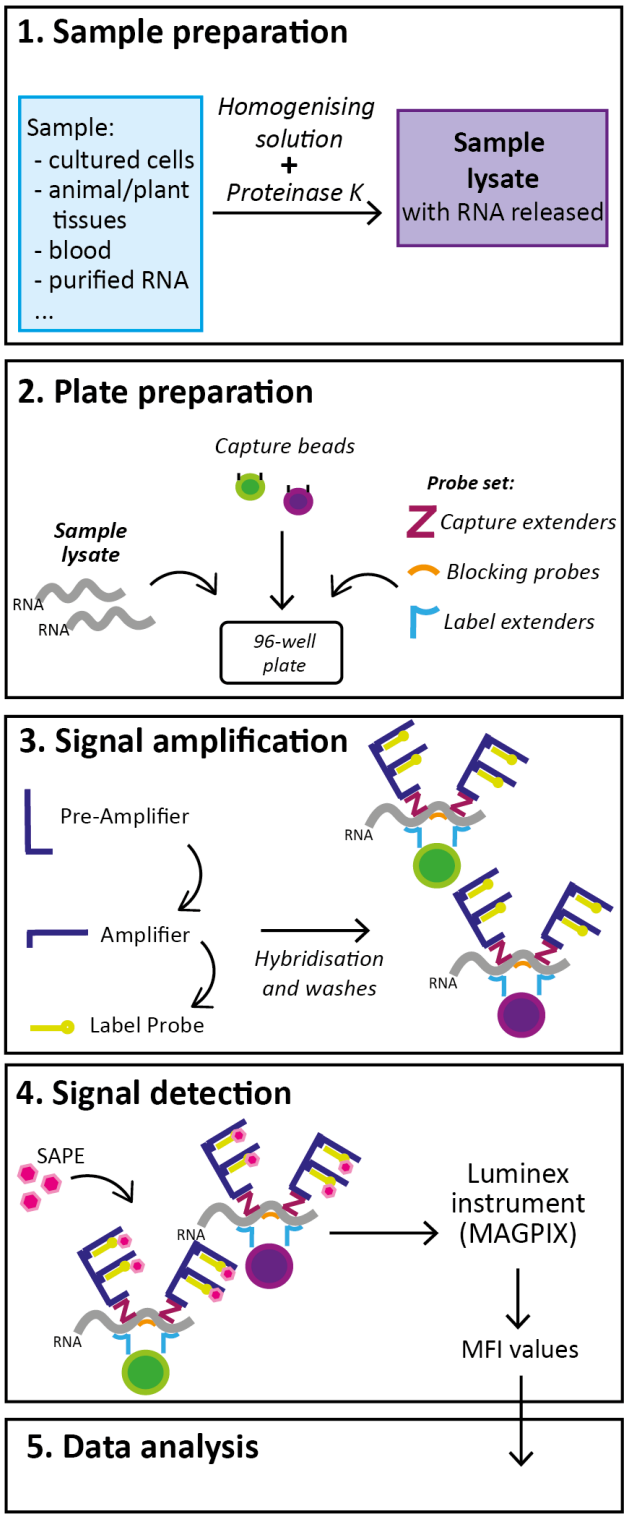

Figure 3.2. Schematic workflow of the QuantiGene methodology.

(1) The QuantiGene technique is initiated by the preparation of samples lysates; samples from any origin are homogenised to release the RNA using a working homogenisation solution containing proteinase K.

(2) Samples are then added individually into the wells of 96-well plates with customised reagents like the magnetic Capture beads and probe set (with capture extenders, blocking probes and label extenders) that are colour-coded and designed specifically to hybridise with the sequences of the RNA targets of interest.

(3) After overnight incubation to allow the hybridisation between RNA targets and Capture beads and probes, based on branched-DNA technology, the signal (not the RNA fragment) is amplified by the sequential addition and washes of oligonucleotide pre-amplifier, amplifier and label probe reagents.

(4) A final chemiluminescent reagent, streptavidin-conjugated R-Phycoerythrin (SAPE) is added, that, by reaction with the previously added biotinylated label probe provides a luminescent signal that is detected in a Luminex instrument and reported as MFI values, which are proportional to the amount of target RNAs present in the samples.

(5) The fluorescence signal is associated with the specific Capture beads and RNA targets and their MFI values are used in the data analysis to determine the expression of the genes of interest.

SAPE = streptavidin-conjugated R-phycoerythrin; MFI = median fluorescent intensity.

As the main aim of the project was the analysis of the heat shock response, characterised by the transcriptional activation of multiple heat shock genes, the features of this QuantiGene methodology were highly aligned to the research interests.

In order to understand this methodology and address whether it could be suitable for the project experiments, a small assay was designed that contained the capture beads and probes for three major heat shock genes: *Hspa1a/b* (HSP70), *Hpsb1* (HSP25) and *Dnajb1* (HSP40), the master regulator of the heat shock response *Hsf1*, *Sirt1* and also several housekeeping genes to be used as reference for normalisation (*Atp5b*, *Canx*, *Rpl13a*, *Eif4a2* and *Ubc*). These housekeeping genes were selected as they had been tested and reported as suitable reference genes for HD RT-qPCR assays (Benn *et al.,* 2008).

3.3.1 Optimisation of sample input for QuantiGene assays

QuantiGene methodology requires the RNA release from the cells in the samples to be analysed. It is essential to obtain a complete lysis of cells in order to achieve good assay precision. An optimal lysis method for the samples should be chosen, as well as a correct ratio of homogenisation solution / proteinase K should be added to the cells or tissues of interest, as per the manufacturer's recommendations, to avoid issues related to poor homogenisation.

To determine the performance of the multiplex assay and the optimal sample input for each of the sample types in the experiments, certain parameters need to be measured:

- Assay limit of detection: the minimum signal that should be obtained for each target RNA to reach any gene expression conclusions. It is calculated as the average of the background MFI values plus 3 standard deviations (SD) of the background signals from each technical replicate.
- Limit of quantification: considered to be the lowest MFI signal to provide an acceptable accuracy of the fold change, related to signals fitting into a linear range.
- Coefficient of variation (CV): an indication of the assay precision; usually less than 15 % for the technical replicates. It is calculated by subtracting the background MFI signal, then averaging the MFI values of technical replicates (AVG) and calculating the standard deviation (SD) of MFI signals from replicates. % CV = (SD / AVG) * 100
- Assay linearity: determines the accuracy of the fold change and validates as suitable all the sample dilutions that show an accuracy of fold change between 80 % – 120 %. To calculate this, serial dilutions experiments need to be performed. The samples are prepared in a dilution series (2-fold, 3-fold…) and the plate is processed as per the manufacturer's instructions. Then, after subtracting the background MFI signal from each sample MFI value, the observed fold change is calculated for each one of the dilutions; the observed

fold change should be within a 20 % range of the 100 % expected fold change (2-fold, 3-fold…), calculated as:

(Observed fold change / expected fold change) * 100 = range of 80 % - 120 %

A sample dilution should then be selected based on showing signals within this range of linearity / accuracy.

- Another important aspect to consider, when choosing the most appropriate dilution, is the signal saturation; this usually corresponds to MFI values over 50,000 in the MAGPIX instrument (Luminex), as per the supplier's indications. It is not advisable to select sample dilutions presenting signal saturation for the gene expression analysis experiments.

In accordance with the protocols for the calculation of these parameters for the 10-plex assay, a set of serial dilutions experiments were conducted. The remaining brain hemisphere and tibialis anterior muscle from the same animals previously dosed with NVP-HSP990 or vehicle (Figure 3.1) were homogenised for QuantiGene analysis. Pools of samples from the same treatment group at equal tissue mass / volume, based on wet tissue weight solubilised (10 mg / 300 µL), were prepared in a series of 3-fold (brain) or 2-fold (tibialis anterior) dilutions. The aims of these optimisation experiments were:

- To elucidate the optimal dilutions of samples from brain hemispheres and tibialis anterior tissues that show a good accuracy and assay linearity without reaching saturation of the signal for any RNA target.
- To ensure the housekeeping genes included in the assay were expressed with consistency in all samples regardless of treatment received.

3.3.2 Optimisation of QuantiGene 10-plex assay for use with mouse brain hemispheres

As explained in the previous section, brain hemispheres samples from each treatment group (vehicle or NVP-HSP990) at equivalent tissue mass / volume (10 mg / 300 µL) were pooled (*n* = 5 - 6 mice per treatment group) and subjected to 3-fold serial dilutions, loading these pools in the plate in duplicate.

As shown on the left side in Figure 3.3, the assay linearity was achieved for housekeeping genes *Atp5b*, *Canx*, *Rpl13a* and *Eif4a2* for both vehicle and NVP-HSP990 samples. The MFI values decreased linearly according to the dilution and, in most cases, all technical replicates from vehicle or treated samples showed a similar MFI signal, indicating that the expression of these four genes was not altered by the treatment with NVP-HSP990 and induction of the heat shock response. However, that was not applicable to *Ubc,* that showed slight differences in expression between vehicle and treatment samples. This is likely to occur because induction of *Ubc* transcription is mediated by HSF1 (Bianchi *et al*., 2018; Vihervaara *et al.,* 2013), and therefore, *Ubc* was not used as a reference gene in the analysis of gene expression in these experiments.

On the right side of Figure 3.3, the heat shock genes *Hspa1a/b*, *Hspb1*, *Dnajb1* and regulators *Hsf1* and *Sirt1* showed good linearity and a proportional decrease of MFI values with the serial dilutions. The levels of expression for *Hsf1* and *Sirt1* were not affected by NVP-HSP990 treatment, and, therefore, both linear regression lines corresponding to the two treatment groups remained similar. The expression of *Hspa1a/b*, *Hspb1* and *Dnajb1* was induced by NVP-HSP990 treatment and the linear regression line corresponding to treated samples appeared with elevated MFI values as compared to the MFI values from vehicle.

Considering the optimisation parameters that were calculated, the 1:9 dilution was an appropriate sample dilution for the QuantiGene gene expression analysis of brain hemispheres. The MFI values for the targets of interest and housekeeping genes at that dilution were over the limit of detection and the signal was not saturated.

Optimisation 10-plex
Brain hemispheres

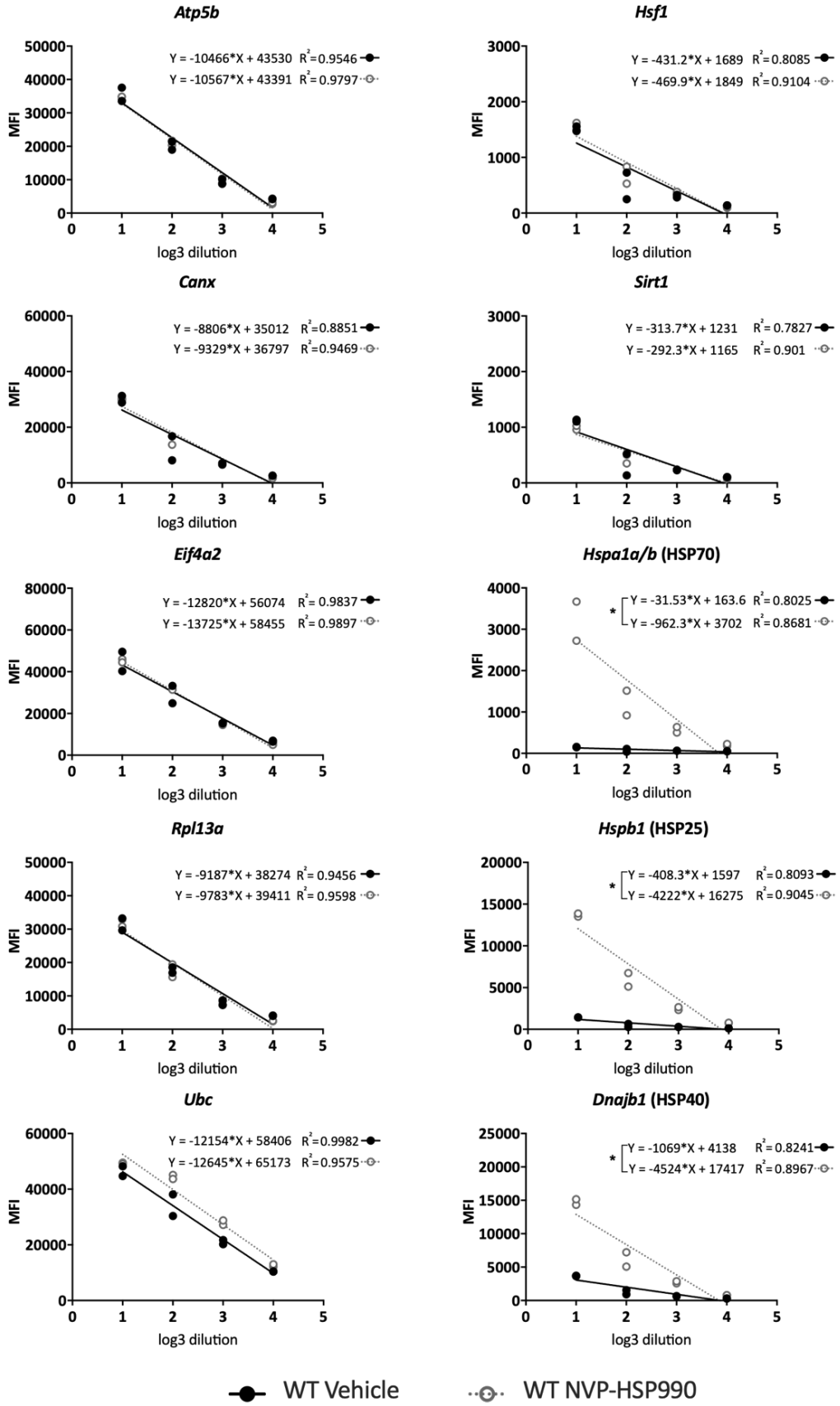

Figure 3.3. Optimisation of sample input in the QuantiGene 10-plex assay for use with wild-type brain hemispheres.

Pools of brain hemisphere samples from either vehicle or NVP-HSP990 treated wild-type animals were prepared with samples at equivalent tissue mass / volume (10 mg / 300 μL), in 3-fold serial dilutions (n = 5 - 6 mice per treatment) and analysed in duplicate. MFI values detected for each dilution from vehicle or NVP-HSP990 samples are shown in the graphs. Assay linearity was calculated for each gene. Housekeeping genes (on the left side) maintained a stable expression between treatment groups, with exception of Ubc. Heat shock genes Hspa1a/b (HSP70)*, Hspb1* (HSP25) *and Dnajb1* (HSP40) *(on the right side) exhibited linear regression lines with significantly different slopes for each treatment group. WT = wild-type; MFI = median fluorescence intensity.*

3.3.3 Optimisation of QuantiGene 10-plex assay for use with mouse tibialis anterior muscle

In a similar approach to that taken for brain hemispheres, tibialis anterior lysates from wild-type mice treated with vehicle or NVP-HSP990 were pooled from each treatment group and subjected to a 2-fold serial dilution. As seen in Figure 3.4, the MFI values corresponding to vehicle or NVP-HSP990 samples followed a linear regression that was equivalent for all the housekeeping genes at all dilutions, indicating a stable expression that was unaffected by treatment conditions. The MFI values for the heat shock genes *Hspa1a/b*, *Hspb1* and *Dnajb1* also followed a linear regression with different slopes in the lines corresponding to each treatment. Taking into consideration the optimisation parameters described, a 1:10 dilution was chosen as an acceptable dilution for tibialis anterior sample input.

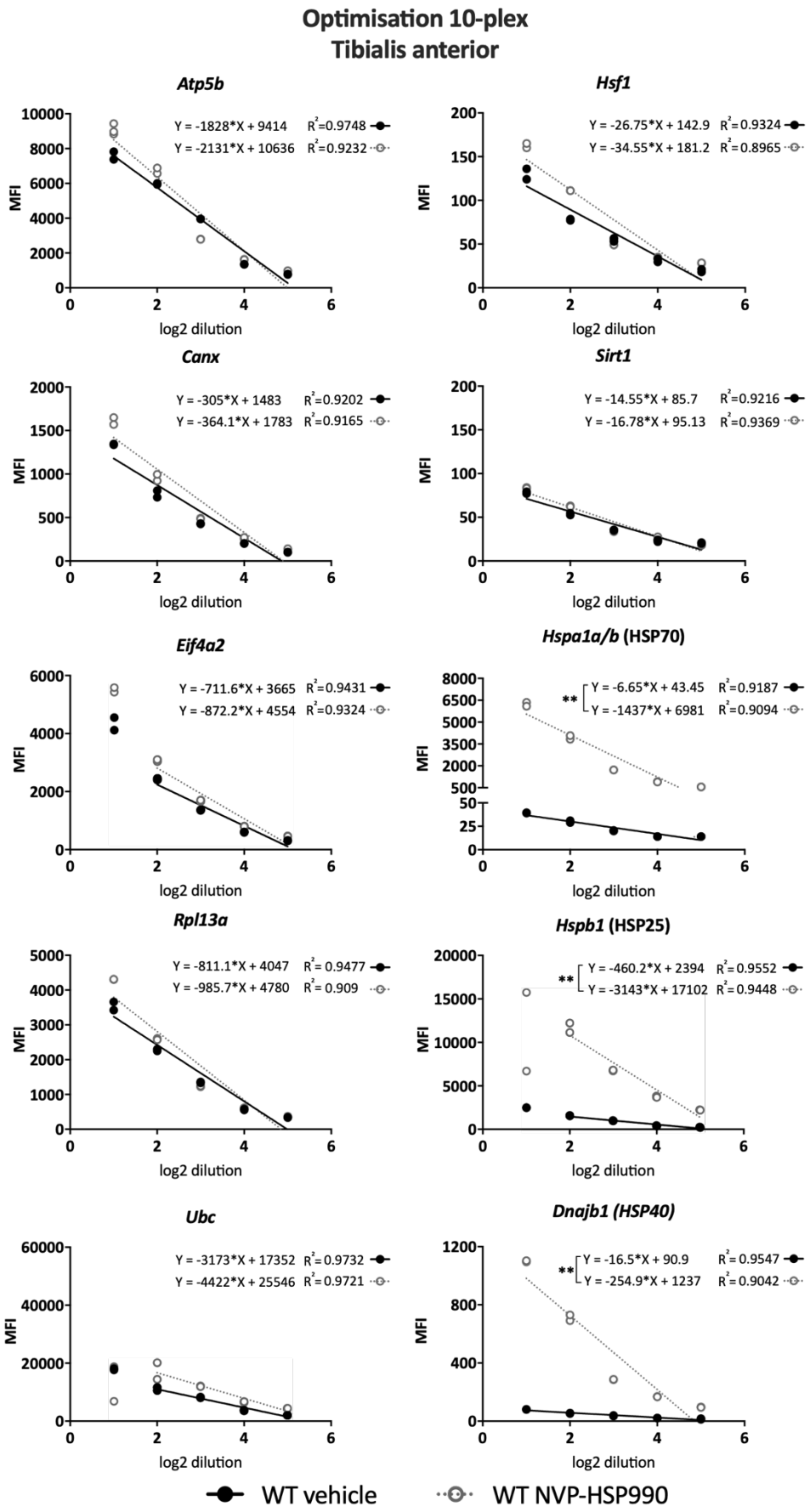
Optimisation 10-plex
Tibialis anterior
Atp5b
Y = -1828*X + 9414 R²=0.9748
Y = -2131*X + 10636 R²=0.9232
Hsf1
Y = -26.75*X + 142.9 R²=0.9324
Y = -34.55*X + 181.2 R²=0.8965
Canx
Y = -305*X + 1483 R²=0.9202
Y = -364.1*X + 1783 R²=0.9165
Sirt1
Y = -14.55*X + 85.7 R²=0.9216
Y = -16.78*X + 95.13 R²=0.9369
Eif4a2
Y = -711.6*X + 3665 R²=0.9431
Y = -872.2*X + 4554 R²=0.9324
Hspa1a/b (HSP70)
**
Y = -6.65*X + 43.45 R²=0.9187
Y = -1437*X + 6981 R²=0.9094
Rpl13a
Y = -811.1*X + 4047 R²= 0.9477
Y = -985.7*X + 4780 R²= 0.909
Hspb1 (HSP25)
**
Y = -460.2*X + 2394 R²= 0.9552
Y = -3143*X + 17102 R²= 0.9448
Ubc
Y = -3173*X + 17352 R²= 0.9732
Y = -4422*X + 25546 R²= 0.9721
Dnajb1 (HSP40)
**
Y = -16.5*X + 90.9 R²= 0.9547
Y = -254.9*X + 1237 R²= 0.9042
MFI
log2 dilution
WT vehicle
WT NVP-HSP990

Figure 3.4. Optimisation of sample input in the QuantiGene 10-plex assay for use with wild-type tibialis anterior.

Pools of tibialis anterior samples from either vehicle or NVP-HSP990 treated wild-type animals were prepared with samples at equivalent tissue mass / volume (10 mg / 300 μL), in 2-fold serial dilutions (n = 5 mice per treatment) and analysed in duplicate. MFI values detected for each dilution from vehicle or NVP-HSP990 samples are shown in the graphs. Assay linearity was calculated for each gene. Housekeeping genes (on the left side) maintain a stable expression between treatment groups. Heat shock genes Hspa1a/b, Hspb1 and Dnajb1 (on the right side) exhibit linear regression lines with significantly different slopes for each treatment group. WT = wild-type; MFI = median fluorescence intensity.

3.4 Validation of the QuantiGene methodology with the 10-plex assay and comparison to RT-qPCR

RT-qPCR is a robust quantitative method that has extensively been used for the analysis of the heat shock response, with a focus on the analysis of expression of major heat shock genes such as *Hspa1a/b* (HSP70), *Hspb1* (HSP25) or *Dnajb1* (HSP40) (Labbadia *et al*., 2011; Carnemolla *et al*., 2014; Neueder *et al*., 2017). This method involves the isolation of RNA from the samples as well as the reverse transcription to complementary DNA (cDNA), followed by amplification of this template cDNA with fluorescently-labelled primers. Due to its high sensitivity, it requires maximum accuracy and precision. Any errors during the steps in the preparation of the samples (e.g., leaving any trace of contamination in the RNA purification or imprecise loading of samples in the plates) may lead to issues like inhibition of the amplification reaction or inaccuracy in the quantification analysis (Bustin, 2002). Also, this methodology presents some limitations related to the number of targets that can be amplified per reaction, which depends on the chemistries of the fluorescence labelling technologies.

As presented in Table 3.1, QuantiGene methodology allows for the multiplexed measurement of gene expression of up to eighty RNA targets in each well, simultaneously and without requiring RNA isolation, reverse transcription or cDNA amplification. Unlike RT-qPCR, the detection of RNA targets is possible from the

homogenised samples directly. In RT-qPCR, the amplification reaction of the cDNA template produces a fluorescence signal proportional to the amount of DNA amplified. Instead, in QuantiGene, probes hybridise directly with the target sequences and, depending on the amount of RNA molecules present in the samples, the signal will be amplified based on the hybridisation.

Table 3.1. Comparison of technical characteristics between QuantiGene and RT-qPCR techniques for the analysis of gene expression

	RT- qPCR	***QuantiGene***
Amplification technology	TaqMan, SYBR-Green, etc. (specific to suppliers)	Branched-DNA hybridisation
RNA extraction and reverse transcription	Both required	Not required; direct detection of RNA targets from homogenates
Number of gene targets per well / reaction	Up to five genes / reaction (if optimised)	Up to eighty genes / reaction simultaneously
Workflow	Requires maximum accuracy and longer processing time	Simple workflow, ELISA-like protocol over 2 days

In order to validate the QuantiGene methodology for the study of the expression of the heat shock genes after pharmacological induction with NVP-HSP990, a comparison of results obtained by QuantiGene and by RT-qPCR was carried out with samples obtained from the same mice.

The brain hemispheres and tibialis anterior tissues previously collected from wild-type mice at 9 weeks of age, were used for the QuantiGene validation experiment. The homogenised samples from vehicle and treated animals were diluted at the selected dilutions after the QuantiGene optimisation (1:9 dilution for brain and 1:10

dilution for tibialis anterior) and, after analysis, the results were compared to those initially obtained by RT-qPCR from the same animals (Figure 3.1).

The housekeeping genes *Atp5b*, *Canx*, *Rpl13a* and *Eif4a2* were considered as reference to calculate the GeoMean and then normalise the expression of the heat shock genes, *Hsf1* and *Sirt1*. As observed in Figure 3.5, both QuantiGene and RT-qPCR techniques provided comparable results for the expression of all genes of interest. Therefore, this validated the QuantiGene methodology as suitable for the measurement of expression levels of heat shock genes after pharmacological induction of the heat shock response with NVP-HSP990.

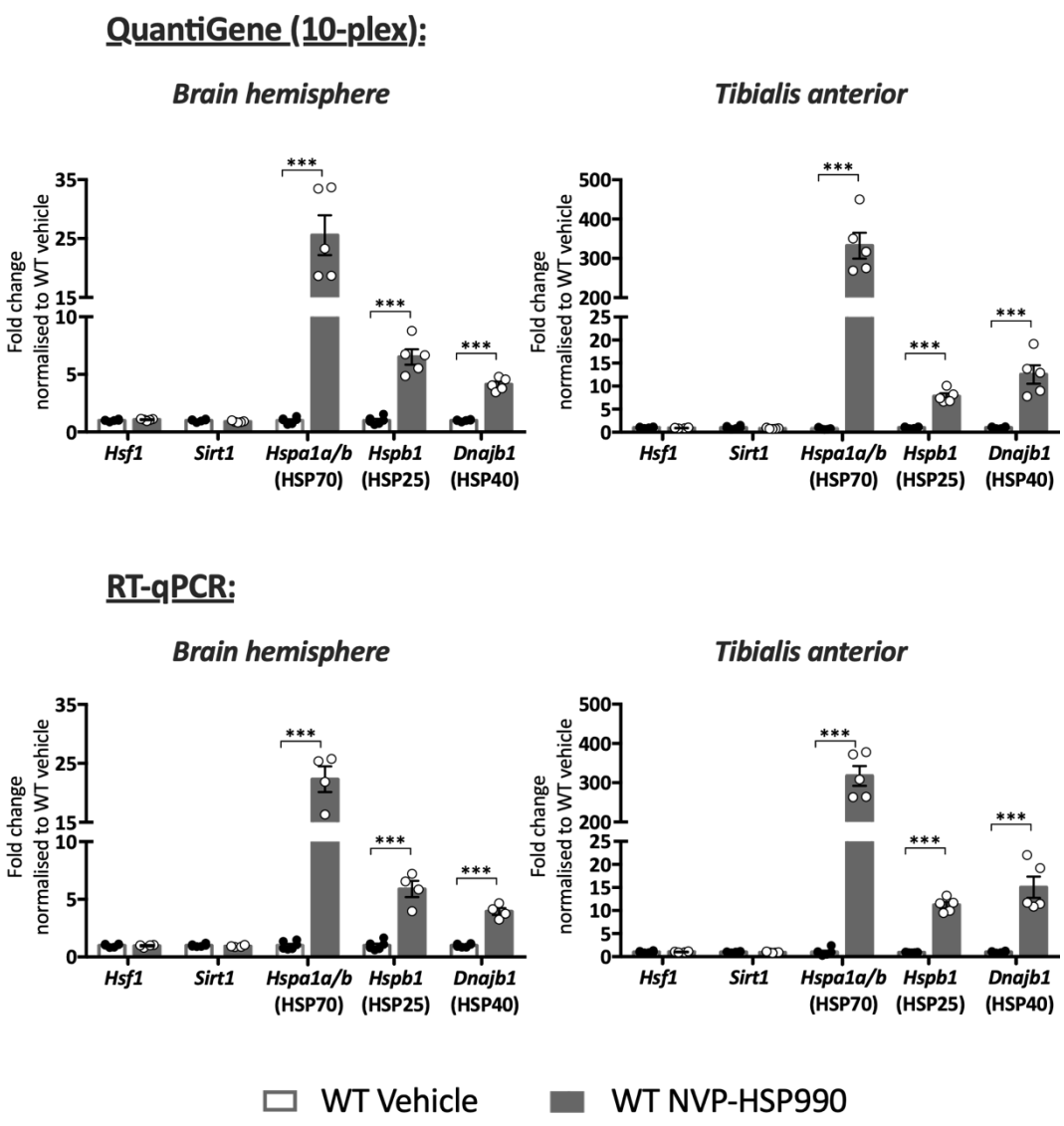

Figure 3.5. Validation of the QuantiGene methodology (10-plex assay) to measure the expression of heat shock genes in mouse brain hemispheres and tibialis anterior after NVP-HSP990 treatment.

The expression of Hsf1, Sirt1, Hspa1a/b (HSP70)*, Hspb1* (HSP25) *and Dnajb1* (HSP40) *after NVP-HSP990 treatment was analysed in brain hemispheres from wild-type mice by QuantiGene (top) and RT-qPCR (bottom), as compared to vehicle. NVP-HSP990 treatment resulted in an increased expression of Hspa1a/b* (HSP70), *Hspb1* (HSP25) *and Dnajb1* (HSP40) *and not of Hsf1 or Sirt1. No differences in the gene expression levels were found between QuantiGene and RT-qPCR. N = 4 - 6 mice per treatment. Statistical analysis was by unpaired Student's t-test. Mean ± SEM. *** p ≤ 0.001. WT = wild-type.*

3.5 Kinetics of the pharmacological induction of the heat shock response with NVP-HSP990

Previous studies assessing the activation of the heat shock response after administration of NVP-HSP990 measured the levels of heat shock genes up to 4 hours or 8 hours after dosing (Labbadia *et al*., 2011; Neueder *et al*., 2017). To corroborate that the time point of tissue collection after dosing corresponded to the highest level of pharmacological induction, a kinetic assessment was conducted. Wild-type mice with a (CBA/Ca x C57BL/6J)F1 background strain were dosed with a single administration of NVP-HSP990 at 12 mg / kg concentration and then brain hemispheres were collected at 4, 8, 12, 16 or 20 hours after treatment (*n* = 4 mice per treatment and per time point).

Brain hemispheres were homogenised and processed for analysis with QuantiGene 10-plex assay at a 1:9 dilution, as optimised (Figure 3.3). The peak of gene expression for *Hspa1a/b* was reached at 4 hours after dosing, and 4 to 8 hours after dosing for *Hspb1* and *Dnajb1* (Figure 3.6). Afterwards, the levels of expression progressively decreased and reached baseline levels by 16 to 20 hours after administration of NVP-HSP990. Although, as observed in the Figure 3.6, the kinetics of the pharmacological induction did not occur at a similar rate for all the heat shock genes studied, 4 hours was selected as an adequate time point for tissue collection after treatment for the following dosing experiments.

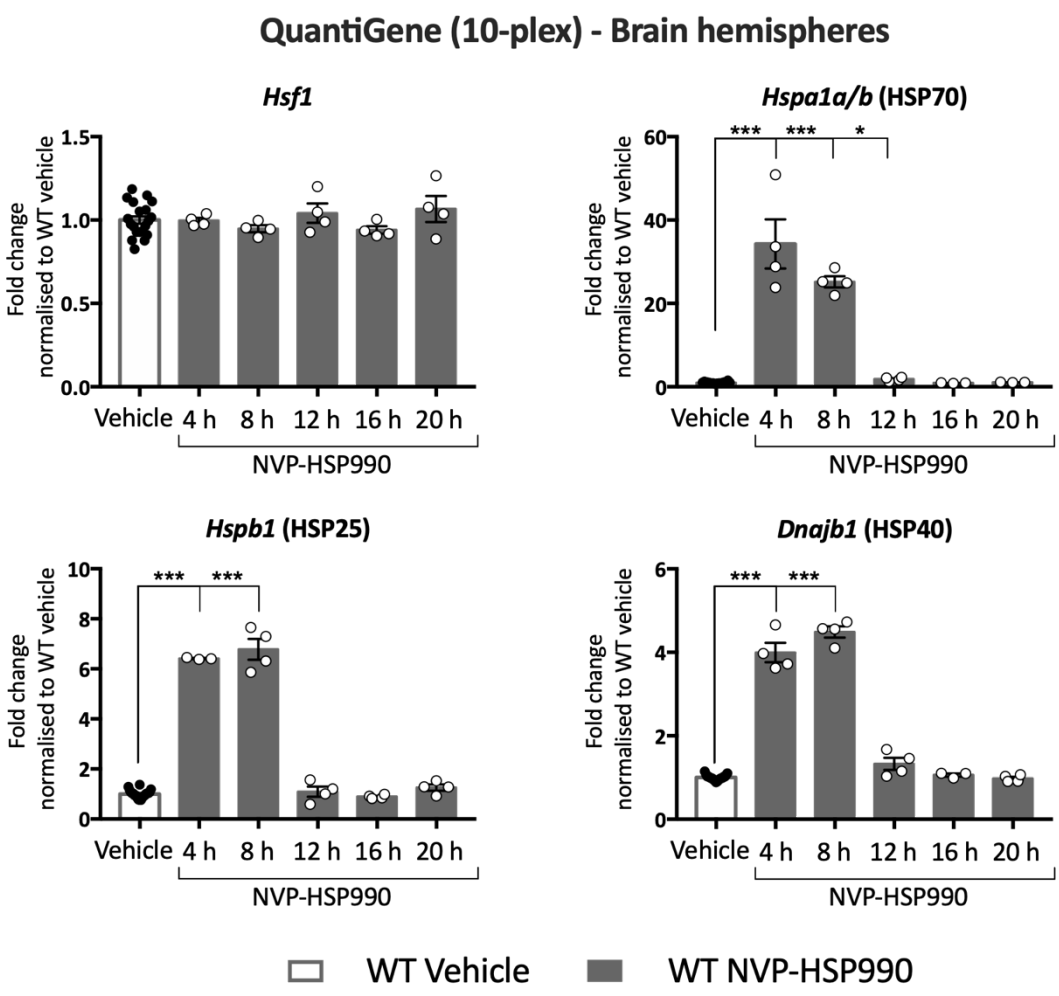

Figure 3.6. Kinetics of the pharmacological induction of the heat shock response after NVP-HSP990 treatment.

Hsf1, Hspa1a/b (HSP70), *Hspb1*(HSP25) *and Dnajb1* (HSP40) *expression levels in brain hemispheres from wild-type mice were measured by QuantiGene 10-plex assay after treatment with vehicle or NVP-HSP990 and tissue collection at 4, 8, 12, 16 and 20 hours post-dosing. For simplicity, all the vehicle samples from each time point for every gene were plotted together in the graphs. A significant increase in the expression of the heat shock genes was found by 4 hours after dosing with NVP-HSP990 and remained until 8 hours post-dosing. By 12 hours after dosing, the expression level of the heat shock genes had declined to baseline levels. N = 3 -4 mice per treatment and per time point. Statistical analysis was by unpaired Student's t-test. Mean ± SEM. *** p value ≤ 0.001; * p value ≤ 0.05. WT = wild-type; h = hours.*

3.6 Design and optimisation of a QuantiGene 20-plex assay

In order to gain a wider perspective on the study of heat shock response, a more extensive QuantiGene multiplex assay (20-plex) was designed, that contained the heat shock genes: *Dnaja1* (HSP40), *Dnaja3* (HSP40), *Dnajb1* (HSP40), *Dnajb5* (HSP40), *Hspb1* (HSP25), *Hspb6* (HSP20), *Hspa1a/b* (HSP70), *Hspa9* (HSP70), *Hspd1* (HSP60), *Hspe1* (HSP10), *Hsph1* (HSP110), *Hsp90aa1* (HSP90) and *Hsp90ab1* (HSP90), regulators *Hsf1* and *Sirt1* and five housekeeping genes (see Table 2.4 in Chapter 2 for details). The selection of these heat shock genes was based on previous microarray and RNA-Seq data (Labbadia *et al*., 2011; Neueder *et al*., 2017) and the validation of the QuantiGene 10-plex assay. A similar optimisation protocol as that described for the 10-plex assay was followed to determine the optimal dilution for sample input in mouse brain hemispheres and tibialis anterior tissues.

3.6.1 Optimisation of QuantiGene 20-plex assay for use with mouse brain hemispheres

Independent pools of brain hemisphere samples (coming from the initial dosing experiment in wild-type mice at 9 weeks of age), at an equivalent tissue mass / volume (10 mg / 300 µL), were prepared in a 2-fold dilution series.

All the genes included in this plex assay adjusted more closely into a linear regression from 1:4 dilution, as shown in Figures 3.7, 3.8, 3.9. The housekeeping genes *Atp5b*, *Canx*, *Rpl13a* and *Eif4a2* maintained a stable expression between treatment groups and followed a decrease of MFI signal proportional to the 2-fold dilution series (Figure 3.7). *Eif4a2* showed signs of saturation at the initial 1:2 dilution. When evaluating the MFI values and the linear regression lines for the genes of interest, in most cases, there were significant differences in the slopes, and this corresponded to the effect of NVP-HSP990. However, the heat shock genes *Dnaja3, Dnajb5* (Figure 3.8), *Hspa9* and *Hspb6* (Figure 3.9) presented linear regression lines with comparable slopes and similar MFI values at all the dilutions tested for both treatment groups. This may be indicating a lack or reduced effect of NVP-HSP990 treatment on the induction of expression of these genes.

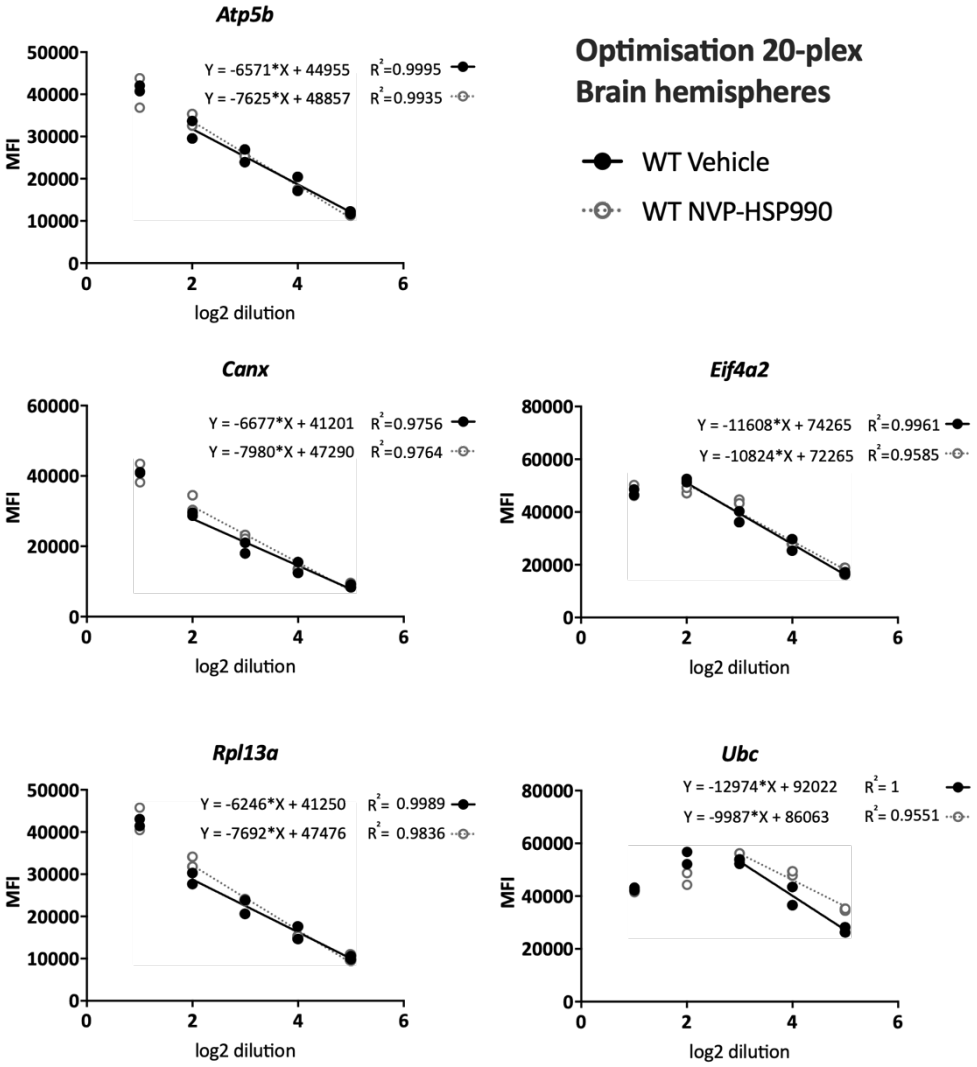

Figure 3.7. Optimisation of sample input in the QuantiGene 20-plex assay (housekeeping genes) for use with wild-type brain hemispheres.

Brain hemisphere samples from either vehicle or NVP-HSP990 treated wild-type mice at equivalent tissue mass / volume (10 mg / 300 µL) were pooled, prepared in 2-fold serial dilutions (n = 5 - 6 mice per treatment) and analysed in duplicate. MFI values detected for each dilution from vehicle or NVP-HSP990 samples are shown in the graphs and linearity was calculated for each housekeeping gene. Eif4a2 and Ubc show a saturated signal at the 1:2 dilutions. All the genes maintained a stable expression between treatment groups, with exception of Ubc. WT = wild-type; MFI = median fluorescence intensity.

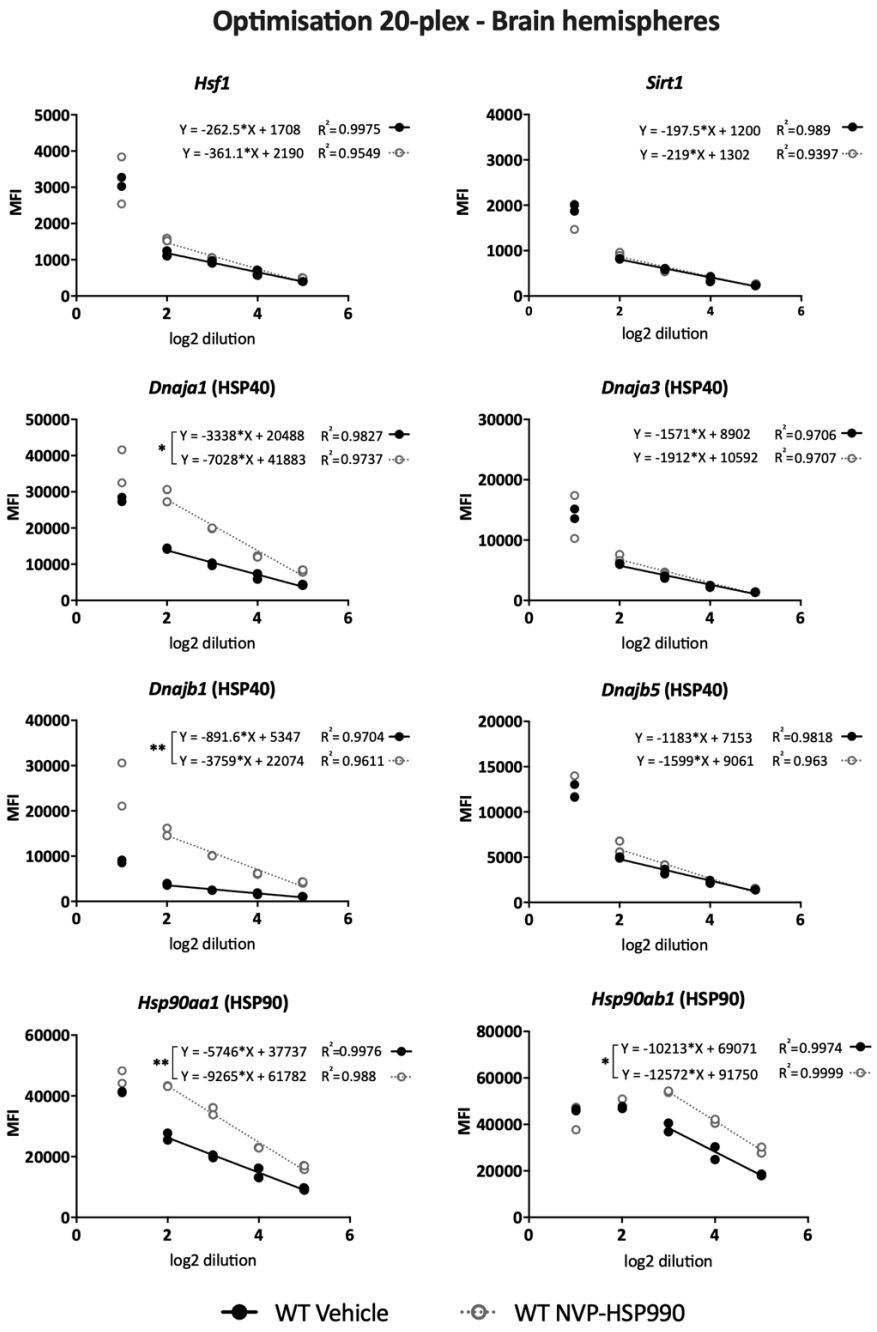

Figure 3.8. Optimisation of sample input of the QuantiGene 20-plex assay for use in wild-type brain hemispheres (heat shock genes).

Brain hemisphere samples from either vehicle or NVP-HSP990 treated wild-type mice at equivalent tissue mass / volume (10 mg / 300 µL) were pooled, prepared in 2-fold serial dilutions (n = 5 - 6 mice per treatment) and analysed in duplicate. MFI values detected for each dilution from vehicle or NVP-HSP990 samples are shown in the graphs and linearity was calculated for each gene of interest. Hsp90ab1 showed signs of signal saturation at the 1:2 dilution. The heat shock genes had linear regression lines with different slopes for each treatment, with exception of Dnaja3 and Dnajb5. WT = wild-type; MFI = median fluorescence intensity.

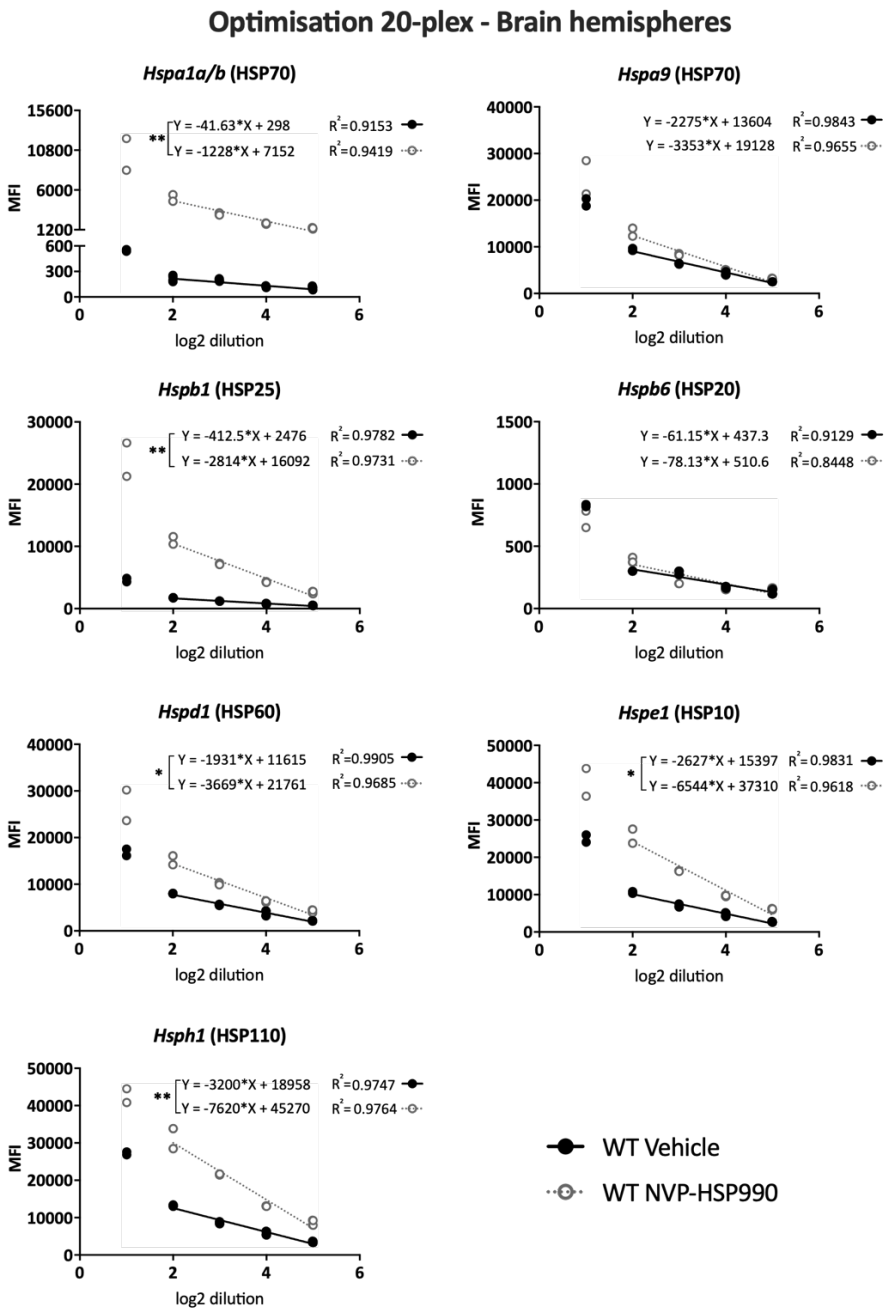

Figure 3.9. Optimisation of sample input of the QuantiGene 20-plex assay for use in wild-type brain hemispheres (heat shock genes).

Brain hemisphere samples from either vehicle or NVP-HSP990 treated wild-type mice at equivalent tissue mass / volume (10 mg / 300 µL) were pooled, prepared in 2-fold serial dilutions (n = 5 - 6 mice per treatment) and analysed in duplicate. MFI values detected for each dilution from vehicle or NVP-HSP990 samples are shown in the graphs and linearity was calculated for each gene of interest. The heat shock genes had linear regression lines with different slopes for each treatment, with exception of Hspa9 and Hspb6. WT = wild-type; MFI = median fluorescence intensity.

3.6.2 Optimisation of QuantiGene 20-plex assay for use with mouse tibialis anterior muscle

A 3-fold dilution series was prepared containing tibialis anterior samples from wild-type mice treated with either vehicle or NVP-HSP990.

A close analysis of the MFI values and linearity of the assay indicated that, similar to what was reported in brain hemispheres, the linear regression was more closely achieved from 1:9 dilution for all the genes included in the assay. Some variability in the expression between treatment groups was exhibited by *Ubc*, as previously (Figure 3.10), and *Canx*. Consistent with what was observed in the brain hemisphere with this 20-plex assay, no evidence of differential expression between treatment groups was found for the heat shock genes *Dnaja3, Dnajb5* (Figure 3.11), *Hspa9* or *Hspb6* (Figure 3.12).

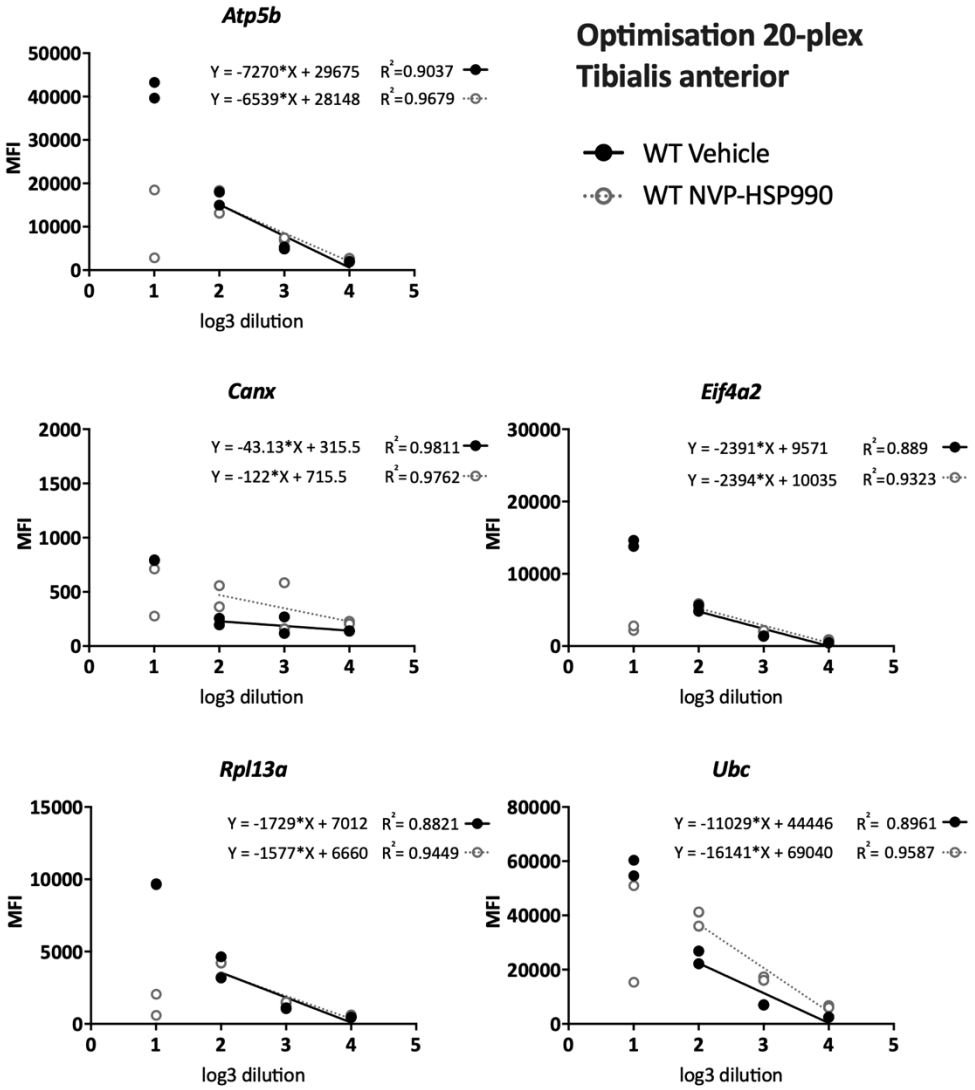

Figure 3.10. Optimisation of sample input of the QuantiGene 20-plex assay (housekeeping genes) for use in wild-type tibialis anterior.

Tibialis anterior samples from either vehicle or NVP-HSP990 treated wild-type mice at equivalent tissue mass / volume (10 mg / 300 μL) were pooled, prepared in 3-fold serial dilutions (n = 5 - 6 mice per treatment) and analysed in duplicate. MFI values detected for each dilution from vehicle or NVP-HSP990 samples are shown in the graphs and linearity was calculated for each housekeeping gene. Atp5b and Ubc show a saturated signal at the 1:3 dilutions. All genes maintain a stable expression between treatment groups, with exception of Ubc and Canx. WT = wild-type; MFI = median fluorescence intensity.

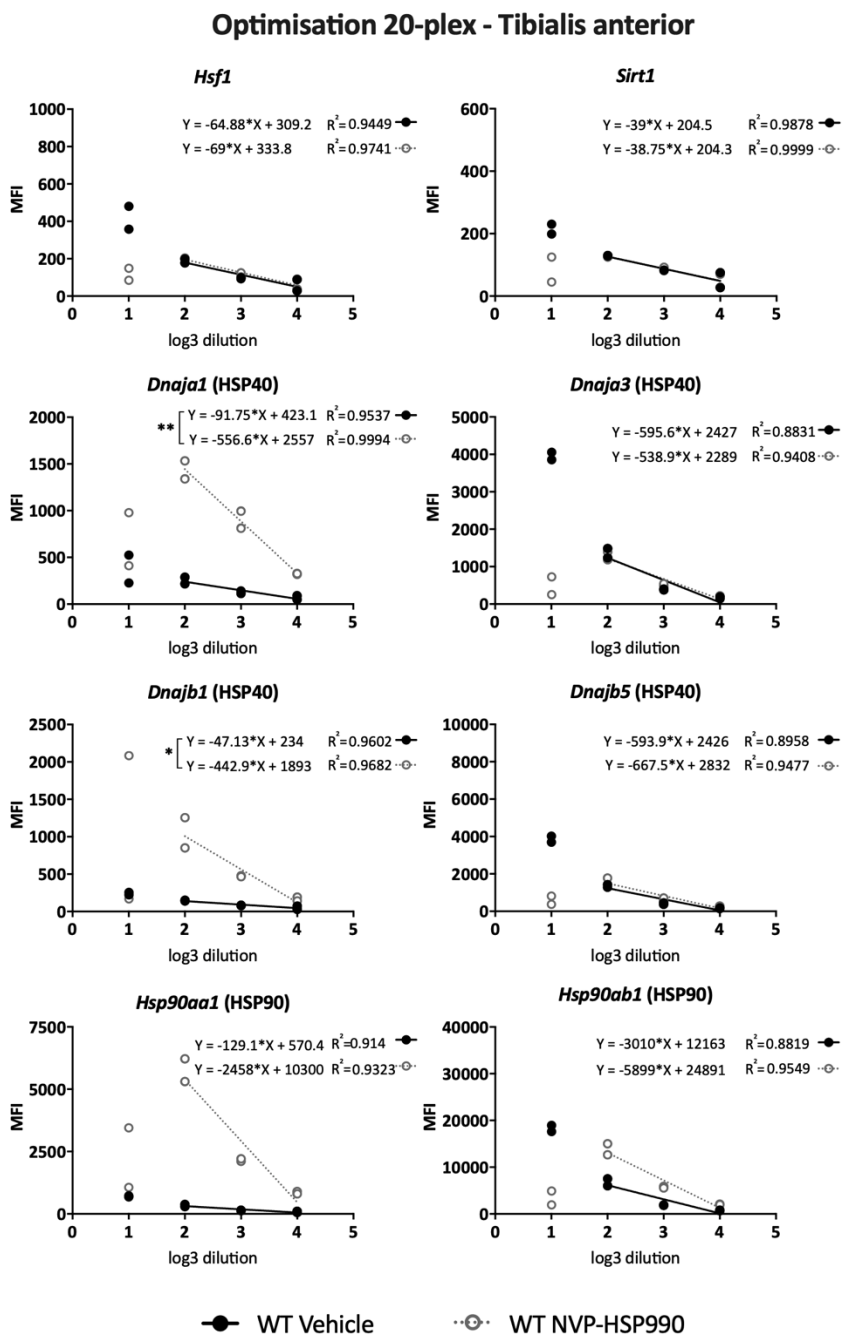

Figure 3.11. Optimisation of sample input of the QuantiGene 20-plex assay for use in wild-type tibialis anterior (heat shock genes).

Tibialis anterior samples from either vehicle or NVP-HSP990 treated wild-type mice at equivalent tissue mass / volume (10 mg / 300 µL) were pooled, prepared in 3-fold serial dilutions (n = 5 - 6 mice per treatment) and analysed in duplicate. MFI values detected for each dilution from vehicle or NVP-HSP990 samples are shown in the graphs and linearity was calculated for each gene of interest. The heat shock genes had linear regression lines with different slopes for each treatment, with exception of Dnaja3 and Dnajb5. WT = wild-type; MFI = median fluorescence intensity.

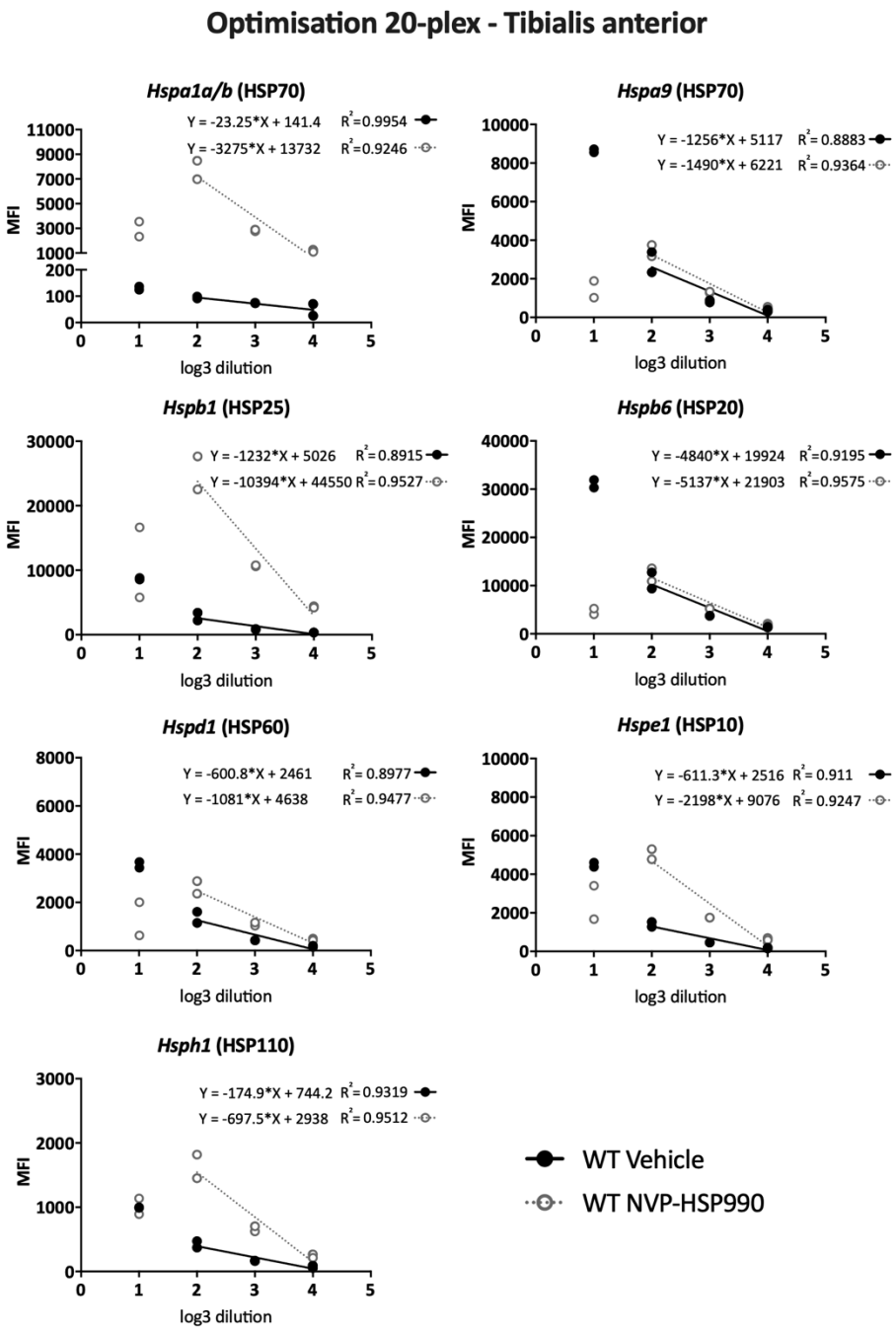

Figure 3.12. Optimisation of sample input of the QuantiGene 20-plex assay for use in wild-type tibialis anterior (heat shock genes).

Tibialis anterior samples from either vehicle or NVP-HSP990 treated wild-type mice at equivalent tissue mass / volume (10 mg / 300 µL), were pooled, prepared in 3-fold serial dilutions (n = 5 - 6 mice per treatment) and analysed in duplicate. MFI values detected for each dilution from vehicle or NVP-HSP990 samples are shown in the graphs and linearity was calculated for each gene of interest. The heat shock genes had linear regression lines with different slopes for each treatment, with exception of Hspa9 and Hspb6. WT = wild-type; MFI = median fluorescence intensity.

3.7 Design of a QuantiGene 18-plex assay

The heat shock genes *Dnaja3* (HSP40)*, Dnajb5* (HSP40)*, Hspa9* (HSP70)*, Hspb6* (HSP20) included in the 20-plex assay were not showing clear signs of induction after treatment with NVP-HSP990, and MFI values in QuantiGene were comparable to those obtained in vehicle samples. This was consistently found in all the serial dilutions tested and both in brain hemispheres and tibialis anterior. For this reason, a new QuantiGene multiplex assay was designed where these four aforementioned genes were excluded. Two additional housekeeping genes were included in the new plex: *Sdha* and *Gapdh*, also reported as stable to be employed as reference genes in the context of HD (Benn *et al*., 2008). The details on the 18-plex designed regarding all the genes included as well as accession numbers and probe regions can be found in Table 2.5 in Chapter 2. This QuantiGene 18-plex assay was used in all the subsequent RNA-based experiments.

3.8 Summary of results and discussion

The boost of protein folding by a coordinated upregulation of multiple heat shock proteins has been proposed as a promising therapeutic approach in the study of protein conformational diseases such as HD (Muchowski and Wacker, 2005; Calamini and Morimoto, 2012; Reis *et al*., 2017; Bose and Cho, 2017). The use of pharmacological compounds to induce the heat shock response via HSF1 activation has been reported in several models of neurodegeneration with variable results (Sittler *et al.,* 2001; Fujikake *et al.,* 2008; Hay *et al.,* 2004; Waza *et al.,* 2005; Neef *et al.,* 2010; Katsuno *et al.,* 2005; Auluck *et al.,* 2005). The HSP90 inhibitors are a type of pharmacological compound that can achieve this purpose. Through their mechanism of action, HSP90 inhibitors release HSF1 from the repressive action by HSP90 inhibitory complex and subsequently lead to the transcriptional activation of the heat shock genes. In the present study, the HSP90 inhibitor NVP-HSP990 has been administered *in vivo* to mice to elicit the activation of the heat shock response. Unlike other HSP90 inhibitors that have reported issues related to toxicity or difficulties in formulation, administration or permeability (Neckers and Workman, 2012), NVP-HSP990 is orally available, brain penetrant and well-tolerated (Menezes *et al.,* 2012).

Previous studies in our group have provided evidence of a potent *in vivo* induction in the expression of the heat shock genes after treatment with NVP-HSP990 (Labbadia *et al*., 2011; Carnemolla *et al*., 2014; Neueder *et al.,* 2017). The experiment illustrated in Figure 3.1 in this Chapter 3 reiterated this effective induction, confirming NVP-HSP990 as a useful tool in the study of the heat shock response.

RT-qPCR has generally been the method of choice for the quantitative analysis of gene expression. Although a highly sensitive and reliable method, RT-qPCR methodology is labour-intensive and, also, presents some challenges, such as the biases or errors associated with the RNA purification and reverse transcription processes that are required for RT-qPCR (Bustin, 2002). With a more simplified protocol and the advantage of detecting multiple transcripts simultaneously and directly from the sample homogenates, QuantiGene appeared as an appropriate methodology to explore for the purposes of the study of the large set of genes implicated in the heat shock response. A QuantiGene assay containing the probes to detect three major heat shock genes, *Hsf1* and *Sirt1* (10-plex assay) was initially designed to understand and validate the methodology for the research aims. A comparison of the results obtained by both QuantiGene and RT-qPCR was conducted using brain hemispheres and tibialis anterior tissues from wild-type mice that had received a dose of NVP-HSP990 or vehicle.

Both RT-qPCR and QuantiGene yielded comparable results (Figure 3.5), demonstrating that QuantiGene methodology was suitable for the detection and reliable analysis of the expression of heat shock genes and regulators of the heat shock response, after pharmacological induction with NVP-HSP990 compound.

QuantiGene 10-plex assay was also used to assess the kinetics of induction after treatment with NVP-HSP990. Previous studies had already pointed out that at 2, 4 and 8 hours post-dosing there was a potent enhancement of expression for the *Hspa1a/b* (HSP70), *Hspb1* (HSP25) and *Dnajb1* (HSP40) genes (Labbadia *et al*., 2011). The magnitude of induction was evaluated with the QuantiGene assay at 4, 8, 12, 16 and 20 hours after dosing in brain hemispheres from wild-type mice. This experiment

confirmed that 4 hours was a peak of induction for the major heat shock genes studied and an adequate time point for harvesting tissues for analysis (Figure 3.6). However, in contrast to *Hspa1a/b*, *Hspb1* and *Dnajb1* seemed to reach the maximal level of induction by 8 hours, with a decline by 12 hours after dosing. This may indicate that, after NVP-HSP990 treatment, the patterns of transcriptional activation of the heat shock genes in brain tissues do not occur at the same time or speed, which may also be applicable to other tissues and would require further evaluation. This aspect would need to be taken into consideration when drawing conclusions from future RNA-based experiments involving the administration of NVP-HSP990, as the peak of induction of all the heat shock genes may not be reached at a single time point of analysis.

In the interest of gaining a wider perspective on the study of the heat shock response at a transcriptional level, another QuantiGene multiplex assay (20-plex) was designed that included thirteen heat shock genes from several families, *Hsf1*, *Sirt1* and housekeeping genes. As for the 10-plex assay, this was optimised to determine the optimal sample input by performing a serial dilution of samples from each treatment group. The MFI values detected for each dilution in each treatment should decrease proportionally to the fold change of the dilution and fit to a linear regression.

After close evaluation of the MFI values and the linearity range, *Dnaja3* (HSP40)*, Dnajb5* (HSP40)*, Hspa9* (HSP70) and *Hspb6* (HSP20) did not exhibit linear regression lines with different slopes between vehicle or NVP-HSP990 treatments in either brain or tibialis anterior (Figures 3.8, 3.9, 3.11, 3.12). *Dnaja3, Dnajb5, Hspa9, and Hspb6* were chosen to be included in the assay based on previous RNA-Seq and microarray data (Labbadia *et al.,* 2011; Neueder *et al.,* 2017); and some of these have been reported as potential therapeutic targets or protective factors in neurodegeneration and other diseases (Edwards *et al*., 2011; Li *et al*., 2017; Zarouchlioti *et al*., 2017; Finka *et al*., 2015). However, the MFI values observed for these genes for each dilution in the NVP-HSP990 group were relatively similar to those observed in vehicle counterparts, suggesting that they were not induced by NVP-HSP990 or, possibly,

that the transcriptional activation occurs at a time point later than 4 hours post dosing.

In summary, the experiments included in this Chapter have provided two main conclusions. First, the confirmation of the efficacy of NVP-HSP990 as a potent pharmacological inducer of the heat shock response *in vivo* in mice and a further understanding on the kinetics of this pharmacological induction. Second, the validation of the QuantiGene methodology and establishment of assays to use for the simultaneous measurement of expression of a large set of heat shock genes and regulators of the heat shock response, after treatment with NVP-HSP990. These provide the main tools to investigate the activation of the heat shock response in the context of HD, as covered in Chapter 4 and Chapter 5 of this thesis.

Chapter 4. Analysing the impairment of the heat shock response in Huntington's disease mouse models

4.1 Introduction

Due to the features of Huntington's disease as an expanded repeat disorder where an aberrantly long polyQ tract in the HTT protein leads to protein aggregation and the formation of insoluble deposits within cells, the heat shock response has been a preferential target of study as a potential therapeutic approach. This has been covered in more detail in the Introduction (Chapter 1).

The coordinated upregulation of heat shock genes and proteins via HSF1 activation has been proposed as a promising avenue to explore, with varied results in the amelioration of the aggregation toxicity in different models of polyQ disease (Waza *et al.,* 2005; Sittler *et al.,* 2001; Fujimoto *et al*., 2005; Fujikake *et al*., 2008). Previous studies of the heat shock response in HD mouse models have used R6/2 mice, which are transgenic for a copy of the exon 1 of the human *HTT* gene (Mangiarini *et al*., 1996), and *Hdh*Q150, which express an expanded repeat of around 150 CAGs inserted in the endogenous *Htt* gene (Lin *et al*., 2001). Labbadia *et al*. (2011), provided evidence of an impaired heat shock response in both models that was correlated with disease progression. Even though a mild improvement in motor phenotypes and reduction of aggregation load could be observed in R6/2 mice during a weekly, dose-escalated treatment with NVP-HSP990 compound, these were not long-lasting effects. As disease worsened, the capacity to elicit a heat shock response was diminished in these mice. However, an impairment in the induction of the heat shock response had not been demonstrated in the zQ175 knock-in model, another extensively used HD mouse model in which mouse *Htt* exon 1 has been replaced with a mutated version of human exon 1 *HTT* (Heikkinen *et al*., 2012; Menalled *et al*., 2012).

A decreased HSF1 availability in the cell, caused by the disease pathology, has been hypothesised as an explanation for the disrupted protein quality control in HD patients and models, including zQ175 mice (Gomez-Pastor *et al*., 2017). To clarify

this, the HSF1 protein expression was quantified in different zQ175 tissues, as shown in the last sections of this Chapter.

This chapter set out to address the following:

1. Determine whether the heat shock response is impaired at the transcript level in brain hemispheres from symptomatic zQ175 mice and compare this to the impairment previously observed in the R6/2 and *Hdh*Q150 models (Labbadia *et al.,* 2011).
2. Optimise the QuantiGene 18-plex assay to determine the working dilutions for brain hemispheres, tibialis anterior, striatum and cortex from zQ175 and R6/2 mice.
3. Extend the analysis of the heat shock response in brain hemispheres to tibialis anterior, striatum and cortex of zQ175 as well as R6/2 by the QuantiGene 18-plex assay, to compare the pattern of impairment between these two widely used HD mouse models.
4. As a potential driving mechanism of heat shock response impairment, study whether HSF1 protein levels are dysregulated in the brain hemispheres, tibialis anterior, striatum and cortex of zQ175 mice and compare this to previous data obtained in the R6/2 and *Hdh*Q150 models (Labbadia *et al.,* 2011).

4.2 Comparative analysis of the heat shock response in brain hemispheres of zQ175, *Hdh*Q150 and R6/2 at late stages of the disease

The impairment in the induction of the heat shock response at the transcript level had been previously analysed in brain tissues of HD mouse models (Labbadia *et al.,* 2011). In that study, after NVP-HSP990 treatment, the expression levels of major heat shock genes *Hspa1a/b* (HSP70), *Hspb1* (HSP25) and *Dnajb1* (HSP40) were measured in the brain hemispheres of R6/2 and *Hdh*Q150 mice at late-stage disease, corresponding to 12 weeks and 22 months of age, respectively (Lin *et al.,* 2001; Mangiarini *et al.,* 1996; Woodman *et al.,* 2007).

However, as stated before, a similar analysis had not been conducted for zQ175 mice. To resolve if an impaired induction of the heat shock response was occurring at the level of transcription, zQ175 mice and their wild-type counterparts at 12 months of age were treated with either NVP-HSP990 (12 mg / kg) or vehicle, and brain hemispheres were collected at 4 hours after dosing. At this age, zQ175 mice are at an early symptomatic stage in their HD phenotype (Heikkinen *et al.,* 2012; Menalled *et al.,* 2012). The following Table 4.1 summarises the study design for the zQ175 model as well as for the previous studies performed in R6/2 and *Hdh*Q150 mice (Labbadia *et al*., 2011).

Table 4.1. Summary of mice allocated for the analysis of the heat shock response in brain hemispheres of HD mouse models at late stages of disease.

	zQ175 Delta Neo	R6/2 *	HdhQ150 *
Age	12 months	12 weeks	22 months
N numbers	8 - 10 mice / genotype / treatment	4 mice / genotype / treatment	4 mice / genotype / treatment
Drug administration	Oral gavage		
Frequency of administration	Single administration		
Dissection time post-dosing	4 hours	2, 4 and 8 hours	
Tissues collected	Brain hemispheres		
Method of analysis	QuantiGene 18-plex assay (9 heat shock genes)	RT-qPCR (3 heat shock genes)	

*R6/2 and *Hdh*Q150 mice were dosed, dissected and the gene expression analysed by Labbadia *et al.,* (2011) (published).

Previous analysis of the heat shock response at the transcriptional level in brain hemispheres of R6/2 and *Hdh*Q150 mice had been done by RT-qPCR (Labbadia *et al.,* 2011). QuantiGene methodology, as explained in Chapter 3, allows for the measurement of multiple RNA targets simultaneously with a plex assay. After optimisation and evaluation of a 10-plex and 20-plex assay, a final 18-plex (Table 2.5 in Chapter 2) was designed that contained the probes to detect nine heat shock genes: *Hspa1a/b* (HSP70), *Dnaja1* (HSP40), *Dnajb1* (HSP40), *Hspb1* (HSP25), *Hspd1* (HSP60), *Hspe1* (HSP10*)*, *Hsph1* (HSP110), *Hsp90aa1* (HSP90α), *Hsp90ab1* (HSP90β), as well as *Hsf1*, *Sirt1* and reference genes *Atp5b*, *Canx*, *Eif4a2*, *Gapdh*, *Rpl13a* and *Sdha*. Although *Ubc* was included in the plex, it was not used as a housekeeping gene, in line with what was concluded in the Chapter 3.

Having established and validated the QuantiGene gene expression assays by a comparison with RT-qPCR (Figure 3.4), the zQ175 brain hemispheres collected 4 hours after dosing were set out to be analysed with the QuantiGene 18-plex assay.

4.2.1 Optimisation of the QuantiGene 18-plex assay for use with zQ175 and wild-type brain hemispheres at 12 months of age

As covered in Chapter 3, an optimal sample dilution needed to be determined for each tissue, genotype and/or experimental condition to be used with the QuantiGene plex assays. In the present study involving HD mouse models, it was particularly relevant to ensure the housekeeping genes were stably expressed between genotypes, as transcriptional dysregulation is a feature of HD mouse models (Benn *et al.,* 2008).

To determine the optimal sample dilution for brain hemispheres from NVP-HSP990 or vehicle treated wild-type and zQ175 mice, independent pools of brain samples at equal concentrations from each treatment group were prepared and subjected to a 2-fold dilution series.

As indicated in Figures 4.1 and 4.2, all the housekeeping genes (Figure 4.1) and genes of interest (Figure 4.2) followed a linear regression from the 1:4 dilution. The initial 1:2 dilution showed signs of instability or signal saturation, indicating that a further dilution of the sample was required. The housekeeping genes *Atp5b*, *Canx*, *Rpl13a*, *Eif4a2*, *Sdha* and *Gapdh* were stably expressed across genotypes and treatment groups, particularly from the 1:8 dilution onwards, with more similar MFI values. For the genes of interest, the different slopes between the linear regression lines corresponding to vehicle or NVP-HSP990 revealed that the expression of all the heat shock genes in the plex was upregulated by NVP-HSP990 treatment. Consequently, taking the optimisation parameters into consideration (section 3.3.1, Chapter 3), a 1:9 dilution was chosen for QuantiGene 18-plex analysis of brain hemispheres.

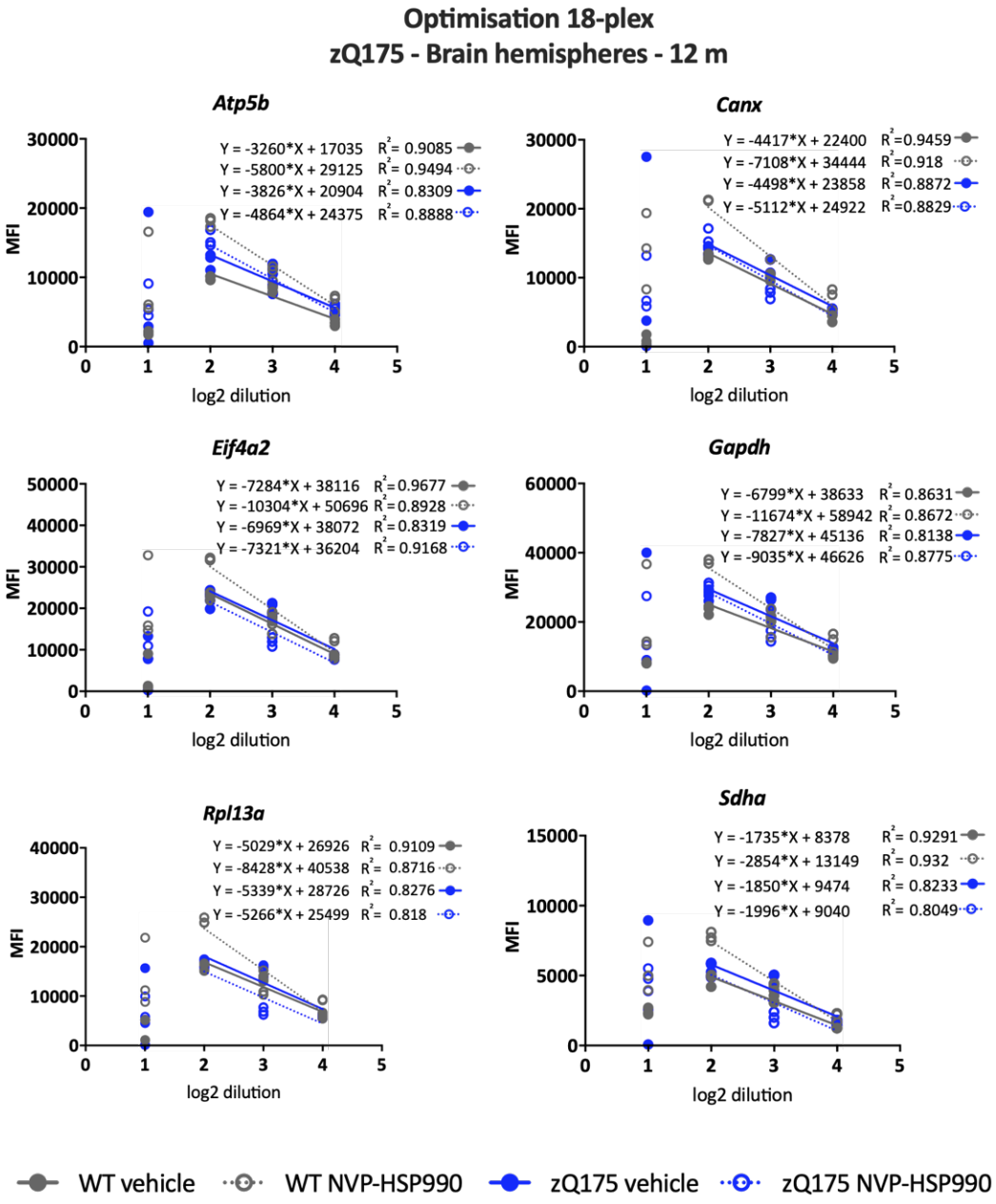

Figure 4.1. Optimisation of sample input in the QuantiGene 18-plex assay for use with zQ175 and wild-type brain hemispheres at 12 months of age (housekeeping genes).

Pools of brain hemisphere samples from zQ175 or wild-type mice (n = 8 - 10 mice / genotype / treatment), at equivalent tissue mass / volume (10 mg / 300 µL), were prepared in a 2-fold dilution series and analysed in triplicate. MFI values that were detected for each dilution from each treatment group are shown. Linear regression was analysed for each housekeeping gene. The initial dilutions (1:2 dilution) showed signs of an unstable or saturated signal. Although with slight differences, all the housekeeping genes maintained a stable expression, especially from 1:8 dilution, unaffected by genotype or treatment. WT = wild-type; MFI = median fluorescence intensity; m = months.

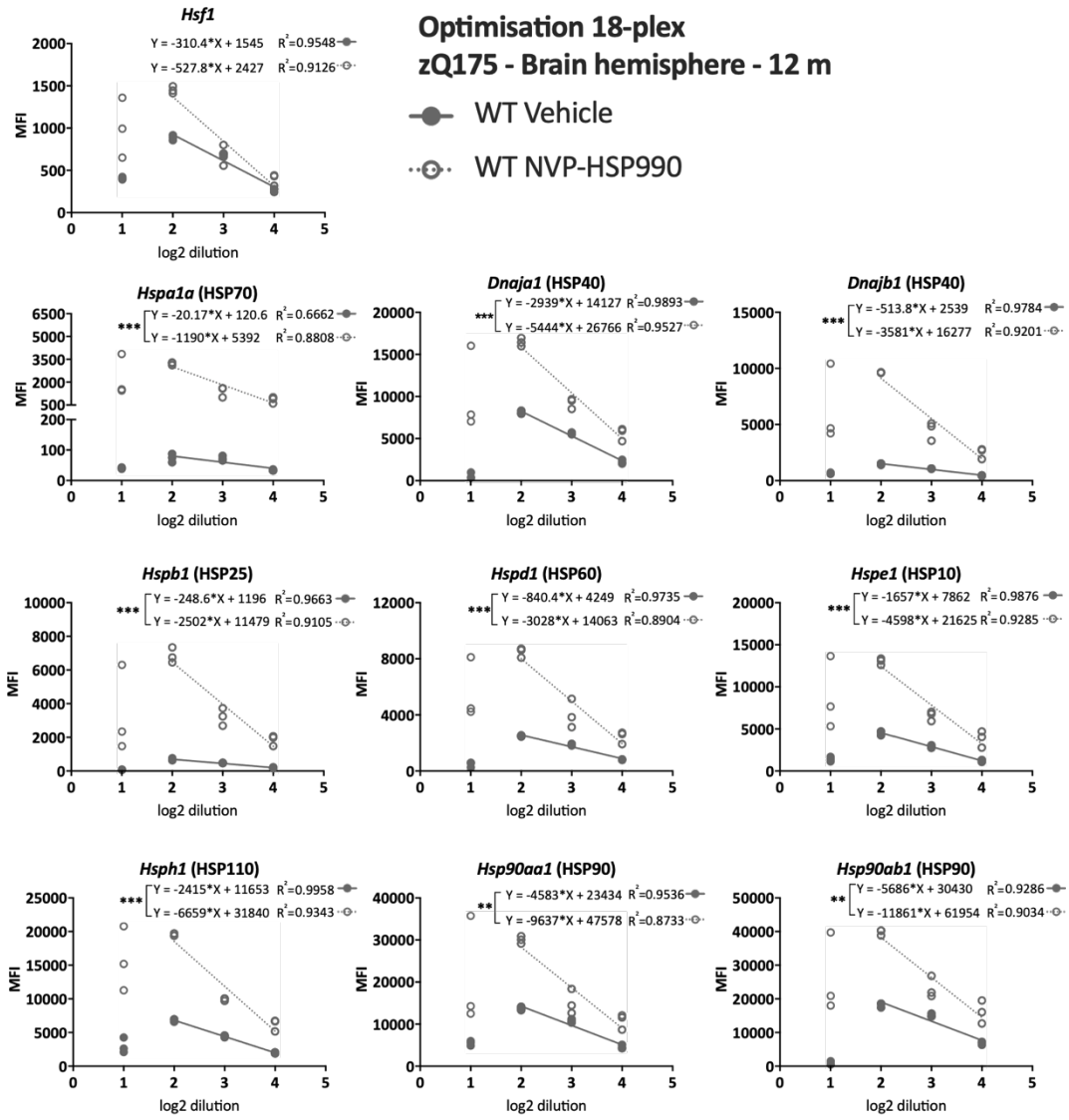

Figure 4.2. Optimisation of sample input in the QuantiGene 18-plex assay for use with zQ175 and wild-type brain hemispheres at 12 months of age (genes of interest).

*Pools of brain hemisphere samples from wild-type mice treated with vehicle or NVP-HSP990 (n = 8 mice / treatment), at equivalent tissue mass / volume (10 mg / 300 µL), were prepared in a 2-fold dilution series and analysed in triplicate. MFI values that were detected for each dilution from each treatment group are shown. Linear regression was analysed for each gene. The initial dilutions (1:2 dilution) showed signs of an unstable or saturated signal. In all cases, the heat shock genes had linear regression lines with significantly different slopes for each treatment group. *** $p \leq 0.001$; ** $p \leq 0.01$. WT = wild-type; MFI = median fluorescence intensity; m = months.*

4.2.2 Analysis of the heat shock response in the brain hemispheres of zQ175 mice and comparison to the impairment observed in R6/2 and *Hdh*Q150

At 12 months of age, as measured by QuantiGene, a significant decrease in the induction of *Hspa1a/b*, *Hspb1* and *Dnajb1* was found in zQ175 brain hemispheres, which presented similarities to the lower induction of these genes in R6/2 and *Hdh*Q150, as analysed by RT-qPCR (Figure 4.3; Labbadia *et al*., 2011). With the QuantiGene 18-plex assay, this impaired induction was also detected in *Dnaja1*, *Hspe1*, *Hsph1*, *Hsp90aa1* and *Hsp90ab1* genes (Figure 4.4), thus indicating a clear dysregulation of the heat shock response in zQ175 brains.

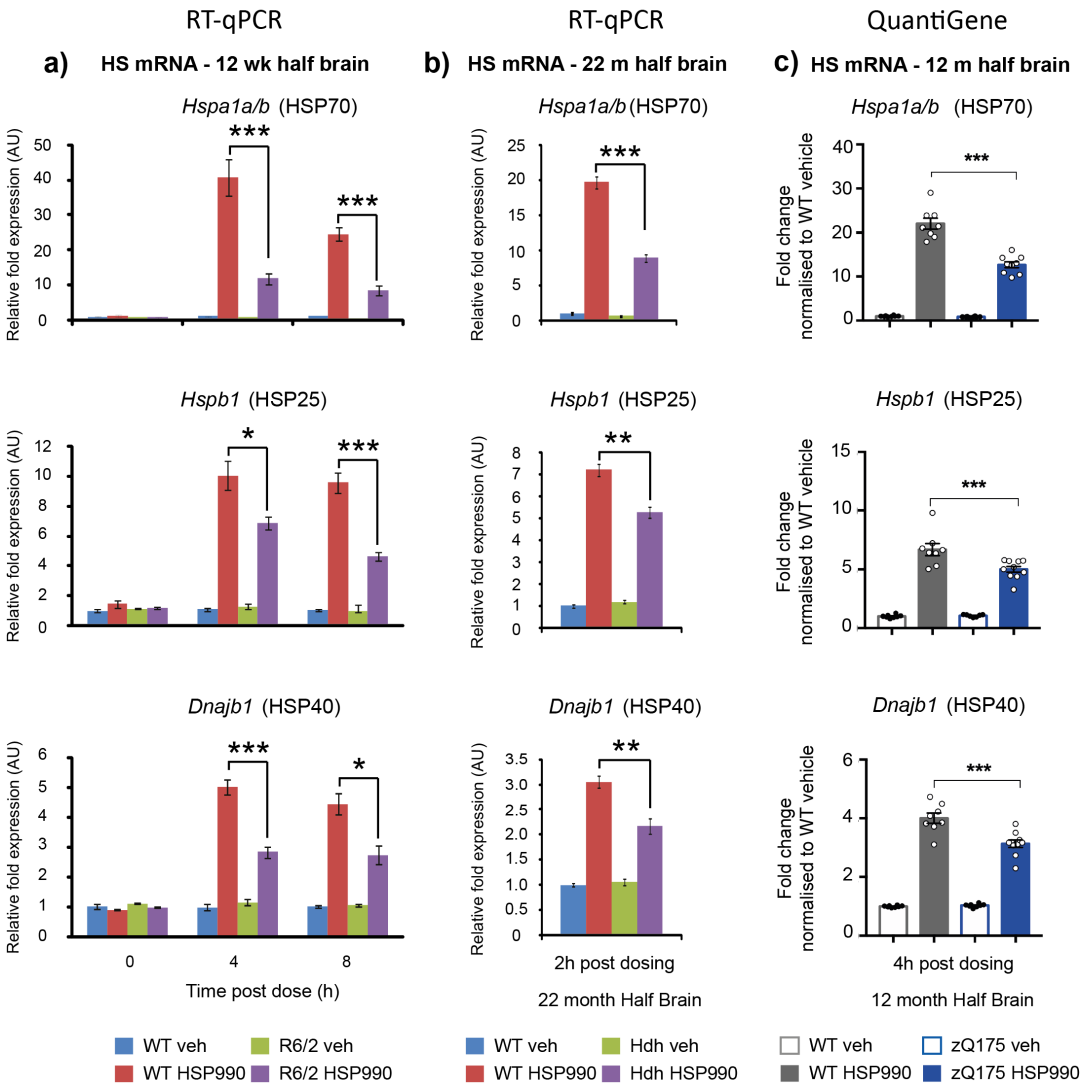

Figure 4.3. Analysis of the heat shock response in brain hemispheres of HD mouse models R6/2, HdhQ150 and zQ175 at late symptomatic stage of disease. ***a)*** *and* ***b)*** *are adapted from a figure in Labbadia et al., (2011) and reproduced with permission. The expression of heat shock genes Hspa1a/a, Hspb1 and Dnajb1 was measured by RT-qPCR (**a, b**) or QuantiGene (**c**) in brain hemispheres of R6/2 at 12 weeks of age (**a**) HdhQ150 at 22 months of age (**b**) and zQ175 at 12 months of age (**c**) after treatment with vehicle or NVP-HSP990 at the indicated time points. NVP-HSP990 samples were normalised to the corresponding wild-type samples treated with vehicle to calculate the fold change in expression. N = 4 mice / genotype / treatment for R6/2 and HdhQ150 mice; N = 6-10 mice / genotype / treatment for zQ175. Statistical analysis by Student's t-test (Labbadia et al., 2011) in **a)** and **b)**; by two-way ANOVA with Bonferroni correction in **c)**. Mean ± SEM. *** p ≤ 0.001; ** p ≤ 0.01; * p ≤ 0.05. WT = wild-type; Hdh = HdhQ150; HSP990 = NVP-HSP990; veh = vehicle; wk = week; AU = arbitrary units; HS = heat shock; h = hours.*

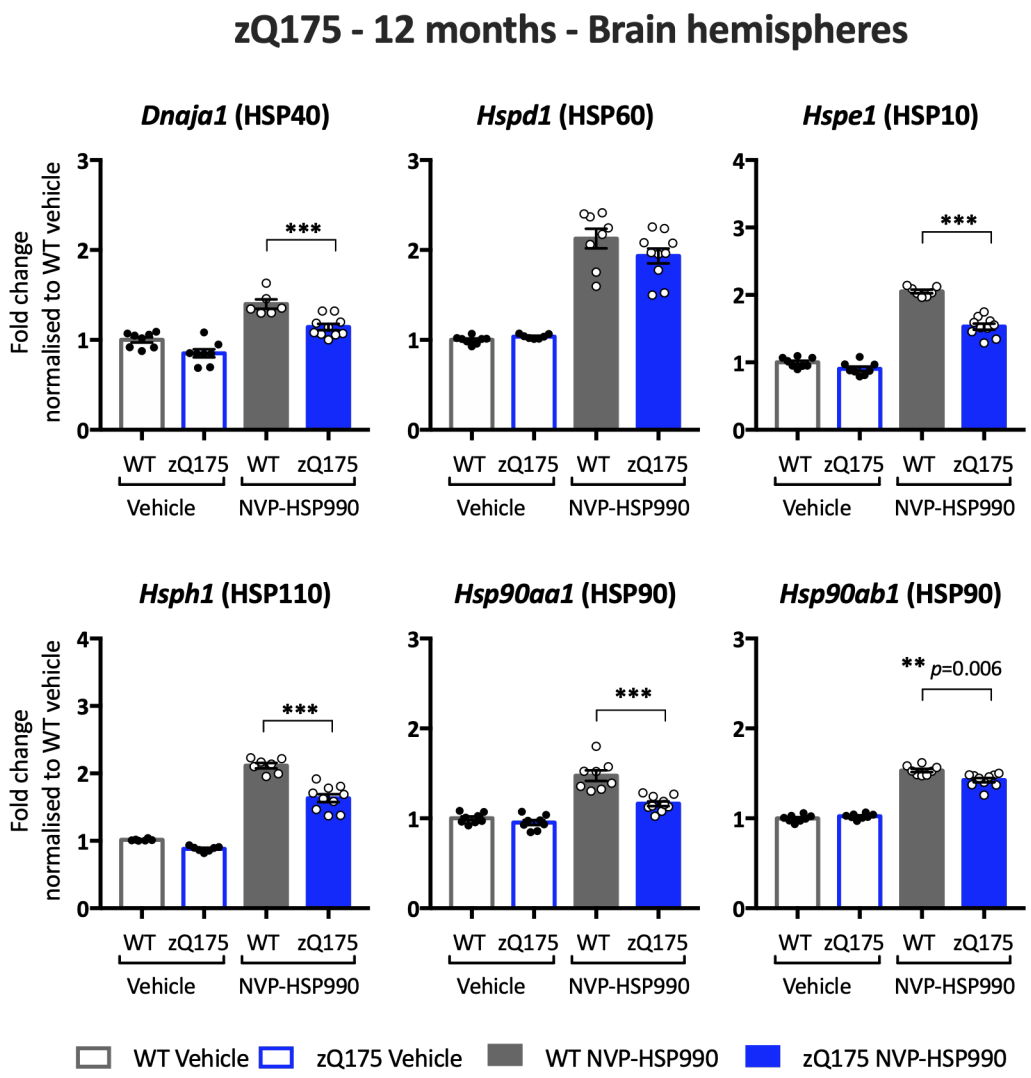

Figure 4.4. Analysis of the heat shock response in the brain hemispheres of zQ175 mice at 12 months of age by QuantiGene.

*The expression of heat shock genes Dnaja1, Hspd1, Hspe1, Hsph1, Hsp90aa1 and Hsp90ab1 was measured in the brain hemispheres of zQ175 at 12 months of age, 4 hours after treatment with vehicle or NVP-HSP990, using the QuantiGene 18-plex assay. NVP-HSP990 samples were normalised to the wild-type samples treated with vehicle. N = 6-10 mice / genotype / treatment. Statistical analysis by two-way ANOVA with Bonferroni correction. Mean ± SEM. *** p ≤ 0.001; ** p ≤ 0.01. WT = wild-type.*

4.3 Comparative analysis of the heat shock response in the cortex, striatum and tibialis anterior of zQ175 and R6/2 with disease progression

The induction of the heat shock response was clearly disrupted in the brain hemispheres of zQ175 mice, as had been demonstrated for R6/2 and *Hdh*Q150 (Labbadia *et al.,* 2011; Figure 4.3 and 4.4). To dissect this in more detail, the heat shock response was assessed in the tibialis anterior muscle, striatum and cortex of zQ175 mice over the course of disease progression. zQ175 mice were dosed with vehicle or NVP-HSP990 (12 mg / kg) at 3 months, 12 months and 20 months of age, corresponding to pre-symtomatic, early symptomatic and late symptomatic stages, respectively (Heikkinen *et al.,* 2012; Menalled *et al*., 2012). The tissues of interest were collected 4 hours after dosing in all cases.

In order to interpret the zQ175 data and obtain a wider understanding and comparison on the impairment of the heat shock response in HD mouse models, R6/2 mice were dosed at 12 weeks of age, corresponding to end-stage of the disease, and the same tissues were collected for analysis 4 hours post-dosing.

The study design is summarised in Table 4.2.

Table 4.2. Summary of mice allocated for the analysis of the heat shock response in the tibialis anterior, striatum and cortex of HD mouse models.

	zQ175 Delta Neo	***R6/2***
Age(s)	*3 months* *12 months* *20 months*	*12 weeks*
N numbers	*6 mice / genotype / treatment / age*	*7-9 mice / genotype / treatment*
Drug administration	*Oral gavage*	
Frequency of administration	*Single administration*	
Dissection time post-dosing	*4 hours*	
Tissues collected	*Tibialis anterior muscle, striatum, cortex*	
Method of analysis	*QuantiGene 18-plex assay*	

4.3.1 Optimisation of the QuantiGene 18-plex assay for use with zQ175, R6/2 and wild-type tissues

As seen in Chapter 3 and section 4.2.1, serial dilution experiments (2-fold) with tibialis anterior, striatal and cortical samples from zQ175, R6/2 and their wild-type counterparts that had received a dose of NVP-HSP990 or vehicle were carried out to identify the optimal dilutions to use with the QuantiGene 18-plex assay. As in previous optimisation experiments, this aimed to ensure that none of the housekeeping genes had saturated MFI signals or were dysregulated between genotypes, treatments or ages. And therefore, samples from the 3- and 20-month cohorts were included. In R6/2, if any of the housekeeping genes were dysregulated, it would be detected in the cohort at 12 weeks of age. For the heat shock genes, as well as avoiding signal saturation, it was important to select a dilution which provided MFI values over the limit of detection. This was especially relevant for *Hspa1a/b*, that gave very low MFI values in the vehicle samples, due to low basal (when non-induced) expression levels.

4.3.1.1 Tibialis anterior

Independent pools of tibialis anterior samples at equivalent tissue mass / volume (10 mg / 300 µL), from each treatment group for the zQ175 and R6/2 cohorts, were prepared and subjected to a 2-fold serial dilution. The housekeeping genes presented a degree of variability in some cases. In particular, for R6/2 and wild-type mice, *Rpl13a* was expressed differently between genotypes and *Gapdh* was saturated and highly variable (Figure 4.8). Although to a lesser extent, this also occurred in the zQ175 and wild-type cohorts at 3 and 20 months of age (Figures 4.5 and 4.6). For these reasons, *Rpl13a* and *Gapdh* were not used as reference genes in the analysis of the heat shock response in tibialis anterior.

In both models, the MFI values for the genes of interest pertaining to either vehicle or NVP-HSP990 treatment, followed a linear regression and the slopes of the regression lines were significantly different between treatment groups. This indicated that transcription of the heat shock genes increased after NVP-HSP990 treatment (Figures 4.7 and 4.9). Taking the MFI values, limits of detection and saturation signals into consideration, a 1:4 dilution was chosen.

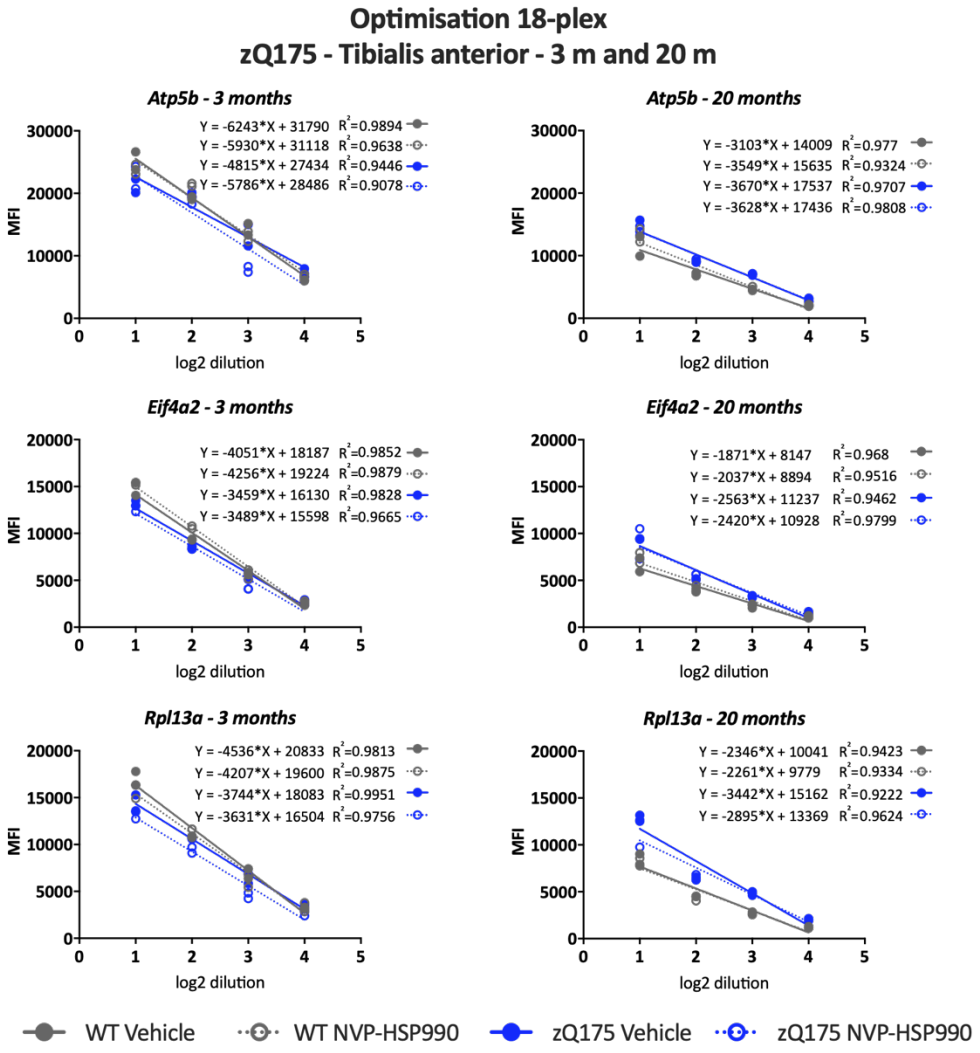

Figure 4.5. Optimisation of sample input in the QuantiGene 18-plex assay for use with zQ175 and wild-type tibialis anterior at 3 and 20 months of age (housekeeping genes).

Pools of tibialis anterior samples from zQ175 or wild-type mice treated with vehicle or NVP-HSP990 (n = 6 mice / genotype / treatment / age), at equivalent tissue mass / volume (10 mg / 300 µL), were prepared in a 2-fold dilution series and analysed in duplicate. MFI values that were detected for each dilution from each treatment group are shown. Linear regression was calculated for each housekeeping gene. All housekeeping genes, except Rpl13a at 20 months of age, maintained a stable expression, with no signs of transcriptional dysregulation between genotypes or treatment. Rpl13a showed slight differences in expression between genotypes at 20 months of age and was excluded as reference gene. WT = wild-type; MFI = median fluorescence intensity; m = months.

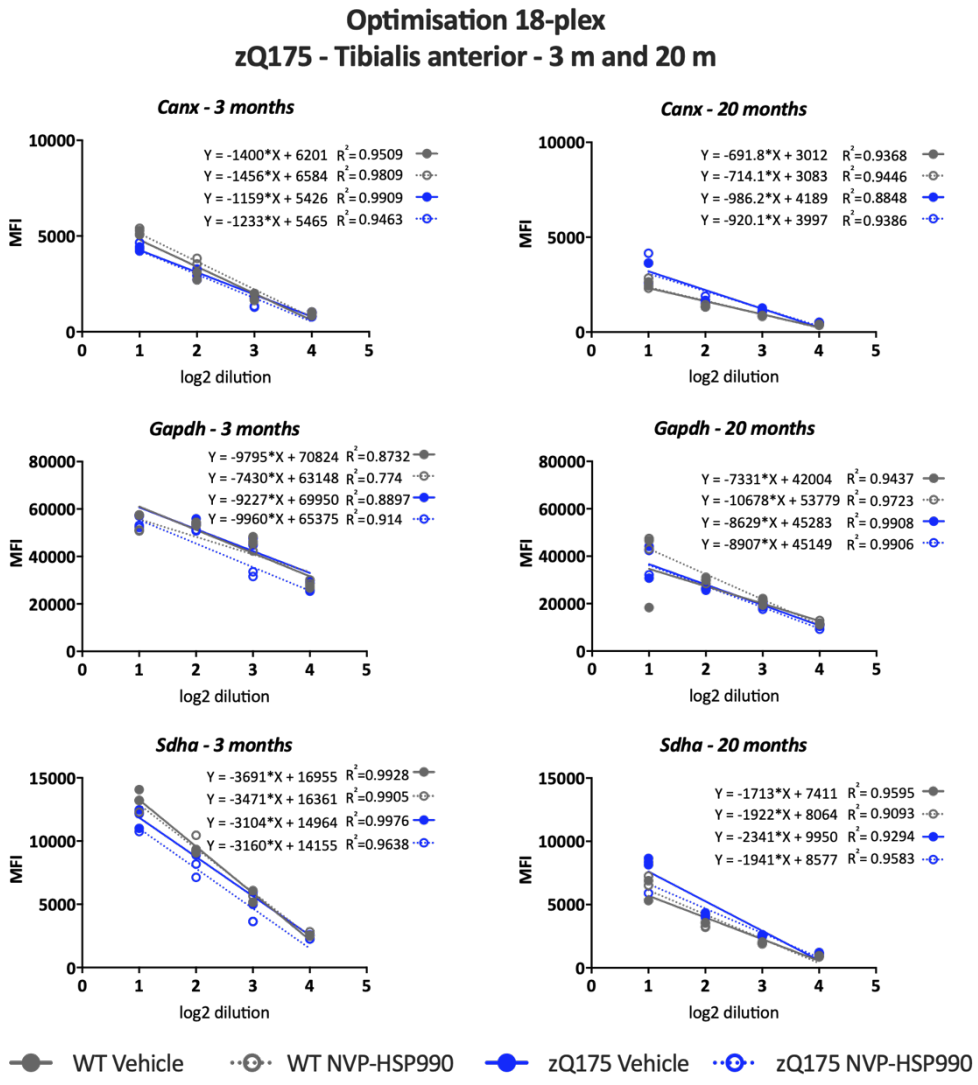

Figure 4.6. Optimisation of sample input in the QuantiGene 18-plex assay for use with zQ175 and wild-type tibialis anterior at 3 and 20 months of age (housekeeping genes).

Pools of tibialis anterior samples from zQ175 or wild-type mice treated with vehicle or NVP-HSP990 (n = 6 mice / genotype / treatment / age), at equivalent tissue mass / volume (10 mg / 300 µL), were prepared in a 2-fold dilution series and analysed in duplicate. MFI values that were detected for each dilution from each treatment group are shown. Linear regression was calculated for each housekeeping gene. All housekeeping genes except Gapdh maintained a stable expression, with no signs of transcriptional dysregulation between genotypes or treatment. Gapdh showed signs of saturation at 3 months or slight differences in expression between genotypes at the initial dilutions and was excluded as reference gene. WT = wild-type; MFI = median fluorescence intensity; m = months.

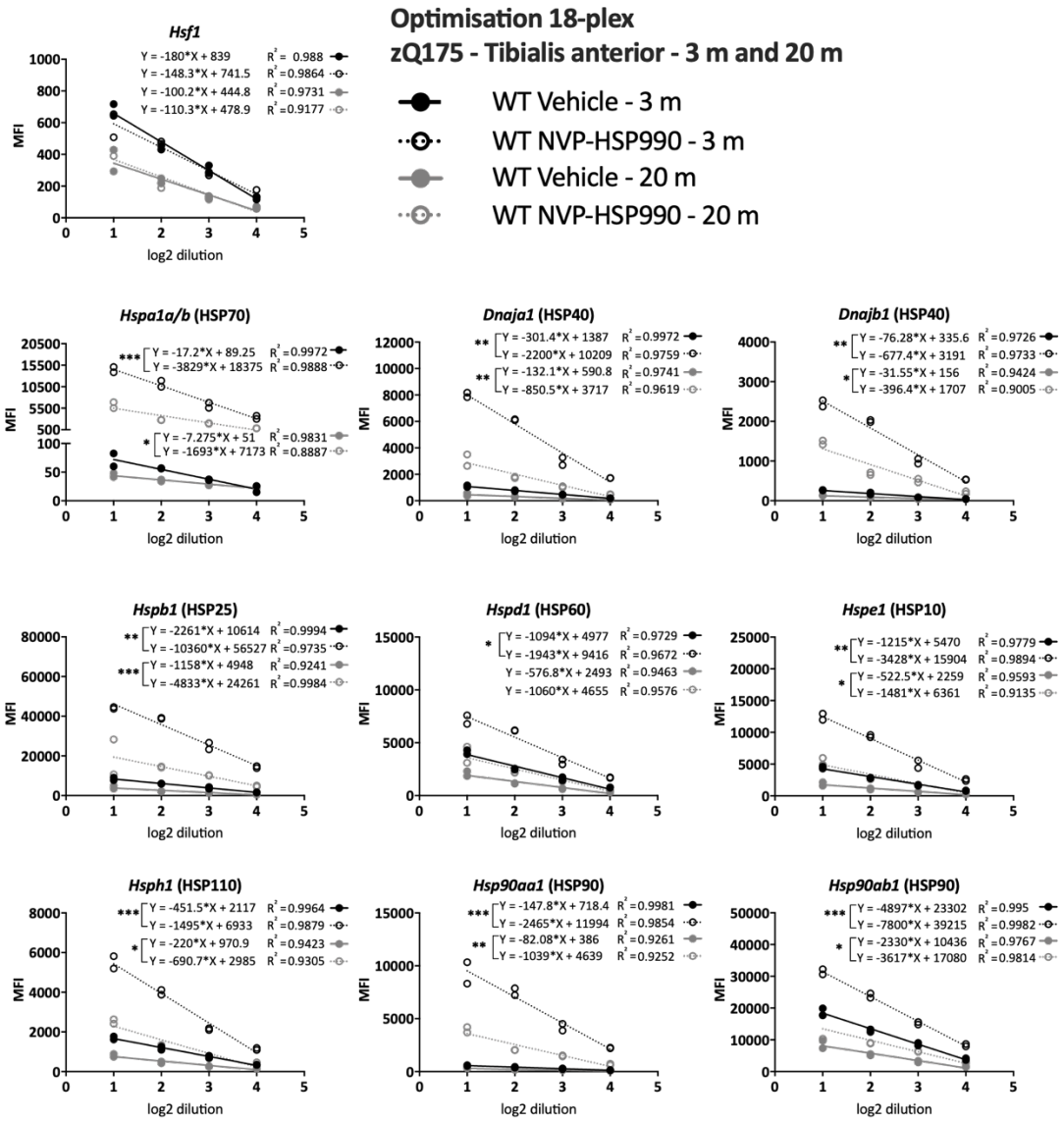

Figure 4.7. Optimisation of sample input in the QuantiGene 18-plex assay for use with zQ175 and wild-type tibialis anterior at 3 and 20 months of age (genes of interest).

*Pools of tibialis anterior samples from wild-type mice treated with vehicle or NVP-HSP990 (n = 6 mice / treatment / age), at equivalent tissue mass / volume (10 mg / 300 µL), were prepared in a 2-fold dilution series and analysed in duplicate. MFI values that were detected for each dilution from each treatment group are shown. Linear regression was calculated for each gene. The MFI values from vehicle samples, corresponding to basal levels of expression, were very low for Hspa1a/b. The heat shock genes had linear regression lines with different slopes for each treatment group. WT = wild-type; MFI = median fluorescence intensity; m = months. *** p ≤ 0.001; ** p ≤ 0.01; * p ≤ 0.05.*

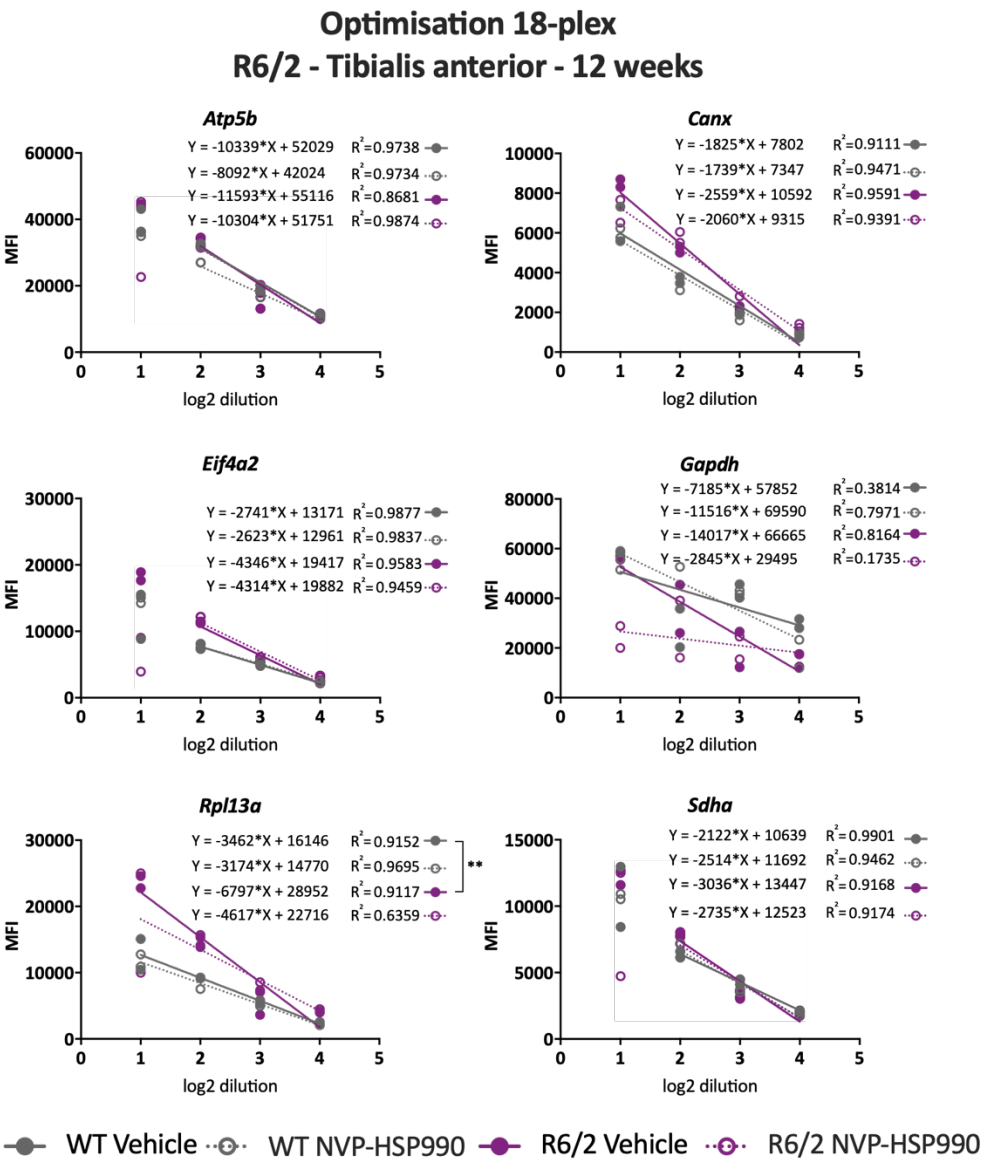

Figure 4.8. Optimisation of sample input in the QuantiGene 18-plex assay for use with R6/2 and wild-type tibialis anterior at 12 weeks of age (housekeeping genes).

*Pools of tibialis anterior samples from R6/2 or wild-type mice treated with vehicle or NVP-HSP990 (n = 7 - 9 mice / genotype / treatment), at equivalent tissue mass / volume (10 mg / 300 µL), were prepared in a 2-fold dilution series and analysed in duplicate. MFI values that were detected for each dilution from each treatment group are shown. Linear regression was analysed for each housekeeping gene. The housekeeping genes Atp5b, Sdha, Canx and Eif4a2 showed a stable expression, especially from 1:4 dilution, across genotypes and/or treatment. Gapdh showed saturation at most of the dilutions and signs of dysregulation. Rpl13a appeared to be dysregulated, with slopes differing between genotypes. Both Gapdh and Rpl13a genes were excluded as reference genes. WT = wild-type; MFI = median fluorescence intensity. ** p ≤ 0.01.*

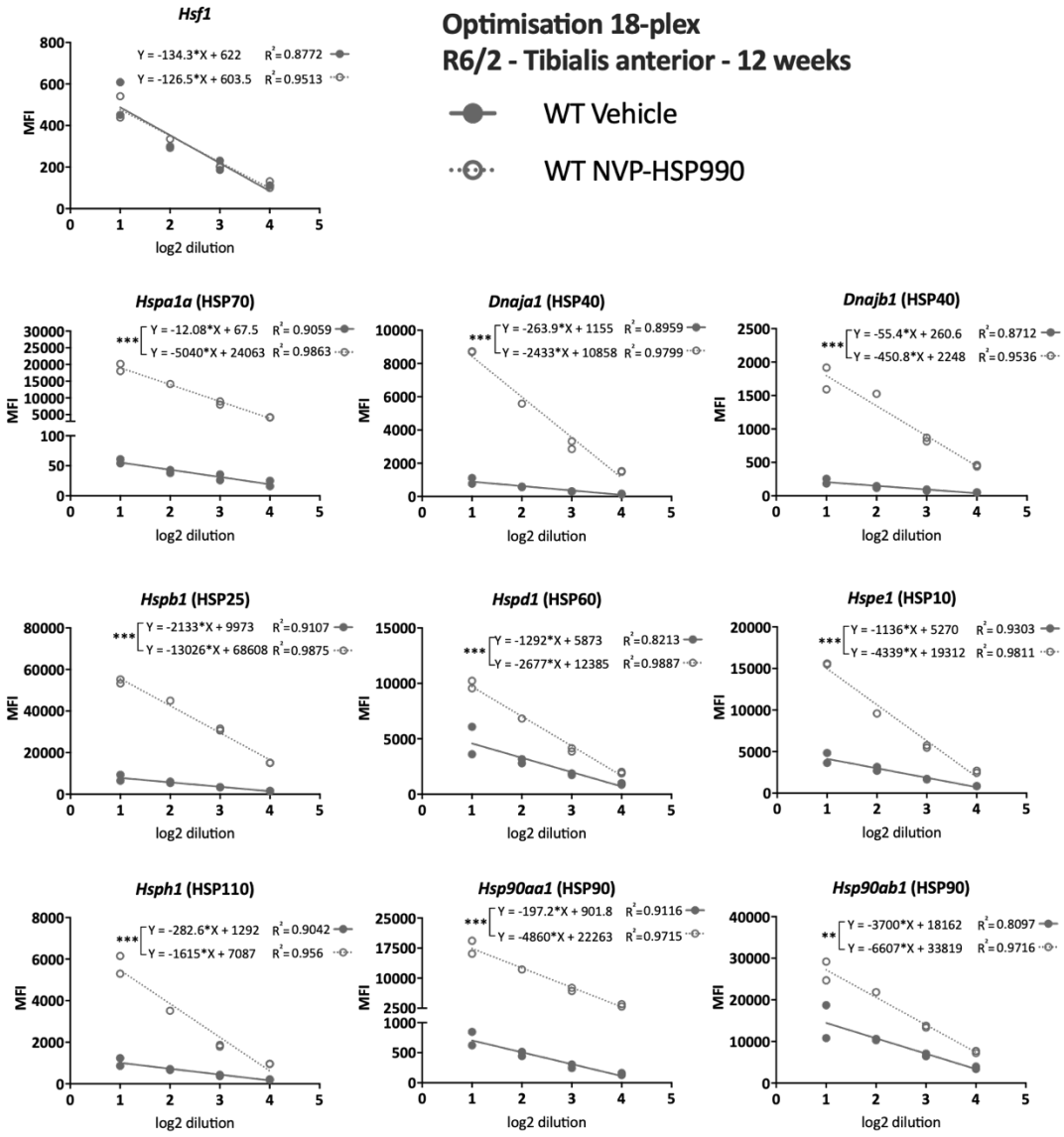

Figure 4.9. Optimisation of sample input in the QuantiGene 18-plex assay for use with R6/2 and wild-type tibialis anterior at 12 weeks of age (genes of interest).

*Pools of tibialis anterior samples from wild-type mice treated with vehicle or NVP-HSP990 (n = 7 - 9 mice/treatment), at equivalent tissue mass / volume (10 mg / 300 µL), were prepared in a 2-fold dilution series and analysed in duplicate. MFI values that were detected for each dilution from each treatment group are shown. Linear regression was calculated for each gene. The MFI values from vehicle samples corresponding to basal levels of expression were very low for Hspa1a/b. The heat shock genes had linear regression lines with significantly different slopes for each treatment group. WT = wild-type; MFI = median fluorescence intensity. *** p ≤ 0.001; ** p ≤ 0.01.*

4.3.1.2 Striatum

The 2-fold dilution series prepared for the 18-plex optimisation of sample input in striatum yielded tight MFI values in the duplicates, that fitted to a linear regression that proportionally decreased with the dilutions. The housekeeping genes had a stable expression that was not affected by the symptomatic stage in zQ175 (Figures 4.10, 4.11) or R6/2 (Figure 4.13) mice. The expression of the heat shock genes was significantly enhanced in the NVP-HSP990 treatment group, with elevated MFI values and significantly different slopes between treatments in both models (Figure 4.12, 4.14). The 1:4 dilution was chosen for this tissue.

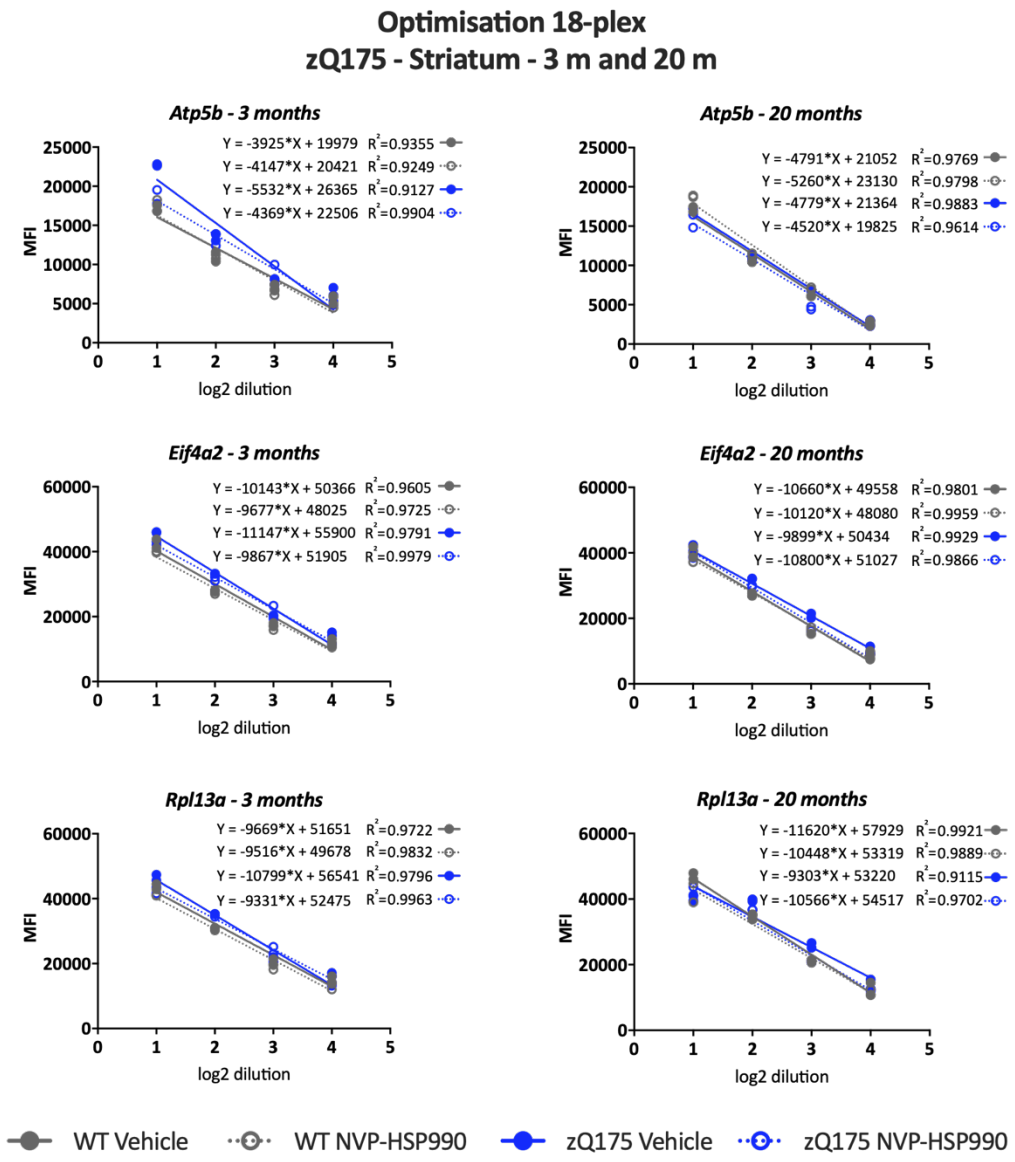

Figure 4.10. Optimisation of sample input in the QuantiGene 18-plex assay for use with zQ175 and wild-type striatum at 3 and 20 months of age (housekeeping genes).

Pools of striatal samples from zQ175 or wild-type mice at 3 or 20 months of age treated with vehicle or NVP-HSP990 (n = 6 mice / genotype / treatment / age), at equivalent tissue mass / volume (10 mg / 300 µL), were prepared in a 2-fold dilution series and analysed in duplicate. MFI values that were detected for each dilution from each treatment group are shown. Linear regression was calculated for each housekeeping gene. All housekeeping genes showed a stable expression at both ages, with no signs of transcriptional dysregulation between genotypes or treatment or with age. WT = wild-type; MFI = median fluorescence intensity; m = months.

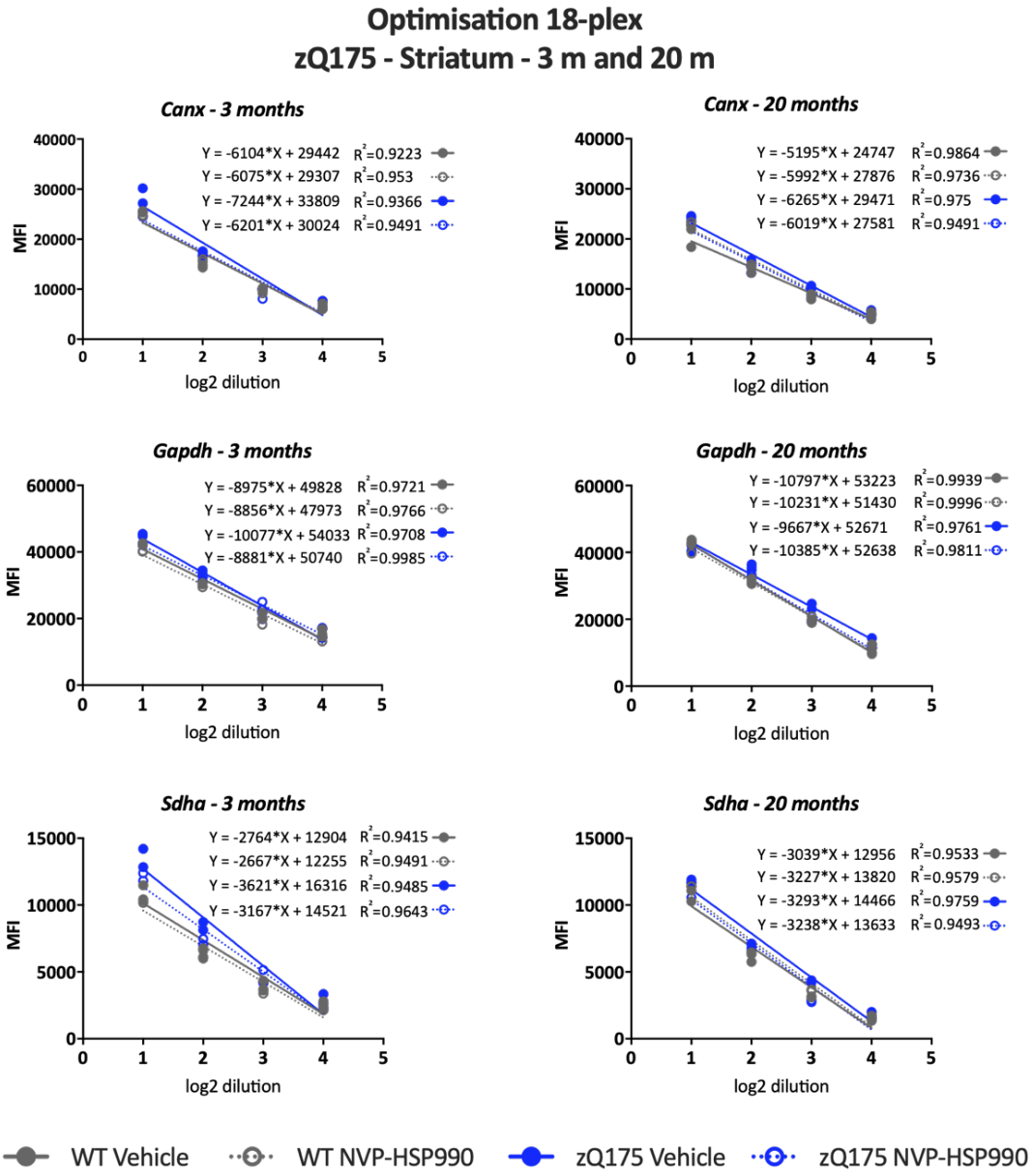

Figure 4.11. Optimisation of sample input in the QuantiGene 18-plex assay for use with zQ175 and wild-type striatum at 3 and 20 months of age (housekeeping genes).

Pools of striatal samples from zQ175 or wild-type mice at 3 or 20 months of age treated with vehicle or NVP-HSP990 (n = 6 mice / genotype / treatment / age), at equivalent tissue mass / volume (10 mg / 300 µL), were prepared in a 2-fold dilution series and analysed in duplicate. MFI values that were detected for each dilution from each treatment group are shown. Linear regression was calculated for each housekeeping gene. All housekeeping genes showed a stable expression at both ages, with no signs of transcriptional dysregulation between genotypes or treatment or with age. WT = wild-type; MFI = median fluorescence intensity; m = months.

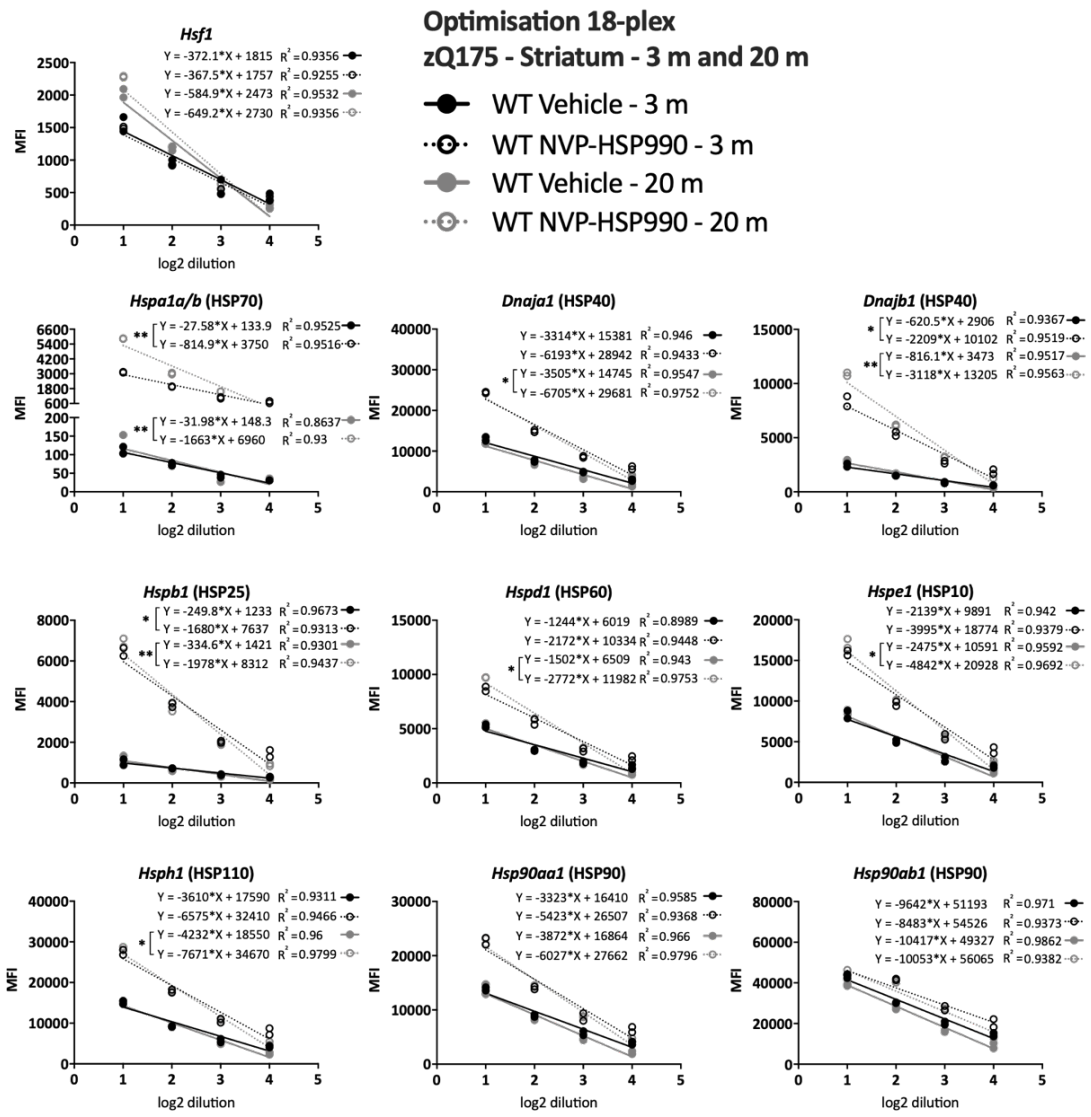

Figure 4.12. Optimisation of sample input in the QuantiGene 18-plex assay for use with zQ175 and wild-type striatum at 3 and 20 months of age (genes of interest).

*Pools of striatal samples from wild-type mice at 3 or 20 months of age treated with vehicle or NVP-HSP990 (n = 6 mice / treatment / age), at equivalent tissue mass / volume (10 mg / 300 µL), were prepared in a 2-fold dilution series and analysed in duplicate. MFI values that were detected for each dilution from each treatment group are shown. Linear regression was calculated for each gene. The MFI values from vehicle samples corresponding to basal levels of expression were very low for Hspa1a/b. Hsp90ab1 showed saturation at the initial 1:2 dilution. The heat shock genes had linear regression lines with different slopes for each treatment group, most of them significantly different. WT = wild-type; MFI = median fluorescence intensity; m = months. ** p ≤ 0.01; * p ≤ 0.05.*

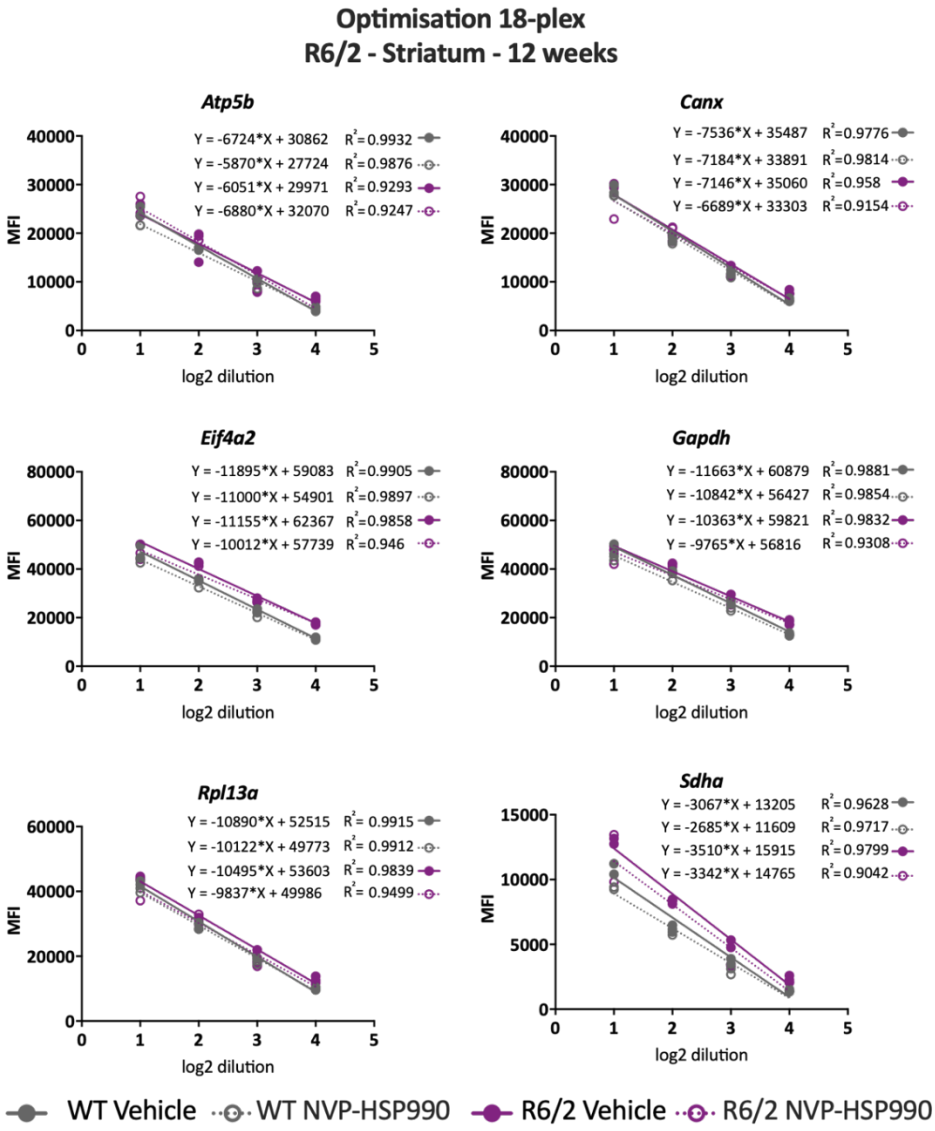

Figure 4.13. Optimisation of sample input in the QuantiGene 18-plex assay for use with R6/2 and wild-type striatum at 12 weeks of age (housekeeping genes). *Pools of striatal samples from R6/2 or wild-type mice treated with vehicle or NVP-HSP990 (n = 7 - 9 mice / genotype / treatment), at equivalent tissue mass / volume (10 mg / 300 µL), were prepared in a 2-fold dilution series and analysed in duplicate. MFI values that were detected for each dilution from each treatment group are shown. Linear regression was calculated for each housekeeping gene. All housekeeping genes showed a stable expression, across genotypes and/or treatment. Eif4a2 and Gapdh showed saturation at 1:2 dilutions. WT = wild-type; MFI = median fluorescence intensity.*

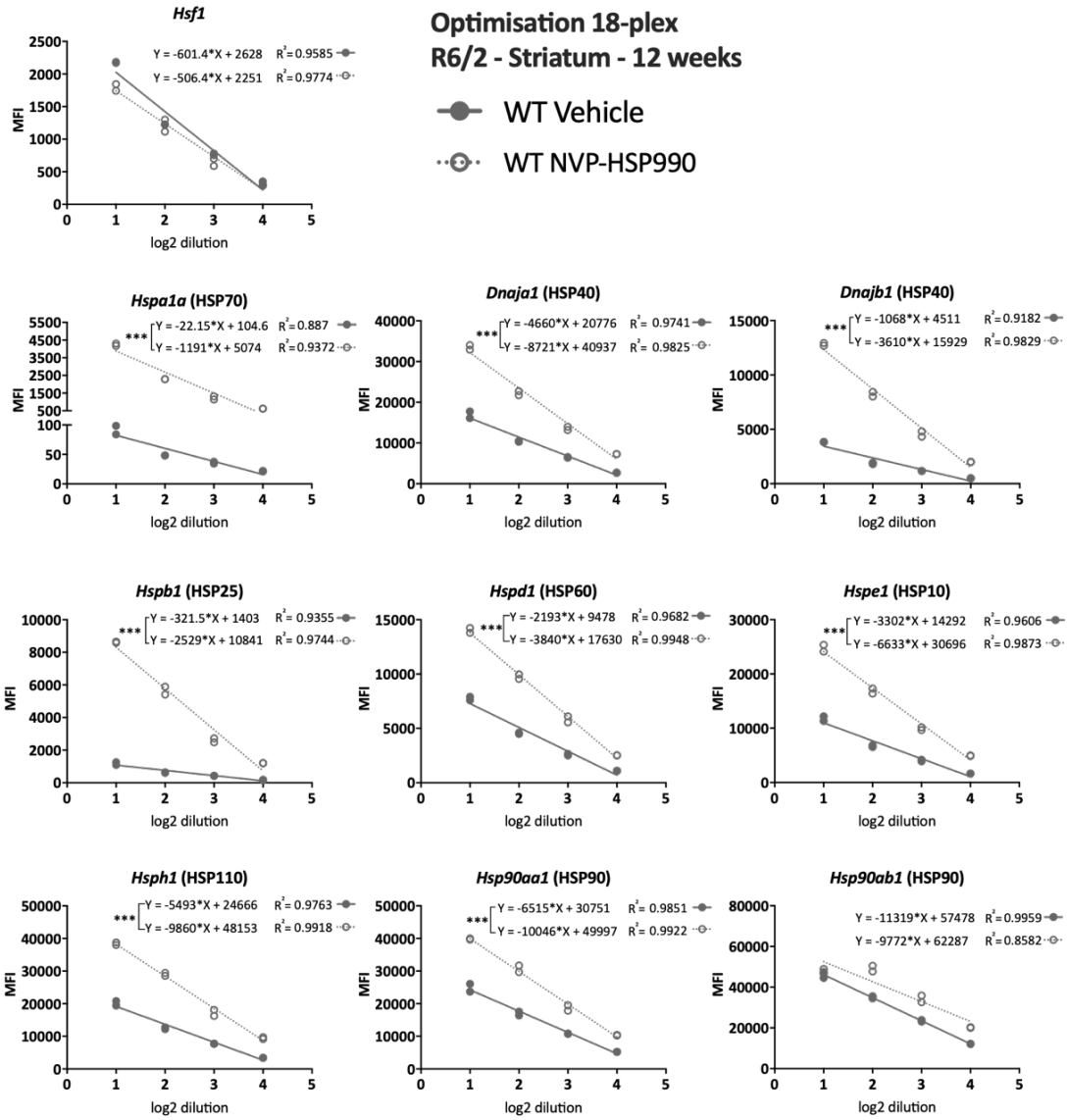

Figure 4.14. Optimisation of sample input in the QuantiGene 18-plex assay for use with R6/2 and wild-type striatum at 12 weeks of age (genes of interest).
*Pools of striatal samples from wild-type mice treated with vehicle or NVP-HSP990 (n = 7 - 9 mice / treatment), at equivalent tissue mass / volume (10 mg / 300 µL), were prepared in a 2-fold dilution series and analysed in duplicate. MFI values that were detected for each dilution from each treatment group are shown. Linear regression was calculated for each gene. The MFI values from vehicle samples corresponding to basal levels of expression were very low for Hspa1a/b. All heat shock genes, except Hsp90ab1, had linear regression lines with significantly different slopes for each treatment group. Hsp90ab1 also showed signs of saturation at the 1:2 dilution. WT = wild-type; MFI = median fluorescence intensity. *** p ≤ 0.001.*

4.3.1.3 Cortex

The MFI values for the cortex, as for striatum, followed a linear regression in both zQ175 and R6/2, with a proportional decrease with increasing sample dilution. The expression of housekeeping genes was again stable across genotypes (Figures 4.15, 4.16, 4.18) and the expression of the heat shock genes was induced by NVP-HSP990 treatment (Figures 4.17, 4.19). Because of slight differences in MFI signals and signs of saturation in some cases at 1:4 dilution, the 1:6 dilution was selected for the cortical region.

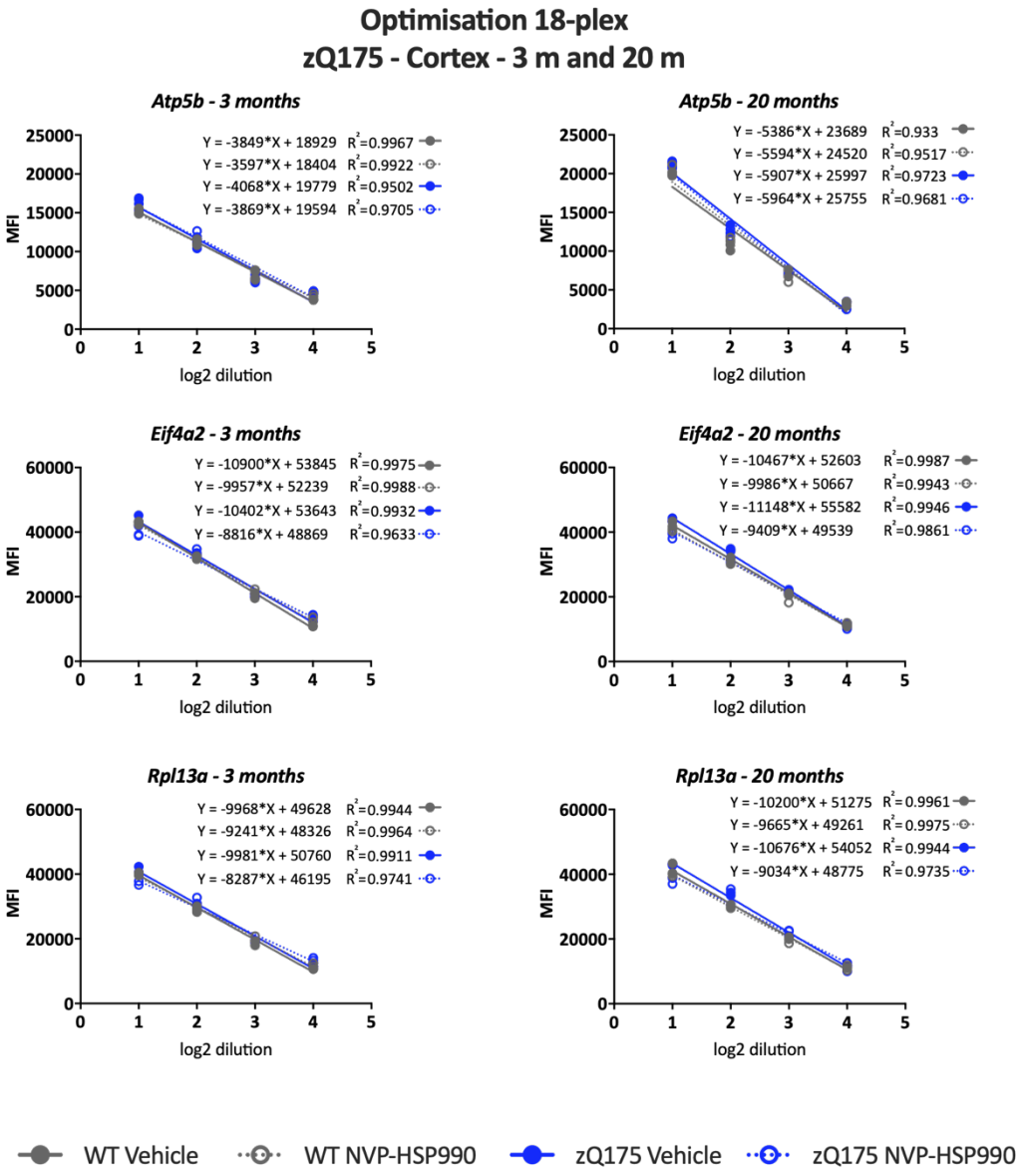

Figure 4.15. Optimisation of sample input in the QuantiGene 18-plex assay for use with zQ175 and wild-type cortex at 3 and 20 months of age (housekeeping genes).

Pools of cortical samples from zQ175 or wild-type mice at 3 and 20 months of age, treated with vehicle or NVP-HSP990 (n = 6 mice / genotype / treatment / age), at equivalent tissue mass / volume (10 mg / 300 µL), were prepared in a 2-fold dilution series and analysed in duplicate. MFI values that were detected for each dilution from each treatment group are shown. Linear regression was calculated for each housekeeping gene. All housekeeping genes showed a stable expression, with no signs of transcriptional dysregulation between genotypes or treatment or with age. WT = wild-type; MFI = median fluorescence intensity; m = months.

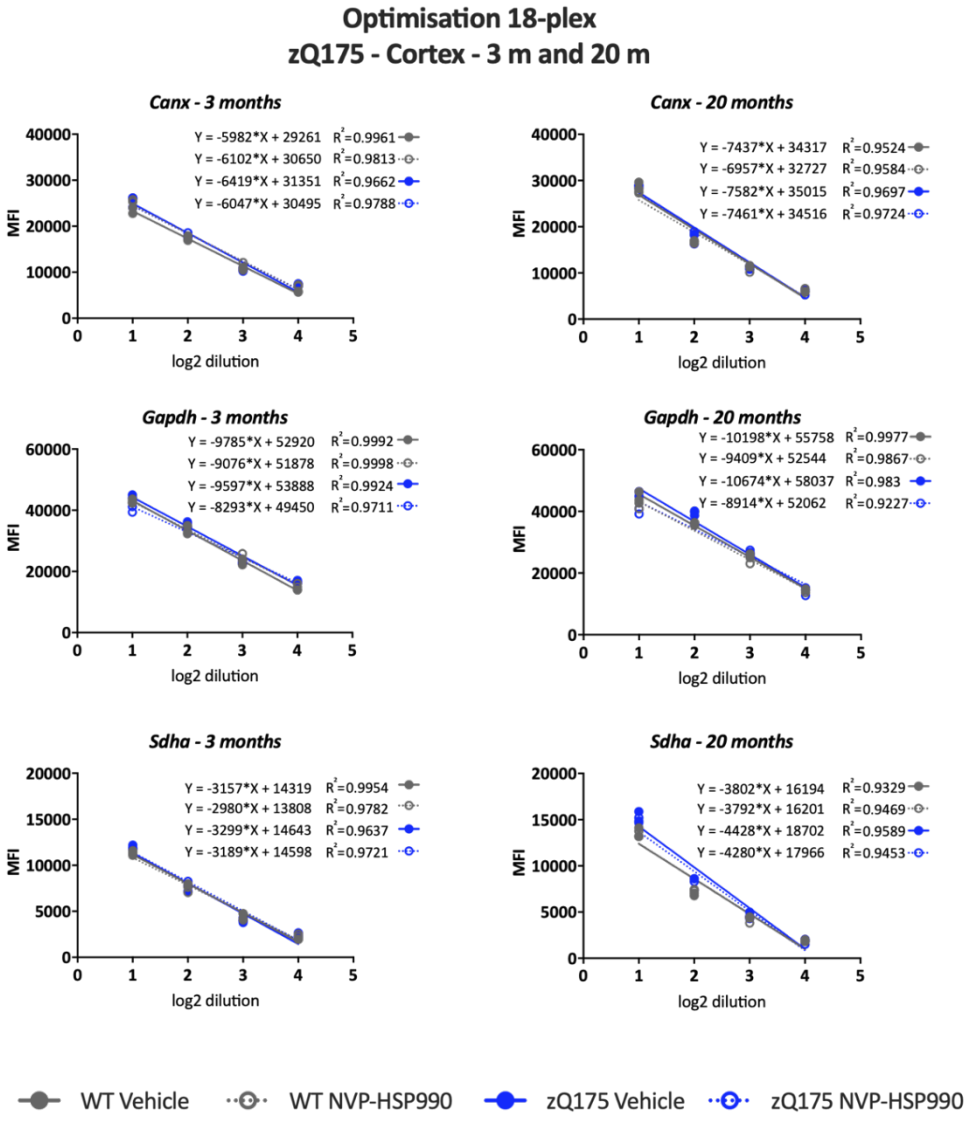

Figure 4.16. Optimisation of sample input in the QuantiGene 18-plex assay for use with zQ175 and wild-type cortex at 3 and 20 months of age (housekeeping genes).

Pools of cortical samples from zQ175 or wild-type mice at 3 and 20 months of age, treated with vehicle or NVP-HSP990 (n = 6 mice / genotype / treatment / age), at equivalent tissue mass / volume (10 mg / 300 µL), were prepared in a 2-fold dilution series and analysed in duplicate. MFI values that were detected for each dilution from each treatment group are shown. Linear regression was calculated for each housekeeping gene. All housekeeping genes showed a stable expression, with no signs of transcriptional dysregulation between genotypes or treatment or with age. WT = wild-type; MFI = median fluorescence intensity; m = months.

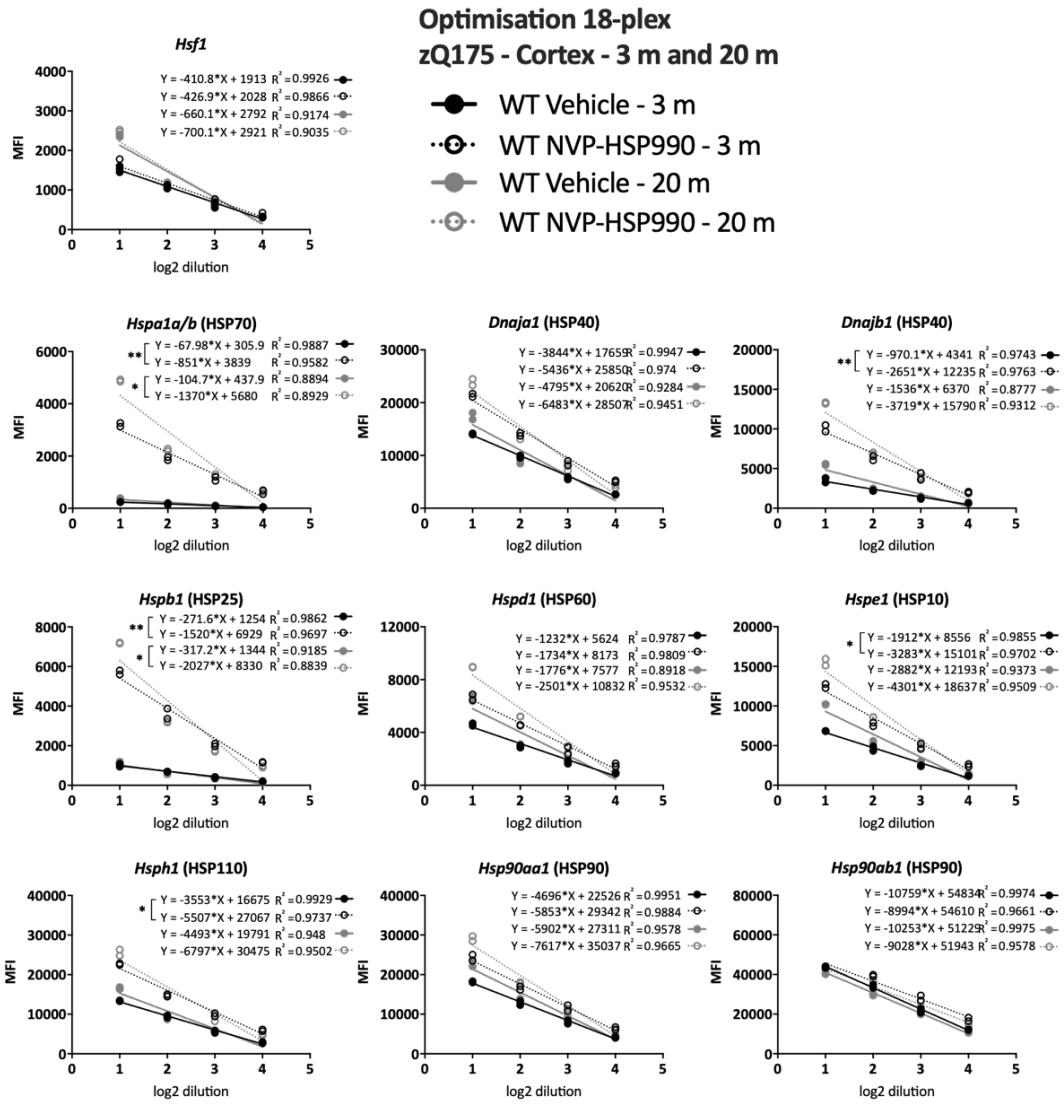

Figure 4.17. Optimisation of sample input in the QuantiGene 18-plex assay for use with zQ175 and wild-type cortex at 3 and 20 months of age (genes of interest).

*Pools of cortical samples from wild-type mice treated with vehicle or NVP-HSP990 (n = 6 mice / treatment / age), at equivalent tissue mass / volume (10 mg / 300 µL), were prepared in a 2-fold dilution series and analysed in duplicate. MFI values that were detected for each dilution from each treatment group are shown. Linear regression was calculated for each gene. The heat shock genes have linear regression lines with different slopes for each treatment group, five of them with significantly different slopes, as indicated. Hsp90ab1 showed some saturation at the initial 1:2 dilution. WT = wild-type; MFI = median fluorescence intensity; m = months. ** p ≤ 0.01; * p ≤ 0.05.*

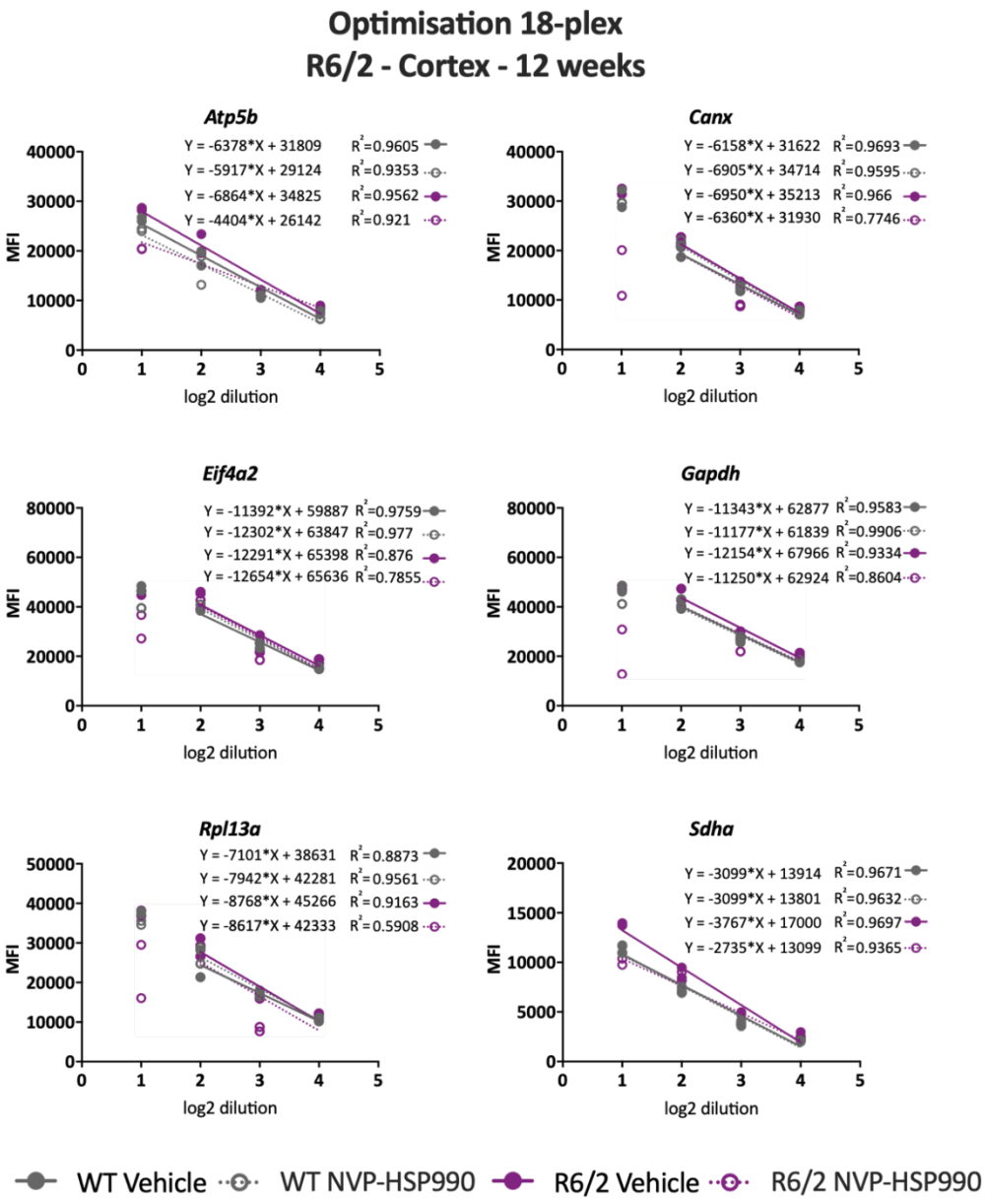

Figure 4.18. Optimisation of sample input in the QuantiGene 18-plex assay for use with R6/2 and wild-type cortex at 12 weeks of age (housekeeping genes).
Pools of cortical samples from R6/2 or wild-type mice treated with vehicle or NVP-HSP990 (n = 7 - 9 mice / genotype / treatment), at equivalent tissue mass / volume (10 mg / 300 µL), were prepared in a 2-fold dilution series and analysed in duplicate. MFI values that were detected for each dilution from each treatment group are shown. Linear regression was calculated for each housekeeping gene. All housekeeping genes showed a stable expression, across genotypes and/or treatment. Eif4a2 and Gapdh showed saturation at 1:2 and 1:4 dilutions. WT = wild-type; MFI = median fluorescence intensity.

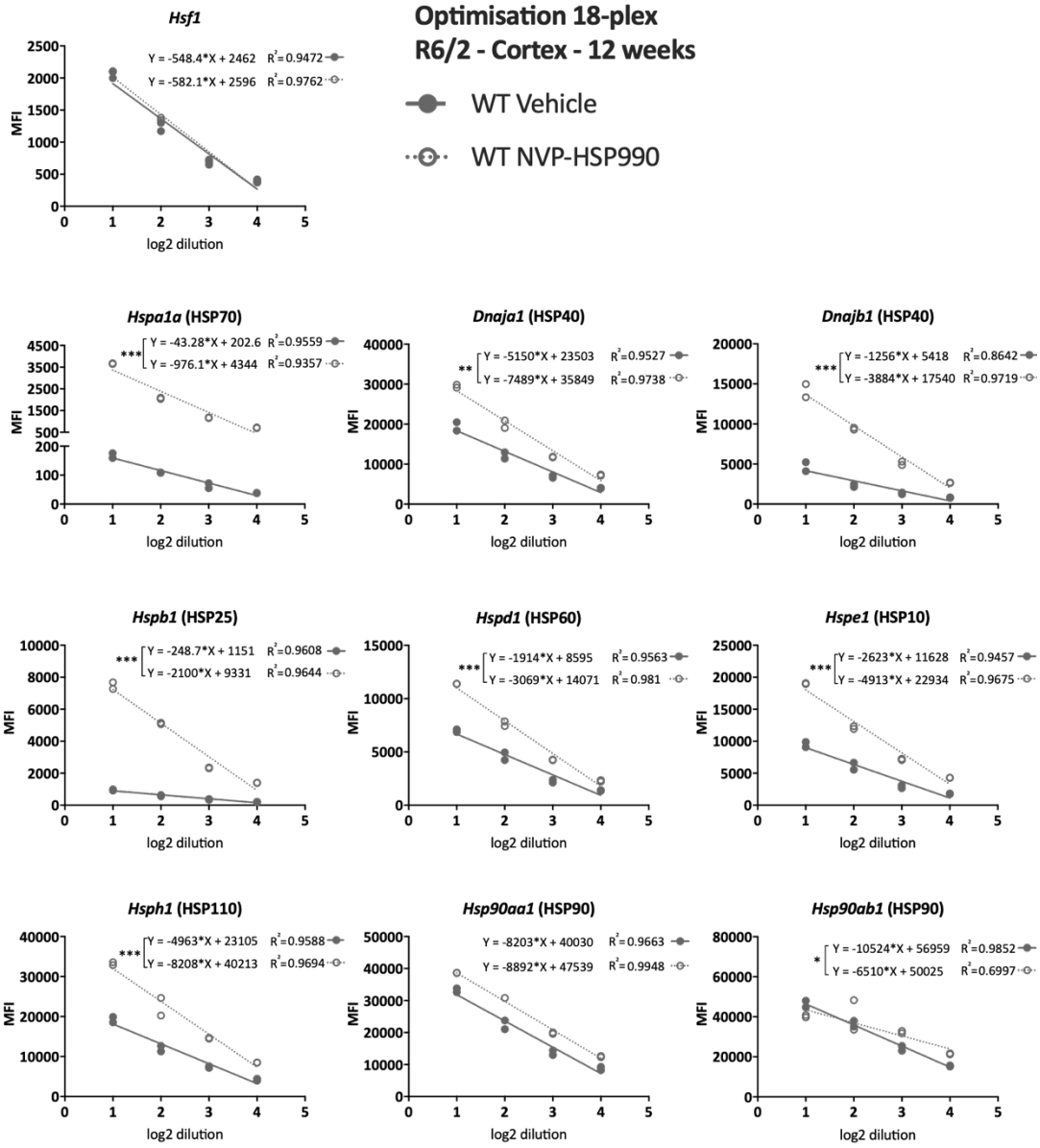

Figure 4.19. Optimisation of sample input in the QuantiGene 18-plex assay for use with R6/2 and wild-type cortex at 12 weeks of age (genes of interest).

*Pools of cortical samples from wild-type mice treated with vehicle or NVP-HSP990 (n = 7 - 9 mice / treatment), at equivalent tissue mass / volume (10 mg / 300 µL), were prepared in a 2-fold dilution series and analysed in duplicate. MFI values that were detected for each dilution from each treatment group are shown. Linear regression was calculated for each gene. All heat shock genes, except Hsp90aa1, have linear regression lines with significantly different slopes for each treatment group. The Hsp90ab1 signal was saturated at 1:2 dilution. WT = wild-type; MFI = median fluorescence intensity; m = months. *** p ≤ 0.001; ** p ≤ 0.01; * p ≤ 0.05.*

The following Table 4.3 is a summary of the dilutions that were selected for each region as optimal to be used with the QuantiGene 18-plex assay.

Table 4.3. Summary of optimal dilutions for QuantiGene 18-plex assay with R6/2 and zQ175 brain and muscle tissues.

QuantiGene assay	Mouse model	Tissue	Dilution of starting material (10 mg / 300 µl)	Final input (µg/µl)
18-plex	zQ175	Brain hemisphere	1:9	3.7
	zQ175 / R6/2	Tibialis anterior	1:4	8.3
	zQ175 / R6/2	Striatum	1:4	8.3
	zQ175 / R6/2	Cortex	1:6	5.5

4.3.2 Analysis of the heat shock response in the tibialis anterior of zQ175 and R6/2 mouse models

After optimisation, the 18-plex assay was applied to assess heat shock gene expression in the tibialis anterior, striatum and cortex of zQ175 and R6/2 mice. zQ175 mice had been dosed with vehicle or NVP-HSP990 (12 mg / kg) at 3 months, 12 months and 20 months of age, R6/2 mice at 12 weeks and tissues had been collected 4 hours after dosing (Table 4.2).

Starting with the tibialis anterior, after close evaluation of the data, five NVP-HSP990 samples, from mice of different ages, had to be removed from the analysis, as the MFI signals and, consequently, fold changes in heat shock gene expression, were very similar to vehicle levels, indicating that NVP-HSP990 treatment had not caused heat shock induction in these mice. Specifically, these samples were: at 3 months of age, two wild-type samples; at 12 months of age, one wild-type sample and at 20 months of age, one wild-type and one zQ175 sample. For consistency, these same samples were also excluded from the analysis of the striatal and cortical regions. No samples were excluded from the R6/2 cohort.

In tibialis anterior, and in line with what was previously observed (Figures 3.1, 3.4; Neueder *et al.,* 2017), the fold changes in heat shock gene expression after treatment with NVP-HSP990 were much more elevated than that observed in brain regions for both the zQ175 and R6/2 models.

In zQ175, eight of the nine genes studied (*Hspa1a/b*, *Dnaja1*, *Dnajb1*, *Hspb1*, *Hspd1*, *Hspe1*, *Hsph1* and *Hsp90aa1*) had a dysregulated induction of expression as compared to the wild-type littermates, that, in all cases, was present by 12 months of age, correlating with the early symptomatic stage of the disease (Figures 4.20, 4.21). An evident dysregulation was also found in the tibialis anterior of R6/2 mice at end-stage of the disease. This involved the same genes as in zQ175, except for *Dnajb1* and *Dnaja1* for which the level of induction was very variable between mice. Interestingly, the impaired induction appeared to be generally more robust in R6/2,

as a greater reduction in the fold change of expression was seen, especially for the *Hspa1a/b*, *Hspb1* and *Hsph1* genes (Figures 4.20, 4.21).

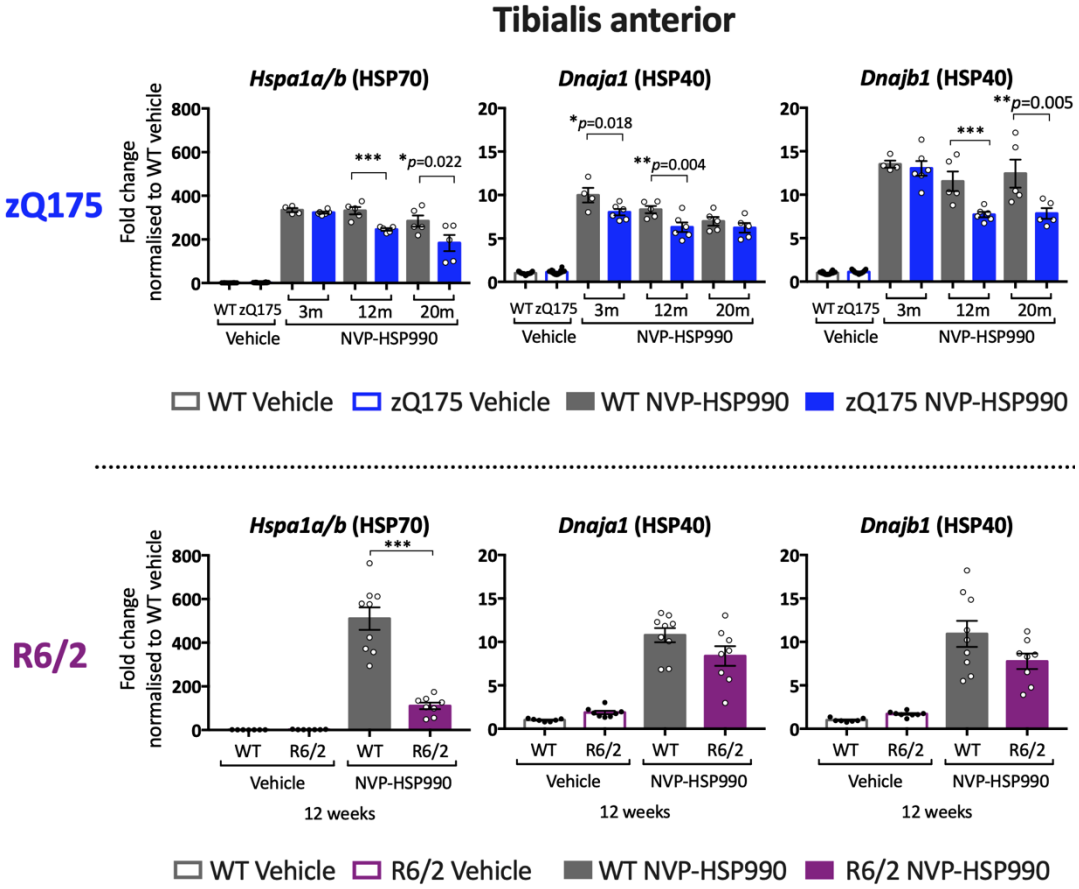

Figure 4.20. Comparative analysis of the heat shock response in the tibialis anterior of zQ175 (at 3, 12 and 12 months of age) and R6/2 mice (at 12 weeks of age).

*The QuantiGene 18-plex assay was used to measure the levels of expression of the heat shock genes Hspa1a/b, Dnaja1 and Dnajb1 in the tibialis anterior of zQ175 at 3, 12 and 20 months of age and R6/2 at 12 weeks of age, 4 hours after treatment with vehicle or NVP-HSP990. All the NVP-HSP990 samples were normalised to the corresponding wild-type vehicle samples. For simplicity, in zQ175 graphs, all the wild-type vehicle samples and all the zQ175 vehicle samples from the three ages were plotted together. N = 6 – 9 mice / genotype / treatment for R6/2 and N = 4 - 6 mice / genotype / treatment / age for zQ175. Data were analysed by two-way ANOVA with Bonferroni correction for multiple comparisons. Mean ± SEM. *** p ≤ 0.001; ** p ≤ 0.01; * p ≤ 0.05. WT = wild-type; m = months.*

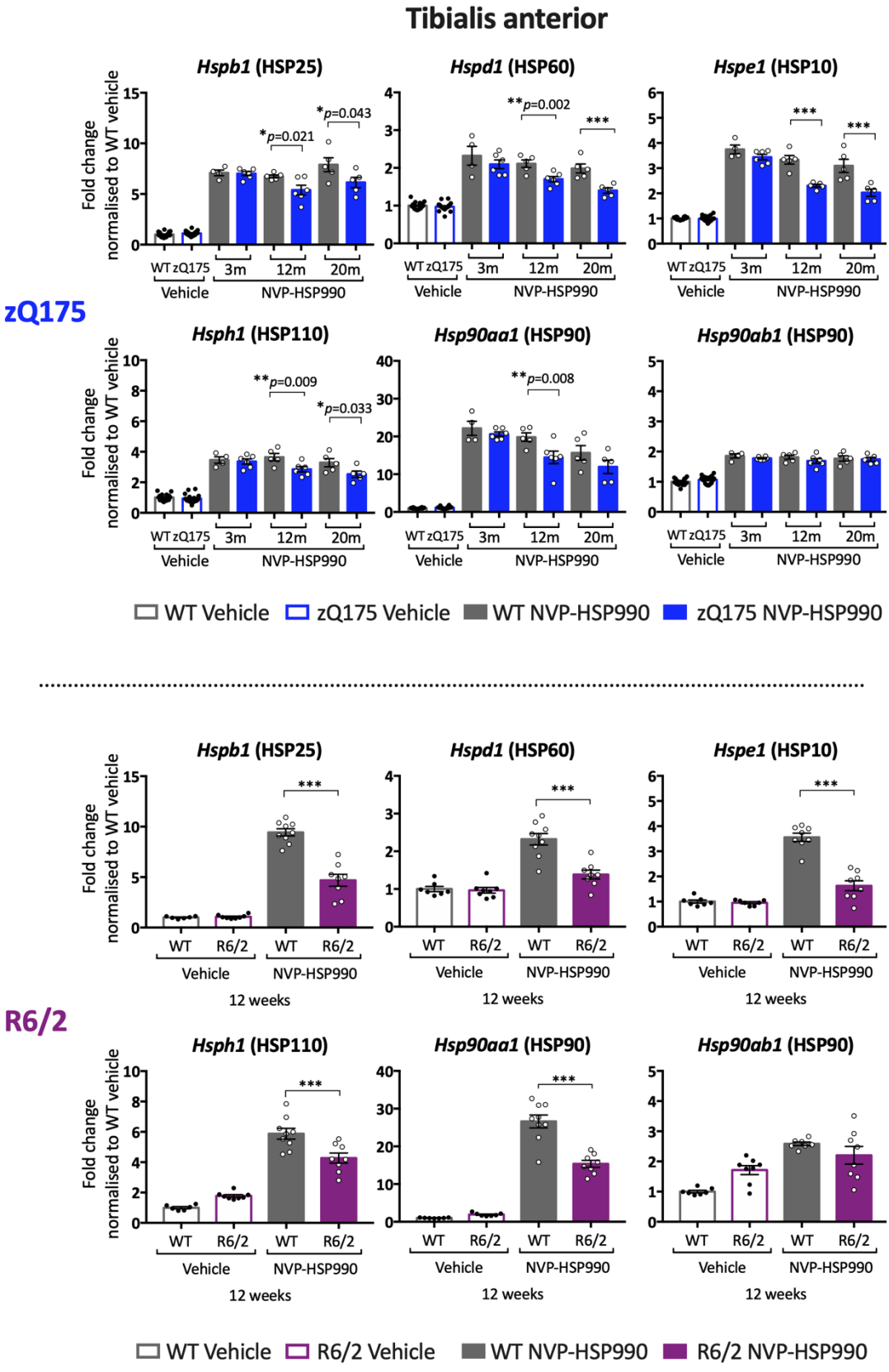
Tibialis anterior
zQ175
R6/2
Hspb1 (HSP25)
Hspd1 (HSP60)
Hspe1 (HSP10)
Hsph1 (HSP110)
Hsp90aa1 (HSP90)
Hsp90ab1 (HSP90)
Fold change normalised to WT vehicle
*p=0.021
*p=0.043
**p=0.002
***
**p=0.009
*p=0.033
**p=0.008
WT zQ175
3m
12m
20m
Vehicle
NVP-HSP990
WT
R6/2
12 weeks
WT Vehicle
zQ175 Vehicle
WT NVP-HSP990
zQ175 NVP-HSP990
R6/2 Vehicle
R6/2 NVP-HSP990

Figure 4.21. Comparative analysis of the heat shock response in the tibialis anterior muscle of zQ175 (at 3, 12 and 12 months of age) and R6/2 mice (at 12 weeks of age).

*The QuantiGene 18-plex assay was used to measure the levels of expression of the heat shock genes Hspb1, Hspd1, Hspe1, Hsph1, Hsp90aa1 and Hsp90ab1 in the tibialis anterior of zQ175 at 3, 12 and 20 months of age and R6/2 at 12 weeks of age, 4 hours after treatment with vehicle or NVP-HSP990. All the NVP-HSP990 samples were normalised to the corresponding wild-type vehicle samples. For simplicity, in zQ175 graphs, all the wild-type vehicle samples and all the zQ175 vehicle samples from the three ages were plotted together. N = 6 – 9 mice / genotype / treatment for R6/2 and N = 4 - 6 mice / genotype / treatment / age for zQ175. Data were analysed by two-way ANOVA with Bonferroni correction for multiple comparisons. Mean ± SEM. *** p ≤ 0.001; ** p ≤ 0.01; * p ≤ 0.05. WT = wild-type; m = months.*

4.3.3 Analysis of the heat shock response in the striatum of zQ175 and R6/2 mouse models

As displayed in Figures 4.22 and 4.23, the impairment that was detected in striatum followed a comparable pattern in both zQ175 and R6/2, generally with similar fold changes of expression and decline in the induction. Five genes were consistently dysregulated in both models: *Hspa1a/b*, *Dnaja1*, *Hspd1*, *Hspe1* and *Hsph1*. Due to a high variability between the NVP-HSP990 samples in R6/2, the decrease in the induced levels of *Hspa1a/b* expression did not reach statistical significance. In zQ175, the dysregulated induction for these genes was apparent in all cases from 3 months of age. Surprisingly, and in contrast to the brain hemisphere data for both zQ175 and R6/2 (Figure 4.3; Labbadia *et al.,* 2011), neither *Dnajb1* nor *Hspb1* were clearly affected in the striatal region.

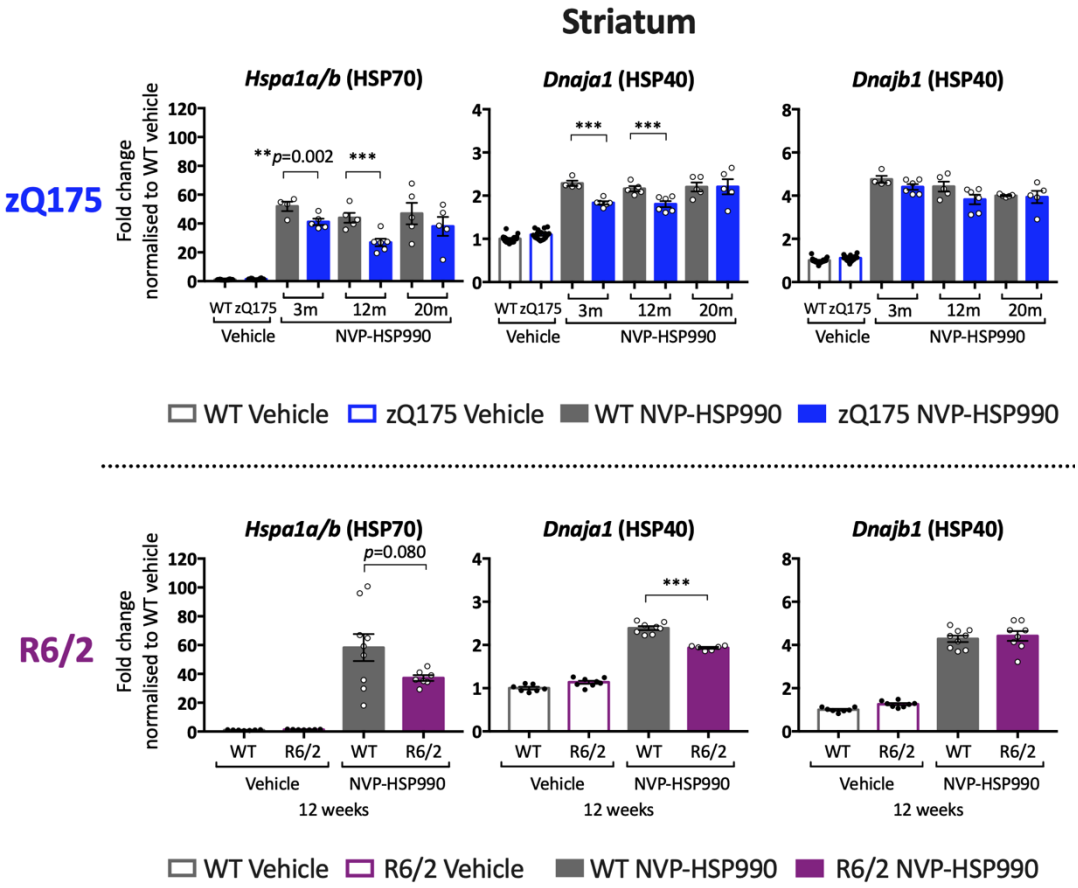

Figure 4.22. Comparative analysis of the heat shock response in the striatum of zQ175 (at 3, 12 and 12 months of age) and R6/2 mice (at 12 weeks of age).
*The QuantiGene 18-plex assay was used to measure the levels of expression of the heat shock genes Hspa1a/b, Dnaja1, Dnajb1 in the striatum of zQ175 at 3, 12 and 20 months of age and R6/2 at 12 weeks of age, 4 hours after treatment with vehicle or NVP-HSP990. All NVP-HSP990 samples were normalised to the corresponding wild-type vehicle samples. For simplicity, in zQ175 graphs, all the wild-type vehicle samples and all the zQ175 vehicle samples from the three ages were plotted together. N = 6 – 9 mice / genotype / treatment for R6/2 and N = 4 - 6 mice / genotype / treatment / age for zQ175. Data were analysed by two-way ANOVA with Bonferroni correction for multiple comparisons. Mean ± SEM. *** p ≤ 0.001; ** p ≤ 0.01. WT = wild-type; m = months.*

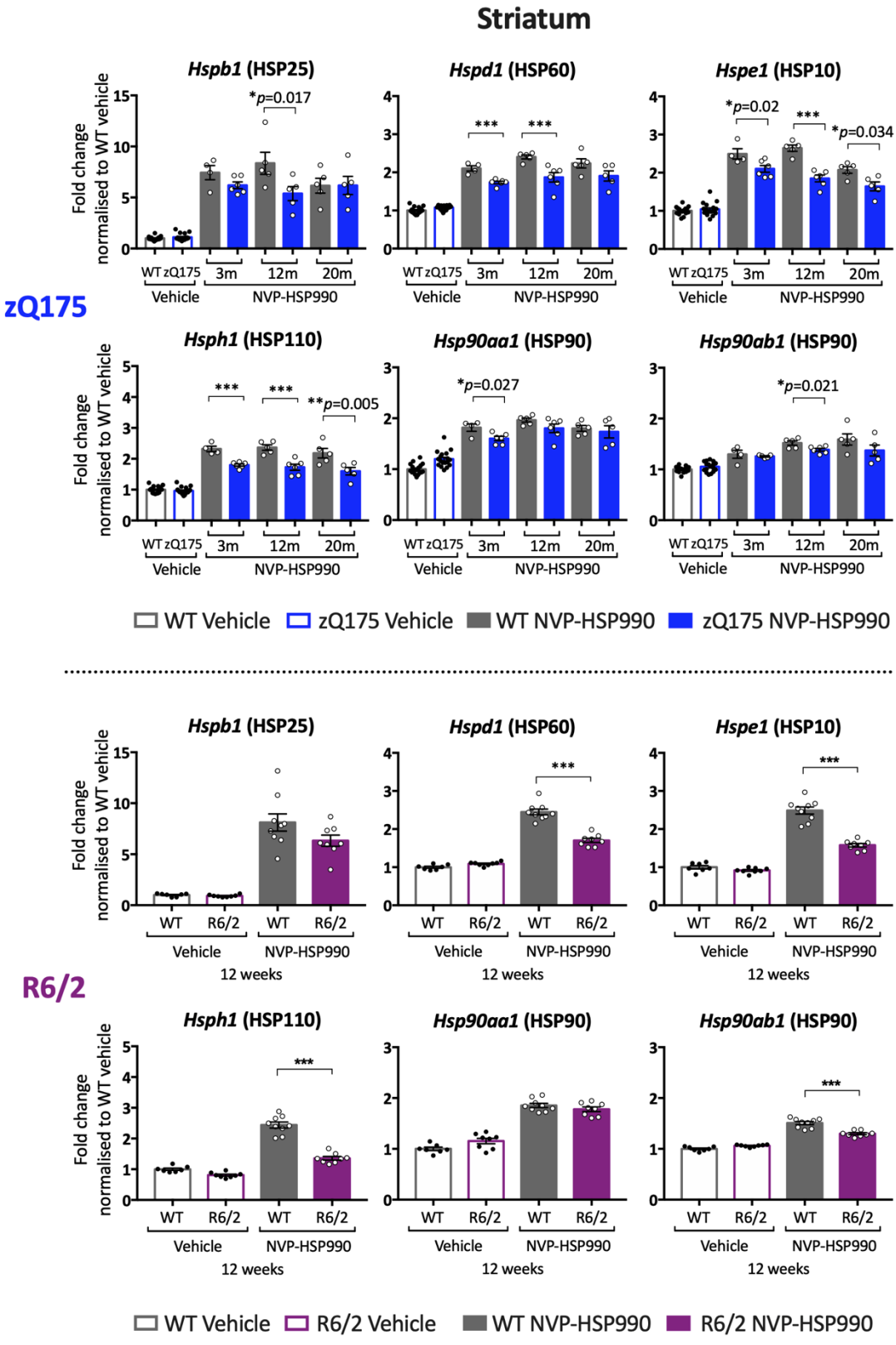
Striatum
zQ175
Hspb1 (HSP25)
Hspd1 (HSP60)
Hspe1 (HSP10)
Hsph1 (HSP110)
Hsp90aa1 (HSP90)
Hsp90ab1 (HSP90)
Fold change normalised to WT vehicle
*p=0.017
***
*p=0.02
*p=0.034
**p=0.005
*p=0.027
*p=0.021
WT zQ175
3m
12m
20m
Vehicle
NVP-HSP990
WT Vehicle
zQ175 Vehicle
WT NVP-HSP990
zQ175 NVP-HSP990
R6/2
WT
R6/2
12 weeks
R6/2 Vehicle
R6/2 NVP-HSP990

Figure 4.23. Comparative analysis of the heat shock response in the striatum of zQ175 (at 3, 12 and 12 months of age) and R6/2 mice (at 12 weeks of age).
*The QuantiGene 18-plex assay was used to measure the levels of expression of the heat shock genes Hspb1, Hspd1, Hspe1, Hsph1, Hsp90aa1 and Hsp90ab1 in the striatum of zQ175 at 3, 12 and 20 months of age and R6/2 at 12 weeks of age, 4 hours after treatment with vehicle or NVP-HSP990. All NVP-HSP990 samples were normalised to the corresponding wild-type vehicle samples. For simplicity, in zQ175 graphs, all the wild-type vehicle samples and all the zQ175 vehicle samples from the three ages were plotted together. N = 6 – 9 mice / genotype / treatment for R6/2 and N = 4 - 6 mice / genotype / treatment / age for zQ175. Data were analysed by two-way ANOVA with Bonferroni correction for multiple comparisons. Mean ± SEM. *** p ≤ 0.001; ** p ≤ 0.01; * p ≤ 0.05. WT = wild-type; m = months.*

4.3.4 Analysis of the heat shock response in the cortex of zQ175 and R6/2 mouse models

When compared to the tibialis anterior and striatum, the heat shock response was impaired to a lesser extent in the cortex. This was especially true for the zQ175 model, where only *Hspa1a/b*, *Hspe1* and *Hsph1* exhibited some level of dysregulation, and only at 12 months, whereas for R6/2, the impairment was more established for these same genes, and *Hspd1* was also affected. Consistent with the striatal data, *Dnajb1* and *Hspb1* did not display signs of reduced induction in any model (Figures 4.24 and 4.25).

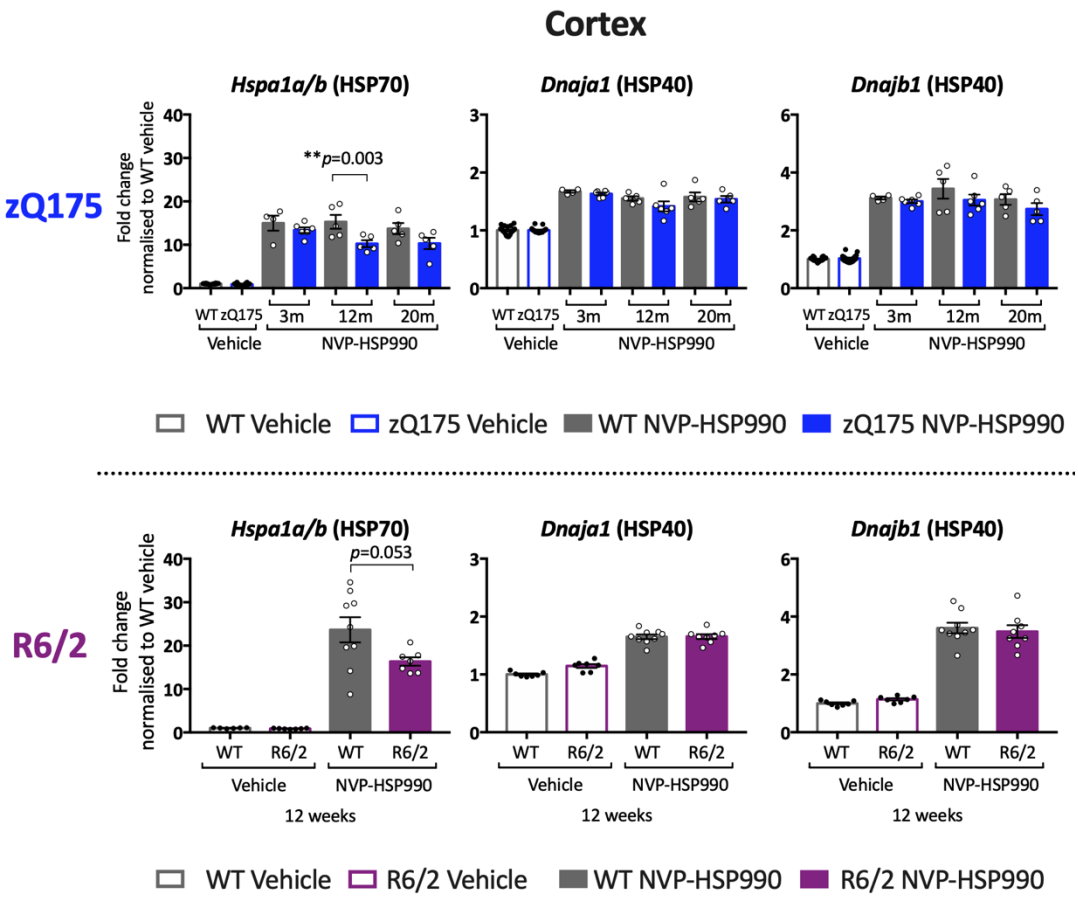

Figure 4.24. Comparative analysis of the heat shock response in the cortex of zQ175 (at 3, 12 and 12 months of age) and R6/2 mice (at 12 weeks of age).
*The QuantiGene 18-plex assay was used to measure the levels of expression of the heat shock genes Hspa1a/b, Dnaja1 and Dnajb1 in the cortex of zQ175 at 3, 12 and 20 months of age and R6/2 at 12 weeks of age, 4 hours after treatment with vehicle or NVP-HSP990. All NVP-HSP990 samples were normalised to the corresponding wild-type vehicle samples. For simplicity, in zQ175 graphs, all the wild-type vehicle samples and all the zQ175 vehicle samples from the three ages were plotted together. N = 6 – 9 mice / genotype / treatment for R6/2 and N = 4 - 6 mice / genotype / treatment / age for zQ175. Data were analysed by two-way ANOVA with Bonferroni correction for multiple comparisons. Mean ± SEM. ** p ≤ 0.01. WT = wild-type; m = months.*

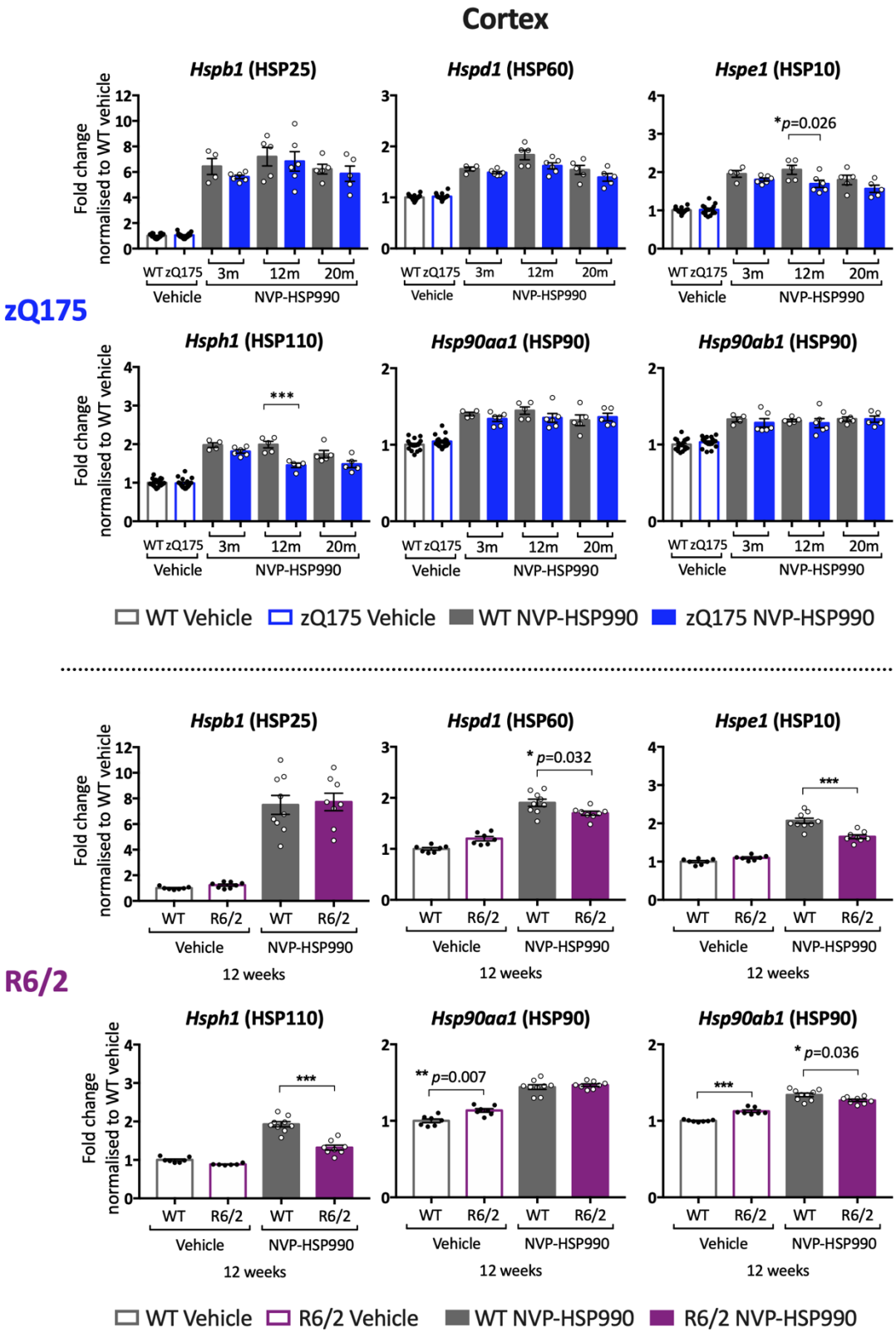
Cortex
zQ175
Hspb1 (HSP25)
Hspd1 (HSP60)
Hspe1 (HSP10)
Hsph1 (HSP110)
Hsp90aa1 (HSP90)
Hsp90ab1 (HSP90)
Fold change normalised to WT vehicle
*p=0.026
***
WT zQ175
3m
12m
20m
Vehicle
NVP-HSP990
WT Vehicle
zQ175 Vehicle
WT NVP-HSP990
zQ175 NVP-HSP990
R6/2
* p=0.032
** p=0.007
* p=0.036
WT
R6/2
12 weeks
R6/2 Vehicle
R6/2 NVP-HSP990

Figure 4.25. Comparative analysis of the heat shock response in the cortex of zQ175 (at 3, 12 and 12 months of age) and R6/2 mice (at 12 weeks of age).
*The QuantiGene 18-plex assay was used to measure the levels of expression of the heat shock genes Hspb1, Hspd1, Hspe1, Hsph1, Hsp90aa1 and Hsp90ab1 in the cortex of zQ175 at 3, 12 and 20 months of age and R6/2 at 12 weeks of age, 4 hours after treatment with vehicle or NVP-HSP990. The NVP-HSP990 samples were normalised to the corresponding wild-type vehicle samples. For simplicity, in zQ175 graphs, all the wild-type vehicle samples and all the zQ175 vehicle samples from the three ages were plotted together. N = 6 – 9 mice / genotype / treatment for R6/2 and N = 4 - 6 mice / genotype / treatment / age for zQ175. Data were analysed by two-way ANOVA with Bonferroni correction for multiple comparisons. Mean ± SEM. *** $p \leq 0.001$; ** $p \leq 0.01$; * $p \leq 0.05$. WT = wild-type; m = months.*

4.4 Analysis of HSF1 expression in Huntington's disease mouse models

The analysis of the heat shock response at the transcriptional level in zQ175 and R6/2 tissues led to the conclusion that a distinct impairment in the ability to activate the heat shock response was present in both the brain and muscle of these two HD mouse models.

A recent publication reported that HSF1 was abnormally degraded in HD cell models, *post-mortem* brains and cells from HD patients and tissues from the zQ175 HD mouse model. The authors proposed that the mutant HTT protein increased HSF1 phosphorylation, leading to its degradation (Gomez-Pastor *et al.,* 2017).

To investigate whether a reduction in HSF1 could cause the heat shock response transcriptional impairment in zQ175 mice, an analysis of HSF1 levels was conducted in zQ175 tissues at late-stage disease.

4.4.1 *Hsf1* gene expression in brain and muscle of zQ175 mice

Before the analysis at the protein level, Figure 4.26 summarises the levels of *Hsf1* gene expression, as measured by QuantiGene in all the regions studied.

There was no difference in the basal levels of *Hsf1* (vehicle treatment) in brain hemispheres, or striatum, and a mild reduction was found in tibialis anterior and cortex at one time point only. There was no difference in *Hsf1* levels after induction with NVP-HSP990 in tibialis anterior, striatum or cortex at any time point, although a reduction was observed in brain hemispheres. However, given that *Hsf1* is not induced, it probably has no biological significance.

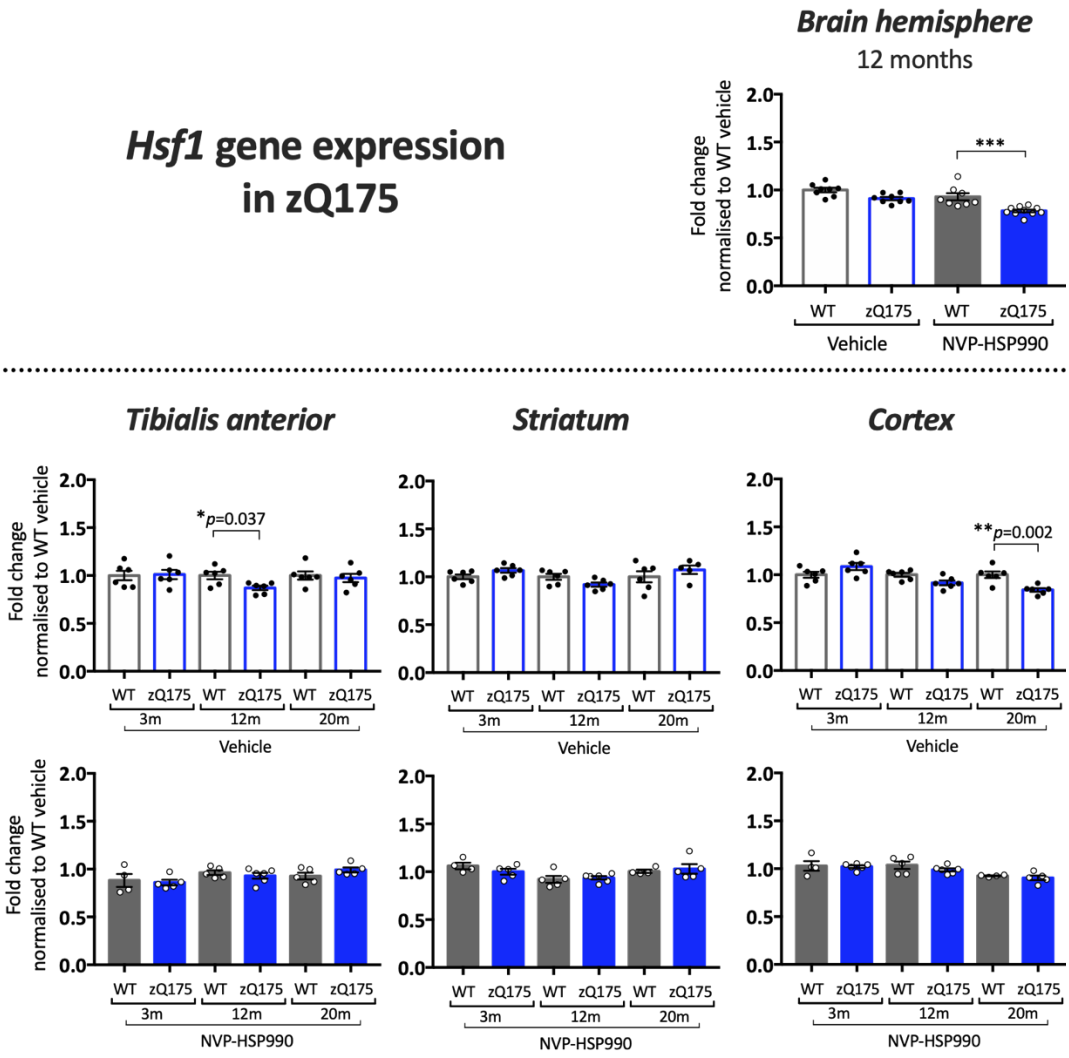

Figure 4.26. Expression of Hsf1 gene in zQ175 tissues as measured by QuantiGene.

*Hsf1 expression was analysed by QuantiGene in the brain hemispheres at 12 months of age and tibialis anterior, striatum and cortex at 3, 12 and 20 months of age, 4 hours after treatment with vehicle or NVP-HSP990. N = 7 - 9 mice / genotype / treatment for brain hemispheres; N = 4 - 6 mice / genotype / treatment / age for tibialis anterior, striatum and cortex. Statistical analysis by two-way ANOVA with Bonferroni correction for multiple comparisons. Mean ± SEM. *** p ≤ 0.001; ** p ≤ 0.01; * p ≤ 0.05. WT = wild-type; m = months.*

4.4.2 Characterisation and optimisation of experimental conditions for HSF1 commercial antibodies

A thorough characterisation of commercial HSF1 antibodies from different suppliers was conducted to select which could be used to measure HSF1 levels in zQ175 tissues.

In order to confirm that the HSF1 antibodies were detecting HSF1, two controls were included in all of the experiments. As a negative control, *Hsf1* knockout samples were used, as the absence of a band in *Hsf1* knockout lysates would indicate the location and size of the correct protein. As a positive control for the HSF1 activated state, samples from wild-type mice that had been dosed with NVP-HSP990 were included. As a consequence of NVP-HSP990 treatment, HSF1 becomes hyperphosphorylated which, as reported (Labbadia *et al.,* 2011; Neueder *et al.,* 2014; Neueder *et al.,* 2017), can be detected as a hypershifted band on western blots.

Brain hemispheres were collected from wild-type mice, *Hsf1* knockout mice, and wild-type mice that had been treated with 12 mg / kg NVP-HSP990. Lysates were prepared in a variety of lysis buffers (RIPA, HEPES, KCl, Triton), including several phosphatase inhibitors as required. The antibodies were tested in a range of dilutions and with two blocking solutions. Additionally, for some of the antibodies, the optimisation also involved a comparison between precast gels (Criterion gels, Bio-Rad) and polyacrylamide gels made in-house. More experimental details can be found in Chapter 2 (section 2.1.6).

Figures 4.27 – 4.30 comprise a series of representative western blot images, all indicating the experimental conditions that were tested. In Figure 4.27, both antibodies from Enzo Life Sciences (ADI-SPA-901F and ADI-SPA-950F) seemed to detect a band that, especially for ADI-SPA-950F, appeared to be hypershifted in the NVP-HSP990 treated samples. These antibodies were further analysed in additional gels, however, the lanes containing *Hsf1* knockout samples consistently showed a band in all cases. In Figure 4.28, the Santa Cruz antibody sc-17757 was interacting with multiple bands, even in the *Hsf1* knockout samples, and therefore, was

discarded. The antibody sc-13516 was more promising and detected the HSF1 activated state, however, even though it was also tested in precast and in-house made gels, a band was always present in the *Hsf1* knockout lanes. In Figure 4.29, representative blots using antibodies from Abcam and Bethyl Laboratories are shown. Both of the Abcam antibodies (ab2923 and ab61382) were very non-specific and there were no differences in the bands for the wild-type, *Hsf1* knockout or induced samples. The same applied to Bethyl Laboratories antibodies A303-174AT and A303-175AT. Finally in Figure 4.30, two examples from blots using antibodies Cell Signalling #4356T and Invitrogen PA3-017 showed a very faint and non-specific signal in all of the samples. None of these antibodies clearly recognised HSF1 and in some cases, multiple, non-specific bands were detected.

Two antibodies, Bethyl A303-176A and Proteintech 51034-1-AP, were found to detect HSF1, as a hypershifted band was observed in the NVP-HSP990-treated samples and this band was absent in the *Hsf1* knockout lanes. These two antibodies were used in the subsequent experiments. Of all of the antibodies tested, these were the only two antibodies that could also be used to reliably detect HSF1 in muscle, especially Proteintech 51034-1-AP antibody, using a similarly comprehensive analysis.

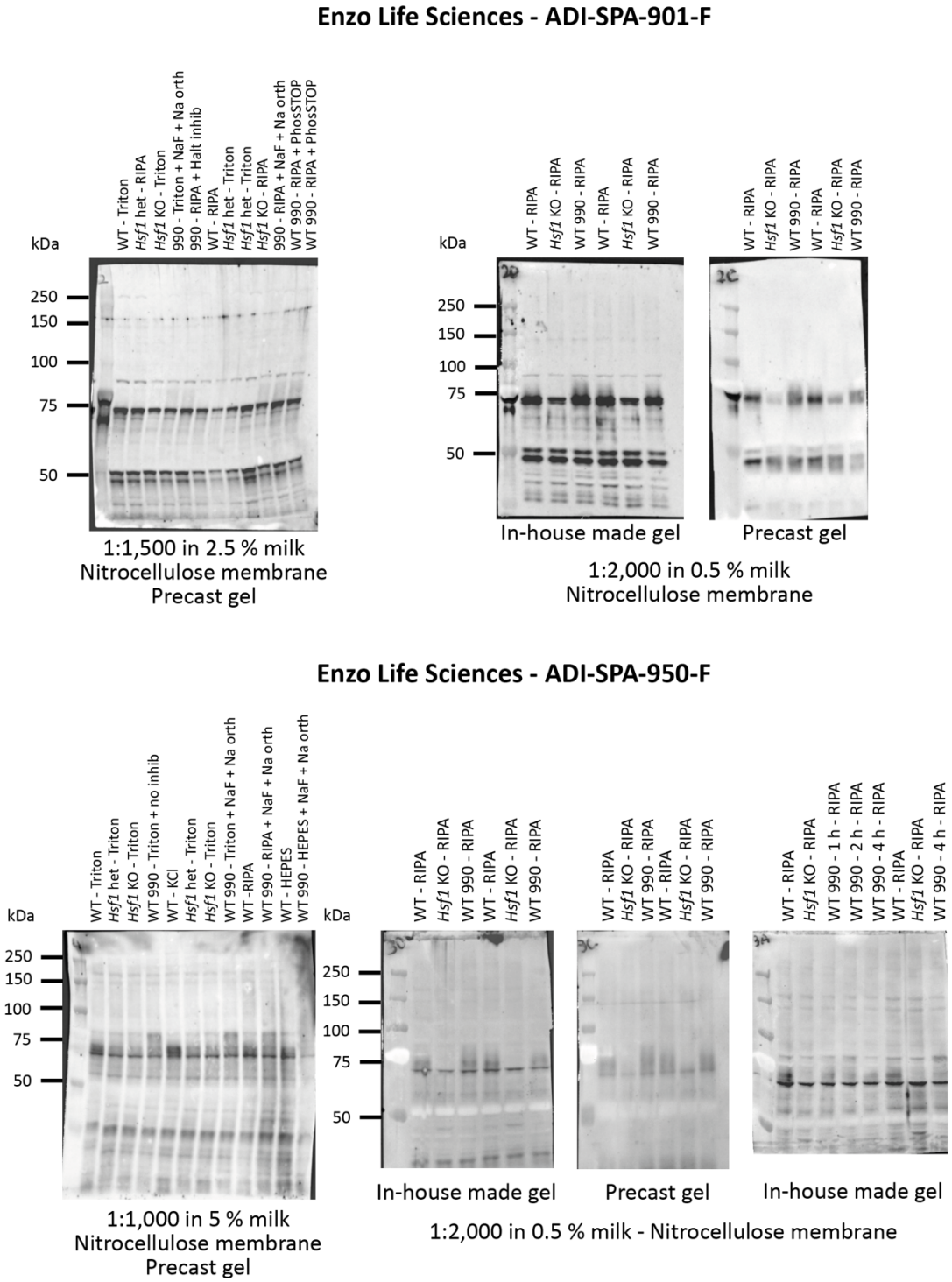

Figure 4.27. Representative western blots with HSF1 antibodies from Enzo Life Sciences, ADI-SPA-901-F (top) and ADI-SPA-950-F (bottom).

Predicted HSF1 band sizes: 80 - 95 kDa (ADI-SPA-901), 85 kDa (ADI-SPA-950). These antibodies seemed to detect a hypershift in lysates from NVP-HSP990 treated mice, however a band was always detected in Hsf1 knockout lanes. WT = wild-type; het = heterozygous; KO = knockout; 990 = NVP-HSP990; Halt inhib. = Halt phosphatase inhibitor cocktail (Thermo Fisher Scientific); Na orth.= Na orthovanadate; PhosSTOP = phosphatase inhibitor tablets (Roche).

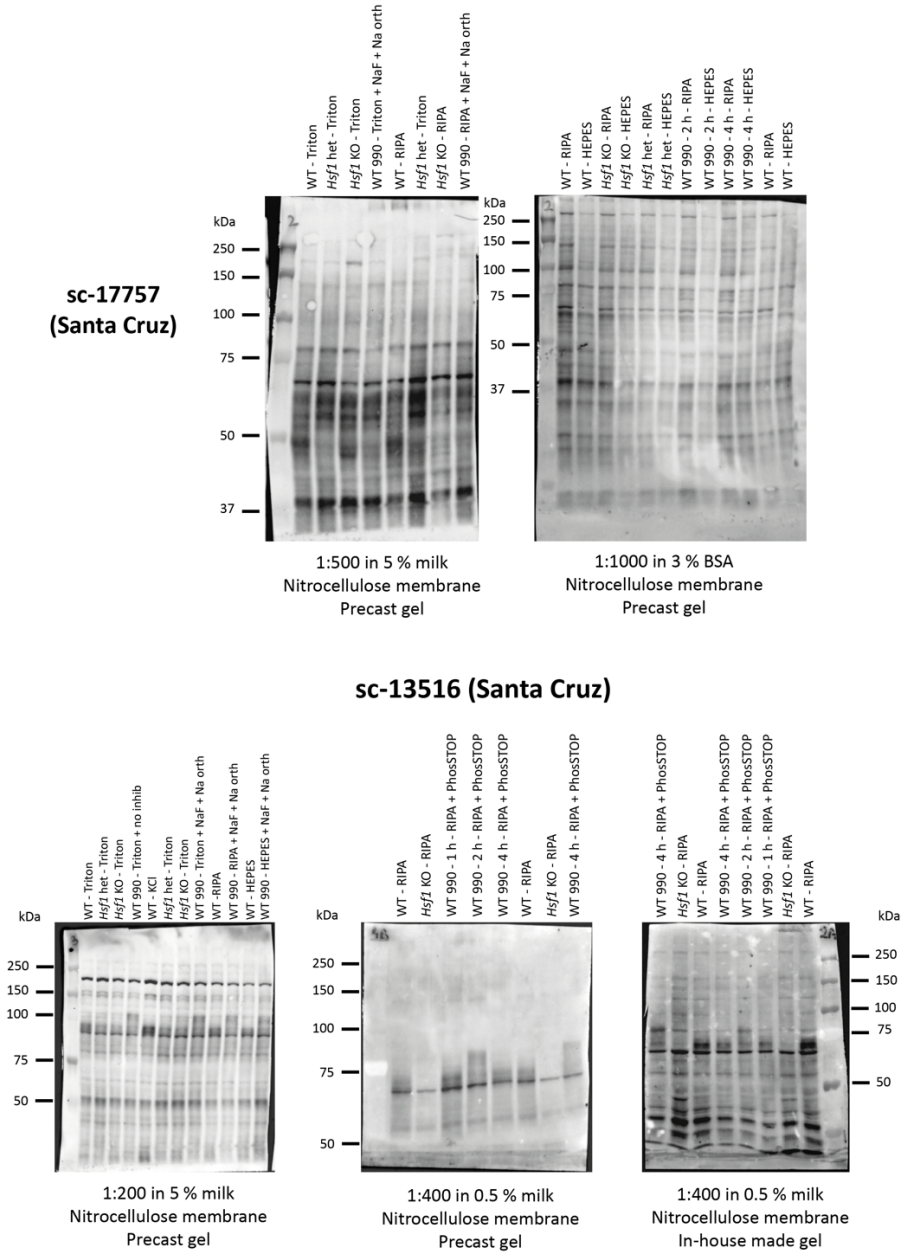

Figure 4.28. Representative western blots with HSF1 antibodies from Santa Cruz Biotechnology, sc-17757 (top) and sc-13516 (bottom).

Predicted HSF1 band sizes: 89-90 kDa (sc-17757 and sc-13516). Multiple proteins were detected by sc-17757, none absent in Hsf1 knockout lanes. A hypershifted band was detected by sc-13516 in lysates from NVP-HSP990 treated mice, but a band was always present in the Hsf1 knockout lanes. WT = wild-type; het = heterozygous; KO = knockout; 990 = NVP-HSP990; Halt inhib. = Halt phosphatase inhibitor cocktail (Thermo Fisher Scientific); Na orth.= Na orthovanadate; PhosSTOP = phosphatase inhibitor tablets (Roche); h = hours.

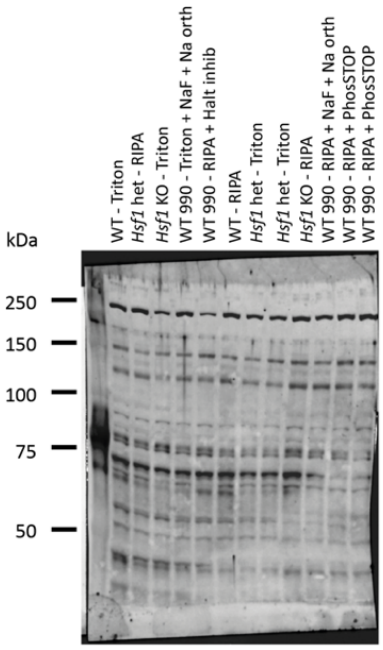

ab2923 (Abcam)
Diluted 1:500 in 2.5 % non-fat milk
Nitrocellulose membrane
Precast gel

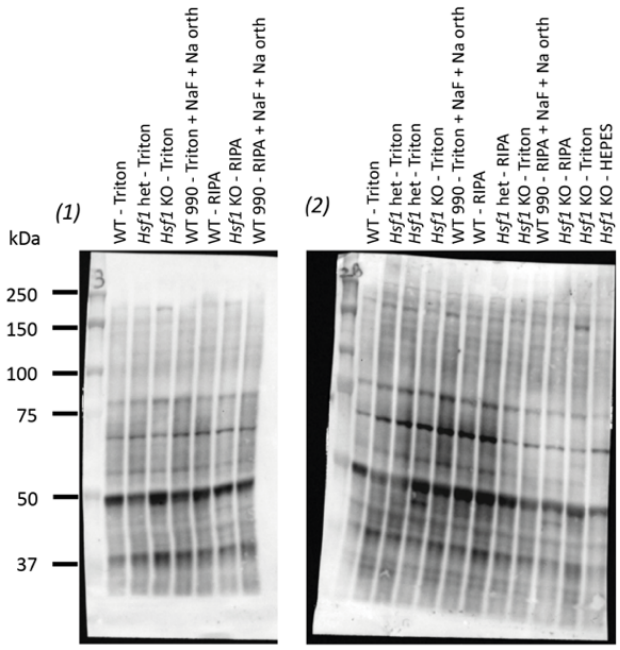

ab61382 (Abcam)
(1) Diluted 1:1,000 in 5 % non-fat milk
(2) Diluted 1:1,000 in 2.5 % BSA
Nitrocellulose membranes
Precast gels

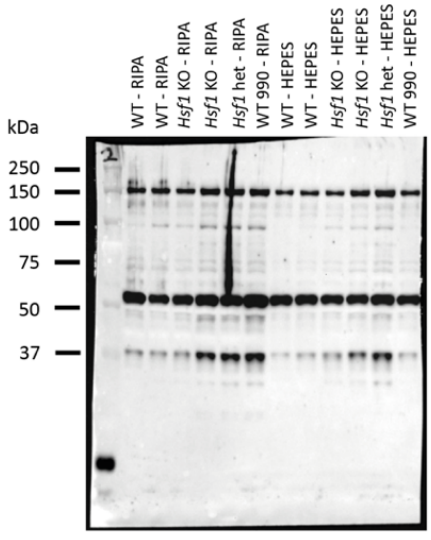

A303-174AT (Bethyl)
Diluted 1:2,000 in 5 % non-fat milk
Nitrocellulose membrane
Precast gel

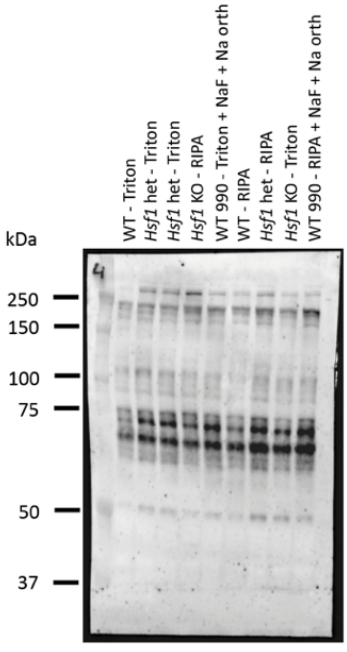

A303-175AT (Bethyl)
Diluted 1:1,000 in 2.5 % non-fat milk
Nitrocellulose membrane
Precast gel

Figure 4.29. Representative western blots with HSF1 antibodies from Abcam ab2923 and ab61382 (top) and from Bethyl Laboratories A303-174AT and A303-175AT (bottom).

Predicted HSF1 band sizes: 83 kDa (ab2923), 57 kDa (ab61382), 70 kDa (Bethyl A303-174AT and A303-175AT). Multiple proteins were detected, none absent in the Hsf1 knockout lanes. WT = wild-type; het = heterozygous; KO = knockout; 990 = NVP-HSP990; Halt inhib. = Halt phosphatase inhibitor cocktail (Thermo Fisher Scientific); Na orth.= Na orthovanadate; PhosSTOP = phosphatase inhibitor tablets (Roche).

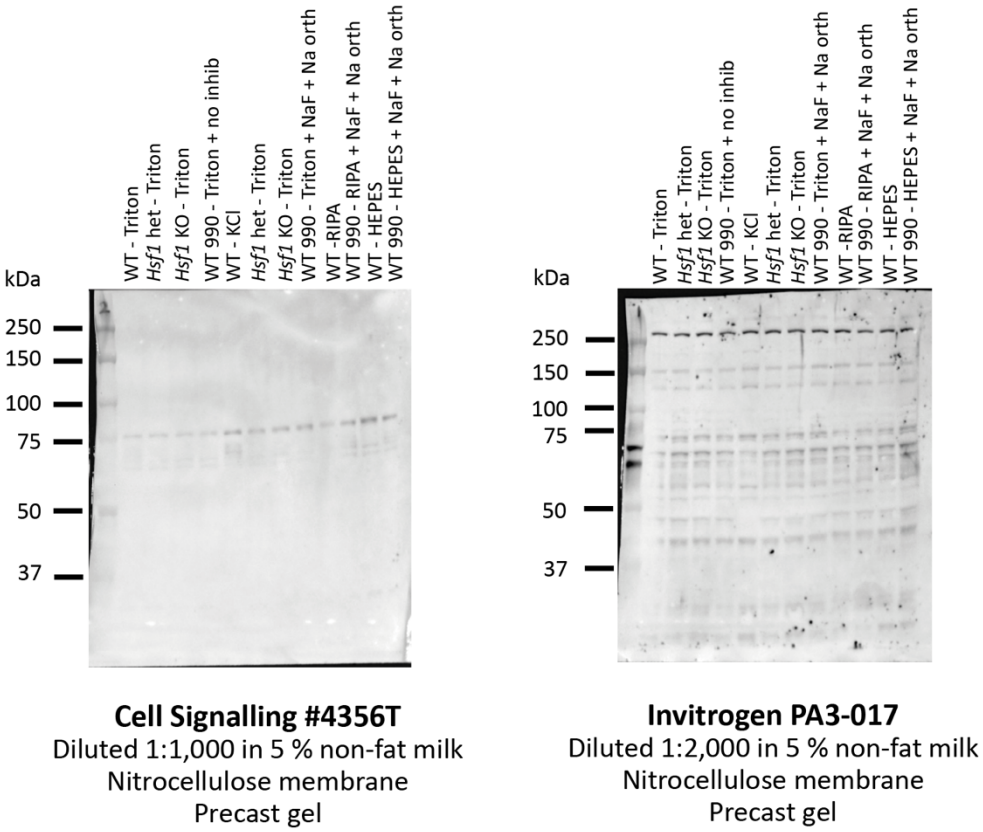

Figure 4.30. Representative western blots with HSF1 antibodies Cell Signalling #4356T (left) and Invitrogen PA3-017 (right).

Predicted size of HSF1 band detected: 80 kDa (Cell Signalling #4356T), 83 kDa (Invitrogen PA3-017). Non-specific or weak signals were detected for Cell Signalling #4356T antibody; multiple bands detected with Invitrogen PA3-017. No band was absent in the Hsf1 knockout lanes. WT = wild-type; het = heterozygous; KO = knockout; 990 = NVP-HSP990; Na orth.= Na orthovanadate.

4.4.3 HSF1 expression in the brain hemispheres of zQ175 mice at 12 months of age and comparison with R6/2 and *Hdh*Q150 mouse models

To begin to elucidate whether the expression of HSF1 was affected by disease progression in the zQ175 model and, potentially, could be responsible for the disruption of the heat shock response at transcriptional level (Figure 4.3), the other brain hemisphere from the 12-month zQ175 cohort (*n* = 6 mice / genotype / treatment), collected 4 hours after NVP-HSP990 or vehicle dosing, was lysed using the optimised conditions for western blotting with HSF1 antibodies determined in the previous section. This was the age at which the zQ175 mice had been analysed by Gomez-Pastor *et al*. (2017).

The levels of HSF1 were quantified separately for each treatment group, normalising to the corresponding wild-type and using ATP5B as the loading control. In the vehicle group (basal expression), HSF1 levels in zQ175 brains were found to be slightly higher than in wild-type brains. Similar levels of HSF1 expression between zQ175 and wild-type were quantified in the NVP-HSP990 group (Figure 4.31, a). A hypershift could be detected for the NVP-HSP990 samples, a consequence of the hyperphosphorylation of HSF1 in the activated state after induction of the heat shock response.

These results were consistent with the data obtained in R6/2 and *Hdh*Q150 by Labbadia *et al.* (2011). HSF1 expression was measured at 12 weeks of age for R6/2 and 22 months of age for *Hdh*Q150, 2 hours after treatment with vehicle or NVP-HSP990. The hypershift was also visible in the NVP-HSP990 samples and the expression was quantified relative to α -tubulin. In both models, as depicted in Figure 4.31 (b, c, d), HSF1 remained unaltered between genotypes.

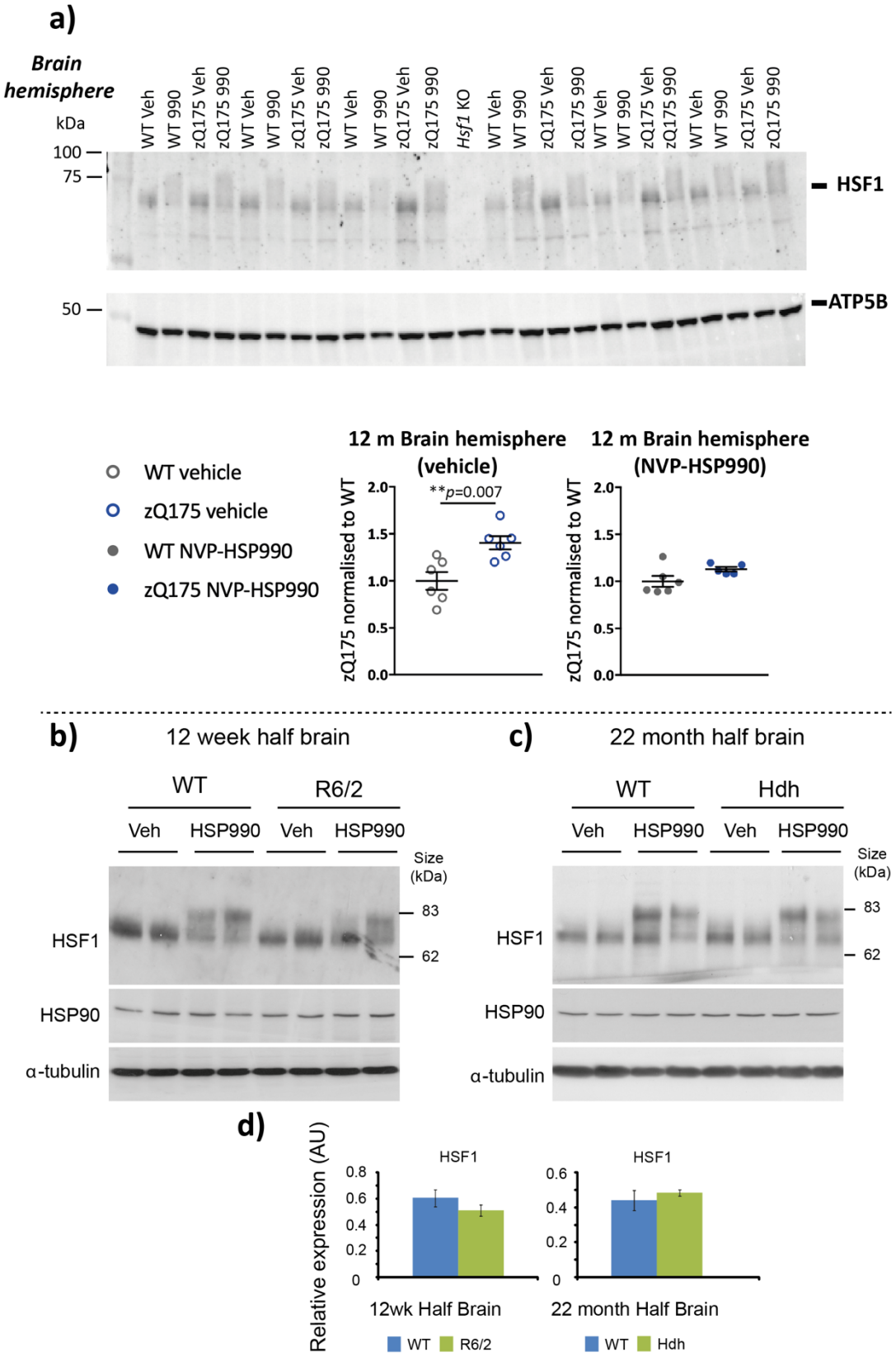
a)
Brain hemisphere
kDa
WT Veh
WT 990
zQ175 Veh
zQ175 990
Hsf1 KO
100
75
50
HSF1
ATP5B
WT vehicle
zQ175 vehicle
WT NVP-HSP990
zQ175 NVP-HSP990
12 m Brain hemisphere (vehicle)
12 m Brain hemisphere (NVP-HSP990)
**p=0.007
zQ175 normalised to WT
b)
12 week half brain
WT
R6/2
Veh
HSP990
Size (kDa)
83
62
HSF1
HSP90
α-tubulin
c)
22 month half brain
Hdh
d)
Relative expression (AU)
12wk Half Brain
22 month Half Brain

Figure 4.31. HSF1 *expression in the brain hemispheres of zQ175 (12 months), R6/2 (12 weeks) and HdhQ150 (22 months) by western blotting.*
a) HSF1 *expression was measured in brain hemispheres of zQ175 at 12 months of age, collected 4 hours after dosing, using the Proteintech 51034-1-AP HSF1 antibody. The levels of* HSF1 *expression were quantified per treatment group, relative to the* ATP5B *loading control and normalised to the corresponding wild-type mice. N = 6 mice / genotype / treatment. Uncropped blots are included in the Appendix Figure 1. Statistical analysis by unpaired Student's t-test. Mean ± SEM. ** p ≤ 0.01.* ***b)*** *and* ***c)*** HSF1 *expression was analysed in brain hemispheres of R6/2 at 12 weeks of age (**b**) and HdhQ150 at 22 months of age (**c**).* ***d)*** *Quantification of* HSF1 *expression detected in* ***b)*** *and* ***c)****, relative to α -tubulin loading control. N = 4 mice / treatment group.* ***b)****,* ***c)*** *and* ***d)*** *are adapted from a figure in Labbadia et al., (2011) and reproduced with permission. WT = wild-type; Hdh = HdhQ150; Veh = vehicle; 990 = NVP-HSP990; wk = weeks; m = months.*

4.4.4 HSF1 expression in the tibialis anterior, striatum and cortex of zQ175 mice at 20 months of age

Following on from the analysis in the brain hemispheres and to complete the picture of HSF1 expression in zQ175, HSF1 expression was evaluated in tibialis anterior muscle, striatum and cortex regions of zQ175 at end-stage of disease (20 months of age), 4 hours after being administered with vehicle or NVP-HSP990. These were the three types of tissues that had been analysed by Gomez-Pastor *et al.* (2017). The remaining tibialis anterior, striatum and half cortex from the zQ175 cohort at 20 months of age used in the transcriptional analysis were processed for western blotting (*n* = 5 - 6 mice / genotype / treatment). The NVP-HSP990 samples that were previously excluded in the transcriptional analysis (section 4.3.2) were also excluded from protein quantification. The uncropped blots can be found in the Appendix, on which the samples removed from the analysis are indicated (Appendix Figures 2, 3, 4).

As for the brain hemispheres (Figure 4.31), the quantification of HSF1 levels was done separately for vehicle and NVP-HSP990 treated samples from each tissue. This expression of HSF1 at basal or activated states in zQ175 was equivalent to the expression in the corresponding wild-type in all of the tissues studied (Figure 4.32).

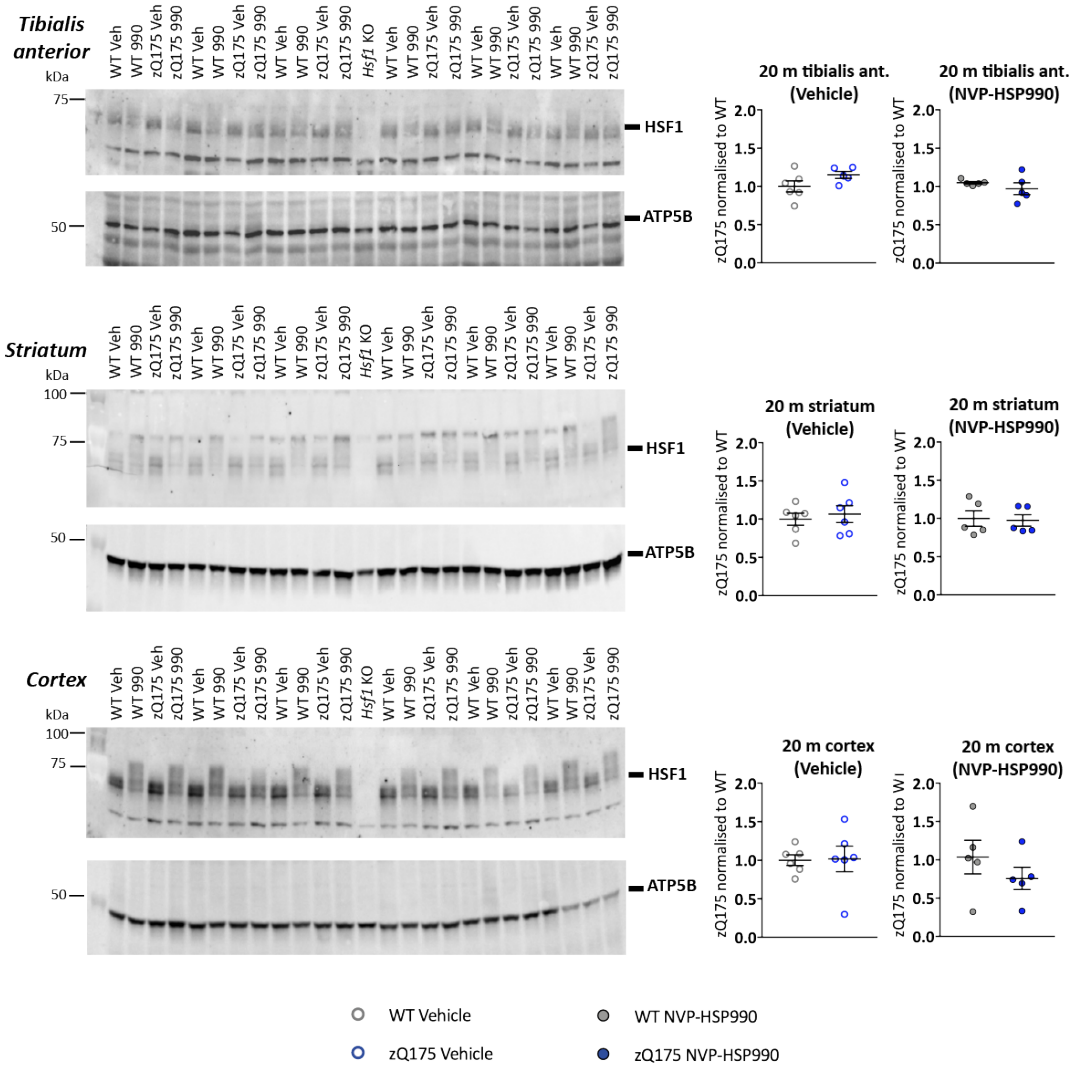

Figure 4.32. HSF1 *expression in the tibialis anterior, striatum and cortex of zQ175 at 20 months of age, by western blotting.*

HSF1 *expression was measured in tibialis anterior, striatum and cortex of zQ175 at 20 months of age, collected 4 hours after dosing, using the Proteintech 51034-1-AP HSF1 antibody for tibialis anterior and cortex and the Bethyl A303-176A antibody for striatum. The levels of* HSF1 *expression were quantified per treatment group, relative to* ATP5B *loading control and normalised to the corresponding wild-type mice. N = 5 - 6 mice / genotype / treatment. Uncropped blots are included in the Appendix Figures 2, 3, 4. Statistical analysis by unpaired Student's t-test. Mean ± SEM. WT = wild-type; 990 = NVP-HSP990; Veh = vehicle; m = months; ant. = anterior.*

4.5 Summary of results and discussion

The heat shock response has been the subject of extensive investigation in HD. Our group participated in this research and provided evidence of a defective induction of the heat shock response in the HD mouse models R6/2 and *Hdh*Q150, and this defect was correlated with the progression of the disease. The pulsed treatment with NVP-HSP990 led to a modest improvement of some HD phenotypes and reduction of aggregation, however, as disease progressed, the HD mice developed an attenuated ability to induce the heat shock response (Labbadia *et al.,* 2011). Studies using the zQ175 mouse model had proposed that this heat shock response impairment was caused by a reduction in HSF1 levels (Gomez-Pastor *et al*., 2017). However, that a disease-related heat shock impairment occurs in zQ175 mice was not shown in that paper and has not been demonstrated elsewhere. Therefore, to further investigate the role of HSF1, a detailed characterisation of the heat shock response in the zQ175 mouse model was performed.

The following tables (Tables 4.4 – 4.7) summarise the results obtained and statistical significance from the gene expression analysis carried out, either by QuantiGene or RT-qPCR, in brain hemispheres, tibialis anterior, striatum and cortex of R6/2 and zQ175 mice, after being dosed with NVP-HSP990 or vehicle, at different ages.

Table 4.4. Summary of results from the gene expression analyses in brain hemispheres of zQ175 at 12 months of age and R6/2 at 12 weeks of age.

	Brain hemispheres		
	zQ175 – 12 months	**R6/2 –** 12 weeks	
Genes	*4 hours*	*4 hours*	*8 hours*
Hspa1a/b	***	***	***
Dnaja1	***	-	-
Dnajb1	***	***	*
Hspb1	***	*	***
Hspd1	n.s.	-	-
Hspe1	***	-	-
Hsph1	***	-	-
Hsp90aa1	***	-	-
Hsp90ab1	**	-	-

The analysis of gene expression in brain hemispheres samples from R6/2 mice was performed by RT-qPCR by Labbadia et al. (2011) only for the Hspa1a/b, Hspb1 and Dnajb1 genes.

*n.s. = not significant; *** $p \leq 0.001$; ** $p \leq 0.01$; * $p \leq 0.05$*

Table 4.5. Summary of results from the gene expression analyses in tibialis anterior of zQ175 at 3, 12 and 20 months of age and R6/2 at 12 weeks of age.

	Tibialis anterior			
	R6/2	zQ175		
Genes	*12 weeks*	*3 months*	*12 months*	*20 months*
Hspa1a/b	***	n.s.	***	*
Dnaja1	n.s.	*	**	n.s.
Dnajb1	n.s.	n.s.	***	**
Hspb1	***	n.s.	*	*
Hspd1	***	n.s.	**	***
Hspe1	***	n.s.	***	***
Hsph1	***	n.s.	**	*
Hsp90aa1	***	n.s.	**	n.s
Hsp90ab1	n.s.	n.s.	n.s.	n.s.

*n.s. = not significant; *** $p \leq 0.001$; ** $p \leq 0.01$; * $p \leq 0.05$*

Table 4.6. Summary of results from the gene expression analyses in striatum of zQ175 at 3, 12 and 20 months of age and R6/2 at 12 weeks of age

	Striatum			
	R6/2	zQ175		
Genes	*12 weeks*	*3 months*	*12 months*	*20 months*
Hspa1a/b	n.s.	**	***	n.s.
Dnaja1	***	***	***	n.s.
Dnajb1	n.s.	n.s.	n.s.	n.s.
Hspb1	n.s.	n.s.	*	n.s.
Hspd1	***	***	***	n.s.
Hspe1	***	*	***	*
Hsph1	***	***	***	**
Hsp90aa1	n.s.	*	n.s.	n.s.
Hsp90ab1	***	n.s.	*	n.s.

*n.s. = not significant; *** $p \leq 0.001$; ** $p \leq 0.01$; * $p \leq 0.05$*

Table 4.7. Summary of results from the gene expression analyses in cortex of zQ175 at 3, 12 and 20 months of age and R6/2 at 12 weeks of age

	Cortex			
	R6/2	zQ175		
Genes	*12 weeks*	*3 months*	*12 months*	*20 months*
Hspa1a/b	n.s.	n.s.	**	n.s.
Dnaja1	n.s.	n.s.	n.s.	n.s.
Dnajb1	n.s.	n.s.	n.s.	n.s.
Hspb1	n.s.	n.s.	n.s.	n.s.
Hspd1	*	n.s.	n.s.	n.s.
Hspe1	***	n.s.	*	n.s.
Hsph1	***	n.s.	***	n.s.
Hsp90aa1	n.s.	n.s.	n.s.	n.s.
Hsp90ab1	*	n.s.	n.s.	n.s.

*n.s. = not significant; *** $p \leq 0.001$; ** $p \leq 0.01$; * $p \leq 0.05$*

The conclusions that could be drawn from the experimental work in this Chapter are:

- **The induction of the heat shock response was impaired in symptomatic zQ175 mice at the transcriptional level.**

As measured by QuantiGene after thorough optimisation (Figures 4.1 and 4.2), a clear impairment was detected in brain hemispheres and this was consistent with previous data obtained for the R6/2 and *Hdh*Q150 models (Labbadia *et al.,* 2011; Figures 4.3 and 4.4). The limitations associated to RT-qPCR had only allowed the analysis of a few heat shock genes in R6/2 and *Hdh*Q150; the QuantiGene methodology allowed for a broader range of heat shock genes to be studied (Figure 4.4).

The development of the QuantiGene multiplex assay for simultaneously measuring the expression levels of many heat shock genes, made a more complete analysis of heat shock impairment in multiple tissues at different stages of disease feasible. Therefore, the pattern of impairment was defined in the tibialis anterior, striatum and cortex of zQ175 mice over the course of the disease: at 3, 12 and 20 months of age. The same regions were also analysed in the R6/2 mice at end-stage of the disease (12 weeks of age) to compare the levels of impairment between two of the most intensively studied mouse models of HD. Optimal lysate dilutions for the QuantiGene 18-plex assay were determined for each tissue and HD mouse model (Figures 4.5 – 4.19 and Table 4.3).

Robust evidence of a deficit in the heat shock response was observed in both models in tibialis anterior and striatum, especially. In tibialis anterior, eight heat shock genes (*Hspa1a/b, Dnaja1*, *Dnajb1*, *Hspb1*, *Hspd1*, *Hspe1*, *Hsph1* and *Hsp90aa1*) appeared to be dysregulated in zQ175 by 12 months of age. In R6/2, most of the heat shock genes studied also showed a lower induction at end-stage (with exception of *Dnaja1* and *Dnajb1* that presented a considerable variability between samples), with a more prominent reduction than in zQ175 (Figures 4.20 and 4.21). Specific features in the progression of muscle pathology and motor phenotypes in HD mouse models may

explain these differences in the decreased levels of expression (Ribchester *et al.,* 2004; Carter *et al.,* 1999; Menalled *et al.,* 2012).

In striatum, the pattern of heat shock response impairment was highly comparable between zQ175 and R6/2 mice, with most of the heat shock genes showing attenuated induction (Figures 4.22 and 4.23). Interestingly, in zQ175 the signs of dysregulation were apparent as early as 3 months of age.

In cortex, a conclusive impairment was seen in R6/2 with five genes affected, however, there was limited proof of such an impairment in zQ175 (Figures 4.24 and 4.25). As in the tibialis anterior, the extent to which the heat shock response is impaired in the cortex may be associated with differences in the cortical pathology between the two mouse models (Li *et al.,* 1999; Davies *et al.,* 1997; Sathasivam *et al.,* 2010; Peng *et al.,* 2016; Carty *et al.,* 2015). Unlike the observation in brain hemispheres (Figures 4.3, 4.4), a clear pattern of dysregulated induction could not be detected for *Dnajb1* and *Hspb1* in striatum and cortex, which may indicate that these two genes are more dysregulated in other areas of the brain.

A higher density and earlier appearance of aggregated huntingtin has been reported in the striatum of zQ175 mice at 3 - 4 months of age, whereas in the cortex, this was not visible until 6 - 8 months of age (Carty *et al.,* 2015). This may explain the more robust and earlier dysregulation of the heat shock response observed in the striatum as compared to the cortex. Additionally, the later observation of an impairment of the heat shock response in the tibialis anterior than in brain regions may be relative to the later formation of inclusions in non-CNS tissues in HD models (Sathasivam *et al.,* 1999; Moffitt *et al.,* 2009).

- **Consistent with previous observations in R6/2 and *Hdh*Q150 models (Labbadia *et al.,* 2011), HSF1 basal or activated levels were not decreased in zQ175 mice.**

The disruption in HSF1 availability is potentially an underlying mechanism that may drive the impairment of the heat shock response observed in HD mice. A recent publication by Gomez-Pastor *et al.* (2017) proposed a model whereby mutant HTT promotes HSF1 degradation by increasing CK2α' kinase and FBXW7 levels, leading to an enhanced HSF1 phosphorylation and ubiquitination. To elucidate whether that may be occurring in zQ175, the HSF1 protein levels were measured in the zQ175 tissues that had been collected.

Prior to any protein experiments with zQ175 tissues, twelve HSF1 commercial antibodies were characterised. In order to confirm that the correct HSF1 band was detected, *Hsf1* knockout samples (negative control) and samples from mice treated with NVP-HS990 (positive control for detection of hyperphosphorylated HSF1) were always included. The characterisation of these antibodies required testing a series of experimental conditions (combinations of lysis buffers, inhibitors, blocking solutions, gels and antibody dilutions). Although some of these antibodies showed promising results, a band was always detected in the *Hsf1* knockout lanes. Only two of the antibodies, A303-176A (Bethyl Laboratories) and 51034-1-AP (Proteintech), were eventually selected as they reliably recognised a band at the expected size, that was hypershifted in NVP-HSP990 samples and absent in *Hsf1* knockout samples.

In contrast to what was reported in cortex, striatum and muscle of zQ175 (Gomez-Pastor *et al.,* 2017), the data presented in this thesis (Figures 4.28 and 4.29) did not agree with the hypothesis that the decreased transcriptional activation of heat shock genes, and subsequent translation of chaperones, may be caused by decreased HSF1 levels. Data in Figure 4.29 indicated that both basal (vehicle) and activated (NVP-HSP990-treated) levels of HSF1 remained unaltered between zQ175 and wild-type tibialis anterior, striatum and cortex at 20 months of age. In line with the previous analysis of R6/2 and *Hdh*Q150 brain hemispheres at end-stage (Labbadia *et al.,* 2011), neither basal nor activated HSF1 levels were decreased in zQ175 brain hemispheres at 12 months of age. Furthermore, at basal conditions (vehicle), HSF1 level was mildly elevated in zQ175 as compared to wild-type (Figure 4.28).

- **Other mechanisms / disease processes need to be considered to explain the heat shock response impairment in HD.**

The data collected regarding HSF1 expression in zQ175 are strongly in accordance with another disease mechanism being responsible for the impairment of the heat shock response with HD progression. Previous work by Labbadia *et al.* (2011) suggested that alterations in the chromatin structure involving a decreased tetra-acetylation of histone H4 may be affecting HSF1 accessibility to heat shock gene promoters. It has been reported that histone modifications could significantly obstruct the binding of HSF1 to the sequence binding motifs in the promoters of heat shock genes (Guertin and Lis, 2010). As a possible explanation, the aggregation of mutant HTT with disease progression may interfere with the acetylation levels of histone H4, as histone acetyl transferases and/or other components may be retained in aggregates (Labbadia *et al.,* 2011; Steffan *et al.,* 2000; Butler and Bates, 2006). The study by Riva *et al.* (2012), analysing the interactions and damaging consequences of polyglutamine expansion on HSF1-dependent gene expression, further supports this proposal.

Chapter 5. Effect of SIRT1 overexpression on the impairment of the heat shock response in R6/2 model with disease progression

5.1 Introduction

Post-translational modifications in HSF1 have a profound effect on HSF1 activity during the heat shock response. Some of these modifications occur during the activation phase of the heat shock response, whereas other modifications have a repressive effect and are present in the attenuation of the response (Gomez-Pastor *et al.,* 2018; Anckar and Sistonen, 2011; Akerfelt *et al*., 2010). One of these inhibitory post-translational modifications for HSF1 is the acetylation of Lys80 in the DNA binding domain, caused by the action of EP300 (Raychaudhuri *et al.,* 2014), and this is essential in the attenuation phase of the heat shock response.

The histone deacetylase SIRT1 has been reported to deacetylate this specific Lys80 residue (Westerheide *et al.,* 2009), which may prolong the interaction between HSF1 and the promoters of the heat shock genes, and consequently, maintain the induced expression of the heat shock genes for a longer period. Previous studies involving overexpression of SIRT1 in neurodegenerative disease mouse models have reported an activation of chaperones and deacetylation of HSF1 (Watanabe *et al.,* 2014).

Transgenic mice overexpressing the *Sirt1* gene under the control of the prion (PrP) promoter (Satoh *et al.,* 2010) were used to investigate whether the *in vivo* overexpression of *Sirt1* may restore or ameliorate the disease-associated impairment of the heat shock response in R6/2 mice, as previously detailed (Figures 4.3 and 4.20-4.25 in Chapter 4). Our group had previously shown that SIRT1 activity is increased in the brains of these *Sirt1* overexpressing transgenic mice (Tulino *et al.,* 2016).

To test the hypothesis that the heat shock impairment in HD mice could be ameliorated by increasing the expression of *Sirt1*, our group had previously performed a small-scale pilot experiment. *Sirt1* transgenic (*Sirt1* tg) female mice were crossed with R6/2 males to obtain four possible genotypes: wild-type, *Sirt1* tg, R6/2

and double mutant *Sirt1* tg::R6/2. These mice were dosed with NVP-HSP990 at 9 weeks of age and brain hemispheres and muscle (quadriceps femoris) were collected at 2, 4, 8 and 20 hours after dosing. The number of mice per treatment group ranged from 2 to 6, and in most cases, there was $n = 4$.

RNA was extracted from the brain hemispheres and quadriceps femoris tissues and the gene expression of *Hspa1a/b* (HSP70), *Hspb1* (HSP25) and *Dnajb1* (HSP40) was analysed by RT-qPCR.

In brain hemispheres, as shown in Figure 5.1, the impairment in the induction of the heat shock response in R6/2 was not apparent until 4 hours after treatment, being evident by 8 hours, especially for the genes *Hspa1a/b* and *Dnajb1*, although not reaching statistical significance in any case due to low numbers of samples. By 4 hours, the level of expression of the three heat shock genes in *Sirt1* tg::R6/2 mice was equivalent to the levels observed in wild-type mice. This improvement was maintained until 8 hours post-dosing, specifically for *Hspa1a/b* and *Hspb1* genes. Interestingly, for *Dnajb1*, the levels of expression in *Sirt1* tg::R6/2 mice were significantly lower than in R6/2. By 20 hours, the levels of gene expression of all the treatment groups had essentially returned to baseline (vehicle) levels.

In quadriceps femoris, the levels of *Hspa1a/b* induction were much greater than in brain hemispheres, reaching a maximum level of expression by 8 hours after dosing. By 4 hours, the impairment in the induction of *Hspa1a/b* gene in R6/2 as compared to wild-type could already be observed, which was restored by *Sirt1* overexpression as detected by 8 hours after treatment (Figure 5.2). A similar observation applied to *Hspb1* gene, where the impairment in R6/2 and restoration of the induction of expression in *Sirt1* tg::R6/2 mice was clear by 8 hours post-dosing (Figure 5.2). There was a great deal of variability between samples for the analysis of *Dnajb1* expression. The impairment in *Dnajb1* induction in R6/2 was apparent at 2 hours and 8 hours after dosing. The expression level of *Dnajb1* in *Sirt1* tg::R6/2 mice 8 hours after treatment was similar to the level reached in wild-type mice, indicating again a possible restoration of the impairment by the overexpression of *Sirt1* (Figure 5.2). As

in brain hemispheres (Figure 5.1), the induced expression of the heat shock genes in quadriceps femoris had diminished almost to baseline levels by 20 hours.

The statistical significance by the *post-hoc* analysis is indicated in Figures 5.1 and 5.2 only between the genotypes: wild-type versus R6/2 and R6/2 versus *Sirt1* tg::R6/2 in the NVP-HSP990-treated groups, not between vehicle and NVP-HSP990 treatments, as most of the comparisons between treatments were significant.

These pilot data were considered to be encouraging and to support the hypothesis that the impairment in the heat shock response in mouse models of HD could be ameliorated by increased SIRT1 activity.

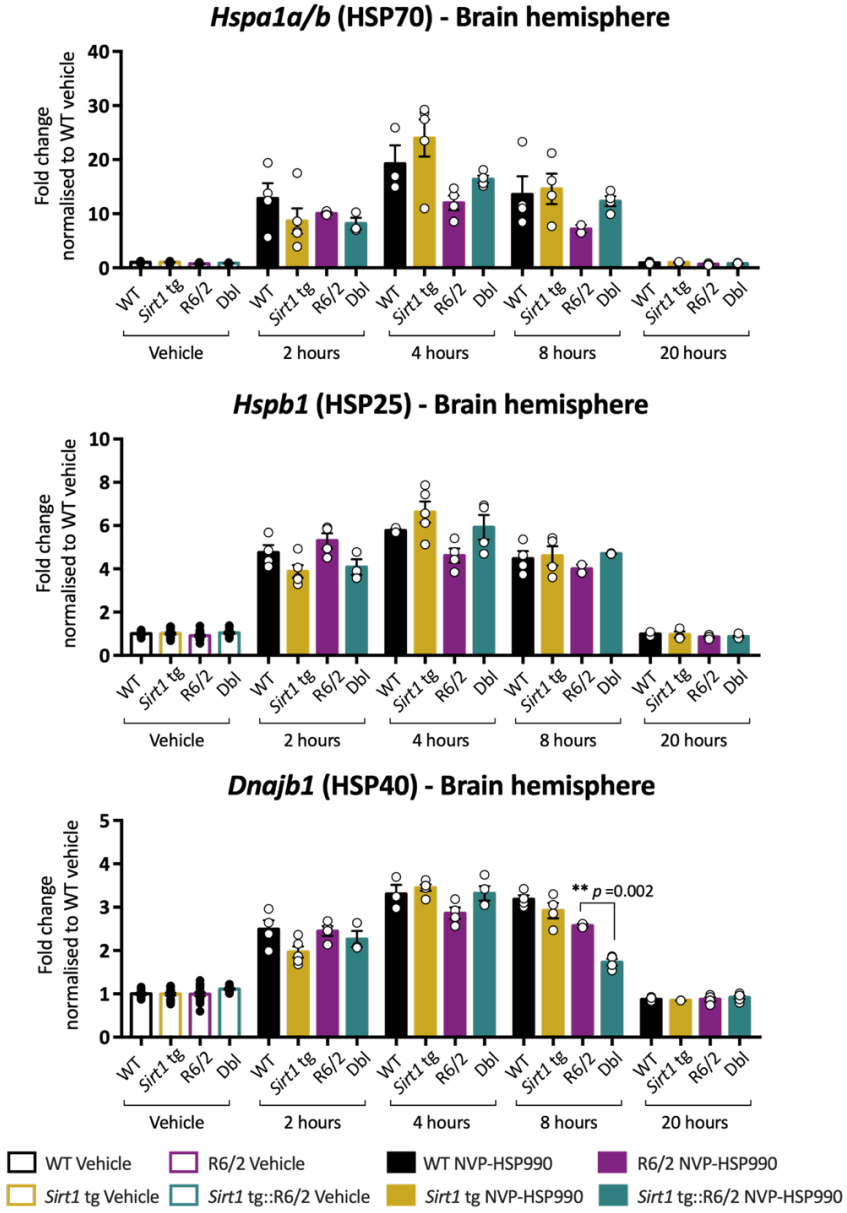

Figure 5.1. Analysis of the expression of heat shock genes Hspa1a/b (HSP70)*, Hspb1* (HSP25) *and Dnajb1* (HSP40) *in brain hemispheres of Sirt1 tg x R6/2 mice at 9 weeks of age by RT-qPCR, after NVP-HSP990 treatment.*

The gene expression of Hspa1a/b (HSP70)*, Hspb1* (HSP25) *and Dnajb1* (HSP40) *was measured by RT-qPCR in brain hemispheres of Sirt1 tg x R6/2 mice at 9 weeks of age, 2, 4, 8 and 20 hours after being treated with NVP-HSP990 or vehicle. N = 2 – 6 mice / genotype / time point / treatment. Atp5b, Canx and Gapdh were used as housekeeping genes for normalisation. Statistical analysis was by two-way ANOVA and Bonferroni correction for multiple comparisons. Statistical significance by the post-hoc analysis is indicated only between genotypes WT vs R6/2 and R6/2 vs Sirt1 tg::R6/2 in NVP-HSP990 groups. Mean ± SEM. ** p ≤ 0.01. WT = wild-type; tg = transgenic; Dbl = double mutant (Sirt1 tg::R6/2).*

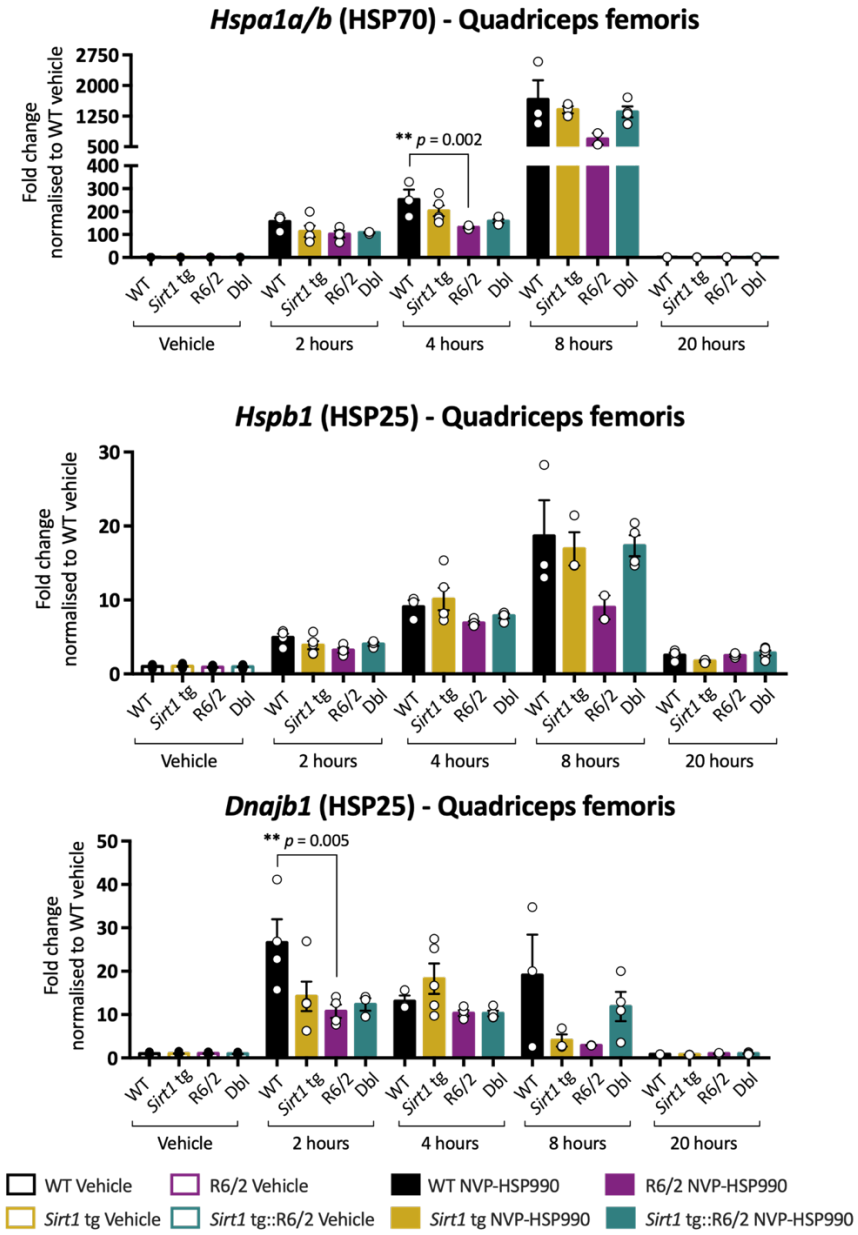

Figure 5.2. Analysis of the expression of heat shock genes Hspa1a/b (HSP70)*, Hspb1* (HSP25) *and Dnajb1* (HSP40) *in quadriceps femoris of Sirt1 tg x R6/2 mice at 9 weeks of age by RT-qPCR, after NVP-HSP990 treatment.*

The gene expression of Hspa1a/b (HSP70)*, Hspb1* (HSP25) *and Dnajb1* (HSP40) *was measured by RT-qPCR in quadriceps femoris of Sirt1 tg x R6/2 mice at 9 weeks of age, 2, 4, 8 and 20 hours after being treated with NVP-HSP990 or vehicle. N = 2 – 6 mice / genotype / time point / treatment. Atp5b, Actb and Sdha were used as housekeeping genes for normalisation. Statistical analysis was by two-way ANOVA and Bonferroni correction for multiple comparisons. Statistical significance by the post-hoc analysis is indicated only between genotypes WT vs R6/2 and R6/2 vs Sirt1 tg::R6/2 in NVP-HSP990 groups. Mean ± SEM. ** p ≤ 0.01. WT = wild-type; tg = transgenic; Dbl = double mutant (Sirt1 tg::R6/2).*

5.2 Study design

To extend the pilot study and further investigate the effect of increasing SIRT1 activity on the heat shock impairment in R6/2 mice, the study was repeated with a greater number of mice per treatment group. It was decided to use two cohorts of mice, at 9 and 14 weeks of age, corresponding to early and late symptomatic disease, so that the effect of increasing SIRT1 activity over the course of the disease could be determined. The greatest potential effect of SIRT1 overexpression had been observed at 8 hours post dosing in the pilot study. Therefore, 4, 7 and 10 hours after treatment were selected, to span this 8-hour time point. The tissues collected were brain hemispheres, tibialis anterior and quadriceps femoris.

5.2.1 Generation of a *Sirt1* tg x R6/2 mouse colony and allocation to NVP-HSP990 dosing trials

To generate sufficient mice for the whole study, firstly, *Sirt1* tg males were bred with C57BL/6J females (Charles River, UK) to obtain a large number of *Sirt1* tg females. These were then crossed with R6/2 males to obtain the four genotypes of interest. Two rounds of breeding provided enough mice to allocate to the dosing trials at 9 and 14 weeks of age, for tissue collection at the three time points, with a minimum *n* of 6 - 7 mice per treatment group. The schematic breeding strategy and study design can be found in Figure 5.3.

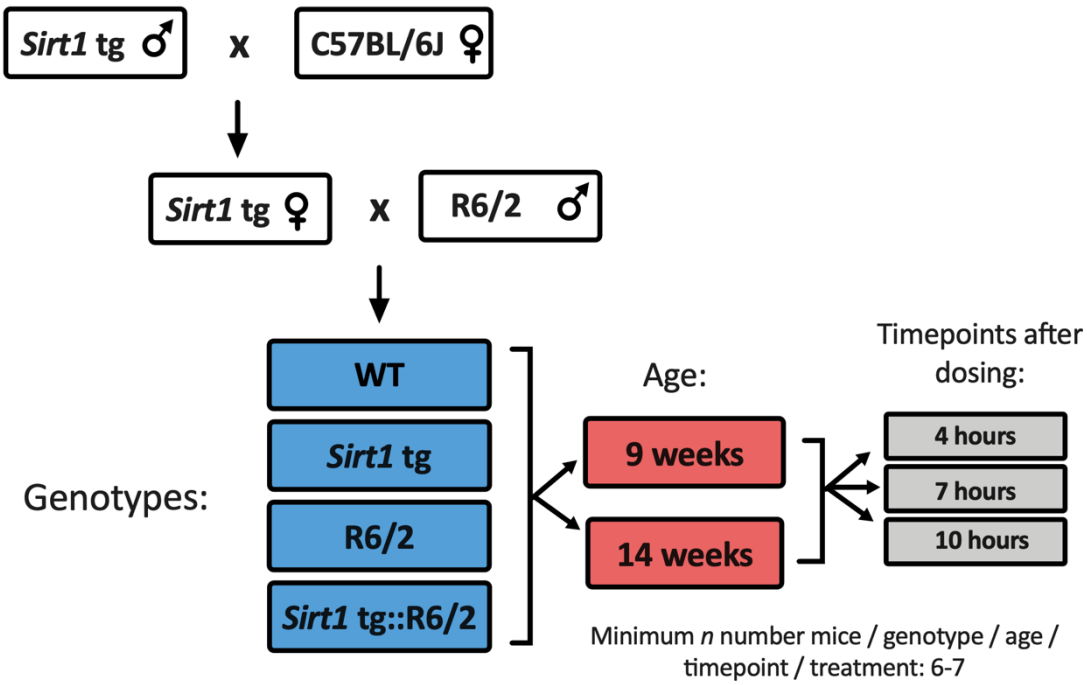

Figure 5.3. Breeding strategy and study design of the Sirt1 tg x R6/2 dosing trials with NVP-HSP990.

Sirt1 tg males were bred with C57BL/6J females (Charles River, UK) to generate Sirt1 tg females that were then crossed with R6/2 males to obtain the genotypes: WT, Sirt1 tg, R6/2 and Sirt1 tg::R6/2. Two cohorts of mice were obtained and assigned as a minimum n = 6 - 7 mice / genotype / treatment / time point for a dosing trial at 9 weeks and another at 14 weeks of age. Each trial contained three groups: for tissue collection at 4, 7 and 10 hours after dosing. WT = wild-type; tg = transgenic.

All mice at both 9 and 14 weeks of age were administered with a single acute dose of NVP-HSP990 (12 mg / kg) or vehicle (2 % methylcellulose in saline solution) by oral gavage and the tissues were harvested at the corresponding time points after dosing. After completing the dosing trials, the genotypes of the samples were confirmed and the total numbers of mice used per genotype per treatment group are indicated in the Table 5.1 below.

Table 5.1. Numbers and genotypes of the Sirt1 tg x R6/2 mice allocated to the NVP-HSP990 dosing trials at 9 and 14 weeks of age.

Age	Time point	Treatment group	Number of mice per genotype			
			WT	*Sirt1* tg	R6/2	*Sirt1* tg::R6/2
9 weeks	4 hours	Vehicle	7	7	7	7
		NVP-HSP990	8	6	9	7
	7 hours	Vehicle	9	5	6	7
		NVP-HSP990	10	8	8	9
	10 hours	Vehicle	5	8	7	7
		NVP-HSP990	10	6	7	6
14 weeks	4 hours	Vehicle	7	7	7	6
		NVP-HSP990	7	7	7	12
	7 hours	Vehicle	8	9	7	9
		NVP-HSP990	9	9	9	10
	10 hours	Vehicle	8	7	7	7
		NVP-HSP990	7	7	7	7

5.3 Optimisation of QuantiGene 18-plex assay for use with *Sirt1* tg x R6/2 mouse tissues

The expression of the heat shock genes in all the treatment groups was analysed by using the QuantiGene 18-plex assay. This was optimised (as described in previous chapters) for use with the *Sirt1* tg x R6/2 cohort of mice to ensure stability of the housekeeping genes between genotypes and treatments as well as to select a sample dilution that provided a signal that was over the limit of detection and without saturation. The cohort at 9 weeks of age, 4 hours after NVP-HSP990 dosing was used for the optimisation as, according to the pilot experiment, a substantial heat shock induction was expected.

5.3.1 *Sirt1* tg x R6/2 brain hemispheres

Independent pools of brain hemisphere samples, at equivalent tissue mass / volume (10 mg / 300 µL), from each of the different treatment groups, were prepared in a 3-fold serial dilution. As indicated in Figures 5.3 and 5.4, the housekeeping genes maintained a stable expression across the different genotypes and were unaffected by treatment, with similar MFI values. However, as there were signs of signal instability in some cases at the 1:3 dilution (such as for *Atp5b* or *Sdha*), the dilution chosen was 1:9 dilution. This 1:9 dilution also proved to be appropriate for the genes of interest (Figure 5.5) as none of the genes had saturated signals and the MFI values were over the limit of detection for each gene.

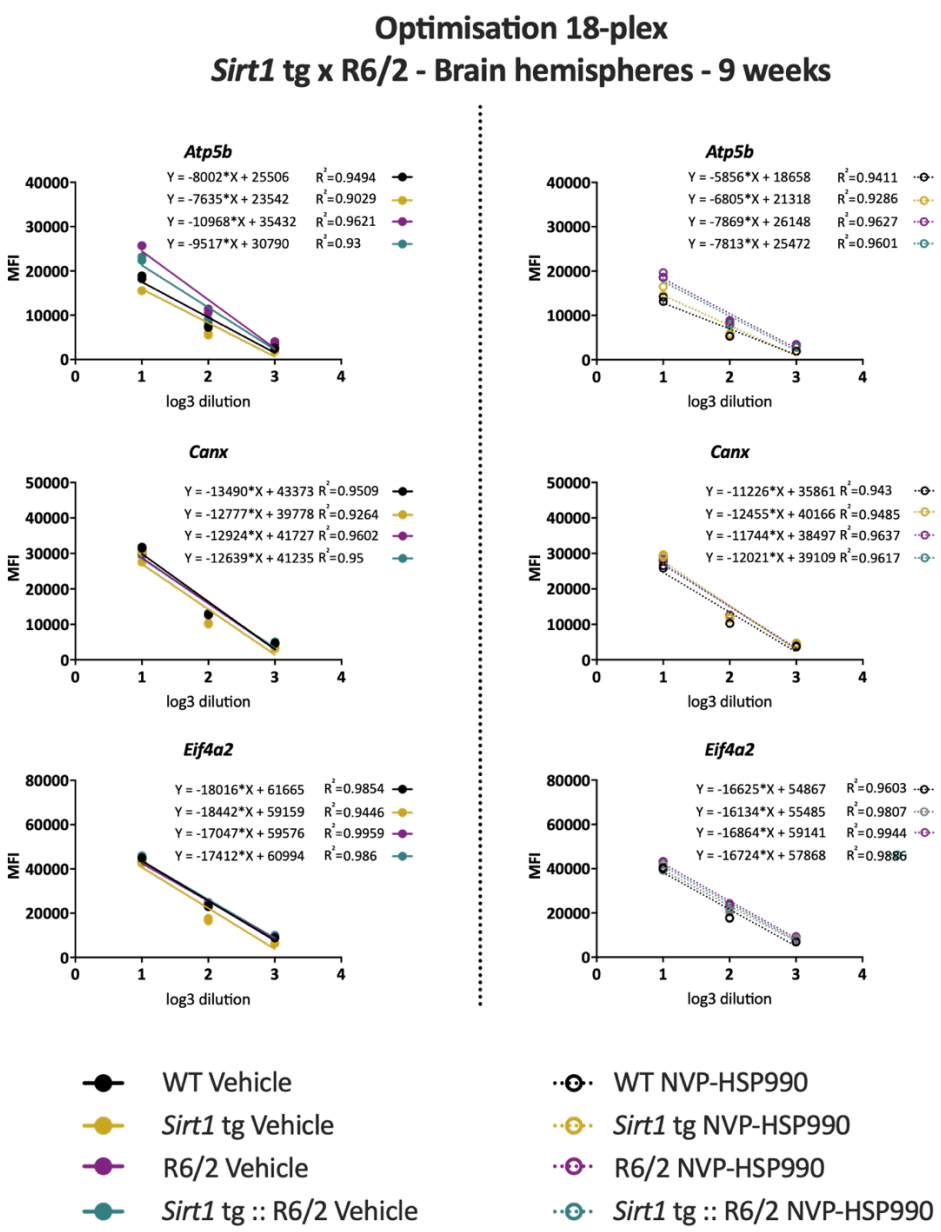

Figure 5.4. Optimisation of sample input in the QuantiGene 18-plex assay for use with Sirt1 tg x R6/2 brain hemispheres (housekeeping genes).

Pools of brain hemisphere samples from Sirt1 tg x R6/2 mice from the 9-week cohort treated with vehicle or NVP-HSP990 (n = 6 mice / genotype / treatment), at equivalent tissue mass / volume (10 mg / 300 µL), were prepared in a 3-fold dilution series and analysed in duplicate. MFI values that were detected for each dilution from each treatment group are shown (vehicle on the left side and NVP-HSP990 on the right side). Linear regression was analysed for each housekeeping gene. The initial dilution (1:3 dilution) showed some signs of unstable signal in Atp5b and possible saturation in Eif4a2 but the rest of the genes maintained a stable expression across genotypes and treatments. WT = wild-type; tg = transgenic; MFI = median fluorescence intensity.

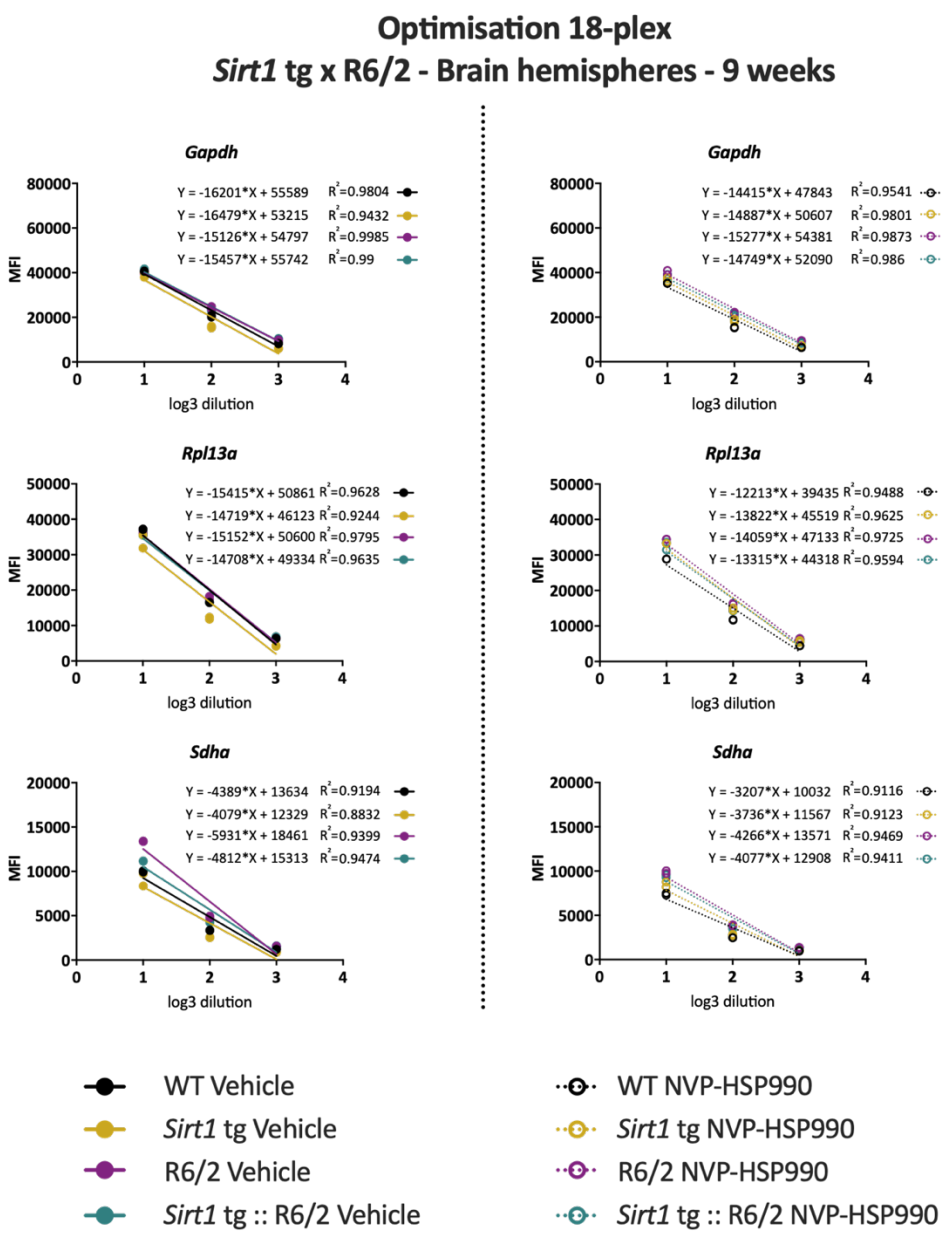

Figure 5.5. Optimisation of sample input in the QuantiGene 18-plex assay for use with Sirt1 tg x R6/2 brain hemispheres (housekeeping genes).

Pools of brain hemisphere samples from Sirt1 tg x R6/2 mice from the 9-week cohort treated with vehicle or NVP-HSP990 (n = 6 mice / genotype / treatment), at equivalent tissue mass / volume (10 mg / 300 µL), were prepared in a 3-fold dilution series and analysed in duplicate. MFI values that were detected for each dilution from each treatment group are shown (vehicle on the left side and NVP-HSP990 on the right side). Linear regression was analysed for each housekeeping gene. The initial dilution (1:3 dilution) showed some signs of unstable signal in Sdha (vehicle) but the rest of the genes maintained a stable expression across genotypes and treatments. WT = wild-type; tg = transgenic; MFI = median fluorescence intensity.

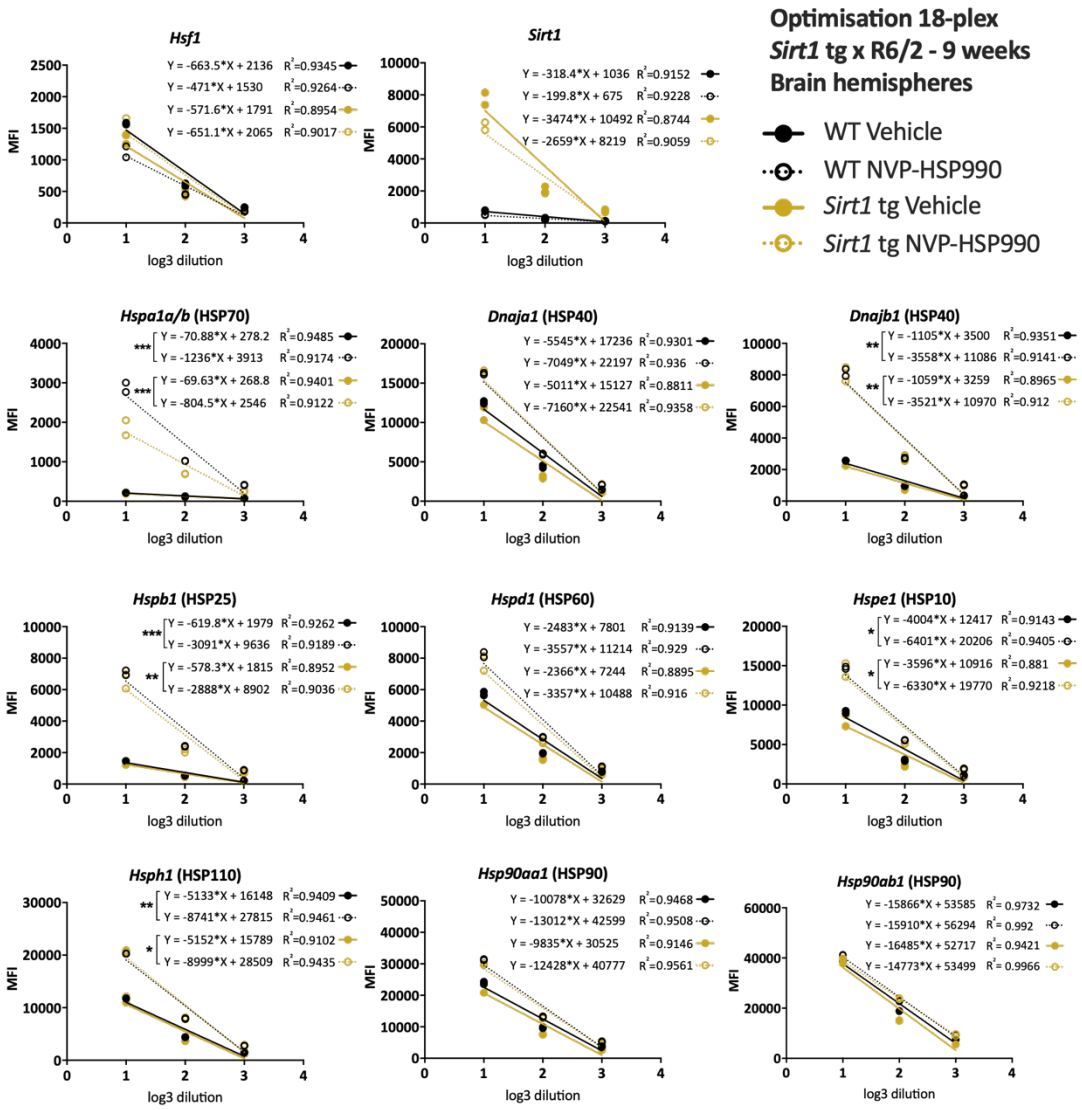

Figure 5.6. Optimisation of sample input in the QuantiGene 18-plex assay for use with Sirt1 tg x R6/2 brain hemispheres (genes of interest).

*Pools of brain hemisphere samples from Sirt1 tg and wild-type mice from the 9-week cohort treated with vehicle or NVP-HSP990 (n = 6 mice / genotype / treatment), at equivalent tissue mass / volume (10 mg / 300 µL), were prepared in a 3-fold dilution series and analysed in duplicate. MFI values that were detected for each dilution from each treatment group are shown. Linear regression was analysed for each gene of interest. None of the dilutions showed signs of saturation. Many of the heat shock genes had linear regression lines with significantly different slopes for each treatment group as a result of the NVP-HSP990 treatment. For the Sirt1 gene, the linear regression lines had significantly different slopes because of Sirt1 overexpression. *** $p \leq 0.001$; ** $p \leq 0.01$; * $p \leq 0.05$. WT = wild-type; tg = transgenic; MFI = median fluorescence intensity.*

5.3.2 *Sirt1* tg x R6/2 tibialis anterior

For the optimisation of the 18-plex assay for use with *Sirt1* tg x R6/2 tibialis anterior, tibialis anterior samples, at equivalent tissue mass / volume (10 mg / 300 µL), were pooled per treatment group and subjected to a 2-fold serial dilution.

For the housekeeping genes, the initial 1:2 dilution showed some variability between groups for all genes but then, from 1:4 dilution, remained stable for *Atp5b*, *Canx*, *Eif4a2* and *Sdha*. *Rpl13a* and *Gapdh*, as previously observed in Chapters 3 and 4, showed signs of variability and/or saturation across the genotypes and therefore were excluded as reference genes for the analysis in tibialis anterior (Figures 5.7, 5.8).

All heat shock genes had linear regression lines corresponding to NVP-HSP990 and vehicle that were significantly different because of the higher expression induced by NVP-HSP990 treatment (Figure 5.9). Considering the low MFI values for the vehicle groups (corresponding to basal levels of expression), a 1:4 dilution was also appropriate as it yielded MFI values over the limit of detection.

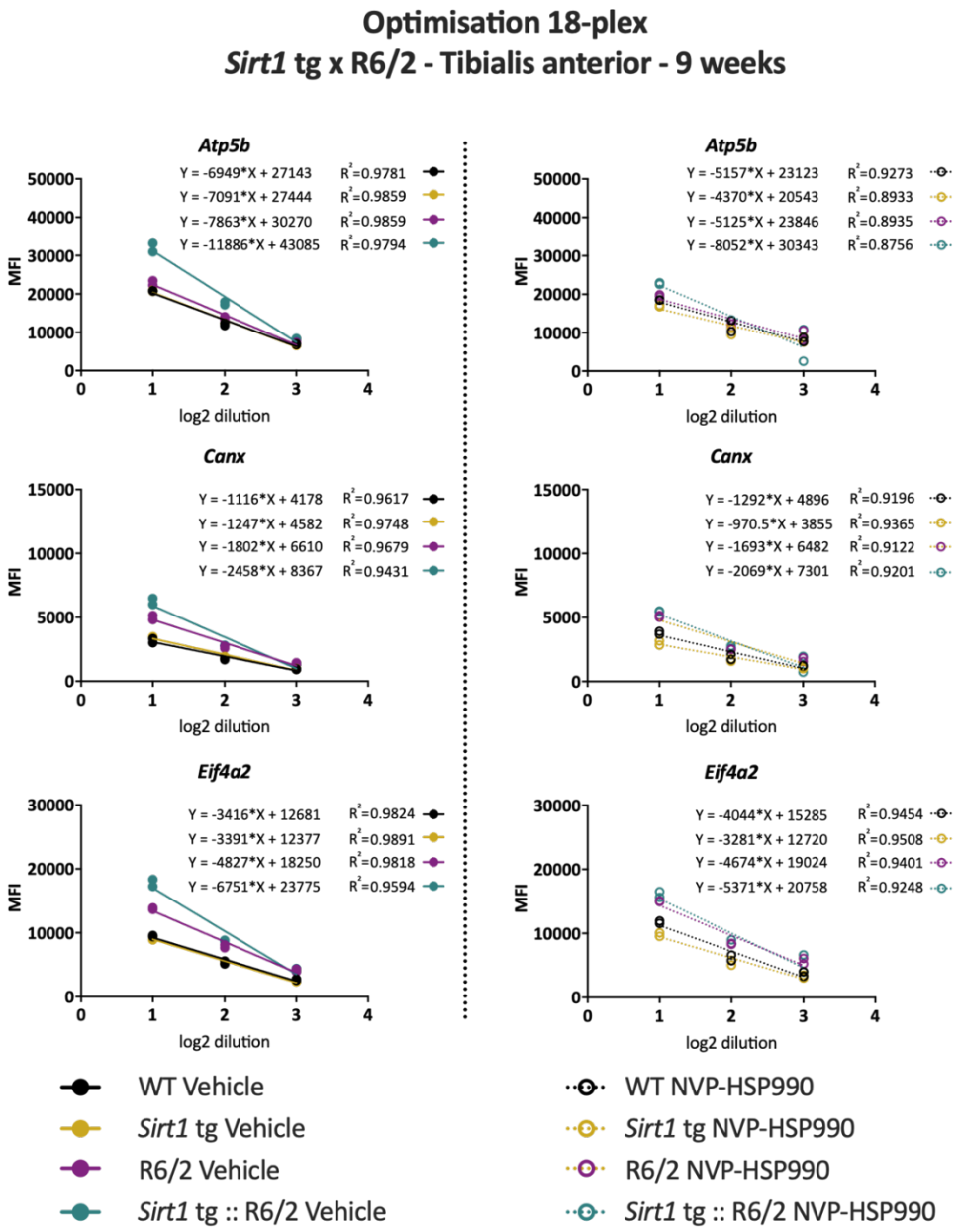

Figure 5.7. Optimisation of sample input in the QuantiGene 18-plex assay for use with Sirt1 tg x R6/2 tibialis anterior (housekeeping genes).

Pools of tibialis anterior samples from Sirt1 tg x R6/2 mice from the 9-week cohort treated with vehicle or NVP-HSP990 (n = 4 mice / genotype / treatment), at equivalent tissue mass / volume (10 mg / 300 µL), were prepared in a 2-fold dilution series and analysed in duplicate. MFI values that were detected for each dilution from each treatment group are shown (vehicle on the left side and NVP-HSP990 on the right side). Linear regression was analysed for each housekeeping gene. The 1:2 dilution showed some signs of an unstable signal in these three genes (in vehicle) but all of them maintained a stable expression and similar MFI values across genotypes and treatments for the 1:4 dilution. WT = wild-type; tg = transgenic; MFI = median fluorescence intensity.

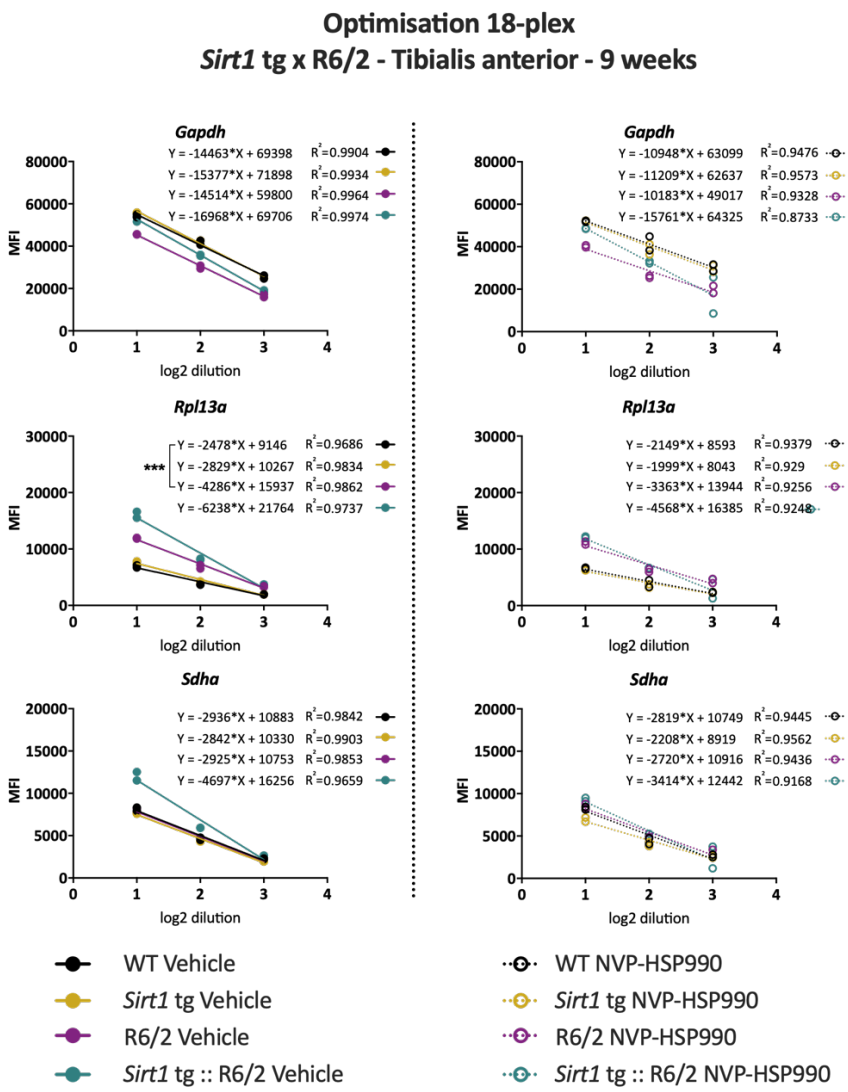

Figure 5.8. Optimisation of sample input in the QuantiGene 18-plex assay for use with Sirt1 tg x R6/2 tibialis anterior (housekeeping genes).

*Pools of tibialis anterior samples from Sirt1 tg x R6/2 mice from the 9-week cohort treated with vehicle or NVP-HSP990 (n = 4 mice / genotype / treatment), at equivalent tissue mass / volume (10 mg / 300 μL), were prepared in a 2-fold dilution series and analysed in duplicate. MFI values that were detected for each dilution from each treatment group are shown (vehicle on the left side and NVP-HSP990 on the right side). Linear regression was analysed for each housekeeping gene. Gapdh showed saturation and different elevations for each linear regression line across all dilutions in both vehicle and NVP-HSP990. The initial dilution (1:2 dilution) showed signs of an unstable signal for Rpl13a (vehicle and NVP-HSP990), and Sdha (vehicle). Sdha then maintained a stable expression and similar MFI values across genotypes and treatments from 1:4 dilution. The linear regression lines for WT and R6/2 in Rpl13a had significantly different slopes in vehicle. Because of these differences and in keeping with previous analyses, Gapdh and Rpl13a were not used as reference genes in the analysis of tibialis anterior. *** $p \leq 0.001$. WT = wild-type; tg = transgenic; MFI = median fluorescence intensity.*

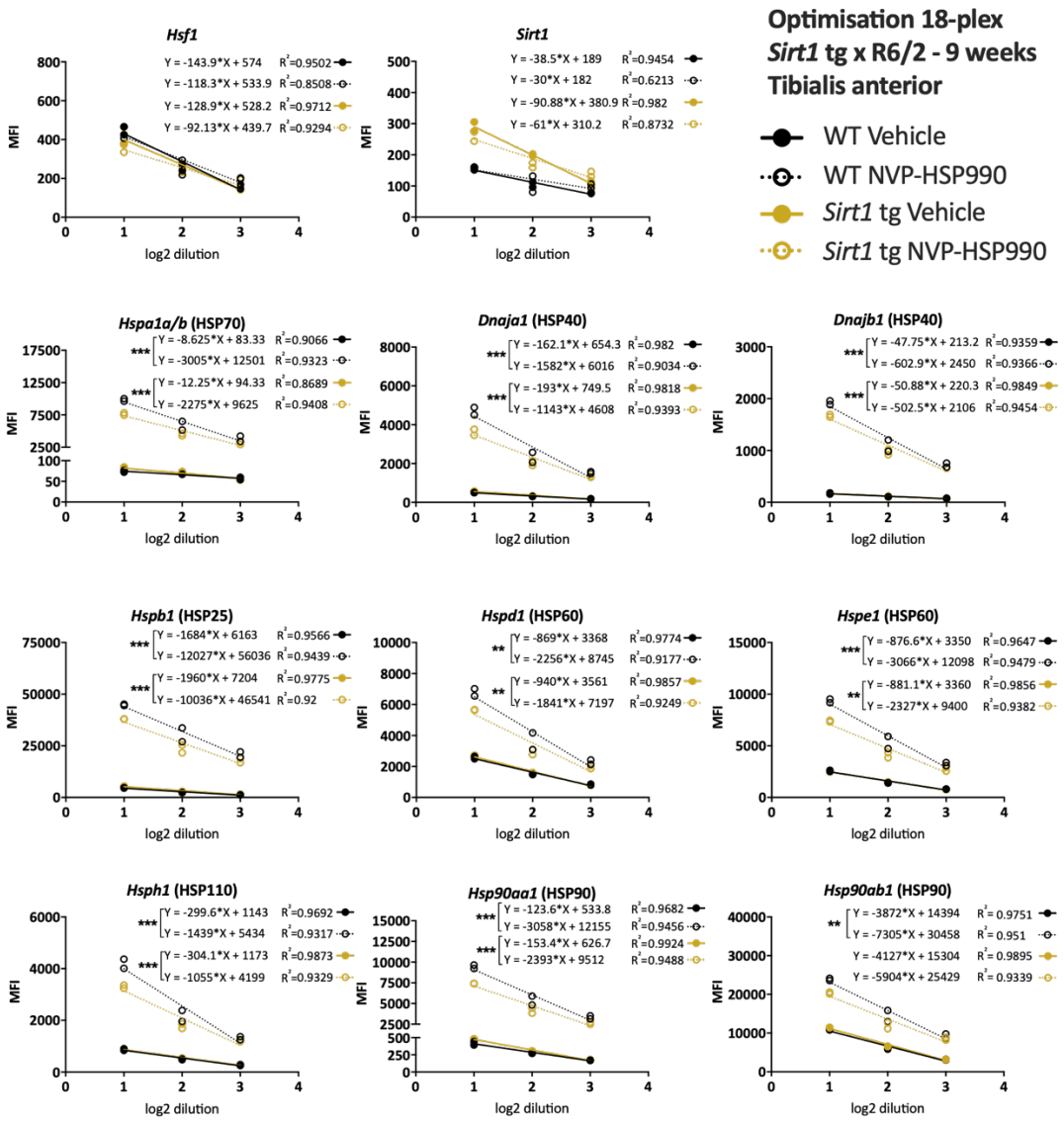

Figure 5.9. Optimisation of sample input in the QuantiGene 18-plex assay for use with Sirt1 tg x R6/2 tibialis anterior (genes of interest).

*Pools of tibialis anterior samples from Sirt1 tg and wild-type mice from the 9-week cohort treated with vehicle or NVP-HSP990 (n = 4 mice / genotype / treatment), at equivalent tissue mass / volume (10 mg / 300 µL), were prepared in a 2-fold dilution series and analysed in duplicate. MFI values that were detected for each dilution from each treatment group are shown. Linear regression was analysed for each gene of interest. None of the dilutions showed signs of saturation. All the heat shock genes had linear regression lines with significantly different slopes for each treatment group as a result of the NVP-HSP990 treatment. For the Sirt1 gene, the linear regression lines had significantly different slopes because of Sirt1 overexpression. *** p ≤ 0.001; ** p ≤ 0.01. WT = wild-type; tg = transgenic; MFI = median fluorescence intensity.*

5.4 Preliminary analysis: Variability in the QuantiGene data

All the tissue samples were homogenised and processed for analysis with the QuantiGene 18-plex assay at the selected dilutions. After analysis, a considerable variability in the fold changes in expression for the NVP-HSP990 samples was observed generally, possibly indicating a differential induction after NVP-HSP990 treatment. Two hypothetical explanations were considered for this variability:

1. The diverse values in the NVP-HSP990 samples could be a result of a technical artifact associated with the QuantiGene technique. To address this potential issue, the gene expression of a set of samples was analysed by RT-qPCR for a comparison.
2. The variable fold changes in expression could be a consequence of differences in exposure to NVP-HSP990 treatment between mice. To clarify this, a pharmacokinetic analysis was conducted for vehicle and NVP-HSP990 quadricep samples to determine the drug concentration.

5.4.1 Re-analysis of data by RT-qPCR

One of the cohorts with the greatest variability was the set of *Sirt1* tg x R6/2 brain samples collected at 14 weeks of age, 4 hours after dosing. In particular, the *Hspa1a/b* gene expression for the wild-type and *Sirt1* tg::R6/2 groups that were dosed with NVP-HSP990 presented remarkable inter-mouse differences.

RNA was extracted from each QuantiGene brain hemisphere homogenate. The protocol for RNA extraction (detailed in Chapter 2, section 2.2.6) was followed without the tissue homogenisation step. The purified RNA was then reverse transcribed and amplified by RT-qPCR. The RT-qPCR analysis of the expression of the *Hspa1a/b*, *Hsph1*, *Hspd1* and *Hspe1* genes (Figure 5.10) yielded very comparable results to QuantiGene. In some cases, the QuantiGene data were tighter (for instance, in *Hspd1* gene). This comparison led to the conclusion that the variability in the data was not due to technical artifacts, but it was rather related to individual effects of NVP-HSP990 treatment in each mouse.

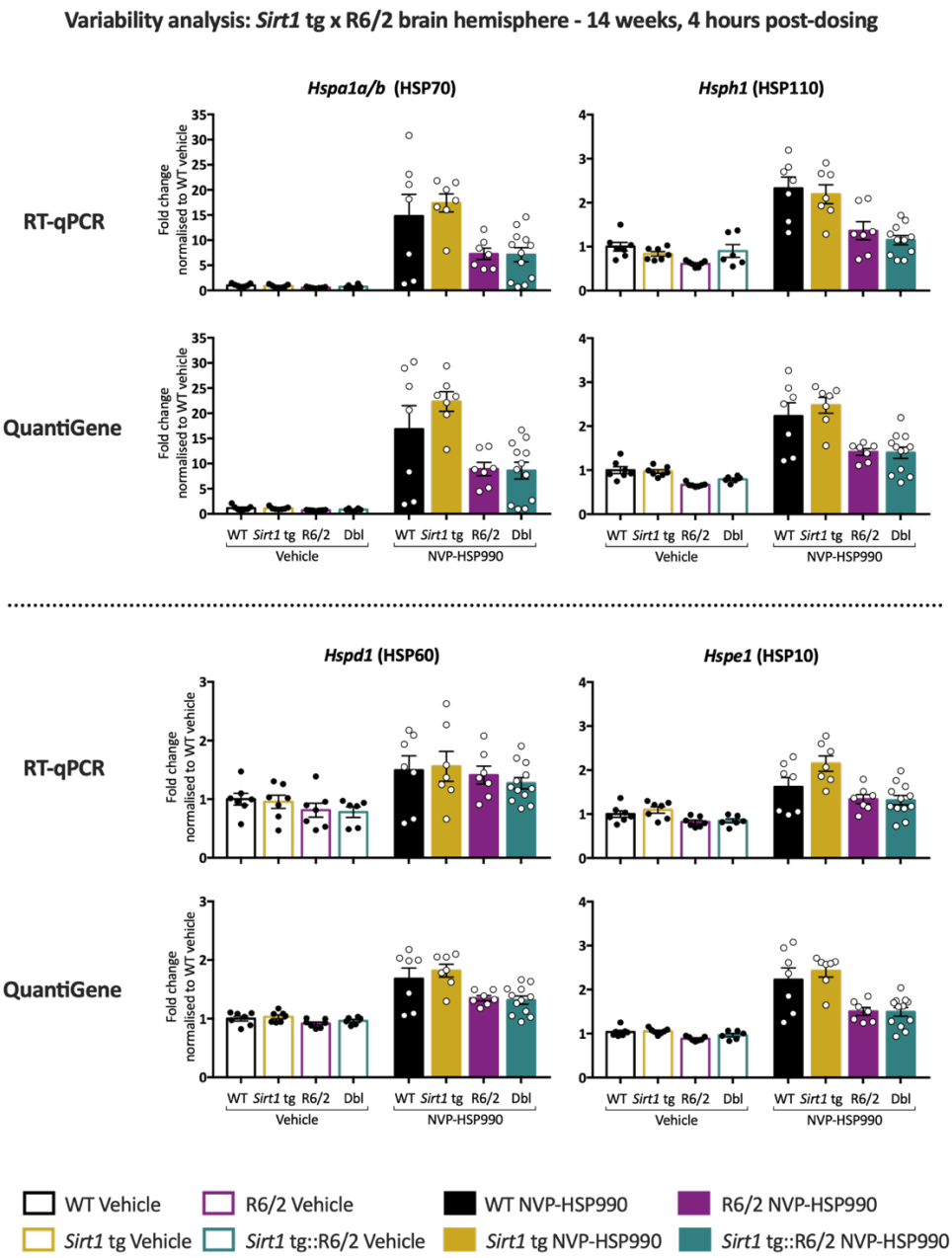

Figure 5.10. Analysis of the expression of Hspa1a/b (HSP70)*, Hsph1* (HSP110)*, Hspd1* (HSP60) *and Hspe1* (HSP10) *in Sirt1 tg x R6/2 brain hemispheres by QuantiGene and RT-qPCR after treatment with NVP-HSP990.*

The gene expression of Hspa1a/b, Hsph1, Hspd1 and Hspe1 was measured in the same Sirt1 tg x R6/2 brain hemispheres at 14 weeks of age, 4 hours after NVP-HSP990 dosing, by RT-qPCR (top) or QuantiGene (bottom). RNA for RT-qPCR was extracted from the QuantiGene brain hemisphere homogenates to investigate the variability of the QuantiGene data. NVP-HSP990 samples were normalised to the corresponding wild-type samples treated with vehicle to calculate the fold change in expression. N = 6 - 12 mice / genotype / treatment. Mean ± SEM. Statistical significance not included. WT = Wild-type; tg = transgenic; Dbl = double mutant (Sirt1 tg::R6/2).

5.4.2 Analysis of NVP-HSP990 concentration in *Sirt1* tg x R6/2 samples

A pharmacokinetic analysis was conducted at IRBM Science Park in Pomezia (Italy) to detect and quantify the presence of NVP-HSP990 in all the vehicle and NVP-HSP990 *Sirt1* tg x R6/2 samples. Quadriceps femoris from all the *Sirt1* tg x R6/2 cohorts were shipped to this location to determine the drug concentration that was present in each sample. The quadriceps femoris samples were homogenised and NVP-HSP990 was extracted and quantified by liquid chromatography and mass spectrometry.

As per their report, in wild-type samples, from 4 hours to 10 hours, the average concentration decreased from 660 ng / g to 392 ng / g in the 9-week cohort and from 492 ng / g to 248 ng / g in the 14-week cohort. In *Sirt1* transgenic samples, from 4 hours to 10 hours, the average concentration decreased from 511 ng / g to 392 ng / g in the 9-week cohort and from 684 ng / g to 399 ng / g in the 14-week cohort. In R6/2 samples, from 4 hours to 10 hours, the average concentration decreased from 507 ng / g to 342 ng / g in the 9-week cohort and from 803 ng / g to 292 ng / g in the 14-week cohort. Finally, in *Sirt1* tg::R6/2 samples, from 4 hours to 10 hours, the average concentration decreased from 891 ng / g to 322 ng / g in the 9-week cohort and from 882 ng / g to 381 ng / g in the 14-week cohort (Figures 5.11 and 5.12). Three vehicle samples were identified that contained a considerable concentration of NVP-HSPP90, probably due to errors during dosing.

To put this information into context and find a correlation between the drug exposure and the individual fold changes in expression after induction, the NVP-HSP990 concentration present in each sample was plotted against the corresponding fold change of *Hspa1a/b* expression in tibialis anterior.

As shown in Figures 5.11 and 5.12, the fold change in *Hspa1a/b* expression and the drug concentration in each mouse do not follow a linear regression and there was no clear correlation. Also, as highlighted in the graphs, the expression of *Hspa1a/b* in some mice was close to baseline and very similar to that in mice treated with vehicle. As the induced expression of *Hspa1a/b* can reach very high levels as compared to

vehicle, this very low expression most likely indicates a lack of induction of the heat shock response after NVP-HSP990 treatment.

In the *Sirt1* tg x R6/2 9-week cohort (Figure 5.11), three samples (one *Sirt1* tg at 4 hours, one *Sirt1* tg at 10 hours and one *Sirt1* tg::R6/2 sample at 7 hours) showed no induction of *Hspa1a/b* expression, which was also applicable to the rest of the heat shock genes. There was a considerable amount of NVP-HSP990 present in these samples, specifically, 363 ng / g and 498 ng / g in *Sirt1* tg samples and 226 ng / g in the *Sirt1* tg::R6/2 sample.

In the *Sirt1* tg x R6/2 14-week cohort, the variability was greater (Figure 5.12). Among the wild-type treated samples, four of them showed no induction which, in these cases, correlated with a lower concentration of NVP-HSP990, ranging from below the limit of quantification (2 ng / g) to 178 ng / g. One *Sirt1* tg sample at 10 hours had a very low *Hspa1a/b* expression, although the NVP-HSP990 concentration was 167 ng / g. Finally, among the *Sirt1* tg::R6/2 group, four samples (three at 4 hours and one at 10 hours) presented with vehicle-like levels of *Hspa1a/b* expression. In these cases, there was no correlation with the NVP-HSP990 concentrations which ranged from 178 to 531 ng / g.

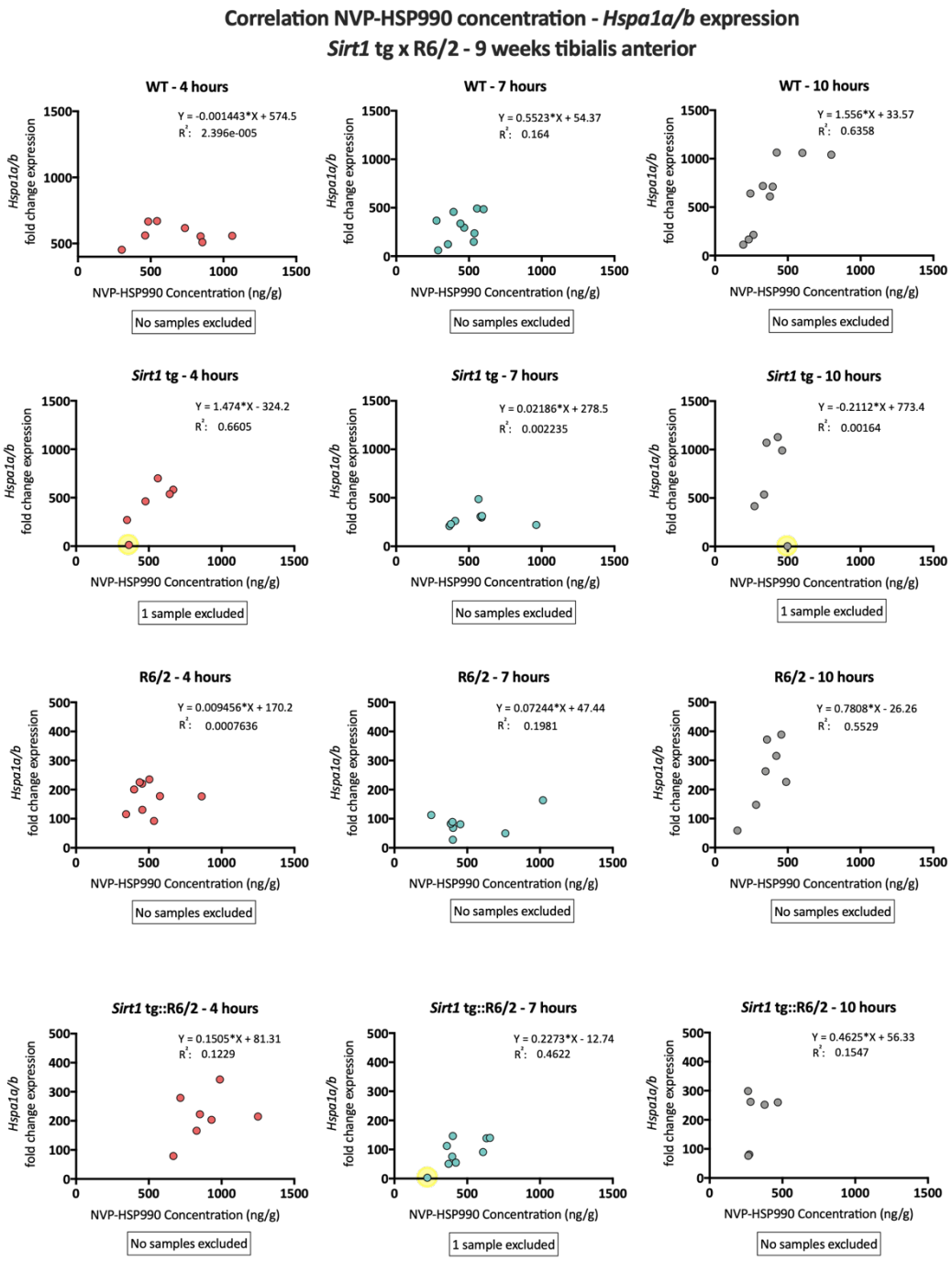

Figure 5.11. Analysis of the correlation between NVP-HSP990 concentration (ng/g) in quadriceps femoris and Hspa1a/b (HSP70) *expression in tibialis anterior of Sirt1 tg x R6/2 at 9 weeks of age, after NVP-HSP990 treatment.*

The concentrations of NVP-HSP990 (ng/g) detected in the quadriceps femoris of Sirt1 tg x R6/2 mice at 9 weeks of age, 4, 7 and 10 hours after being dosed with NVP-HSP990 (on the x axis) were plotted with their fold changes in expression of Hspa1a/b in tibialis anterior (normalised to wild-type vehicle) as measured by QuantiGene (on the y axis). The dots highlighted in yellow indicate samples that were excluded from analysis as no induction of Hspa1a/b expression had occurred. WT = wild-type; tg = transgenic.

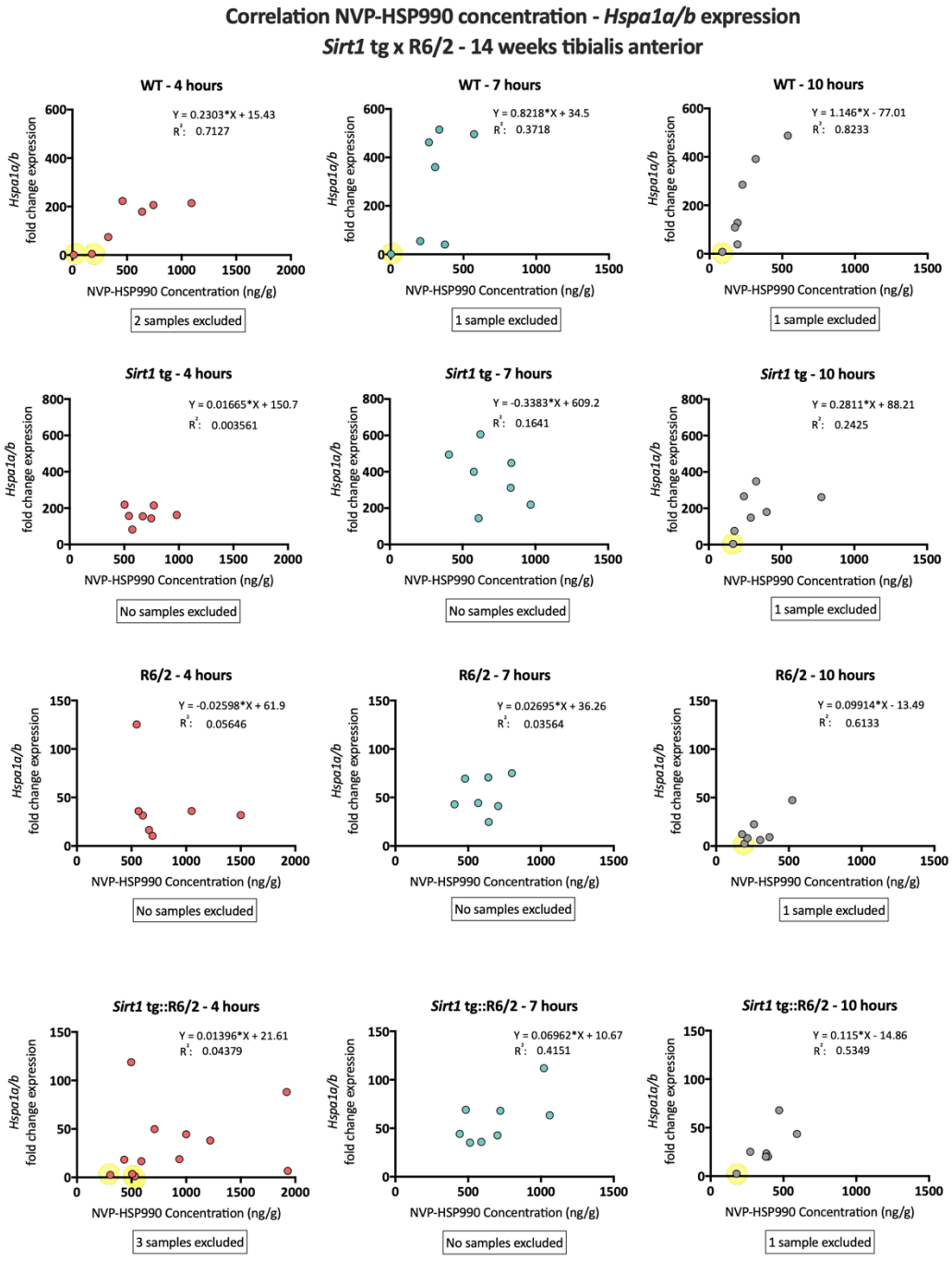

Figure 5.12. Analysis of the correlation between NVP-HSP990 concentration (ng/g) in quadriceps femoris and Hspa1a/b (HSP70) *expression in tibialis anterior of Sirt1 tg x R6/2 at 14 weeks of age, after NVP-HSP990 treatment.*
The concentrations of NVP-HSP990 (ng/g) detected in the quadriceps femoris of Sirt1 tg x R6/2 mice at 14 weeks of age, 4, 7 and 10 hours after being dosed with NVP-HSP990 (on the x axis) were plotted with their fold changes in expression of Hspa1a/b in tibialis anterior (normalised to wild-type vehicle) as measured by QuantiGene (on the y axis). The dots highlighted in yellow indicate samples that were excluded from analysis as no induction of Hspa1a/b expression had occurred. WT = wild-type; tg = transgenic.

5.4.3 Removal of outliers or non-induced samples

The information obtained from the comparison of the NVP-HSP990 pharmacokinetic analysis with *Hspa1a/b* expression identified samples in which induction after NVP-HSP990 treatment had not occurred. These were removed from the final analysis, together with the three "vehicle"-treated samples that had most likely received NVP-HSP990 during dosing. All of the non-induced samples removed from analysis showed no induction in either tibialis anterior or brain hemisphere samples. Below is the complete list of samples that were excluded from analysis:

In the *Sirt1* tg x R6/2 9-week cohort:

- Two *Sirt1* tg::R6/2 vehicle samples: dosed with NVP-HSP990.
- Two *Sirt1* tg treated samples, one at 4 hours and one at 10 hours: not induced.
- One *Sirt1* tg::R6/2 treated sample at 10 hours: not induced.
- Additionally, two wild-type treated samples at 10 hours were excluded as there were discrepancies between the genotyping and repeat sizing results and therefore the genotypes were not confirmed.

In the *Sirt1* tg x R6/2 14-week cohort:

- One wild-type vehicle sample at 7 hours as it received NVP-HSP990 dosing.
- Four wild-type treated samples (two at 4 hours, one at 7 hours and one at 10 hours): not induced.
- One *Sirt1* tg treated sample at 10 hours: not induced.
- One R6/2 treated sample at 10 hours: not induced.
- Four *Sirt1* tg::R6/2 treated samples (three at 4 hours and one at 10 hours): not induced.

The final numbers of samples included in the analysis (mice per genotype, age, treatment and time point) can be found in Table 5.3.

Table 5.2. Final numbers of the Sirt1 tg x R6/2 mice per genotype, included in the analysis of the NVP-HSP990 dosing trials at 9 and 14 weeks of age, after exclusion of outliers.

Age	Time point	Treatment group	Number of mice per genotype			
			WT	*Sirt1* tg	R6/2	*Sirt1* tg::R6/2
9 weeks	4 hours	Vehicle	7	7	7	7
		NVP-HSP990	8	5	9	7
	7 hours	Vehicle	9	5	6	7
		NVP-HSP990	10	8	8	8
	10 hours	Vehicle	5	8	7	5
		NVP-HSP990	8	5	7	6
14 weeks	4 hours	Vehicle	7	7	7	6
		NVP-HSP990	5	7	7	9
	7 hours	Vehicle	7	9	7	9
		NVP-HSP990	8	9	9	10
	10 hours	Vehicle	8	7	7	7
		NVP-HSP990	6	6	6	6

5.5 Effect of *Sirt1* overexpression on the induction of expression of heat shock genes in brain hemispheres and tibialis anterior of R6/2 mice with disease progression

After removal of the outliers, the QuantiGene data from the *Sirt1* tg x R6/2 dosing trials at 9 and 14 weeks of age was re-analysed.

For simplicity, the statistical significance after *post-hoc* analysis added to the graphs in Figures 5.13 to 5.34 is only between the genotypes: wild-type versus R6/2 and R6/2 versus *Sirt1* tg::R6/2 in the NVP-HSP990-treated groups; not between vehicle and NVP-HSP990 treatments, as most of the comparisons between treatments were significant.

5.5.1 Expression of *Sirt1* and *Hsf1*

The overexpression of *Sirt1* in brain was consistent in the *Sirt1* tg and *Sirt1* tg::R6/2 groups in brain hemispheres, with an average incremental expression of 8.6-fold ± 2, as compared to wild-type conditions (Figure 5.13). A slightly higher variability in the *Sirt1* overexpression between samples in these two groups could be seen in the brain hemispheres at 14 weeks, especially in the 4-hour cohort.

On the contrary, this consistent *Sirt1* overexpression in brain was not achieved in the tibialis anterior of the same mice, where a greater variability could be seen in the *Sirt1* tg and *Sirt1* tg::R6/2 groups. This was especially the case in the 14-week cohort, with overexpression levels ranging from 0.1-fold to 15-fold (an average of 3.7-fold ± 2.3) as compared to wild-type (Figure 5.14). This indicated that the more stable overexpression detected in brain was not present in muscle.

Hsf1 expression remained constant in brain hemispheres and tibialis anterior across genotypes and treatments at both ages (Figures 5.15, 5.16).

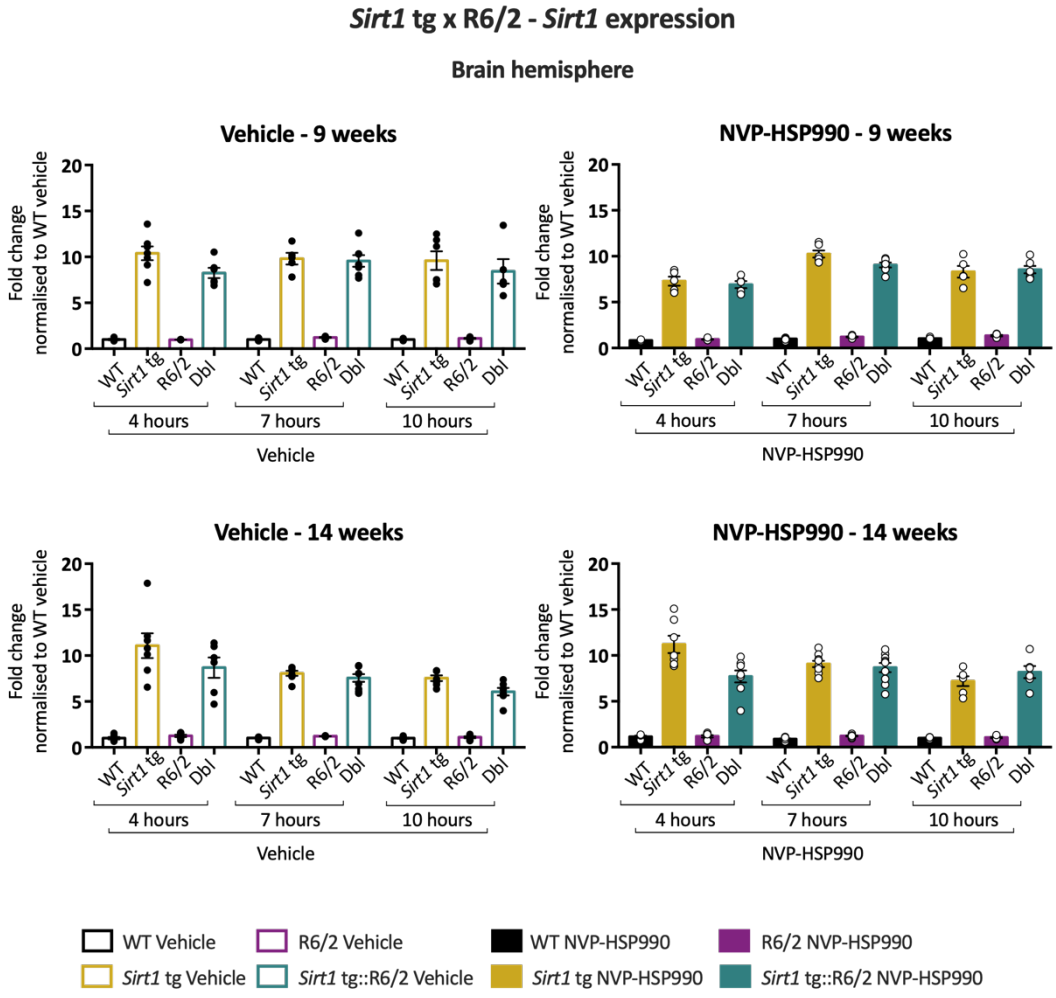

Figure 5.13. Sirt1 expression in brain hemispheres of Sirt1 tg x R6/2 mice at 9 and 14 weeks of age, after treatment with NVP-HSP990.

Sirt1 expression was measured by QuantiGene in the brain hemispheres of Sirt1 tg x R6/2 mice at 9 and 14 weeks of age, 4, 7 and 10 hours after receiving a dose of NVP-HSP990 (right side) or vehicle (left side). The fold changes in expression for the NVP-HSP990 groups were normalised to the corresponding WT vehicle. N = 5 - 10 mice / genotype / treatment at 9 weeks and at 14 weeks. Mean ± SEM. Statistical significance between genotypes is not shown. WT = wild-type; tg = transgenic; Dbl = double mutant (Sirt1 tg::R6/2).

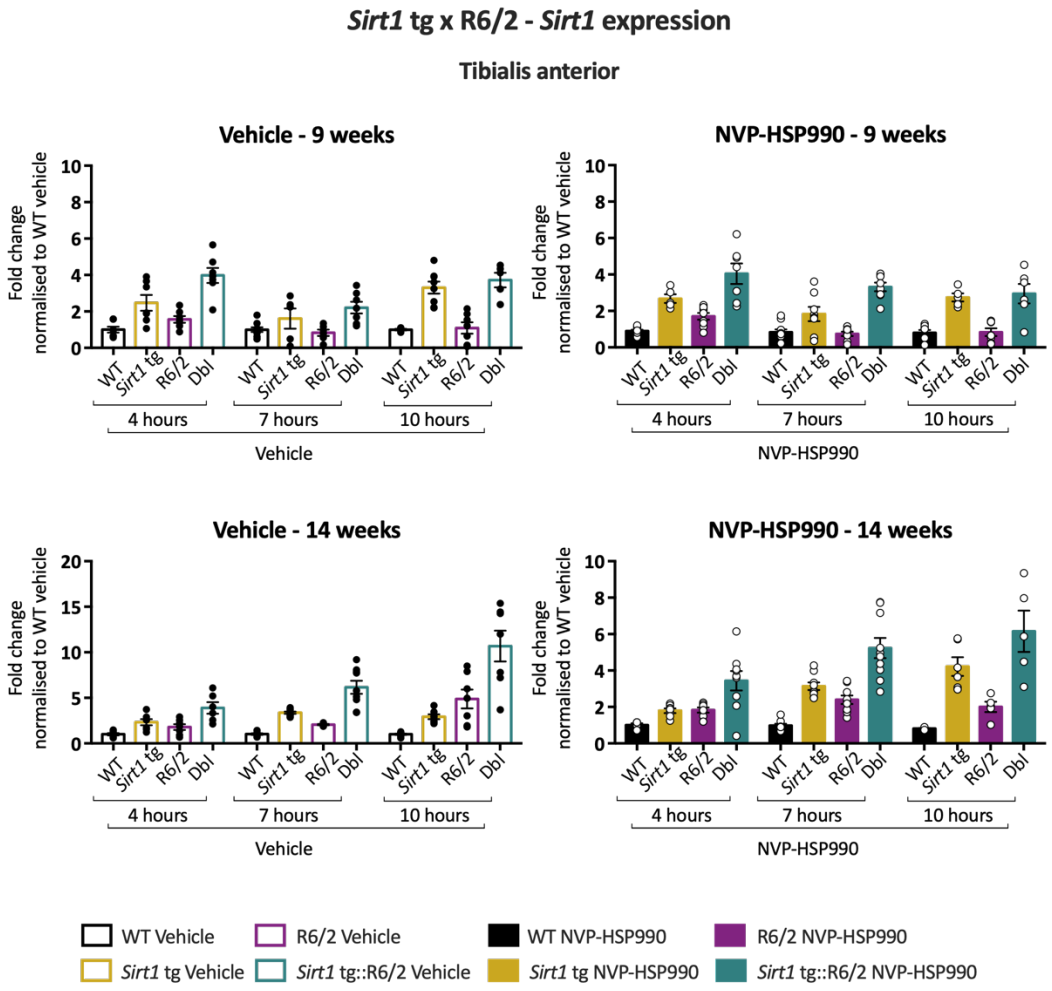

Figure 5.14. Sirt1 expression in tibialis anterior of Sirt1 tg x R6/2 mice at 9 and 14 weeks of age, after treatment with NVP-HSP990.

Sirt1 expression was measured by QuantiGene in the tibialis anterior of Sirt1 tg x R6/2 mice at 9 and 14 weeks of age, 4, 7 and 10 hours after receiving a dose of NVP-HSP990 (right side) or vehicle (left side). The fold changes in expression for the NVP-HSP990 groups were normalised to the corresponding WT vehicle. N = 5 - 10 mice / genotype / treatment at 9 weeks and 4 - 10 mice / genotype / treatment at 14 weeks. Mean ± SEM. Statistical analysis was by two-way ANOVA and Bonferroni correction for multiple comparisons. Statistical significance between genotypes is not shown. WT = wild-type; tg = transgenic; Dbl = double mutant (Sirt1 tg::R6/2).

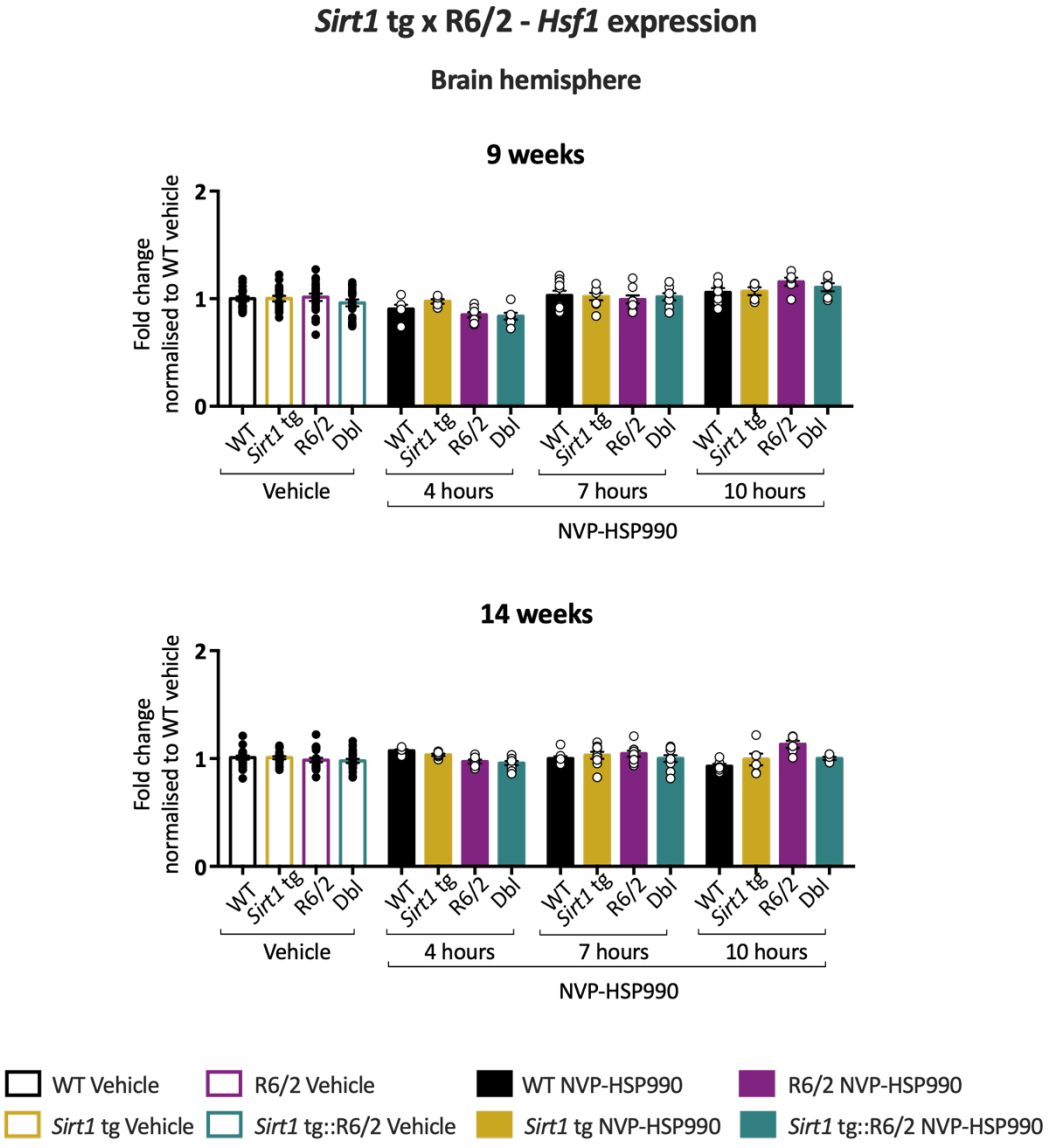

Figure 5.15. Hsf1 expression in brain hemispheres of Sirt1 tg x R6/2 mice at 9 and 14 weeks of age, after treatment with NVP-HSP990.

Hsf1 expression was measured by QuantiGene in the brain hemispheres of Sirt1 tg x R6/2 mice at 9 and 14 weeks of age, 4, 7 and 10 hours after receiving a dose of NVP-HSP990 or vehicle. The fold changes in expression for the NVP-HSP990 groups were normalised to the corresponding WT vehicle. N = 5 - 10 mice / genotype / treatment at 9 weeks and at 14 weeks. Statistical analysis was by two-way ANOVA and Bonferroni correction for multiple comparisons. Mean ± SEM. WT = wild-type; tg = transgenic; Dbl = double mutant (Sirt1 tg::R6/2).

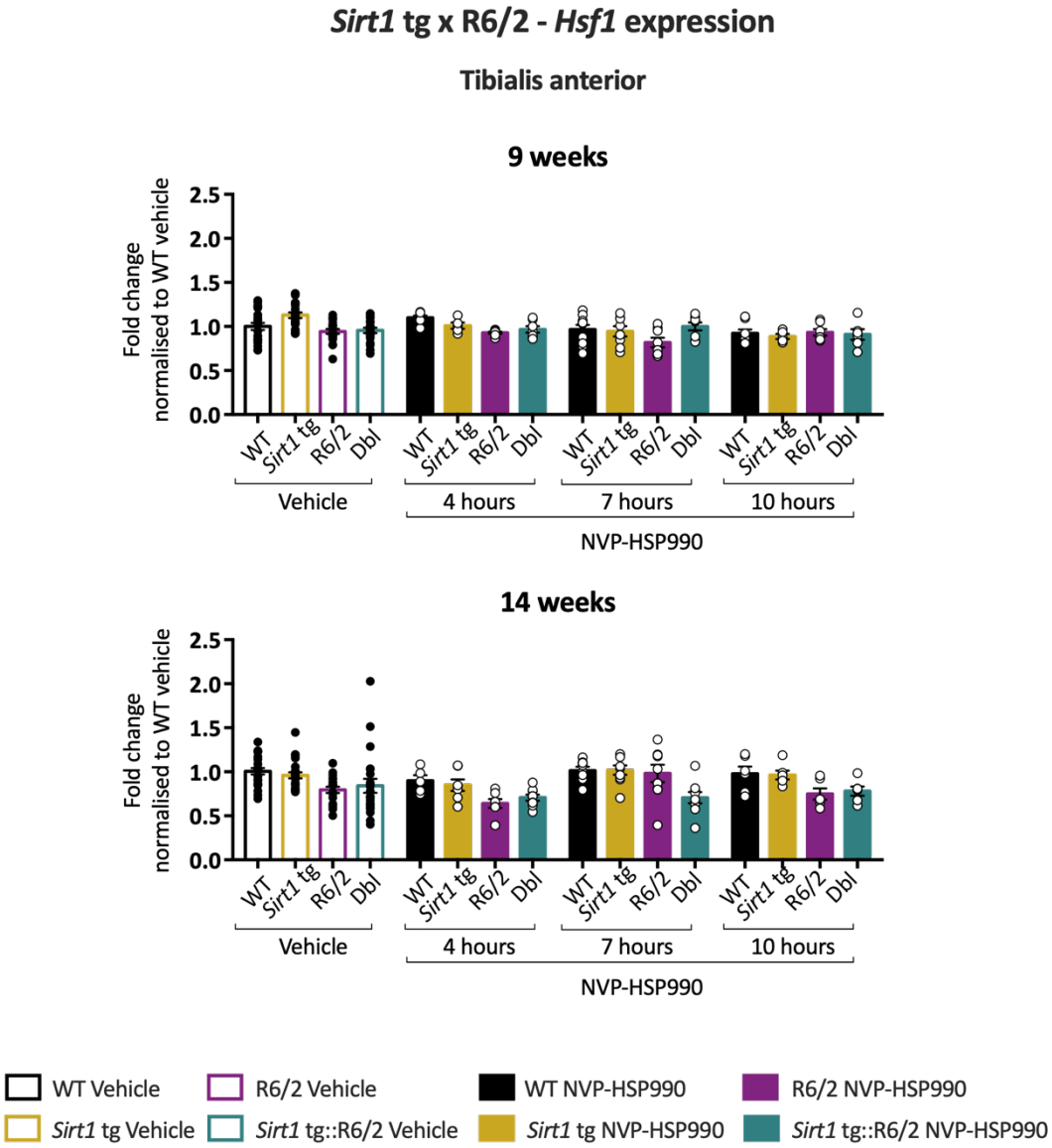

Figure 5.16. Hsf1 expression in tibialis anterior of Sirt1 tg x R6/2 mice at 9 and 14 weeks of age, after treatment with NVP-HSP990.

Hsf1 expression was measured by QuantiGene in the tibialis anterior of Sirt1 tg x R6/2 mice at 9 and 14 weeks of age, 4, 7 and 10 hours after receiving a dose of NVP-HSP990 or vehicle. The fold changes in expression for the NVP-HSP990 groups were normalised to the corresponding WT vehicle. N = 5 - 10 mice / genotype / treatment at 9 weeks and at 14 weeks. Statistical analysis was by two-way ANOVA and Bonferroni correction for multiple comparisons. Mean ± SEM. WT = wild-type; tg = transgenic; Dbl = double mutant (Sirt1 tg::R6/2).

5.5.2 Expression of *Hspa1a/b* (HSP70)

In brain (Figure 5.17), the induced expression of *Hspa1a/b* (HSP70) was clearly impaired in R6/2 as compared to wild-type by 4 hours after NVP-HSP990 treatment both at 9 and 14 weeks of age. At 9 weeks, this impairment was still in place by 8 hours after dosing. This was not the case at 14 weeks, when wild-type levels of expression were not as high as at 9 weeks of age. Although at 9 weeks the overexpression of *Sirt1* was causing an apparently higher level of induction than in R6/2 both at 4 and 8 hours after treatment, this mild improvement did not reach statistical significance.

As expected from previous data, the levels of induced expression of *Hspa1a/b* were dramatically higher in tibialis anterior than in brain tissues (Figure 5.18). At early and late symptomatic stages of the disease, R6/2 had a significant decrease in the capacity to elicit a heat shock response which was maintained up to 10 hours after dosing. For all the treatment groups, the level of induction of *Hspa1a/b* expression was diminished at 14 weeks of age. Although by 10 hours at 14 weeks of age, there was a mild increase in the expression level in *Sirt1* tg::R6/2 mice compared to R6/2, this was not statistically significant (Figure 5.18).

In both tissues, there was still a considerable level of variability in *Hspa1a/b* induction at both ages and all time points, which will have decreased the power to detect differences between treatment groups.

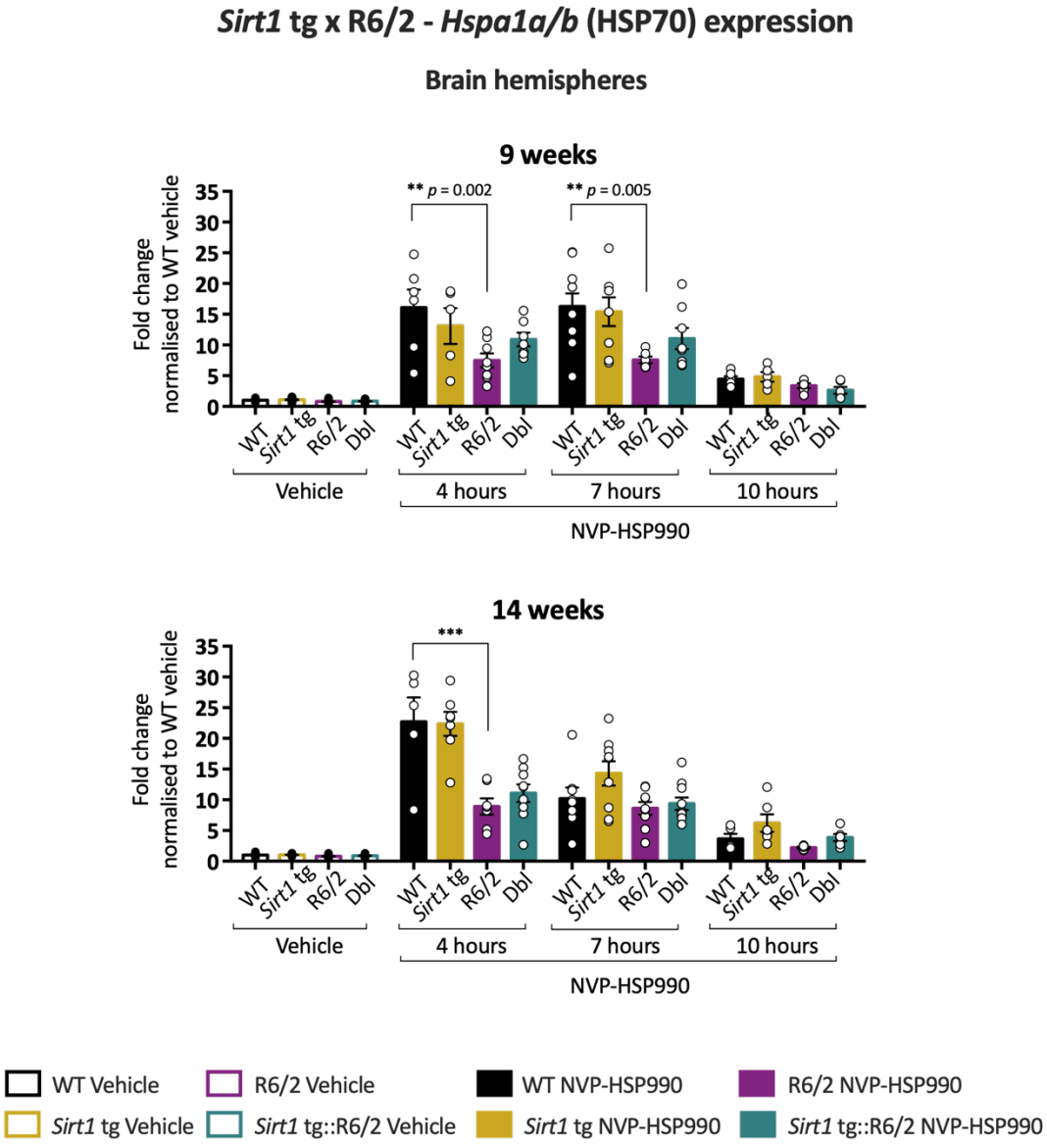

Figure 5.17. Hspa1a/b (HSP70) *expression in brain hemispheres of Sirt1 tg x R6/2 mice at 9 and 14 weeks of age, after treatment with NVP-HSP990.*
Hspa1a/b (HSP70) *expression was measured by QuantiGene in the brain hemispheres of Sirt1 tg x R6/2 mice at 9 and 14 weeks of age, 4, 7 and 10 hours after receiving a dose of NVP-HSP990 or vehicle. The fold changes in expression for the NVP-HSP990 groups were normalised to the corresponding WT vehicle. For simplicity, the vehicle data for each time point were plotted together for each genotype, as no differences between time points were found. N = 5 - 10 mice / genotype / treatment at 9 weeks and at 14 weeks. Statistical analysis was by two-way ANOVA and Bonferroni correction for multiple comparisons. Only the statistical significance values between WT vs R6/2 and R6/2 and Sirt1 tg::R6/2 in NVP-HSP990 groups are shown. Mean ± SEM. *** p ≤ 0.001; ** p ≤ 0.01. WT = wild-type; tg = transgenic; Dbl = double mutant (Sirt1 tg::R6/2).*

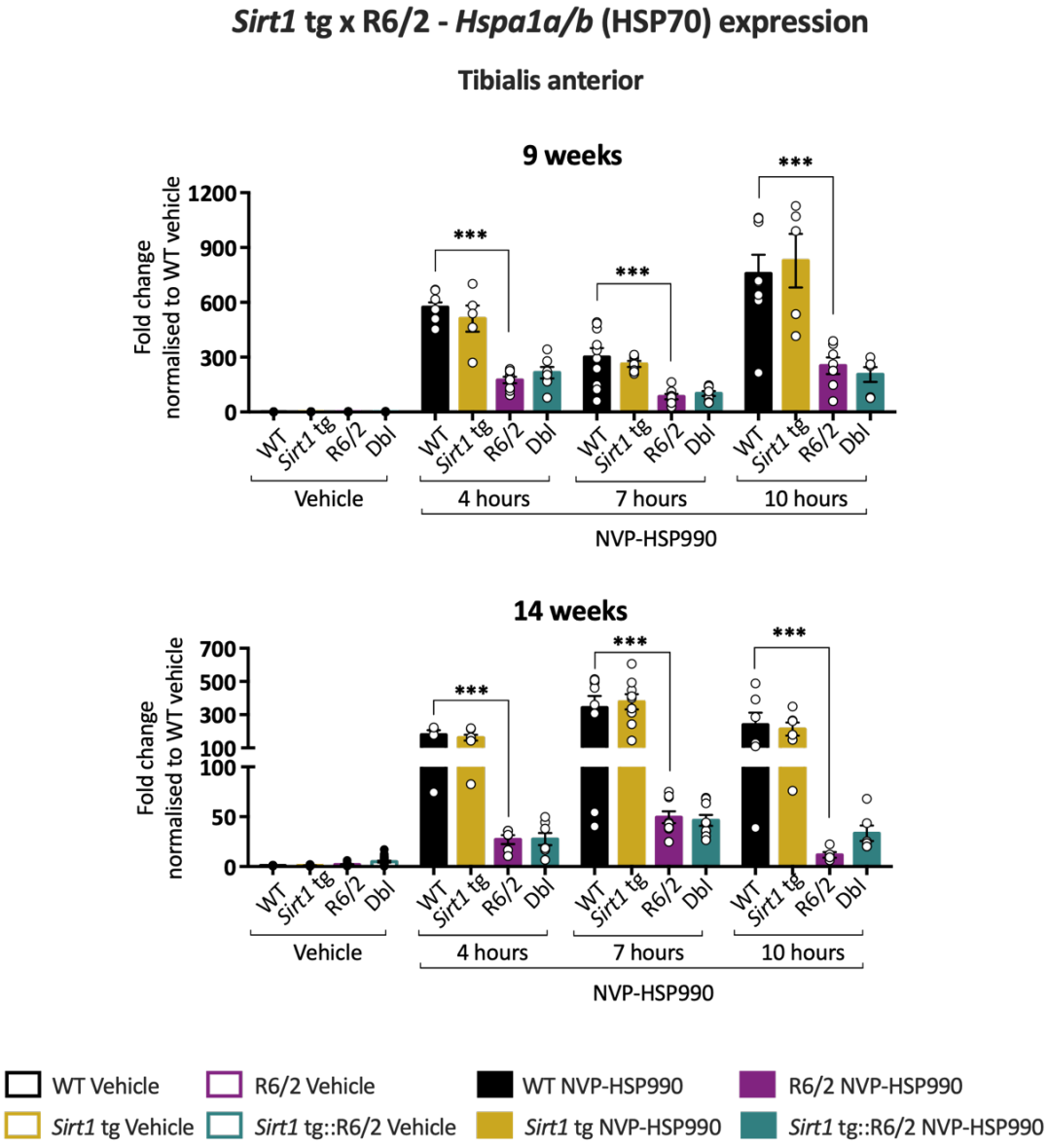

Figure 5.18. Hspa1a/b expression in tibialis anterior of Sirt1 tg x R6/2 mice at 9 and 14 weeks of age, after treatment with NVP-HSP990.

Hspa1a/b (HSP70) *expression was measured by QuantiGene in the tibialis anterior of Sirt1 tg x R6/2 mice at 9 and 14 weeks of age, 4, 7 and 10 hours after receiving a dose of NVP-HSP990 or vehicle. The fold changes in expression for the NVP-HSP990 groups were normalised to the corresponding WT vehicle. For simplicity, the vehicle data for each time point were plotted together for each genotype, as no differences between time points were found. N = 5 - 10 mice / genotype / treatment at 9 weeks and 5 - 9 mice / genotype / treatment at 14 weeks. Statistical analysis was by two-way ANOVA and Bonferroni correction for multiple comparisons. Only the statistical significance values between WT vs R6/2 and R6/2 and Sirt1 tg::R6/2 in NVP-HSP990 groups are shown. Mean ± SEM. *** $p \leq 0.001$. WT = wild-type; tg = transgenic; Dbl = double mutant (Sirt1 tg::R6/2).*

5.5.3 Expression of *Hspb1* (HSP25)

A clear impairment in the induced expression of *Hspb1* (HSP25) was observed in R6/2 tibialis anterior as compared to wild-type littermates, which was present from 4 to 10 hours after dosing at 9 weeks of age and to a lesser extent at 14 weeks of age (Figure 5.20). This impairment was not as consistent in brain (Figure 5.19). The capacity to maintain a heat shock response was also reduced with age, especially in tibialis anterior. The overexpression of *Sirt1* did not have an ameliorating effect on the impaired response in R6/2 mice, and only a mild increase in expression could be seen at 4 hours in brain hemispheres at 9 and 14 weeks of age, which did not reach statistical significance (Figure 5.19).

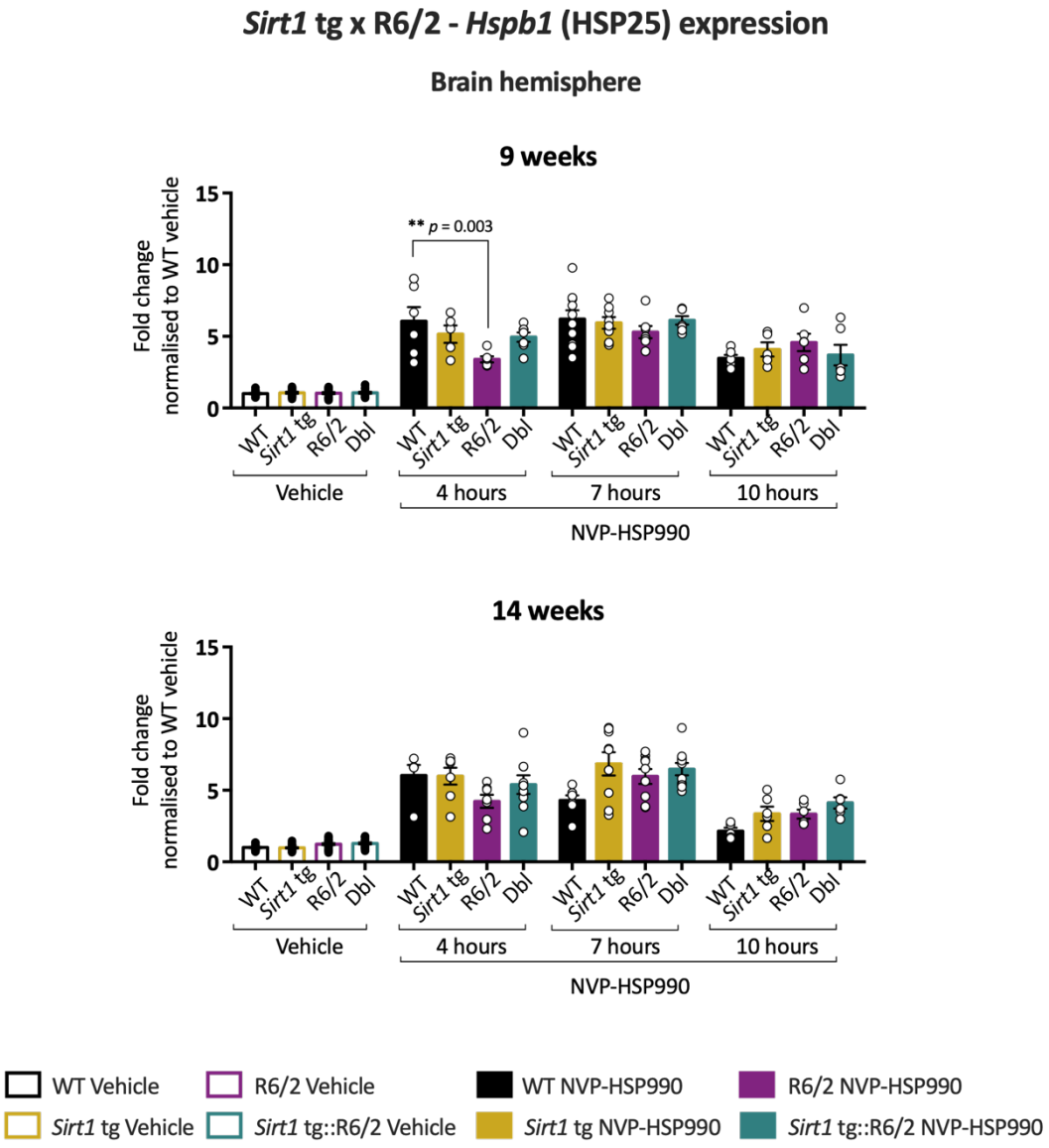

Figure 5.19. Hspb1 expression in brain hemispheres of Sirt1 tg x R6/2 mice at 9 and 14 weeks of age, after treatment with NVP-HSP990.

Hspb1 (HSP25) *expression was measured by QuantiGene in the brain hemispheres of Sirt1 tg x R6/2 mice at 9 and 14 weeks of age, 4, 7 and 10 hours after receiving a dose of NVP-HSP990 or vehicle. The fold changes in expression for the NVP-HSP990 groups were normalised to the corresponding WT vehicle. For simplicity, the vehicle data for each time point were plotted together for each genotype, as no differences between time points were found. N = 5 - 10 mice / genotype / treatment at 9 weeks at 14 weeks. Statistical analysis was by two-way ANOVA and Bonferroni correction for multiple comparisons. Only the statistical significance values between WT vs R6/2 and R6/2 and Sirt1 tg::R6/2 in NVP-HSP990 groups are shown. Mean ± SEM. ** p ≤ 0.01. WT = wild-type; tg = transgenic; Dbl = double mutant (Sirt1 tg::R6/2).*

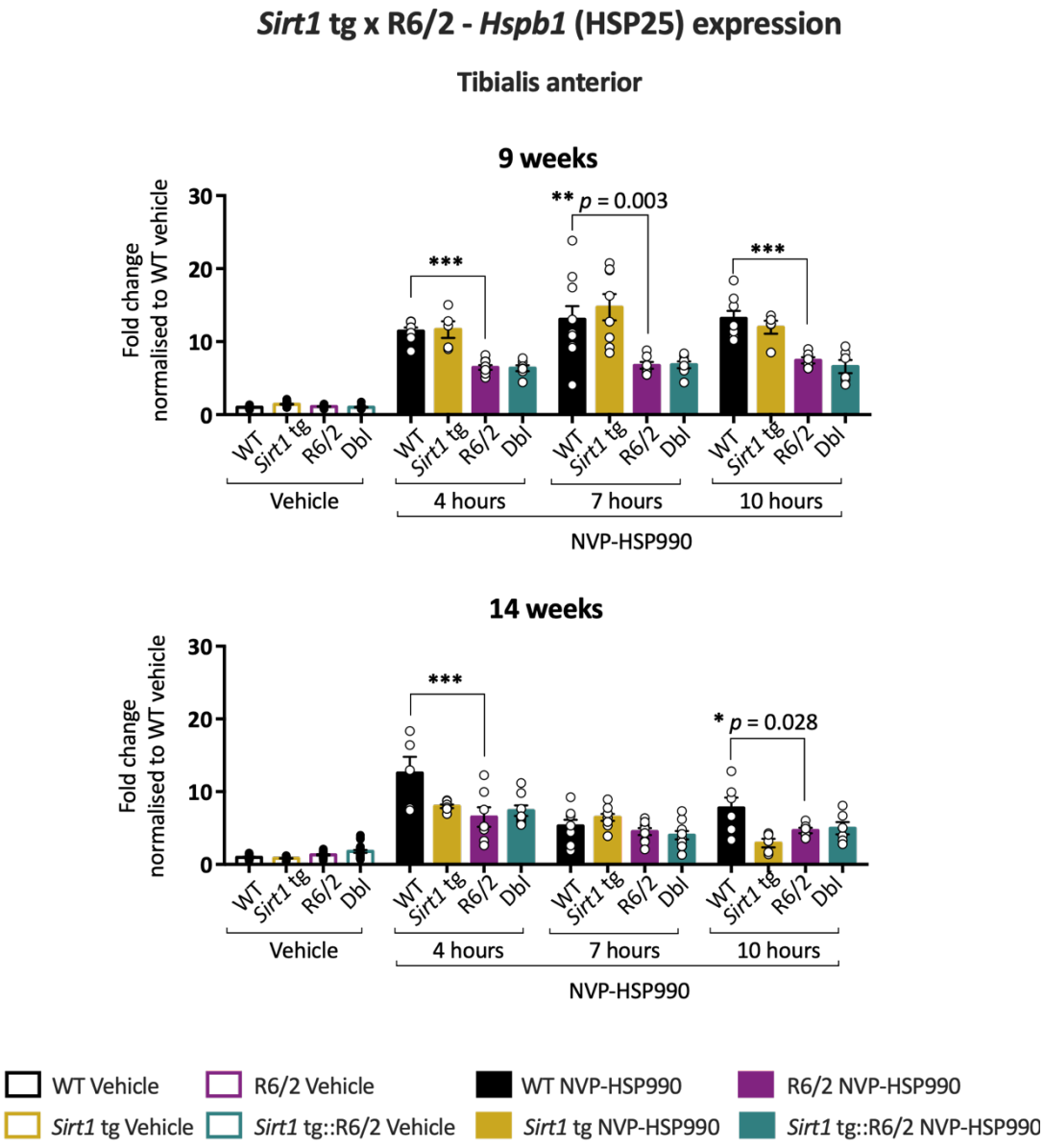

Figure 5.20. Hspb1 expression in tibialis anterior of Sirt1 tg x R6/2 mice at 9 and 14 weeks of age, after treatment with NVP-HSP990.

Hspb1 (HSP25) *expression was measured by QuantiGene in the tibialis anterior of Sirt1 tg x R6/2 mice at 9 and 14 weeks of age, 4, 7 and 10 hours after receiving a dose of NVP-HSP990 or vehicle. The fold changes in expression for the NVP-HSP990 groups were normalised to the corresponding WT vehicle. For simplicity, the vehicle data for each time point were plotted together for each genotype, as no differences between time points were found. N = 5 - 10 mice / genotype / treatment at 9 weeks at 14 weeks. Statistical analysis was by two-way ANOVA and Bonferroni correction for multiple comparisons. Only the statistical significance values between WT vs R6/2 and R6/2 and Sirt1 tg::R6/2 in NVP-HSP990 groups are shown. Mean ± SEM. *** p ≤ 0.001; ** p ≤ 0.01; * p ≤ 0.05. WT = wild-type; tg = transgenic; Dbl = double mutant (Sirt1 tg::R6/2).*

5.5.4 Expression of *Dnaja1* (HSP40)

For brain hemispheres, the level of *Dnaja1* (HSP40) induction was fairly similar across all time points and genotypes at both ages, although, at 4 hours, it was significantly reduced in R6/2 as compared to wild-type (Figure 5.21).

A more pronounced impairment in R6/2 was detected at all time points in tibialis anterior but only at 9 weeks of age, as at 14 weeks of age, the differences between R6/2 and wild-type did not reach statistical significance (Figure 5.22).

The overexpression of *Sirt1* did not influence the induction of *Dnaja1* expression in R6/2 in brain or tibialis anterior.

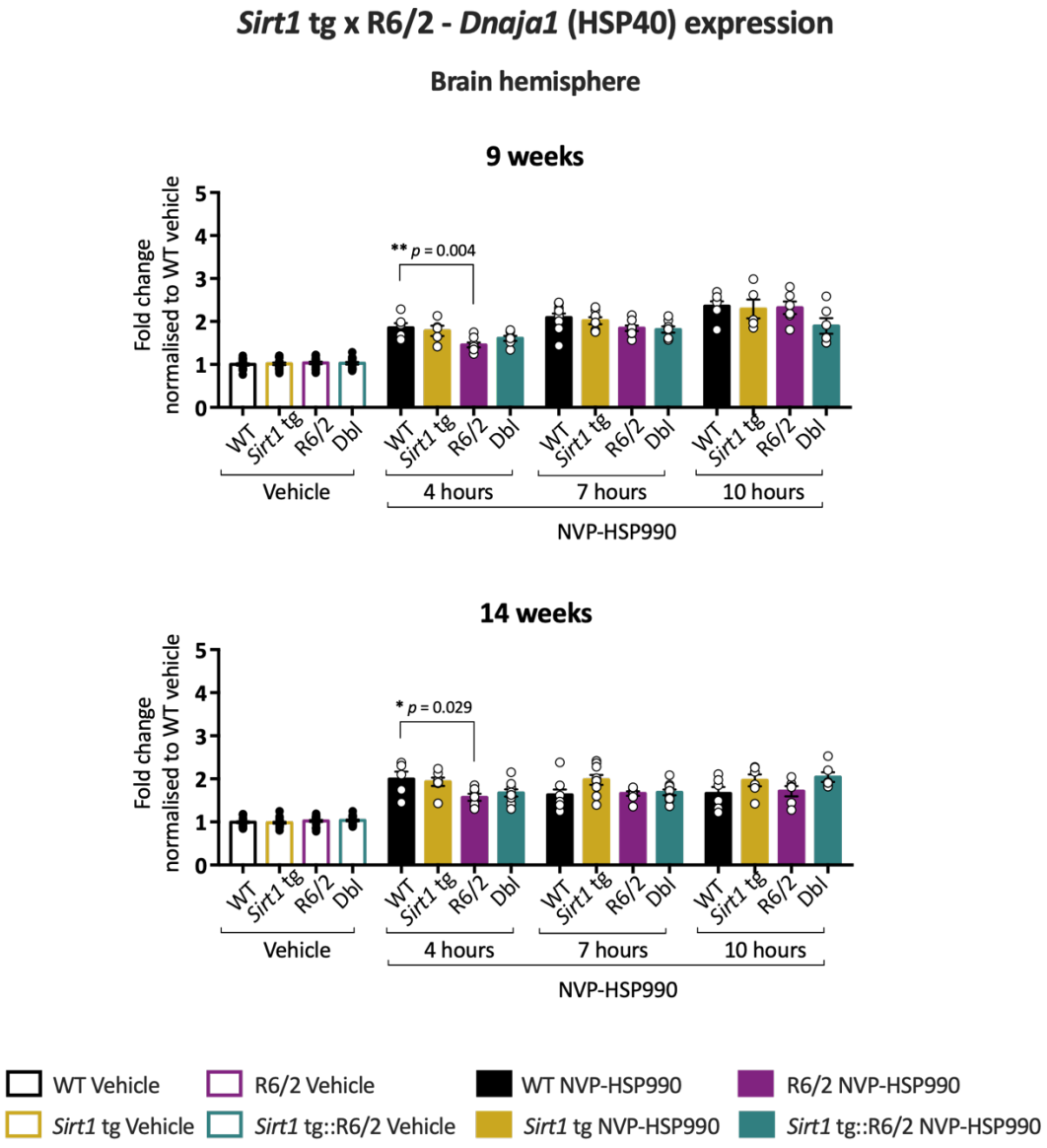

Figure 5.21. Dnaja1 (HSP40) *expression in brain hemispheres of Sirt1 tg x R6/2 mice at 9 and 14 weeks of age, after treatment with NVP-HSP990.*

Dnaja1 (HSP40) *expression was measured by QuantiGene in the brain hemispheres of Sirt1 tg x R6/2 mice at 9 and 14 weeks of age, 4, 7 and 10 hours after receiving a dose of NVP-HSP990 or vehicle. The fold changes in expression for the NVP-HSP990 groups were normalised to the corresponding WT vehicle. For simplicity, the vehicle data for each time point were plotted together for each genotype, as no differences between time points were found. N = 5 - 10 mice / genotype / treatment at 9 weeks at 14 weeks. Statistical analysis was by two-way ANOVA and Bonferroni correction for multiple comparisons. Only the statistical significance values between WT vs R6/2 and R6/2 and Sirt1 tg::R6/2 in NVP-HSP990 groups are shown. Mean ± SEM. ** p ≤ 0.01; * p ≤ 0.05. WT = wild-type; tg = transgenic; Dbl = double mutant (Sirt1 tg::R6/2).*

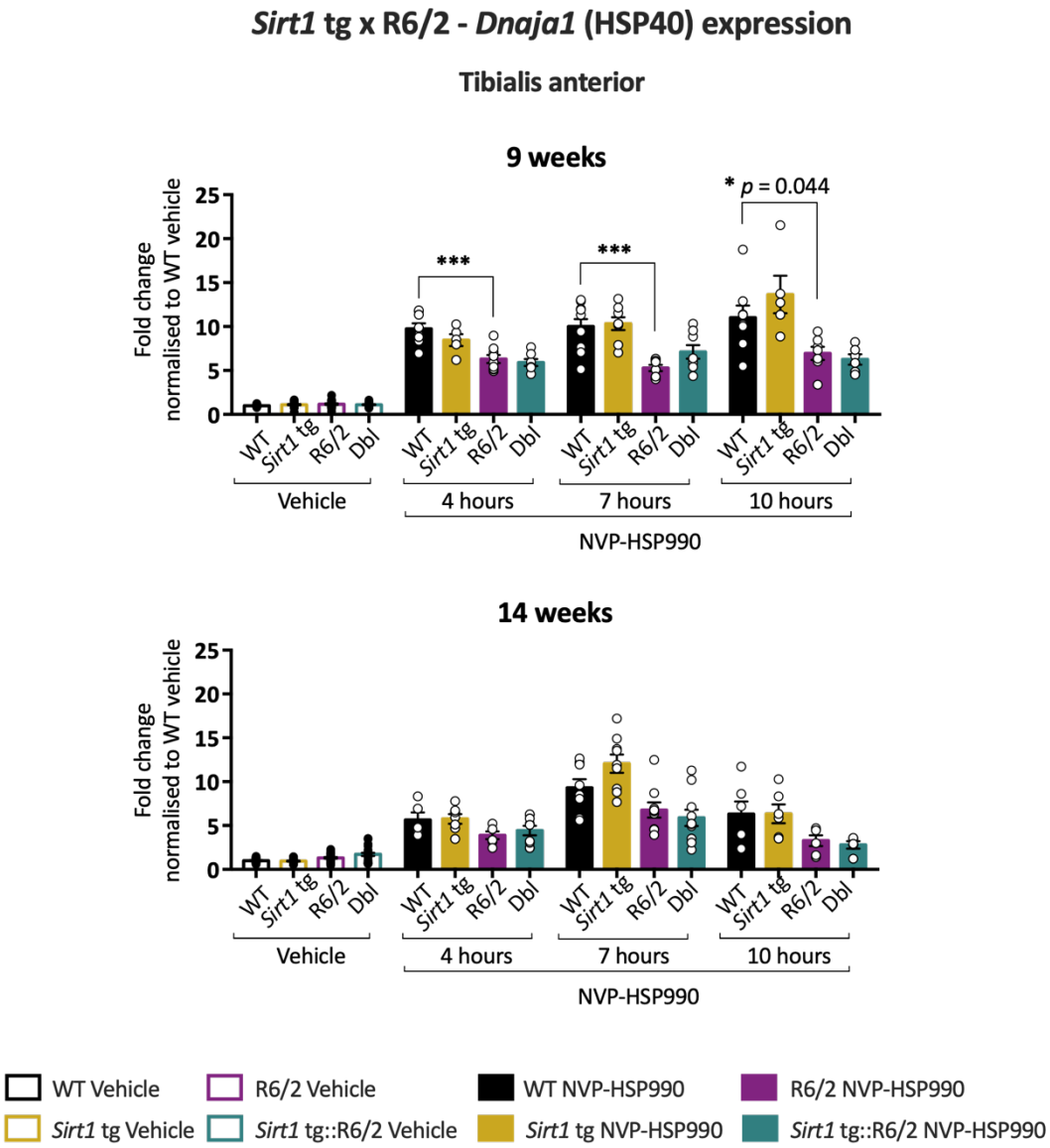

Figure 5.22. Dnaja1 (HSP40) *expression in tibialis anterior of Sirt1 tg x R6/2 mice at 9 and 14 weeks of age, after treatment with NVP-HSP990.*

Dnaja1 (HSP40) *expression was measured by QuantiGene in the tibialis anterior of Sirt1 tg x R6/2 mice at 9 and 14 weeks of age, 4, 7 and 10 hours after receiving a dose of NVP-HSP990 or vehicle. The fold changes in expression for the NVP-HSP990 groups were normalised to the corresponding WT vehicle. For simplicity, the vehicle data for each time point were plotted together for each genotype, as no differences between time points were found. N = 5 - 10 mice / genotype / treatment at 9 weeks at 14 weeks. Statistical analysis was by two-way ANOVA and Bonferroni correction for multiple comparisons. Only the statistical significance values between WT vs R6/2 and R6/2 and Sirt1 tg::R6/2 in NVP-HSP990 groups are shown. Mean ± SEM. *** p ≤ 0.001; * p ≤ 0.05. WT = wild-type; tg = transgenic; Dbl = double mutant (Sirt1 tg::R6/2).*

5.5.5 Expression of *Dnajb1* (HSP40)

In a similar pattern as to that observed for *Dnaja1* (HSP40) in brain, the levels of *Dnajb1* (HSP40) induction remained equivalent for all the genotypes at all time points at 9 and 14 weeks of age. The exception was at 14 weeks of age, by 10 hours post-dosing, where the fold change in *Dnajb1* expression of *Sirt1* tg::R6/2 was significantly higher than in R6/2 (Figure 5.23); however, as both R6/2 and wild-type levels of expression were lower at that time point, this significantly higher expression of *Dnajb1* in *Sirt1* tg ::R6/2 mice was probably not biologically significant.

The pattern of impairment in tibialis anterior was more evident for R6/2 at 9 weeks of age, when there were statistically significant decreases in *Dnajb1* expression in R6/2 as compared to wild-type at 4 and 7 hours after dosing. Generally, by 14 weeks of age, the induction in tibialis anterior was less notable than at 9 weeks, without significant differences between genotypes (Figure 5.24).

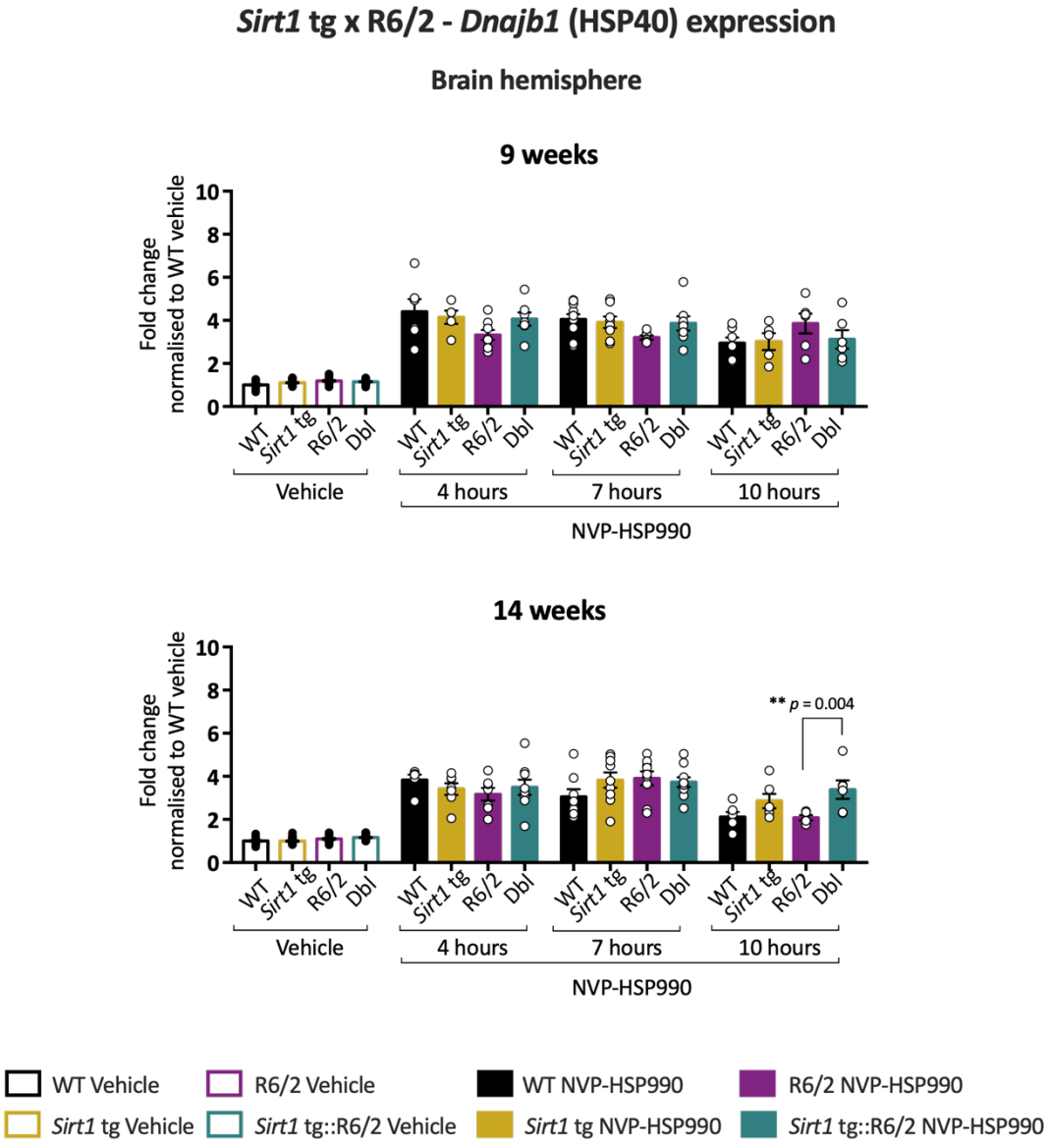

Figure 5.23. Dnajb1 (HSP40) *expression in brain hemispheres of Sirt1 tg x R6/2 mice at 9 and 14 weeks of age, after treatment with NVP-HSP990.*

Dnajb1 (HSP40) *expression was measured by QuantiGene in the brain hemispheres of Sirt1 tg x R6/2 mice at 9 and 14 weeks of age, 4, 7 and 10 hours after receiving a dose of NVP-HSP990 or vehicle. The fold changes in expression for the NVP-HSP990 groups were normalised to the corresponding WT vehicle. For simplicity, the vehicle data for each time point were plotted together for each genotype, as no differences between time points were found. N = 5 - 10 mice / genotype / treatment at 9 weeks at 14 weeks. Statistical analysis was by two-way ANOVA and Bonferroni correction for multiple comparisons. Only the statistical significance values between WT vs R6/2 and R6/2 and Sirt1 tg::R6/2 in NVP-HSP990 groups are shown. Mean ± SEM. ** p ≤ 0.01. WT = wild-type; tg = transgenic; Dbl = double mutant (Sirt1 tg::R6/2).*

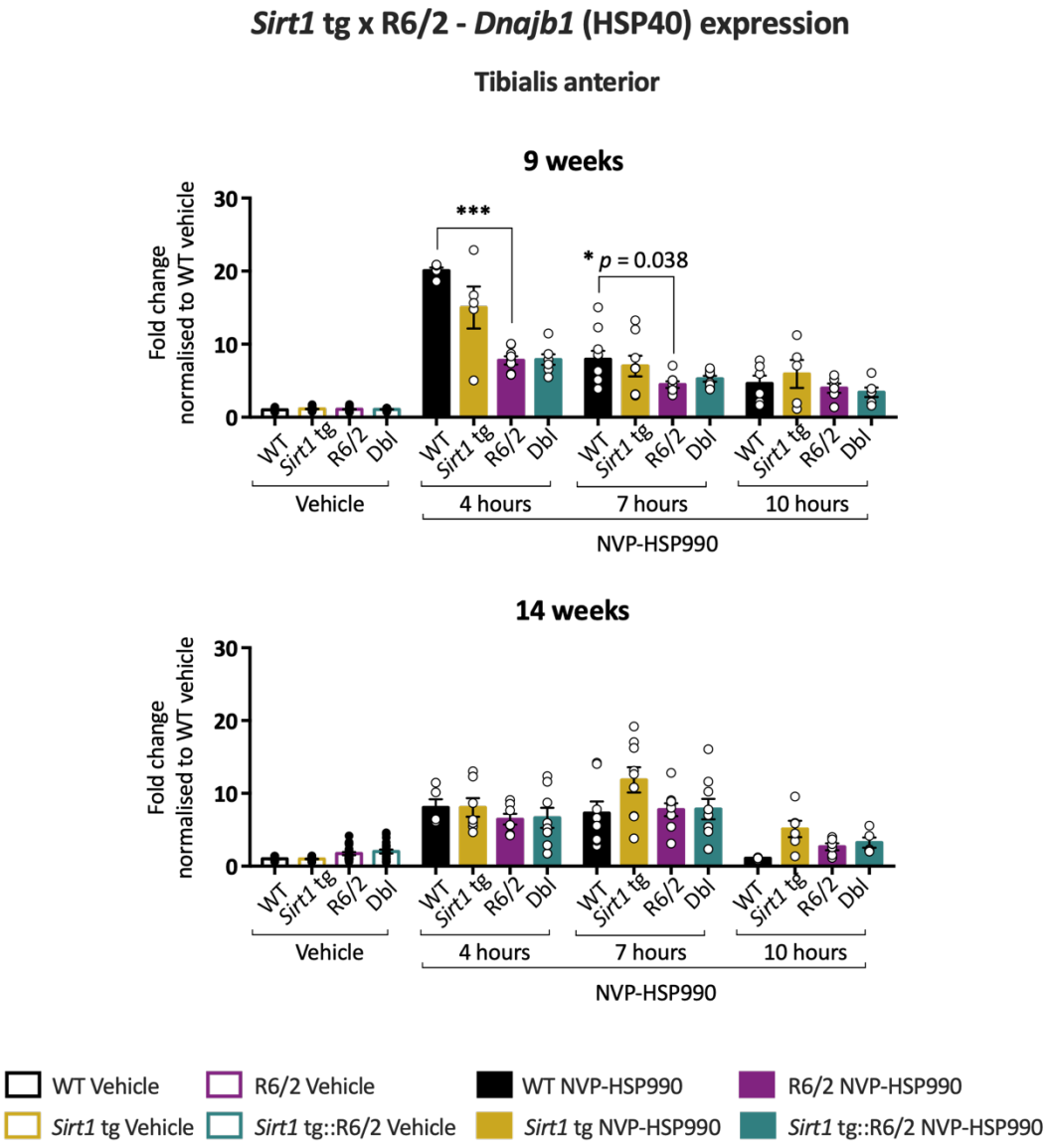

Figure 5.24. Dnajb1 (HSP40) *expression in tibialis anterior of Sirt1 tg x R6/2 mice at 9 and 14 weeks of age, after treatment with NVP-HSP990.*

Dnajb1 (HSP40) *expression was measured by QuantiGene in the tibialis anterior of Sirt1 tg x R6/2 mice at 9 and 14 weeks of age, 4, 7 and 10 hours after receiving a dose of NVP-HSP990 or vehicle. The fold changes in expression for the NVP-HSP990 groups were normalised to the corresponding WT vehicle. For simplicity, the vehicle data for each time point were plotted together for each genotype, as no differences between time points were found. N = 5 - 10 mice / genotype / treatment at 9 weeks and 4 - 10 mice / genotype / treatment at 14 weeks. Statistical analysis was by two-way ANOVA and Bonferroni correction for multiple comparisons. Only the statistical significance values between WT vs R6/2 and R6/2 and Sirt1 tg::R6/2 in NVP-HSP990 groups are shown. Mean ± SEM. *** p ≤ 0.001; * p ≤ 0.05. WT = wild-type; tg = transgenic; Dbl = double mutant (Sirt1 tg::R6/2).*

5.5.6 Expression of *Hspd1* (HSP60)

A decrease in *Hspd1* (HSP60) induction in R6/2 was evident at all time points and ages in the tibialis anterior (Figure 5.26), with some variability between samples in the wild-type group at 7 and 10 hours as compared to the rest of the treatment groups.

In brain, the evidence of impairment in R6/2 as compared to wild-type was present at 4 hours for 9 and 14 weeks of age and maintained to 7 hours at 9 weeks of age only. By 10 hours after dosing, at both ages, the levels of expression in wild-type and R6/2 brains were comparable (Figure 5.25).

No differences in the levels of expression or kinetics of induction could be detected when *Sirt1* was overexpressed, either in brain or in tibialis anterior (Figures 5.25 and 5.26).

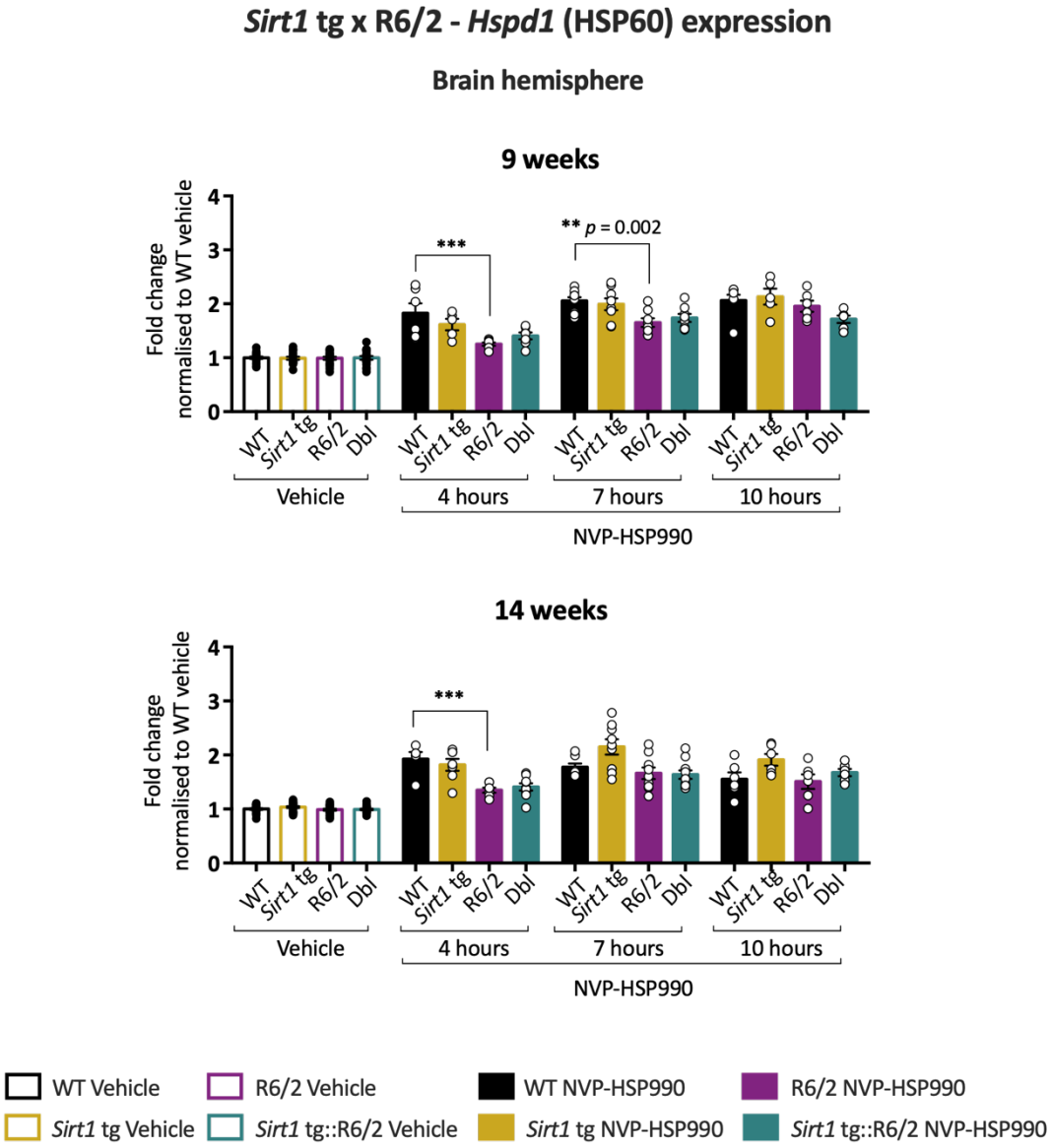

Figure 5.25. Hspd1 (HSP60) *expression in brain hemispheres of Sirt1 tg x R6/2 mice at 9 and 14 weeks of age, after treatment with NVP-HSP990.*

Hspd1 (HSP60) *expression was measured by QuantiGene in the brain hemispheres of Sirt1 tg x R6/2 mice at 9 and 14 weeks of age, 4, 7 and 10 hours after receiving a dose of NVP-HSP990 or vehicle. The fold changes in expression for the NVP-HSP990 groups were normalised to the corresponding WT vehicle. For simplicity, the vehicle data for each time point were plotted together for each genotype, as no differences between time points were found. N = 5 - 9 mice / genotype / treatment at 9 weeks and 5 - 10 mice / genotype / treatment at 14 weeks. Statistical analysis was by two-way ANOVA and Bonferroni correction for multiple comparisons. Only the statistical significance values between WT vs R6/2 and R6/2 and Sirt1 tg::R6/2 in NVP-HSP990 groups are shown. Mean ± SEM. *** p ≤ 0.001; ** p ≤ 0.01. WT = wild-type; tg = transgenic; Dbl = double mutant (Sirt1 tg::R6/2).*

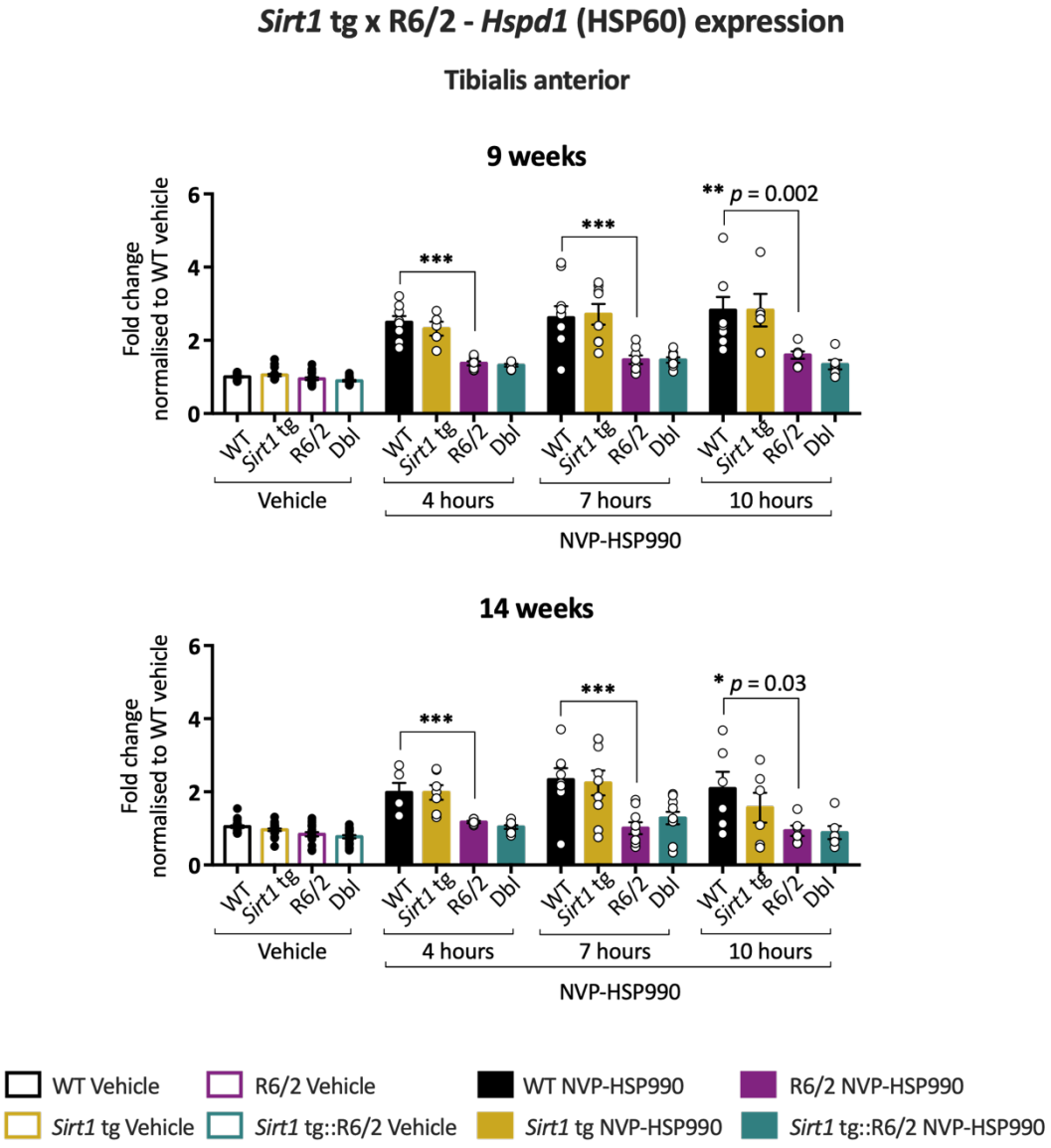

Figure 5.26. Hspd1 (HSP60) *expression in tibialis anterior of Sirt1 tg x R6/2 mice at 9 and 14 weeks of age, after treatment with NVP-HSP990.*

Hspd1 (HSP60) *expression was measured by QuantiGene in the tibialis anterior of Sirt1 tg x R6/2 mice at 9 and 14 weeks of age, 4, 7 and 10 hours after receiving a dose of NVP-HSP990 or vehicle. The fold changes in expression for the NVP-HSP990 groups were normalised to the corresponding WT vehicle. For simplicity, the vehicle data for each time point were plotted together for each genotype, as no differences between time points were found. N = 5 - 10 mice / genotype / treatment at 9 weeks and at 14 weeks. Statistical analysis was by two-way ANOVA and Bonferroni correction for multiple comparisons. Only the statistical significance values between WT vs R6/2 and R6/2 and Sirt1 tg::R6/2 in NVP-HSP990 groups are shown. Mean ± SEM. *** p ≤ 0.001; ** p ≤ 0.01; * p ≤ 0.05. WT = wild-type; tg = transgenic; Dbl = double mutant (Sirt1 tg::R6/2).*

5.5.7 Expression of *Hspe1* (HSP10)

For *Hspe1* (HSP10) induction, a consistent pattern of impairment was found at both ages and practically at all time points in R6/2 mice as compared to wild-type, with a greater decrease in expression in R6/2 in tibialis anterior (Figures 5.27 and 5.28). This pattern of impairment remained relatively unaltered for both tissues at both ages. However, the *Sirt1* overexpression did not have any influence on the kinetics or levels of induction in R6/2 mice.

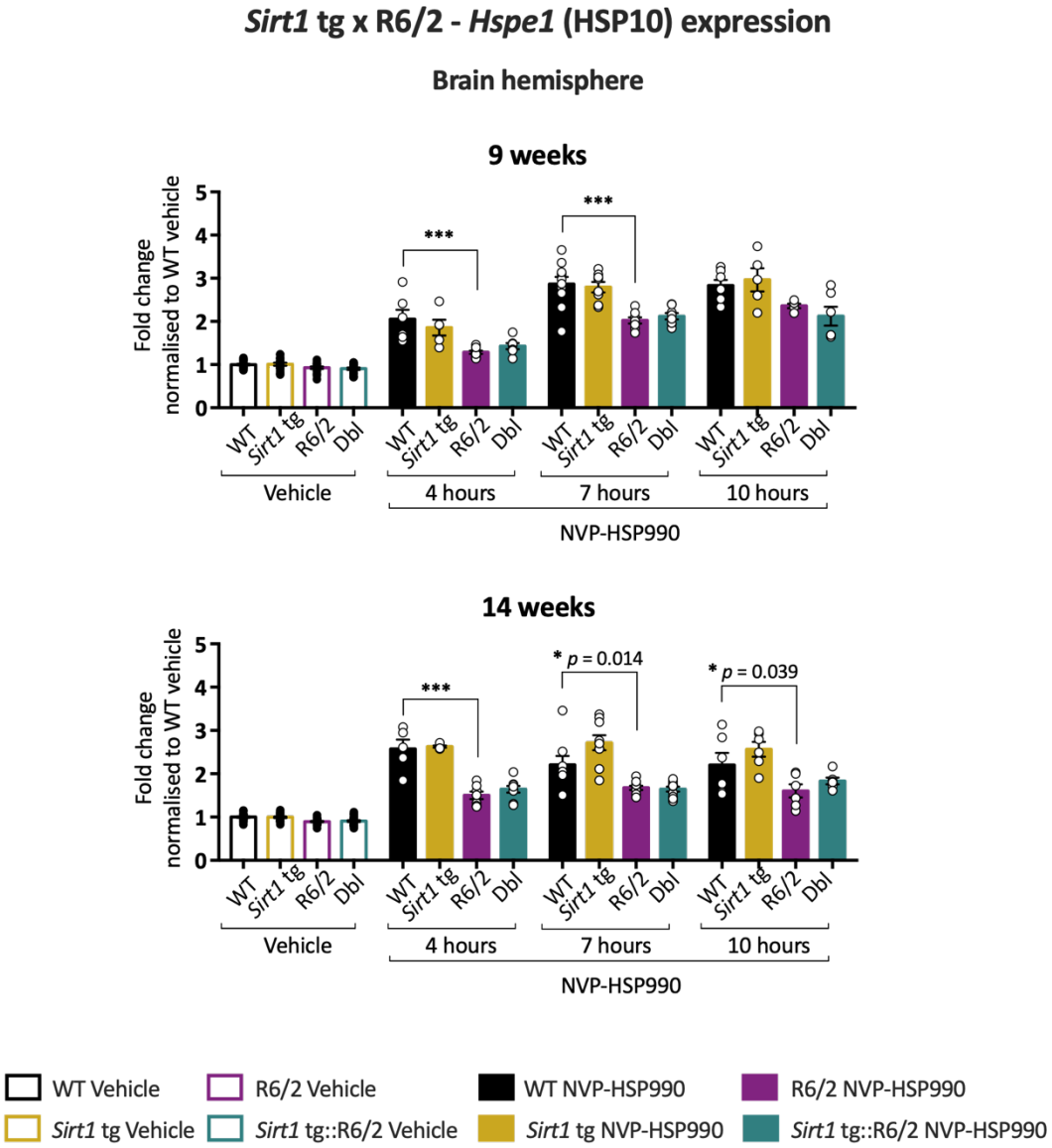

Figure 5.27. Hspe1 (HSP10) *expression in brain hemispheres of Sirt1 tg x R6/2 mice at 9 and 14 weeks of age, after treatment with NVP-HSP990.*

Hspe1 (HSP10) *expression was measured by QuantiGene in the tibialis anterior of Sirt1 tg x R6/2 mice at 9 and 14 weeks of age, 4, 7 and 10 hours after receiving a dose of NVP-HSP990 or vehicle. The fold changes in expression for the NVP-HSP990 groups were normalised to the corresponding WT vehicle. For simplicity, the vehicle data for each time point were plotted together for each genotype, as no differences between time points were found. N = 5 - 10 mice / genotype / treatment at 9 weeks and at 14 weeks. Statistical analysis was by two-way ANOVA and Bonferroni correction for multiple comparisons. Only the statistical significance values between WT vs R6/2 and R6/2 and Sirt1 tg::R6/2 in NVP-HSP990 groups are shown. Mean ± SEM. *** p ≤ 0.001; * p ≤ 0.05. WT = wild-type; tg = transgenic; Dbl = double mutant (Sirt1 tg::R6/2).*

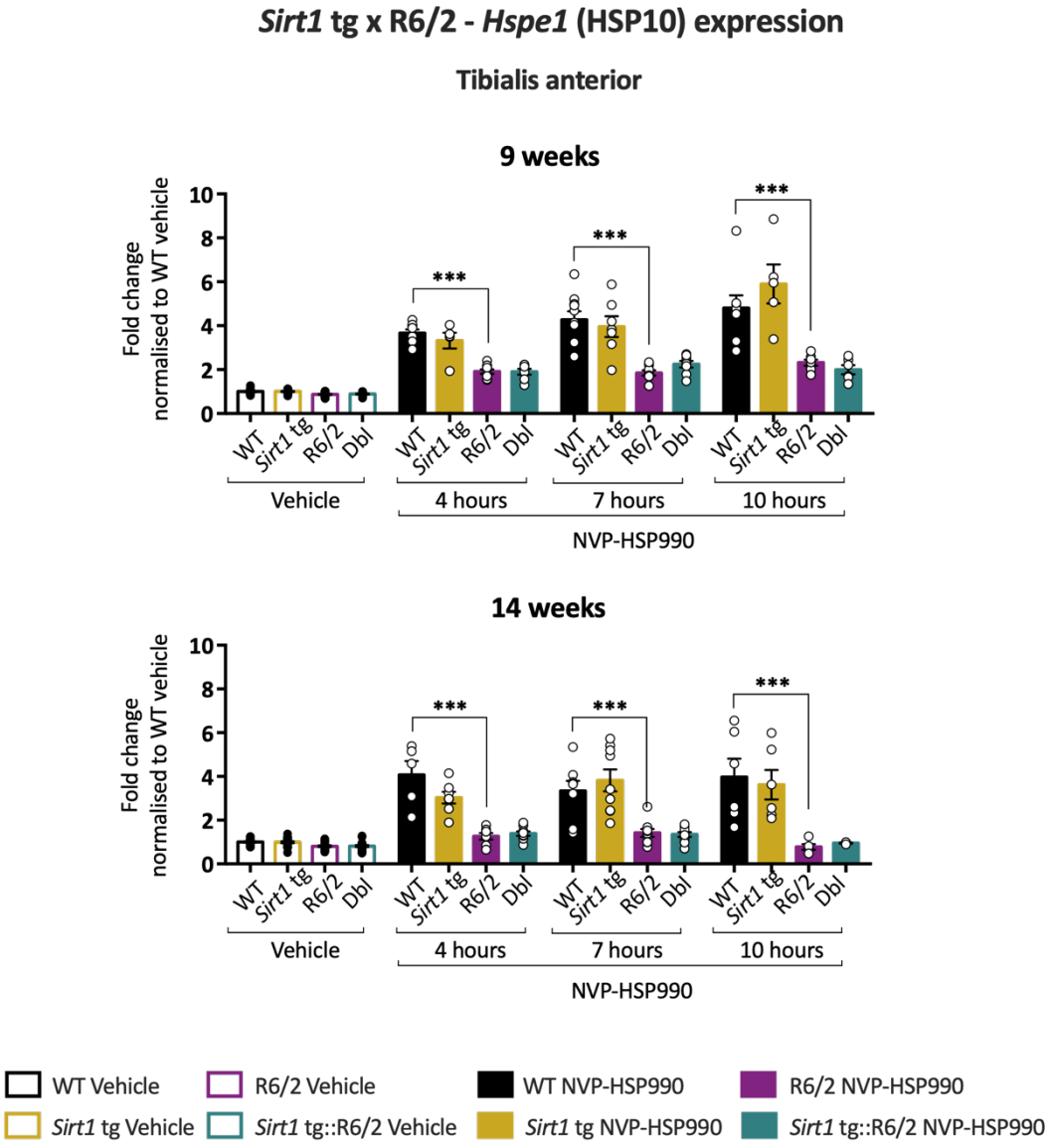

Figure 5.28. Hspe1 (HSP10) *expression in tibialis anterior of Sirt1 tg x R6/2 mice at 9 and 14 weeks of age, after treatment with NVP-HSP990.*

Hspe1 (HSP10) *expression was measured by QuantiGene in the tibialis anterior of Sirt1 tg x R6/2 mice at 9 and 14 weeks of age, 4, 7 and 10 hours after receiving a dose of NVP-HSP990 or vehicle. The fold changes in expression for the NVP-HSP990 groups were normalised to the corresponding WT vehicle. For simplicity, the vehicle data for each time point were plotted together for each genotype, as no differences between time points were found. N = 4 - 10 mice / genotype / treatment at 9 weeks and at 14 weeks. Statistical analysis was by two-way ANOVA and Bonferroni correction for multiple comparisons. Only the statistical significance values between WT vs R6/2 and R6/2 and Sirt1 tg::R6/2 in NVP-HSP990 groups are shown. Mean ± SEM. *** $p \leq 0.001$. WT = wild-type; tg = transgenic; Dbl = double mutant (Sirt1 tg::R6/2).*

5.5.8 Expression of *Hsph1* (HSP110)

As observed in previous sections for *Hspd1* and *Hspe1*, a clear and consistent decrease in the induction of *Hsph1* (HSP110) expression was found in R6/2 at both ages for all time points in both brain and tibialis anterior (Figures 5.29 and 5.30).

The patterns of expression remained generally equivalent in each tissue and unaffected by age. A high degree of variability was found particularly in the wild-type group at 4 hours post-dosing at 14 weeks of age in tibialis with one sample showing an unusually high level of expression as compared to the rest of the samples. Even though a slightly higher level of expression could be seen in *Sirt1* tg::R6/2 by 10 hours at 14 weeks of age in both tissues, this was not statistically significant (Figures 5.29 and 5.30).

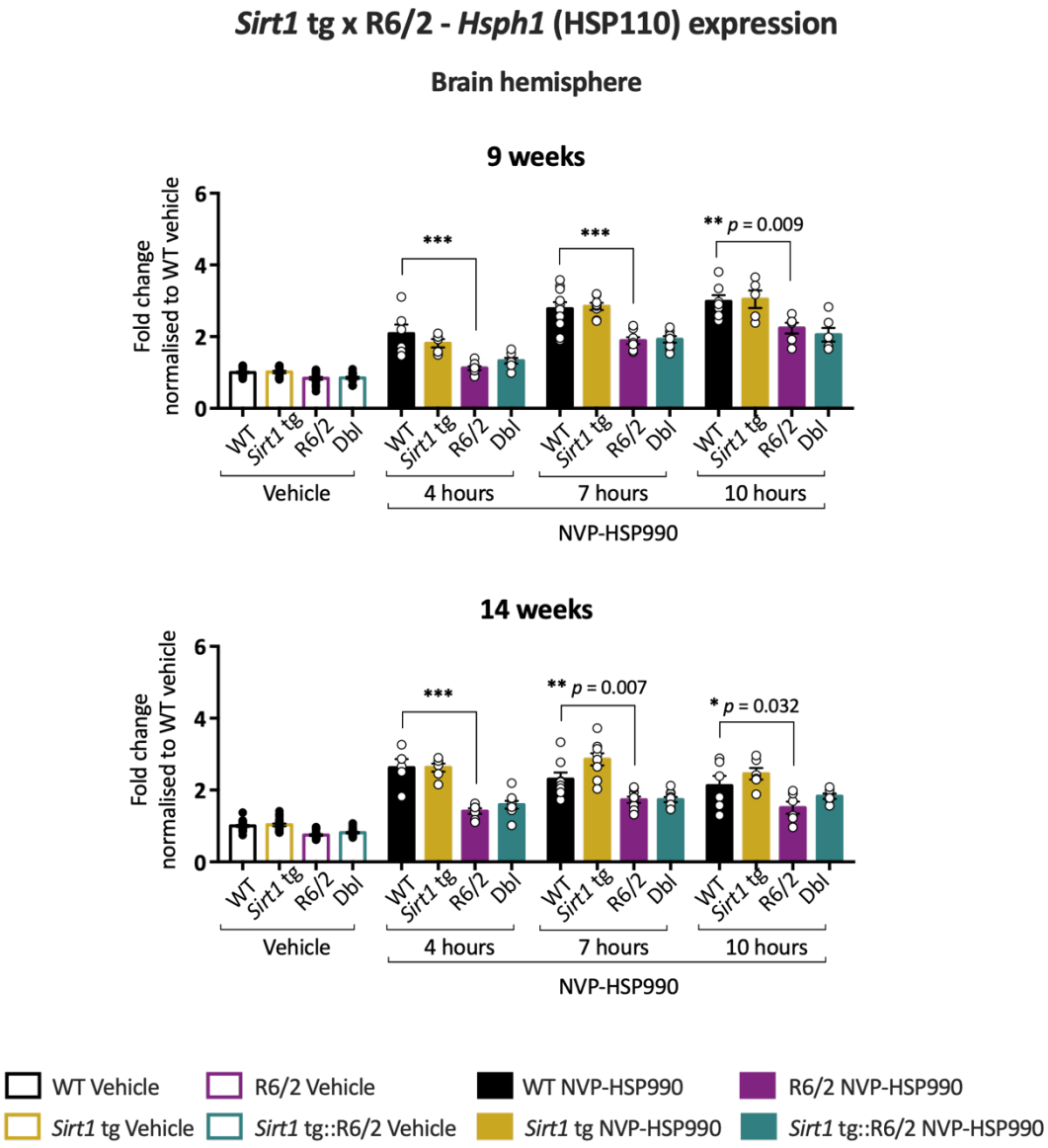

Figure 5.29. Hsph1 (HSP110) *expression in brain hemispheres of Sirt1 tg x R6/2 mice at 9 and 14 weeks of age, after treatment with NVP-HSP990.*

Hsph1 (HSP110) *expression was measured by QuantiGene in the brain hemispheres of Sirt1 tg x R6/2 mice at 9 and 14 weeks of age, 4, 7 and 10 hours after receiving a dose of NVP-HSP990 or vehicle. The fold changes in expression for the NVP-HSP990 groups were normalised to the corresponding WT vehicle. For simplicity, the vehicle data for each time point were plotted together for each genotype, as no differences between time points were found. N = 5 - 10 mice / genotype / treatment at 9 weeks and at 14 weeks. Statistical analysis was by two-way ANOVA and Bonferroni correction for multiple comparisons. Only the statistical significance values between WT vs R6/2 and R6/2 and Sirt1 tg::R6/2 in NVP-HSP990 groups are shown. Mean ± SEM. *** p ≤ 0.001; ** p ≤ 0.01; * p ≤ 0.05. WT = wild-type; tg = transgenic; Dbl = double mutant (Sirt1 tg::R6/2).*

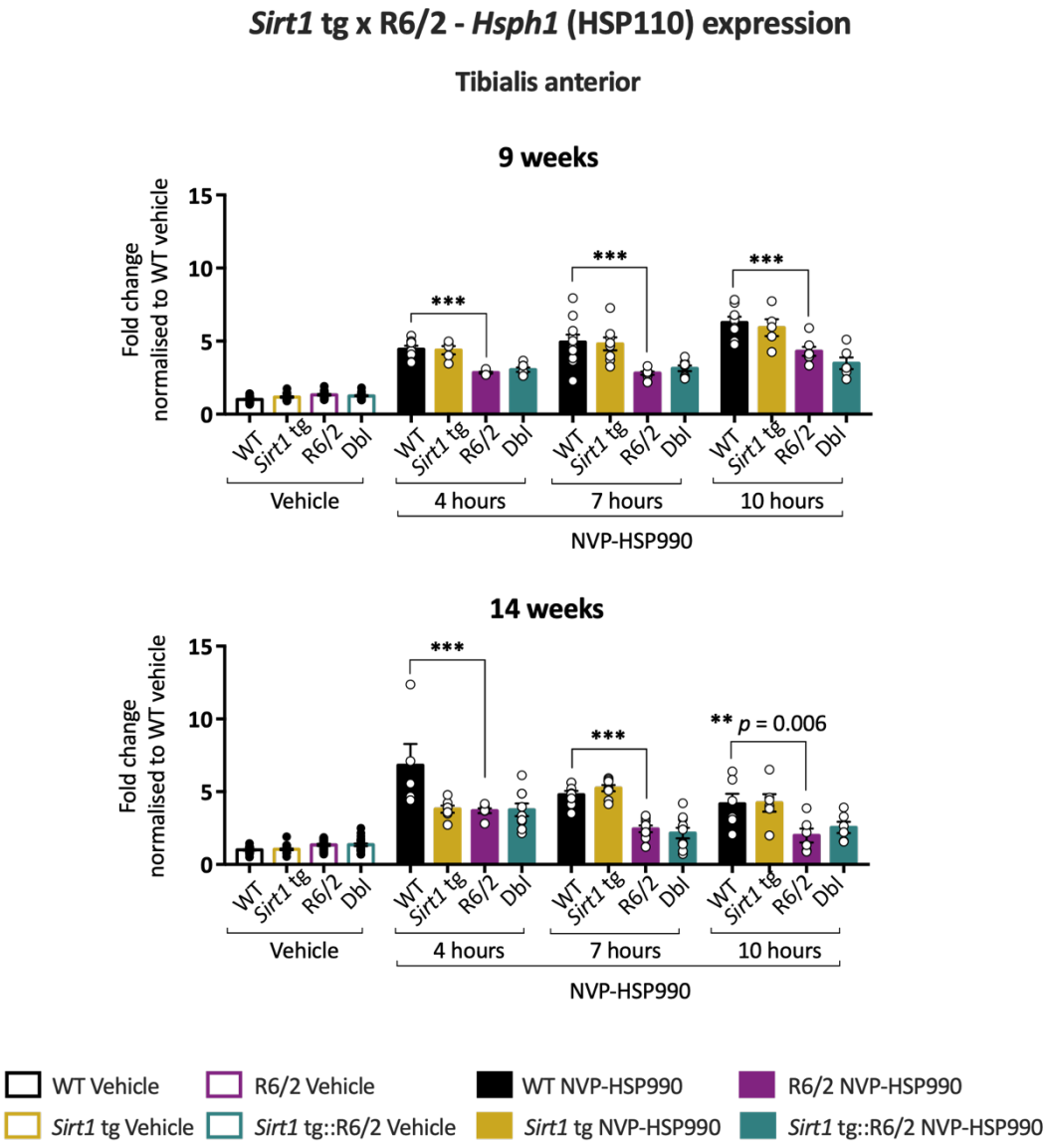

Figure 5.30. Hsph1 (HSP110) *expression in tibialis anterior of Sirt1 tg x R6/2 mice at 9 and 14 weeks of age, after treatment with NVP-HSP990.*

Hsph1 (HSP110) *expression was measured by QuantiGene in the tibialis anterior of Sirt1 tg x R6/2 mice at 9 and 14 weeks of age, 4, 7 and 10 hours after receiving a dose of NVP-HSP990 or vehicle. The fold changes in expression for the NVP-HSP990 groups were normalised to the corresponding WT vehicle. For simplicity, the vehicle data for each time point were plotted together for each genotype, as no differences between time points were found. N = 4 - 10 mice / genotype / treatment at 9 weeks and 5 - 10 mice / genotype / treatment at 14 weeks. Statistical analysis was by two-way ANOVA and Bonferroni correction for multiple comparisons. Only the statistical significance values between WT vs R6/2 and R6/2 and Sirt1 tg::R6/2 in NVP-HSP990 groups are shown. Mean ± SEM. *** p ≤ 0.001; ** p ≤ 0.01. WT = wild-type; tg = transgenic; Dbl = double mutant (Sirt1 tg::R6/2).*

5.5.9 Expression of *Hsp90aa1* (HSP90)

A significant decrease in the level of induction of the inducible *Hsp90aa1* (HSP90) was found in R6/2 brains, but only at 4 hours after dosing, as compared to wild-type counterparts, at both 9 and 14 weeks of age (Figure 5.31). In tibialis anterior, this impairment in R6/2 was more substantial and maintained by 7 hours post-dosing at 9 weeks of age (Figure 5.32).

Sirt1 overexpression caused a significant increase in *Hsp90aa1* expression in brain of R6/2 mice at 14 weeks of age, as detected by 10 hours after NVP-HSP990 treatment (Figure 5.31). However, although a slight increase was also visible in tibialis anterior at the same time point and age, this was not significantly different as compared to R6/2 (Figure 5.32).

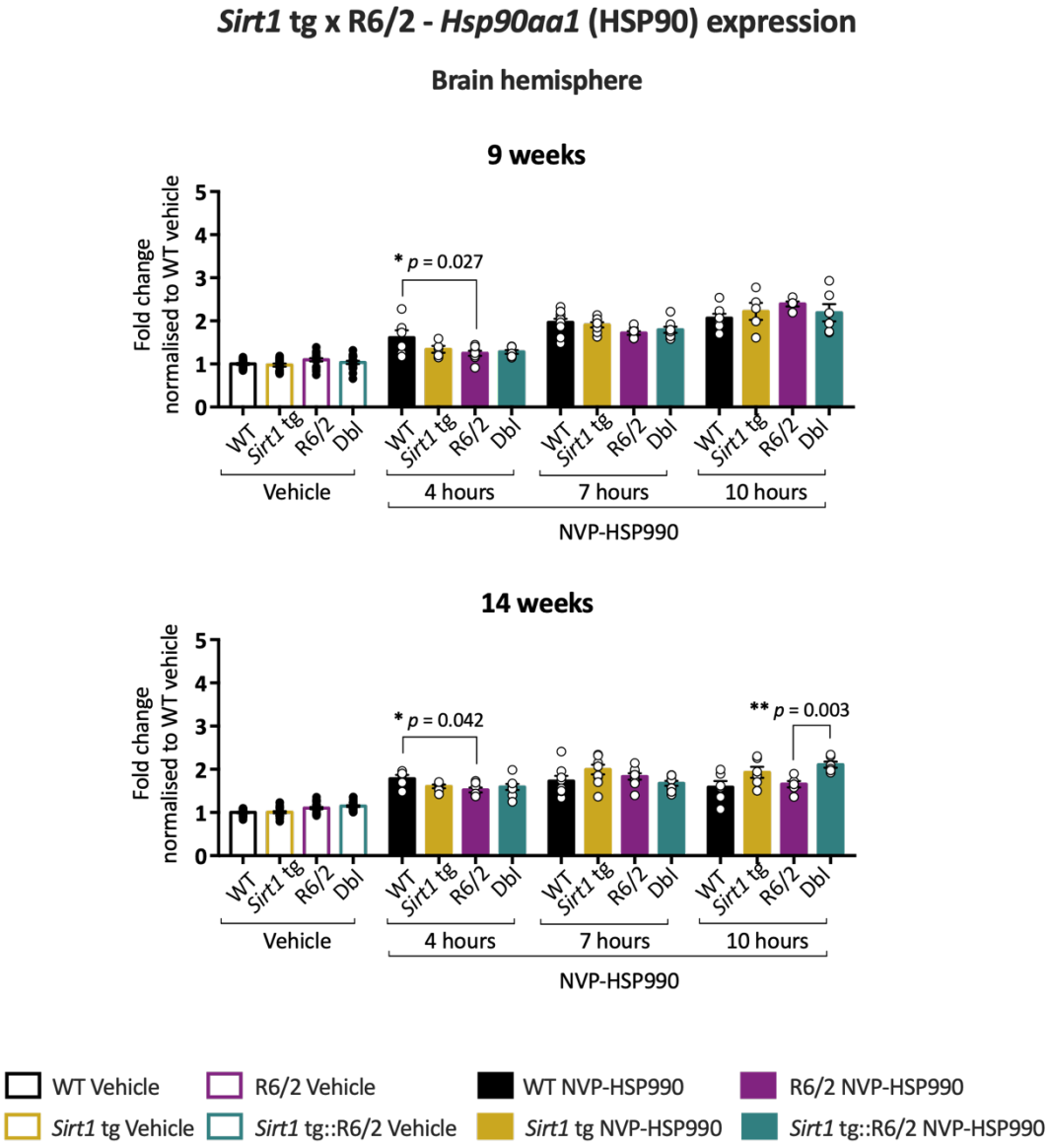

Figure 5.31. Hsp90aa1 (HSP90) *expression in brain hemispheres of Sirt1 tg x R6/2 mice at 9 and 14 weeks of age, after treatment with NVP-HSP990.*

Hsp90aa1 (HSP90) *expression was measured by QuantiGene in the brain hemispheres of Sirt1 tg x R6/2 mice at 9 and 14 weeks of age, 4, 7 and 10 hours after receiving a dose of NVP-HSP990 or vehicle. The fold changes in expression for the NVP-HSP990 groups were normalised to the corresponding WT vehicle. For simplicity, the vehicle data for each time point were plotted together for each genotype, as no differences between time points were found. N = 5 - 10 mice / genotype / treatment at 9 weeks and at 14 weeks. Statistical analysis was by two-way ANOVA and Bonferroni correction for multiple comparisons. Only the statistical significance values between WT vs R6/2 and R6/2 and Sirt1 tg::R6/2 in NVP-HSP990 groups are shown. Mean ± SEM. ** p ≤ 0.01; * p ≤ 0.05. WT = wild-type; tg = transgenic; Dbl = double mutant (Sirt1 tg::R6/2).*

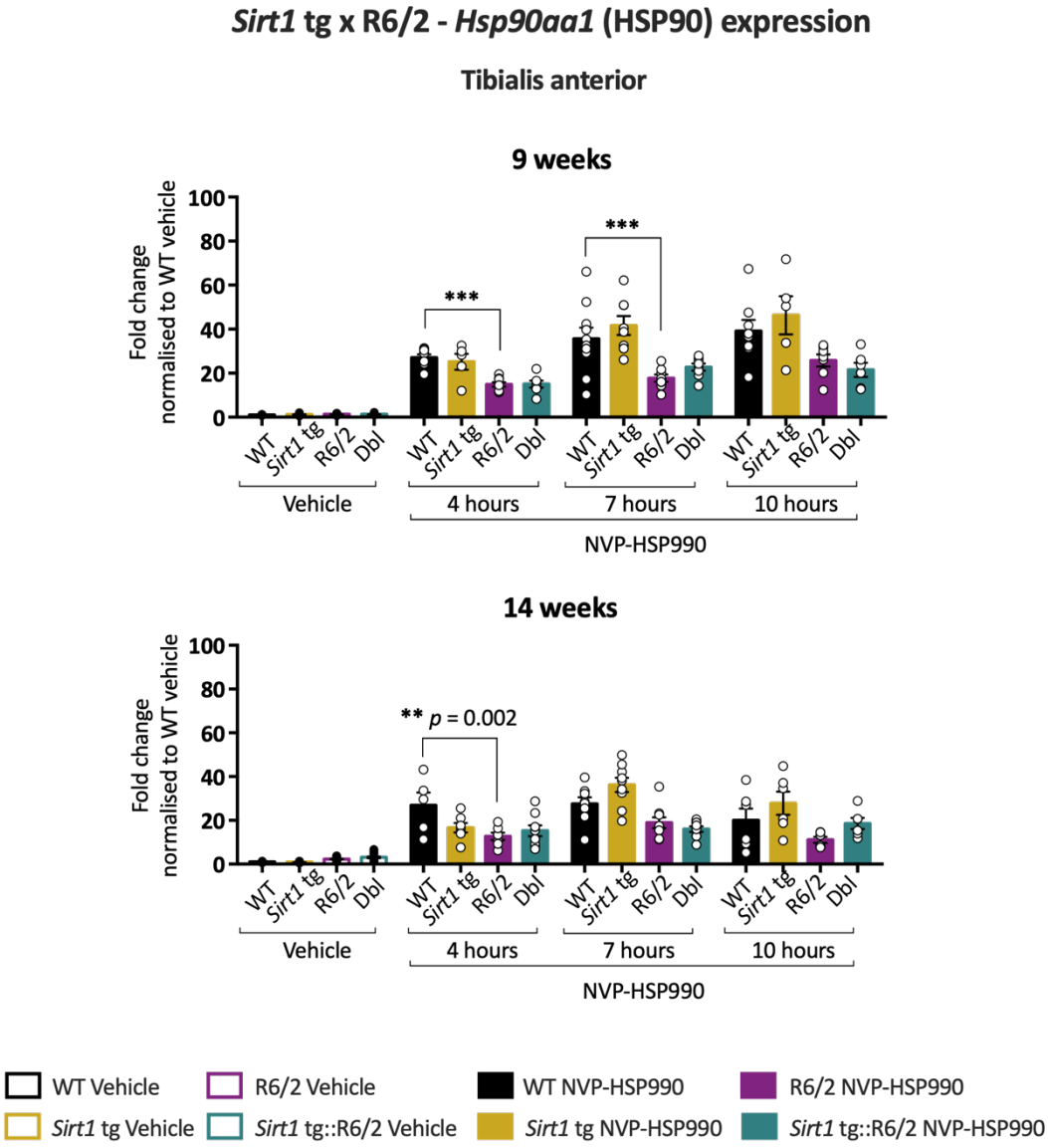

Figure 5.32. Hsp90aa1 (HSP90) *expression in tibialis anterior of Sirt1 tg x R6/2 mice at 9 and 14 weeks of age, after treatment with NVP-HSP990.*

Hsp90aa1 (HSP90) *expression was measured by QuantiGene in the tibialis anterior of Sirt1 tg x R6/2 mice at 9 and 14 weeks of age, 4, 7 and 10 hours after receiving a dose of NVP-HSP990 or vehicle. The fold changes in expression for the NVP-HSP990 groups were normalised to the corresponding WT vehicle. For simplicity, the vehicle data for each time point were plotted together for each genotype, as no differences between time points were found. N = 5 - 10 mice / genotype / treatment at 9 weeks and 5 - 9 mice / genotype / treatment at 14 weeks. Statistical analysis was by two-way ANOVA and Bonferroni correction for multiple comparisons. Only the statistical significance values between WT vs R6/2 and R6/2 and Sirt1 tg::R6/2 in NVP-HSP990 groups are shown. Mean ± SEM. *** p ≤ 0.001; ** p ≤ 0.01. WT = wild-type; tg = transgenic; Dbl = double mutant (Sirt1 tg::R6/2).*

5.5.10 Expression of *Hsp90ab1* (HSP90)

There was no compelling evidence for an impairment in the constitutively expressed *Hsp90ab1* (HSP90) induction as compared to wild-type in either R6/2 brain at the ages studied (although it was significant at the 7 hours time point) or in tibialis at 9 weeks of age (Figures 5.33 and 5.34). At 14 weeks of age, in tibialis anterior, more visible differences were observed between R6/2 and wild-type, although there was a high degree of variability within the groups, and this difference was only statistically significant at 10 hours after dosing (Figure 5.34).

Similar to that described for *Hsp90aa1*, a mild but statistically significant difference in the levels of expression was detected in brain between *Sirt1* tg::R6/2 and R6/2 mice at 14 weeks of age, 10 hours after being dosed (Figure 5.33).

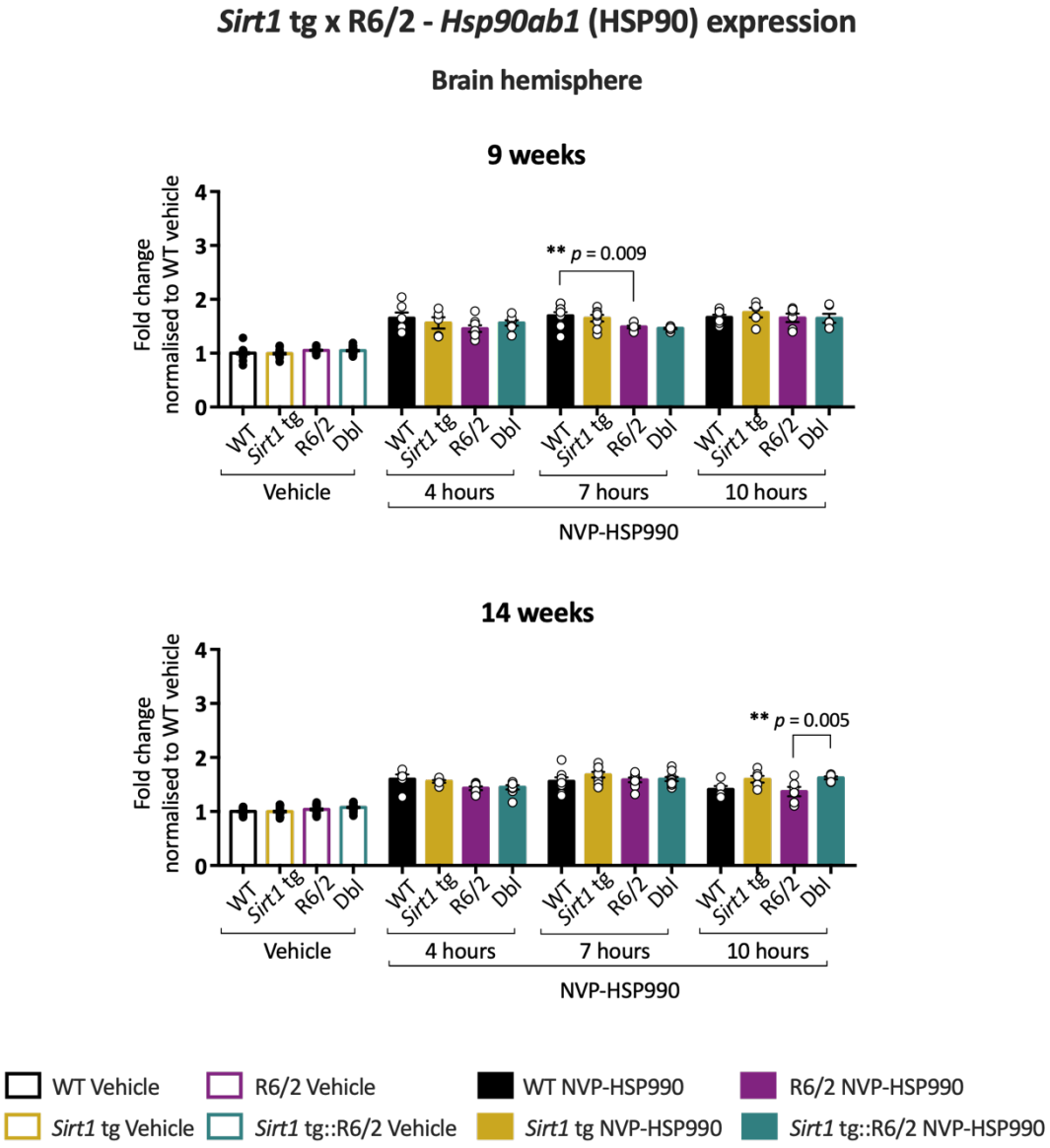

Figure 5.33. Hsp90ab1 (HSP90) *expression in brain hemispheres of Sirt1 tg x R6/2 mice at 9 and 14 weeks of age, after treatment with NVP-HSP990.*

Hsp90ab1 (HSP90) *expression was measured by QuantiGene in the brain hemispheres of Sirt1 tg x R6/2 mice at 9 and 14 weeks of age, 4, 7 and 10 hours after receiving a dose of NVP-HSP990 or vehicle. The fold changes in expression for the NVP-HSP990 groups were normalised to the corresponding WT vehicle. For simplicity, the vehicle data for each time point were plotted together for each genotype, as no differences between time points were found. N = 5 - 10 mice / genotype / treatment at 9 weeks and at 14 weeks. Statistical analysis was by two-way ANOVA and Bonferroni correction for multiple comparisons. Only the statistical significance values between WT vs R6/2 and R6/2 and Sirt1 tg::R6/2 in NVP-HSP990 groups are shown. Mean ± SEM. ** p ≤ 0.01. WT = wild-type; tg = transgenic; Dbl = double mutant (Sirt1 tg::R6/2).*

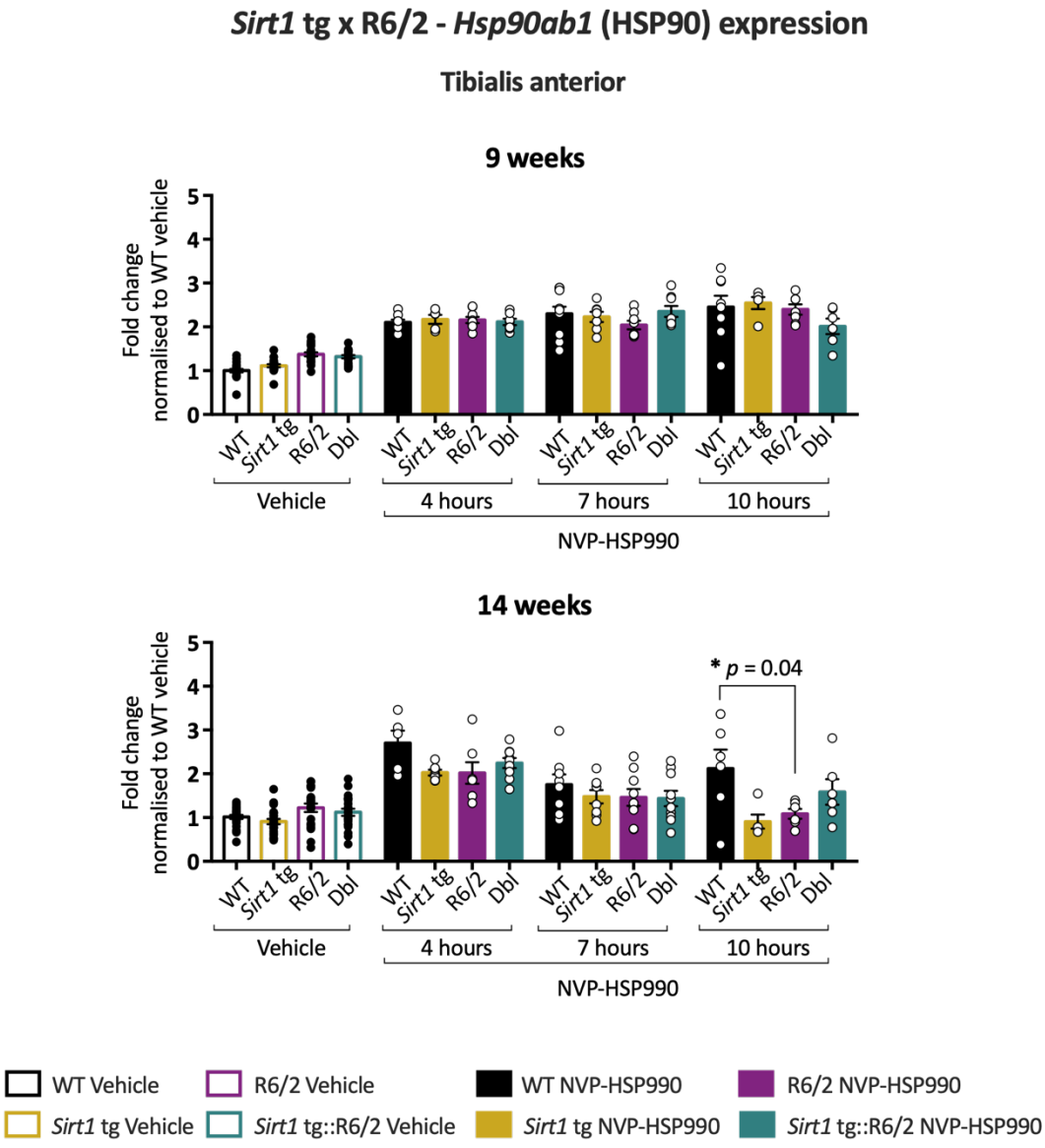

Figure 5.34. Hsp90ab1 (HSP90) *expression in tibialis anterior of Sirt1 tg x R6/2 mice at 9 and 14 weeks of age, after treatment with NVP-HSP990.*

Hsp90ab1 (HSP90) *expression was measured by QuantiGene in the tibialis anterior of Sirt1 tg x R6/2 mice at 9 and 14 weeks of age, 4, 7 and 10 hours after receiving a dose of NVP-HSP990 or vehicle. The fold changes in expression for the NVP-HSP990 groups were normalised to the corresponding WT vehicle. For simplicity, the vehicle data for each time point were plotted together for each genotype, as no differences between time points were found. N = 5 - 10 mice / genotype / treatment at 9 weeks and at 14 weeks. Statistical analysis was by two-way ANOVA and Bonferroni correction for multiple comparisons. Only the statistical significance values between WT vs R6/2 and R6/2 and Sirt1 tg::R6/2 in NVP-HSP990 groups are shown. Mean ± SEM. * p ≤ 0.05. WT = wild-type; tg = transgenic; Dbl = double mutant (Sirt1 tg::R6/2).*

5.6 Summary of results and discussion

The modulation of HSF1 for the activation of the heat shock response is a potential therapeutic strategy for HD, as discussed in Chapters 3 and 4. As shown in Chapter 4, the heat shock response is impaired in brain regions and tibialis anterior muscle from R6/2 mice (Figures 4.3 and 4.20 to 4.25). This is consistent with the study by Labbadia *et al.* (2011), where the pulsed treatment with NVP-HSP990 provided mild but transient improvements in some HD phenotypes, as the capacity of R6/2 mice to elicit a heat shock response became impaired as the disease progressed.

Over the course of the heat shock response, HSF1 undergoes many post-translational modifications (Gomez-Pastor *et al.,* 2018; Anckar and Sistonen, 2011; Akerfelt *et al*., 2010). During the activation phase, the hyperphosphorylation of specific residues in HSF1 domains is essential for initiating the transcriptional activation of heat shock genes. In contrast, during the attenuation phase, the acetylation of Lys80 in the DNA binding domain of HSF1 is a critical post-translational modification, which is facilitated by the acetyltransferase EP300 (Raychaudhuri *et al.,* 2014). Lys80 acetylation in HSF1 affects its interaction with heat shock gene promoters and leads to the eventual inactivation of HSF1. A report by Westerheide *et al.* (2009) provided evidence for an interaction between HSF1 and the histone deacetylase SIRT1, which led to the deacetylation of this Lys80 residue.

SIRT1 has been studied as a potential disease modifier for HD due to its involvement in diverse aspects of cell biology such as aging, apoptosis, mitochondrial function and inflammation (Haigis and Sinclair, 2010). The *in vivo* neuroprotective effects of increased SIRT1 activity that have been described in the context of HD and polyglutamine toxicity include prolonged survival, reduced brain atrophy and amelioration of motor function (Parker *et al.,* 2005; Jeong *et al.,* 2012; Jiang *et al.,* 2012). In contrast, in some studies, the genetic or pharmacological inhibition of SIRT1 showed a decrease in HD symptoms (Pallos *et al.,* 2008; Smith *et al.*, 2014). These contrasting results may be explained by a dual function: on one hand, a pro-survival effect in cells might be caused by an enhanced SIRT1 activity and, on the other hand,

the inhibition of SIRT1 may lead to the increased acetylation of mutant HTT which could promote its degradation (Jeong *et al.*, 2009). In our group, SIRT1 activity was found to be decreased in the brains of HD models R6/2 and *Hdh*Q150 (Tulino *et al.,* 2016). The phosphorylation levels of SIRT1 were dysregulated in the striatum and cerebellum of these HD models from 9 weeks of age by the presence of mutant HTT, subsequently affecting SIRT1 activity.

The main research aim in this chapter was to investigate whether an increase in SIRT1 activity resulting from *Sirt1* overexpression (Tulino *et al*., 2016) could alleviate the heat shock response impairment that occurs in HD mouse models with disease progression.

An intercross between R6/2 and *Sirt1* overexpressing mice (*Sirt1* tg) provided the four genotypes of interest: wild-type, *Sirt1* tg, R6/2 and double mutant *Sirt1* tg::R6/2. An initial small-scale pilot study in which the expression of *Hspa1a/b*, *Hspb1* and *Dnajb1* was analysed in brain and quadriceps femoris in these four genotypes at 9 weeks of age in response to treatment with NVP-HSP990 or vehicle, suggested that increasing SIRT1 activity in R6/2 mice had a restorative effect on the expression of these genes, with levels of *Hspa1a/b* and *Hspb1* comparable to that in wild-type mice at 8 hours post-dosing (Figures 5.1 and 5.2). However, the study was underpowered due to a low sample size and therefore needed to be expanded to determine whether these results could be confirmed.

A large-scale study was designed with a greater number of mice per treatment group. Two cohorts of mice were selected, at 9 weeks and 14 weeks of age, to cover the early and late symptomatic stages of disease in the R6/2 model. These mice were administered with NVP-HSP990 or vehicle and then brain and tibialis anterior were dissected at three time points after dosing to study the kinetics and levels of expression of the heat shock genes in all the treatment groups by the QuantiGene 18-plex assay (Figure 5.3).

The following tables (Tables 5.3, 5.4) summarise the results obtained and statistical significance from the gene expression analysis by QuantiGene in brain hemispheres and tibialis anterior of R6/2 (as compared to wild-type) and *Sirt1* tg::R6/2 (as compared to R6/2) mice at 9 and 14 weeks of age, at different time points after being dosed with NVP-HSP990 or vehicle.

Table 5.3. Summary of results from the gene expression analyses in brain hemisphere of R6/2 and Sirt1 tg::R6/2 mice at 9 and 14 weeks of age, at different time points after dosing with NVP-HSP990.

	Brain hemisphere											
	R6/2 (as compared to WT)						***Sirt1* tg::R6/2** (as compared to R6/2)					
	9 weeks			**14 weeks**			**9 weeks**			**14 weeks**		
Gene	*4 h*	*7 h*	*10 h*	*4 h*	*7 h*	*10 h*	*4 h*	*7 h*	*10 h*	*4 h*	*7 h*	*10 h*
Hspa1a/b	**	**	n.s.	***	n.s.	n.s.	n.s.	n.s.	n.s.	n.s.	n.s.	n.s.
Hspb1	**	n.s.	n.s.	n.s.	n.s.	n.s.	n.s.	n.s.	n.s.	n.s.	n.s.	n.s.
Dnaja1	**	n.s.	n.s.	*	n.s.	n.s.	n.s.	n.s.	n.s.	n.s.	n.s.	n.s.
Dnajb1	n.s.	n.s.	n.s.	n.s.	n.s.	n.s.	n.s.	n.s.	n.s.	n.s.	n.s.	**
Hspd1	***	**	n.s.	***	n.s.	n.s.	n.s.	n.s.	n.s.	n.s.	n.s.	n.s.
Hspe1	***	***	n.s.	***	*	*	n.s.	n.s.	n.s.	n.s.	n.s.	n.s.
Hsph1	***	***	**	***	**	*	n.s.	n.s.	n.s.	n.s.	n.s.	n.s.
Hsp90aa1	*	n.s.	n.s.	*	n.s.	n.s.	n.s.	n.s.	n.s.	n.s.	n.s.	**
Hsp90ab1	n.s.	**	n.s.	n.s.	n.s.	n.s.	n.s.	n.s.	n.s.	n.s.	n.s.	**

*n.s. = not significant; *** $p \leq 0.001$; ** $p \leq 0.01$; * $p \leq 0.05$*

Table 5.4. Summary of results from the gene expression analyses in tibialis anterior of R6/2 and Sirt1 tg::R6/2 mice at 9 and 14 weeks of age, at different time points after dosing with NVP-HSP990.

	Tibialis anterior											
	R6/2 (as compared to WT)						***Sirt1* tg::R6/2** (as compared to R6/2)					
	9 weeks			**14 weeks**			**9 weeks**			**14 weeks**		
Gene	*4 h*	*7 h*	*10 h*	*4 h*	*7 h*	*10 h*	*4 h*	*7 h*	*10 h*	*4 h*	*7 h*	*10 h*
Hspa1a/b	***	***	***	***	***	***	n.s.	n.s.	n.s.	n.s.	n.s.	n.s.
Hspb1	***	**	***	***	n.s.	*	n.s.	n.s.	n.s.	n.s.	n.s.	n.s.
Dnaja1	***	***	*	n.s.	n.s.	n.s.	n.s.	n.s.	n.s.	n.s.	n.s.	n.s.
Dnajb1	***	*	n.s.	n.s.	n.s.	n.s.	n.s.	n.s.	n.s.	n.s.	n.s.	n.s.
Hspd1	***	***	**	***	***	*	n.s.	n.s.	n.s.	n.s.	n.s.	n.s.
Hspe1	***	***	***	***	***	***	n.s.	n.s.	n.s.	n.s.	n.s.	n.s.
Hsph1	***	***	***	***	***	**	n.s.	n.s.	n.s.	n.s.	n.s.	n.s.
Hsp90aa1	***	***	n.s.	**	n.s.	n.s.	n.s.	n.s.	n.s.	n.s.	n.s.	n.s.
Hsp90ab1	n.s.	n.s.	n.s.	n.s.	n.s.	*	n.s.	n.s.	n.s.	n.s.	n.s.	n.s.

*n.s. = not significant; *** $p \leq 0.001$; ** $p \leq 0.01$; * $p \leq 0.05$*

Some conclusions can be summarised from the findings:

- **R6/2 mice had a dysregulation in the induction of the heat shock response in brain and tibialis anterior at 9 and 14 weeks of age**

In keeping with the previous data described in Chapter 4 (Figures 4.3 and 4.20 to 4.25) and as was reported by Labbadia *et al.* (2011), a consistent impairment in the induction of the heat shock response was evident in R6/2 mice by 9 weeks of age and maintained to 14 weeks of age, with all the heat shock genes included in the analysis showing dysregulation at one or more time points after dosing.

- **The induction of the heat shock genes in brain and tibialis anterior was highly variable between samples of the same groups.**

QuantiGene analysis showed highly variable fold changes of expression within NVP-HSP990-treated groups. To investigate this further, RNA was extracted from QuantiGene homogenates, and the samples were re-analysed by RT-qPCR, which corroborated the variability observed by QuantiGene. This excluded the possibility of a technical issue in the QuantiGene methodology (Figure 5.10).

Next, to understand the exposure to NVP-HSP990 drug, the quadriceps femoris samples from all the vehicle and treated *Sirt1* tg x R6/2 mice were shipped to the IRBM institute (Pomezia, Italy) to measure the tissue concentrations of NVP-HSP990. This concentration (ng / g) was plotted against the fold changes in expression of *Hspa1a/b* measured in the tibialis anterior of *Sirt1* tg x R6/2 mice by QuantiGene (Figures 5.11 and 5.12). Interestingly, in some samples, even though a considerable amount of drug was present, the heat shock response had not been induced, as the *Hspa1a/b* expression levels were comparable to those in vehicle groups in both brain and muscle. The samples where no clear induction had occurred were excluded from the final analysis (as highlighted in Figures 5.11 and 5.12).

- **In contrast to the pilot data, *Sirt1* overexpression did not restore the heat shock response impairment in R6/2, neither in brain nor in tibialis anterior.**

Even though on a few occasions the overexpression of *Sirt1* did cause a very mild but significant increase in the expression of *Dnajb1*, *Hps90aa1*, *Hsp90ab1* in brain at 14 weeks of age by 10 hours after dosing (Figures 5.23, 5.31, 5.33), the potential results of the pilot experiment failed to transfer into the large-scale study. A very mild amelioration in the expression of *Hspa1a/b* could be observed in *Sirt1* tg::R6/2 brains as compared to R6/2 by 4 hours after dosing at 9 weeks of age, but this did not reach statistical significance (Figure 5.17).

There are several possible explanations as to why the *Sirt1* overexpression did not restore the heat shock response:

- The data in the pilot experiment may not be fully comparable to the data obtained in the large-scale study. The mice used in the pilot experiment were bred and housed in a different environment in another mouse facility which may have affected in the response to NVP-HSP990 treatment.
- As pointed out in previous Chapter 3 (Figure 3.5) and observed in the Figures 5.13 to 5.33 in this chapter, the heat shock genes showed different kinetics of induction, meaning that the maximal level of induction may have not been reached between 4 to 10 hours after treatment for some genes. It is possible that the *Sirt1* overexpression modified the kinetics of induction and could have a more significant effect on the impairment at a later time point post-dosing. This may be supported by the fact that, on the few occasions when a significant improvement on the expression was achieved by *Sirt1* overexpression, this occurred by 10 hours-post dosing.
- The study by Jiang *et al.* (2012) described an interaction between mutant HTT and SIRT1, which significantly affected SIRT1 deacetylase function and SIRT1 targets were hyperacetylated. It may be that the abundance of mutant HTT at symptomatic stages of the disease (at 9 and 14 weeks of age in R6/2 in the present study) could hinder SIRT1 deacetylase activity, and therefore *Sirt1*

overexpression may not be sufficient to restore SIRT1 activity and, by extension, the heat shock response in HD. Other factors controlling SIRT1 activity, such as AROS and DBC1, could be modulating the heat shock response as well (Raynes *et al.,* 2013), although their influence in the HD context is unknown. Also, in R6/2, as reported by Tulino *et al.* (2016), SIRT1 phosphorylation levels and therefore its activity, are altered by the presence of mutant HTT, and this could be a contributor of the diminished heat shock response in HD and may have influenced the results of the present study.

An investigation of the levels of acetylation of HSF1 in R6/2 mice (and other HD models) as well as an analysis of the interaction between SIRT1 and HTT may shed some light into the mechanism/s behind the impairment of the heat shock response in HD, which could have applications in other protein conformational disorders.

Chapter 6. Discussion

6.1 Summary of the thesis and main results

The heat shock response and its dysregulation has been a subject extensively investigated in HD and other protein conformational disorders. Diverse approaches to modulate the heat shock response, either by genetic manipulation of chaperones or pharmacologically via HSF1 activation, have been explored as potential strategies to enhance the protein folding capacity and prevent aggregation in these diseases.

In HD, the study by Labbadia *et al*. (2011) demonstrated the impairment of the heat shock response in two HD mouse models, R6/2 and *Hdh*Q150, after the *in vivo* administration of HSP90 inhibitor NVP-HSP990. The pulsed pharmacological induction of the heat shock response in these mice, via NVP-HSP990 treatment, resulted in a transient amelioration of some HD phenotypes and a decrease in mutant HTT aggregation, but the ability to elicit the heat shock response became impaired with disease progression. The capacity of HSF1 to dissociate from HSP90 repression, translocate to the nucleus and hyperphosphorylate were confirmed not to be compromised. An altered chromatin structure and accessibility to promoters due to reduced levels of acetylated histone H4 caused by mutant HTT presence were proposed as possible mechanisms underlying this impairment. Another recent study proposed an abnormal degradation of HSF1 as a potential cause for the dysregulation of the heat shock response, providing evidence of reduced levels of HSF1 in HD cellular models, post-mortem tissues from HD patients and zQ175 mice (Gomez-Pastor *et al*., 2017). However, an HD-related dysregulation of heat shock response was not demonstrated in zQ175 in that study.

In this thesis, two main research aims were pursued. First, a descriptive analysis of the heat shock response impairment in brain and muscle of zQ175, at 3, 12 and 20 months of age, covering the disease course in this model, after *in vivo* administration of the compound NVP-HSP990. A QuantiGene approach was taken to measure the transcriptional expression of a set of heat shock genes. This methodology for this was

optimised and validated through the design of several multiplex assays and by comparison with established RT-qPCR assays (Figure 3.4). The final and optimised QuantiGene 18-plex assay simultaneously detected the expression of regulators of the heat shock response, *Hsf1* and *Sirt1*, as well as of nine heat shock genes encoding chaperones belonging to different subfamilies, straight from mouse tissue lysates. An initial analysis in brain hemispheres of zQ175 mice at a symptomatic stage (12 months of age) corroborated the deficit in the heat shock response, consistent with that previously observed in R6/2 and *Hdh*Q150 (Labbadia *et al*., 2011; Figures 4.3 and 4.4). To further characterise the pattern of heat shock response impairment, the QuantiGene analyses were extended to tibialis anterior and cortical and striatal regions of zQ175 mice, collected at 3, 12 and 20 months of age, 4 hours after NVP-HSP990 treatment. The same dosing strategy and tissue collection was carried out with late symptomatic stage R6/2 mice, at 12 weeks of age, for a comparative analysis. A clear and comparable deficiency in the induction of the heat shock response was identified in the striatum and tibialis anterior of both models, with most of the heat shock genes dysregulated in zQ175 by 3 and 12 months of age, respectively per tissue (Figures 4.20-4.23). The impairment was not as evident in cortex, especially for zQ175, where only a few genes were affected (Figures 4.24, 4.25).

To understand whether a decrease in HSF1 availability could be responsible for this deficiency, HSF1 levels were measured in all tissues collected from zQ175 mice at late symptomatic stages (12 months of age in brain hemispheres and 20 months of age in tibialis anterior, striatum and cortex). No reduction of HSF1 was found, either in basal or activated levels, in any of these zQ175 tissues, as compared to wild-type counterparts, in contrast to what was reported (Gomez-Pastor *et al*., 2017) and in line with previous data in R6/2 and *Hdh*Q150 (Labbadia *et al*., 2011; Figure 4.28).

The second aim of this thesis focused on HSF1 regulation. Post-translational modifications of HSF1 significantly regulate the activation and attenuation of the heat shock response. One of the most significant modifications is the acetylation of the

residue Lys80 by EP300, which disrupts HSF1 binding to the promoters of heat shock genes (Raychaudhuri *et al*., 2014). This residue can be deacetylated by SIRT1 (Westerheide *et al*., 2009), which can subsequently prolong HSF1 binding to DNA and the transcriptional activation of heat shock genes. SIRT1 activity was previously found to be reduced in brains of R6/2 and *Hdh*Q150 mice (Tulino *et al*., 2016). To investigate whether the decrease in SIRT1 activity was causal to the heat shock response impairment observed in HD mice, an intercross between *Sirt1* overexpressing mice and R6/2 mice was carried out, to obtain the four genotypes of interest (Figure 5.3). These mice were dosed with NVP-HSP990 at 9 (early symptomatic) and 14 (late symptomatic) weeks of age, and brain hemispheres and muscle tissues were harvested at 4, 7 and 10 hours post-dosing (Tables 5.2, 5.3). The analysis by QuantiGene 18-plex assay indicated that *Sirt1* overexpression was not able to restore or significantly ameliorate the deficient heat shock response in brain or tibialis anterior of R6/2 mice at any age or time point (Figures 5.3 – 5.34), thus suggesting that other mechanism/s must be playing a role in this impairment.

6.2 Relevance of findings and considerations

- **Continuous induction of the heat shock response as a therapeutic strategy: the paradox of HSF1 activation in neurodegeneration and carcinogenesis**

Given that some beneficial effects have been detected in HD and polyglutamine models after pharmacological induction of the heat shock response (Sittler *et al*., 2001; Fujimoto *et al*., 2005; Fujikake *et al*., 2008), a sustained treatment with one of these inducers may be considered as a potential therapeutic strategy. However, this needs to be carefully addressed. This pharmacological induction mostly relies on the activation of HSF1, as shown in this thesis. Even though HSF1 has been mostly studied in its canonical role as master regulator of the heat shock response, other non-heat shock functions related to development, reproduction, metabolism or tumorigenesis have been described (Li *et al*., 2017; Xiao *et al*., 1999; Li *et al*., 2016; Scherz-Shouval *et al*., 2014).

The metabolic and energetic condition of the cell may promote or repress the activation of HSF1 as the heat shock response is regulated by cellular conditions and needs (Labbadia and Morimoto, 2015; Prahlad *et al*., 2008). For instance, under conditions of low energy or availability of amino acids, HSF1 becomes inactivated by factors like AMPK or mTORC1 through phosphorylation at residues Ser121 or Ser326, respectively (Chou *et al*., 2012; Dai *et al*., 2015).

The cellular proliferation demands of the organism, such as in the context of development or cancer, affect the activation and regulation of the heat shock response. Several regulators of HSF1 such as the E3 ubiquitin ligase FBXW7 (Kourtis *et al*., 2015) or kinases like MEK (of the MAPK signaling pathway) (Tang *et al*., 2015) are also implicated in the regulation of other factors involved in the cell cycle and cellular growth (Wang *et al*., 2012; Hilger *et al*., 2002; Guo *et al*., 2020).

During development, HSF1 is involved in the regulation of the meiotic cell cycle, but in a manner that is independent of the heat shock response, as demonstrated in nematodes and mammals (Le Masson *et al*., 2011; Li *et al*., 2016). The study by Li *et al*. (2016) showed that the transcription of common chaperones, involved in either the protein synthesis required for cell growth during development or prevention of protein misfolding during heat shock response, is induced by HSF1 but through binding to different heat shock elements in the promoters of the heat shock genes.

One of the main concerns for the continuous activation of HSF1 is the alleged oncogenic consequences, due to the potential of HSF1 as a facilitator of malignant transformation by enhancing protein synthesis and cell survival (Dai *et al*., 2007; Scherz-Shouval *et al*., 2014; Alasady and Mendillo, 2020). In this context, it has been reported that, in a range of cancers, the levels of heat shock proteins are elevated and HSF1 is constitutively activated, to support the uncontrolled proliferation and maintenance of cancerous cells (Santagata *et al*., 2011; Wu *et al*., 2017; Calderwood and Gong, 2016; Dai and Sampson, 2016). The pro-survival role of chaperones is beneficial under developmental conditions but can have negative consequences in carcinogenesis, when the cell death capacity of cancer cells is diminished and,

consequently, cells could have limitless proliferation (Wei *et al*., 1995). Accordingly, the inhibition of HSF1 and/or chaperones is considered a therapeutic strategy in cancer treatment to reduce the survival of cancer cells and their potential metastasis (Dai *et al*., 2007; Scherz-Shouval *et al*., 2014; Gong *et al*., 2015). A study by Mendillo *et al*. (2012) revealed that the profile of genomic transcriptional activation led by HSF1 and its occupancy of promoters in human cancer cells was found to be comparable to that detected during developmental stages in *C. elegans* (Li *et al*., 2016). And, similar to that occurring during development, this program was significantly distinct from the heat shock response induced under stress conditions, with many heat shock proteins being uniquely regulated (Mendillo *et al*., 2012). The regulatory mechanisms and cellular triggers underlying the preferential binding of HSF1 to specific promoters that drive each transcriptional activation program are not fully elucidated. Certain regulatory factors, as well as a cell, tissue and condition type-specific regulation might be behind this (Guisbert *et al*., 2013; Prahlad *et al*., 2008; Sala *et al*., 2017; Morimoto, 2020).

In brief, these studies suggest that HSF1 drives two separate transcriptional activation programs: one during stress and initiation of the heat shock response and another during cell growth and proliferation. It is unclear whether the elevated expressions of HSF1 and heat shock proteins in cancerous cells are a consequence of the increasing cell proliferation demands or if, by contrast, these aberrantly high levels of expression are causal to cancer pathogenesis. Nevertheless, as it is still largely unexplored in neurodegeneration and protein conformational disorders such as HD, an outstanding question is whether a continuously activated HSF1, to combat protein aggregation, may eventually re-engage in these other non-canonical, stress-independent transcriptional programs, and lead to oncogenic transformation (Arneaud and Douglas, 2016). Therefore, a cautiously designed genetic manipulation or treatment plan (if using a pharmacological approach), including a benefit/risk analysis would be of upmost importance.

- **A long-term treatment with HSP90 inhibitors may lead to unknown consequences in neurodegeneration**

In line with the previous section, the extended pharmacological induction of the heat shock response, particularly via HSP90 inhibition, as occurs with NVP-HSPP90, raises additional concerns as a treatment option in neurodegeneration.

As stated before, many heat shock proteins are upregulated in cancerous cells and are important in supporting oncogenesis and tumor formation. HSP90 is relevant in aspects of cancer development and maintenance, as some of its client proteins are critical factors in cell signaling pathways implicated in the malignant cellular growth and tissue invasion, as they become mutated or highly expressed. For instance, some of these HSP90 clients participate in the Raf/MEK/ERK signaling cascade (Taipale *et al*., 2012), which is key in allowing undiscriminated cell proliferation. Hence, HSP90 inhibition is an important therapeutic strategy to block oncogenic signaling pathways, as it facilitates the loss of function of HSP90 client proteins and their clearance by ubiquitin proteasome and autophagy systems (Trepel *et al*., 2010). Many inhibitors have been described, are in use as anticancer treatments and are generally well tolerated (Neckers *et al*., 2018; Serwetnyk and Blagg, 2021). However, the use of HSP90 inhibitors may lead to off target effects, such as the non-selective inhibition of other HSP90 isoforms or members of the ATPase family where HSP90 belongs and that share structural similarities (Neckers *et al*., 2018; Serwetnyk and Blagg, 2021).

HSP90 plays stabilising and functional roles in complex and diverse pathways, with several hundred client proteins, such as transcription factors, protein kinases, hormone receptors and other factors (Taipale *et al*., 2012). The downstream effects of HSP90 inhibition are beneficial for cancer therapeutics, as HSP90 client proteins would no longer support the undiscriminated cell proliferation and survival. However, a chronic HSP90 inhibition to treat neurodegeneration may have unforeseen consequences (Peterson and Blagg, 2009), which may include disruption of essential cellular signaling transduction or even potential compensatory mechanisms by other members of the proteostasis network, resulting in cytotoxicity.

- **Alternative approaches to induce the heat shock response**

The induction of the heat shock response via HSF1 activation is dependent on HSF1 trimerisation and, also, post-translational modifications on HSF1 domains that tightly regulate the response. For instance, the acetyltransferase EP300 acetylates HSF1 on several residues. Under absence of stress, the acetylation of Lys208 and Lys298 residues of HSF1 by EP300 stabilises HSF1 and its presence in a monomeric state. However, under stress conditions and during the heat shock response, the additional acetylation of residues Lys80 and Lys118 by EP300 not only attenuates the heat shock response but also enhances HSF1 degradation via the UPS system (Raychaudhuri *et al*., 2014). SIRT1 deacetylation of Lys80 reverses the reduced DNA binding and prolongs the heat shock response (Westerheide *et al*., 2009). Perhaps, the modulation/inhibition of EP300 in combination with SIRT1 activation or overexpression may be an interesting approach to investigate in HD.

Other alternative options to investigate, as suggested by Neef *et al*. (2011), could focus on compounds that target HSF1 directly rather than through the targeted inhibition of HSP90 that may lead to unwanted consequences. This could be by manipulating the post-translational modifications on HSF1 (either enhancing the activating post-translational modifications or inhibiting the repressive ones [Rimoldi *et al*., 2001]), or by binding to HSF1 and disrupting its interaction with HSP90 without inhibiting HSP90 (e.g., targeting co-chaperones of HSP90). To that end, further investigation of the specific interaction sites between HSF1 and HSP90 (Kijima *et al*., 2018) as well as the enzymes and pathways responsible for the post-translational modifications on HSF1 would be needed. Additionally, as the interaction between HSF1 and HSP90 is believed to be weak (Zou *et al*., 1998), another option would be the use of compounds that may disrupt the inhibitory complex between HSP70 and HSF1 (Shi *et al*., 1998).

The transcriptional activation of heat shock genes is a complex and multifactor process. It is mainly mediated by HSF1, although some studies have also indicated

the participation of other transcription factors (Mendillo *et al*., 2012; Sasi *et al*., 2014).

- **SIRT1 overexpression was not sufficient to restore the heat shock response impairment in R6/2 mice: other potential regulatory mechanisms that may be involved**

SIRT1 ability to deacetylate HSF1 in specific residues affects its binding to heat shock gene promoters (Westerheide *et al*., 2009) and makes it an interest target to investigate in the amelioration of the heat shock response impairment in protein conformational diseases. The important role of SIRT1 in HSF1 stabilisation and function was highlighted, for instance, in a study by Kim *et al*. (2016), where the application of SIRT1 inhibitors in cell culture caused an increased acetylation and degradation of HSF1 by ubiquitination.

The collapse of proteostasis with aging (Hipp *et al*., 2019; Ben-Zvi *et al*., 2009), correlated with a diminished SIRT1 activity (Tulino *et al*., 2016), may help to explain the deficit in the heat shock response that is observed in HD mouse models (Dues *et al*., 2016). The expression of mutant HTT may exacerbate cellular aging (Horvath *et al*., 2016; Gasset-Rosa *et al*., 2017) or conversely, the age-related decline of proteostasis mechanisms may lead to an increased cell vulnerability and the aggregation of mutant HTT (Diguet *et al*., 2009). Previous studies from our group did not observe an impairment in the induction of the heat shock response in older wild-type mice but did detect an age-related reduction of chaperones, HSF1 and SIRT1, although only in cardiac tissues (Carnemolla *et al*., 2014).

The reduced SIRT1 activity observed in HD mice was attributed to dysregulated phosphorylation levels by the metabolic sensor AMPK-α1, a known regulator of SIRT1 (Lau *et al*., 2014), which had an abnormal expression and subcellular distribution. AMPK has also been linked to the repression of HSF1, mediating its phosphorylation on residue Ser121 to inhibit its nuclear translocation (Dai *et al*., 2015; Su *et al*., 2019). Measuring the acetylation levels of HSF1 in the four genotypes of *Sirt1* tg x R6/2 mice

could indicate whether SIRT1 activity had been restored in HD mice and whether it was effective in deacetylating HSF1.

In addition to this, Gomez-Pastor *et al*. (2017) proposed that the increases in CK2α' (a catalytic subunit of CK2 kinase) and FBXW7 caused by the presence of mutant HTT were behind an abnormal degradation of HSF1. However, the evidence gathered in this thesis, regarding HSF1 expression at late stages of the disease in HD mouse models, does not support that proposal (Figures 4.31, 4.32). It is feasible, though, that the indicated regulatory mechanism of HSF1 is dysregulated in HD, not necessarily causing an increased HSF1 degradation, but rather affecting its post-translational modifications and activity. Interestingly, CK2 also regulates SIRT1 and affects its deacetylating activity (Choi *et al*., 2017).

It may then be speculated that the presence of mutant HTT severely induces the dysregulation of some important factors of metabolic stress and cell viability such as AMPK, CK2 or FBXW7, which may lead to a deficit or suppression of HSF1 activity, subsequently affecting the activation/maintenance of the heat shock response, in an interplay mechanism including SIRT1. The investigation and modulation of factors that regulate both HSF1 and SIRT1 could be a strategy to explore.

Thus, it could be concluded that the investigation of other molecular components that regulate HSF1 function at different levels along its activation and inactivation/degradation, as well as other HSF1 targets (aside from the heat shock proteins) may be an interesting avenue to examine in the field of neurodegeneration.

6.3 Study limitations and potential approaches

- **Interpreting the heat shock response impairment and induction characteristics**

Some limitations may have played a role when interpreting the characteristics of the heat shock response induction and, therefore, its impairment in mouse tissues. For instance, a potential difference in the kinetics of induction for each heat shock gene

(Diller, 2006). It is conceivable that the maximal induction of each heat shock gene is achieved in a time-dependent manner after initiation of the heat shock response. As the analysis was conducted on tissues collected at 4 hours (in zQ175) and up to 10 hours (in *Sirt1* tg x R6/2) after NVP-HSP990 administration, it is possible that the highest transcriptional activation had not been reached for some of the genes and, therefore, some differences between genotypes might not have been detected. Choosing appropriate time points after dosing for tissue collection, when the induced expression of all the heat shock genes of interest is at the highest levels, is challenging. In this thesis, the levels of induced expression of three major heat shock genes (*Hspa1a/b*, *Hspb1* and *Dnajb1*) were measured in brains of wild-type mice after treatment with NVP-HSP990. The maximal induction of *Hspa1a/b* was reached at 4 hours post-dosing, after which it progressively declined to basal levels; for *Hspb1* and *Dnajb1*, this maximal induction was still seen at 8 hours after dosing. By 12 hours post-dosing, the expression levels of all three genes had returned to baseline levels (Figure 3.5). A similar kinetic study was conducted by Neueder *et al*. (2017), who showed that the heat stress-induced heat shock response in wild-type mice led to the upregulation of these same heat shock genes in quadriceps femoris muscle, with a maximal induction at 4 hours after the heat treatment and clear return to baseline levels by 8 hours (Neueder *et al*., 2017).

Neueder and colleagues, by transcriptomic and gene ontology enrichment analyses, also found that there were some discrepancies in the set of upregulated genes after induction of the heat shock response when using different inducers. When using a heat stress treatment, the upregulated genes were associated with energy metabolism and response to oxidative stress; when using NVP-HSP990 to inhibit HSP90, the upregulated genes were related to biological processes of focal adhesion, extracellular matrix organization or angiogenesis (Neueder *et al*., 2017). Therefore, these discrepancies in transcriptional activation may need to be taken into account when drawing conclusions.

Finally, the contribution of a differential pattern of expression of the heat shock proteins in each tissue, related to a cell type and tissue-specific regulations should also be taken into consideration (Guisbert *et al*., 2013; Morimoto, 2020).

- **NVP-HSP990 treatment and *in vivo* limitations**

Highly variable data was observed in the NVP-HSP990- induced expression of the heat shock genes in animals from the same treatment group. This was particularly evident in the *Sirt1* tg x R6/2 cohorts of mice. Because of this, a comparison was made between the results obtained by QuantiGene and RT-qPCR, which were found to be highly comparable (Figure 5.10). Additionally, a pharmacokinetic analysis was performed externally, at the IRBM institute, which corroborated the individual exposure to the NVP-HSP990 drug in many subjects (Figures 5.11 and 5.12) and allowed the exclusion of samples where a clear induction had not happened. These variabilities could be due to a differential biodistribution of the compound in each animal (related to age, weight or other intrinsic metabolic characteristics). Alternatively, it may be associated with a minimal threshold of drug concentration that is required for an effective HSP90 inhibition to take place, determined by other unknown factors.

Some limitations may have also been related to the use of R6/2 as a model for the *Sirt1* overexpression screening. The HD phenotype is pronounced and progresses very quickly in R6/2 mice, and possibly the effects of mutant HTT on the protein homeostasis mechanisms may be too deleterious in this model and not possible to be overcome or ameliorated only by SIRT1 overexpression. Perhaps the SIRT1 overexpression in other HD model with a slower rate of disease progression such as zQ175 may have provided a different outcome; however, it would have required breeding and maintenance of that mouse colony for a longer period to cover different stages of the disease.

6.4 Conclusions and future perspectives

Some concluding remarks may be made from the work presented in this thesis, with potential future applications:

- **Impairment of the heat shock response in HD and other diseases**

The disruption of the proteostasis machineries, including the heat shock response, is a feature of HD that is shared with other neurodegenerative disorders such as Alzheimer's disease (AD) (Bruni *et al*., 2020), Parkinson's disease (PD) (Aridon *et al*., 2011) or amyotrophic lateral sclerosis (ALS) (Chen *et al*., 2016; Kalmar and Greensmith, 2017). Experimental approaches focused on enhancing the clearance of their toxic aggregated proteins are an ongoing strategy to slow down the disease progression (Boland *et al*., 2018), with beneficial results in several disease models (Chen *et al*., 2013; Auluck *et al*., 2005, Putcha *et al*., 2010; Novoselov *et al*., 2013; Kalmar *et al*., 2008).

- **Usefulness of the QuantiGene plex assays to measure the induction of the heat shock response**

The development and optimisation of a QuantiGene multiplex assay to detect the expression of a large set of heat shock genes has proven to be useful in the characterisation of the heat shock response in HD mouse models, to measure both the basal and induced expression of these genes after pharmacological induction of the response. This QuantiGene assay may be a valuable tool to evaluate the effectiveness of other treatments and experimental approaches aimed to restore the heat shock response or study aspects of proteostasis, not only in HD but in other protein conformational disorders featuring a presence of aggregates, such as AD, PD or ALS.

- **The possibility of treatments involving the induction of the heat shock response in the human disease**

Evidence of dysregulated proteostasis and clearance of mutant HTT has been reported in the human disease, in post-mortem tissues or cells derived from HD patients (Bennet *et al*., 2007; Martinez-Vicente *et al*., 2010).

The long-term application of treatments targeting the heat shock response may not be an ideal therapeutic strategy for the reasons previously discussed. Perhaps, a short-term or pulsed treatment in combination with other UPS and autophagy inducers may be successful in the prevention of misfolding and degradation of the already aggregated forms. These approaches may also be considered as a preventative therapeutic intervention to reduce smaller, oligomeric species at early or pre-symptomatic stages of the disease, before the formation of inclusions.

In conclusion, the maintenance of protein homeostasis is complex and critical in cellular physiology and health, as its disruption is a feature in many protein conformational diseases. A deep understanding of the mechanisms and regulators governing this disruption is essential, to apply this knowledge in the development of refined therapeutic strategies. The work contained in this thesis may shed some light on these dysregulated mechanisms and address some valuable points, which may hopefully be useful in elucidating novel ways to cope with proteotoxicity.

Appendix

Full-length blots from Figures in Chapter 4, corresponding to Figures 4.31 and 4.32 (from next page).

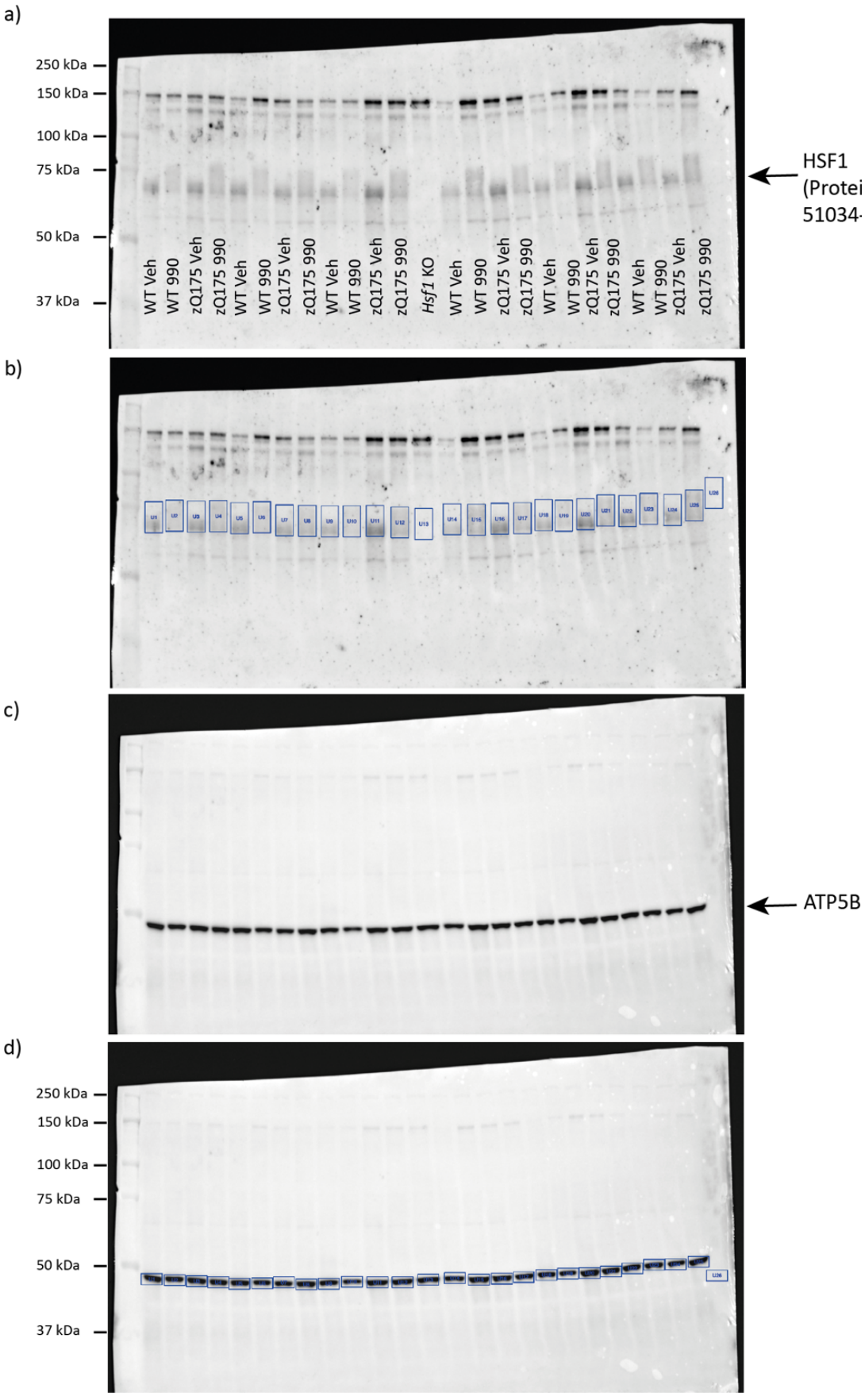
a)
250 kDa
150 kDa
100 kDa
75 kDa
50 kDa
37 kDa
WT Veh
WT 990
zQ175 Veh
zQ175 990
WT Veh
WT 990
zQ175 Veh
zQ175 990
WT Veh
WT 990
zQ175 Veh
zQ175 990
Hsf1 KO
WT Veh
WT 990
zQ175 Veh
zQ175 990
WT Veh
WT 990
zQ175 Veh
zQ175 990
WT Veh
WT 990
zQ175 Veh
zQ175 990
HSF1
(Protei
51034
b)
c)
ATP5B
d)
250 kDa
150 kDa
100 kDa
75 kDa
50 kDa
37 kDa

Appendix Figure 1. Full-length western blots of HSF1 in brain hemispheres of zQ175 and wild-type mice at 12 months of age.

Ful-length western blots brain hemispheres of zQ175 and wild-type mice at 12 months of age, corresponding to Figure 4.31; (a) immunoprobed with HSF1 Proteintech 51034-1-AP antibody, (b) areas that were used for the quantification from the HSF1 antibody probed blot, (c) immunoprobed with ATP5B antibody and (d) areas selected for the quantification from the ATP5B antibody probed blot. Veh = vehicle; 990 = NVP-HSP990; WT = wild-type.

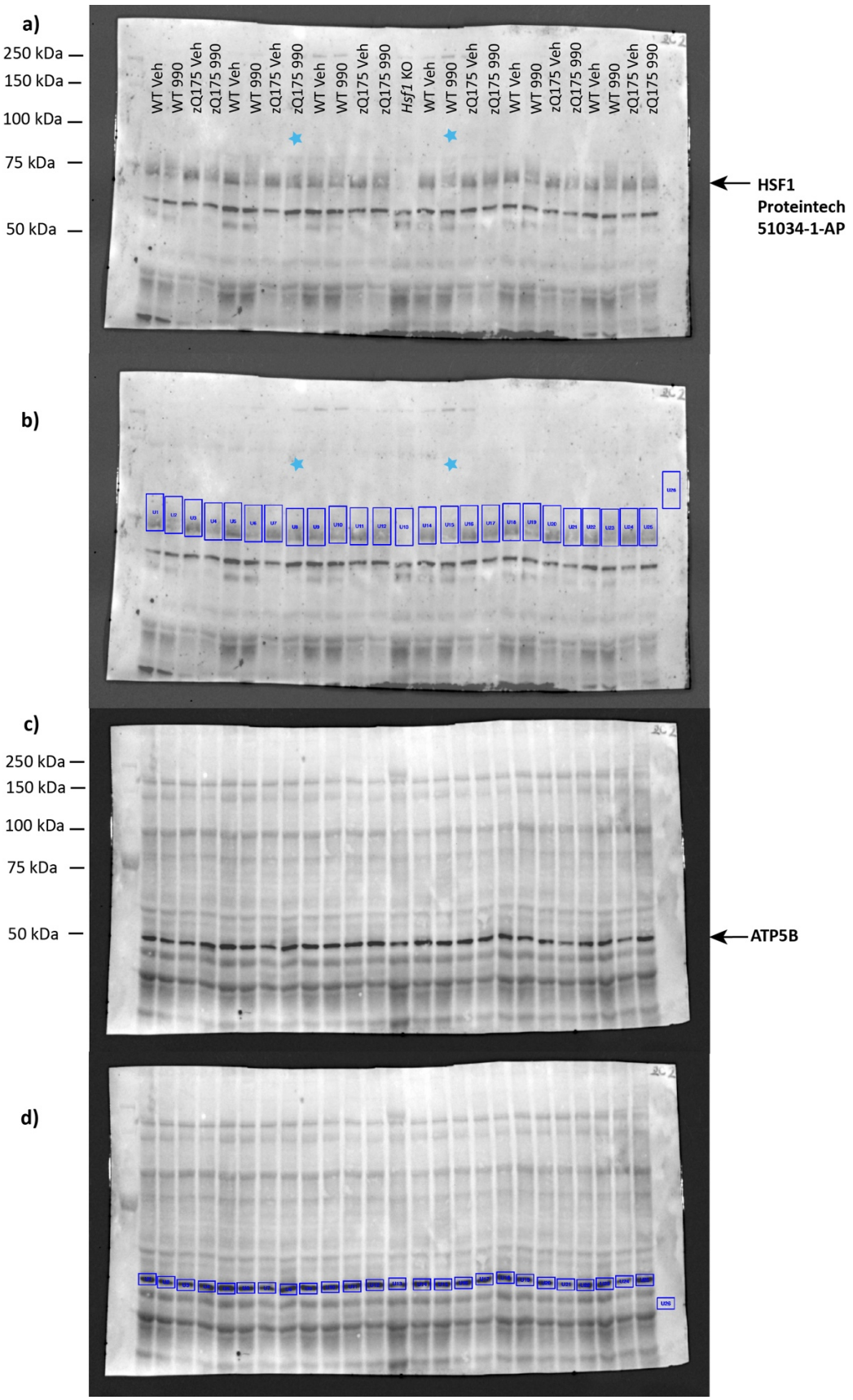
a)
250 kDa
150 kDa
100 kDa
75 kDa
50 kDa
WT Veh
WT 990
zQ175 Veh
zQ175 990
WT Veh
WT 990
zQ175 Veh
zQ175 990
WT Veh
WT 990
zQ175 Veh
zQ175 990
Hsf1 KO
WT Veh
WT 990
zQ175 Veh
zQ175 990
WT Veh
WT 990
zQ175 Veh
zQ175 990
WT Veh
WT 990
zQ175 Veh
zQ175 990
HSF1
Proteintech
51034-1-AP
b)
c)
250 kDa
150 kDa
100 kDa
75 kDa
50 kDa
ATP5B
d)

Appendix Figure 2. Full-length western blots of HSF1 in tibialis anterior of zQ175 and wild-type mice at 20 months of age.

Full-length western blot in tibialis anterior of zQ175 and wild-type mice at 20 months of age, corresponding to Figure 4.32, (a) immunoprobed with HSF1 Proteintech 51034-1-AP antibody, (b) the areas that were used in the quantification, from the HSF1 antibody probed blot; (c) immunoprobed with ATP5B antibody, and (d) areas selected for quantification, from the ATP5B antibody probed blot. The blue stars refer to samples that were excluded from the quantification because of poor induction of the heat shock response (indicated in section 4.4.4). Veh = vehicle; 990 = NVP-HSP990; WT = wild-type.

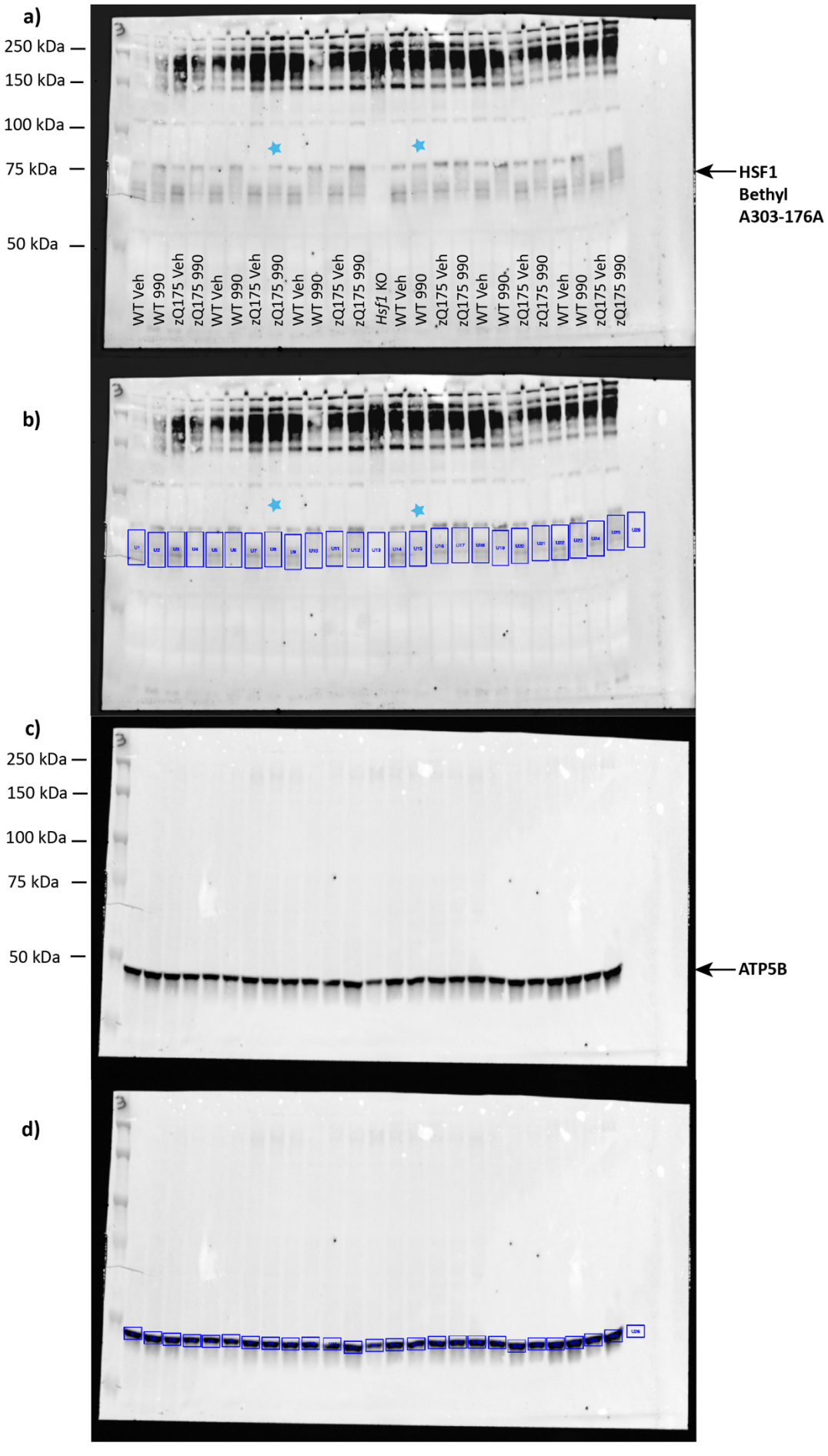
a)
250 kDa
150 kDa
100 kDa
75 kDa
50 kDa
WT Veh
WT 990
zQ175 Veh
zQ175 990
WT Veh
WT 990
zQ175 Veh
zQ175 990
WT Veh
WT 990
zQ175 Veh
zQ175 990
Hsf1 KO
WT Veh
WT 990
zQ175 Veh
zQ175 990
WT Veh
WT 990
zQ175 Veh
zQ175 990
WT Veh
WT 990
zQ175 Veh
zQ175 990
HSF1
Bethyl
A303-176A
b)
c)
250 kDa
150 kDa
100 kDa
75 kDa
50 kDa
ATP5B
d)

Appendix Figure 3. Full-length western blots of HSF1 in striatum of zQ175 and wild-type mice at 20 months of age.

Full-length western blot in striatum of zQ175 and wild-type mice at 20 months of age, corresponding to Figure 4.32, (a) immunoprobed with HSF1 Bethyl A303-176A antibody, (b) the areas that were used in the quantification, from the HSF1 antibody probed blot; (c) immunoprobed with ATP5B antibody, and (d) areas selected for quantification, from the ATP5B antibody probed blot. The blue stars refer to samples that were excluded from the quantification because of poor induction of the heat shock response (indicated in section 4.4.4). Veh = vehicle; 990 = NVP-HSP990; WT = wild-type.

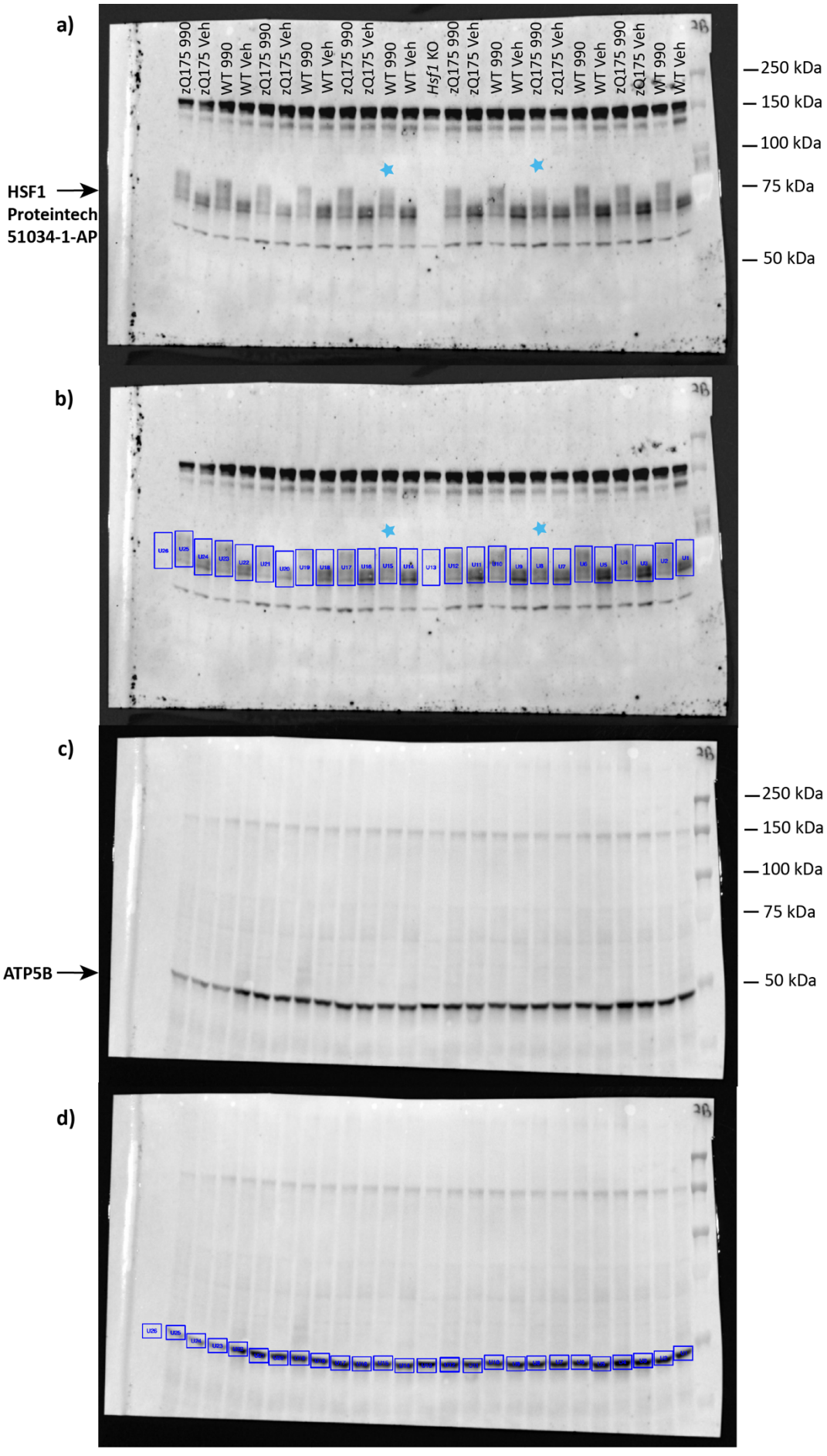
a)
zQ175 990
zQ175 Veh
WT 990
WT Veh
zQ175 990
zQ175 Veh
WT 990
WT Veh
zQ175 990
zQ175 Veh
WT 990
WT Veh
Hsf1 KO
zQ175 990
zQ175 Veh
WT 990
WT Veh
zQ175 990
zQ175 Veh
WT 990
WT Veh
zQ175 990
zQ175 Veh
WT 990
WT Veh
250 kDa
150 kDa
100 kDa
75 kDa
50 kDa
HSF1
Proteintech
51034-1-AP
b)
c)
250 kDa
150 kDa
100 kDa
75 kDa
50 kDa
ATP5B
d)

Appendix Figure 4. Full-length western blots of HSF1 in cortex of zQ175 and wild-type mice at 20 months of age.

Full-length western blot in cortex of zQ175 and wild-type mice at 20 months of age, corresponding to Figure 4.32, (a) immunoprobed with HSF1 Proteintech 51034-1-AP antibody, (b) the areas that were used in the quantification, from the HSF1 antibody probed blot; (c) immunoprobed with ATP5B antibody, and (d) areas selected for quantification, from the ATP5B antibody probed blot. The blue stars refer to samples that were excluded from the quantification because of poor induction of the heat shock response (indicated in section 4.4.4). Veh = vehicle; 990 = NVP-HSP990; WT = wild-type.

References

Abravaya, K., Myers, M. P., Murphy, S. P., & Morimoto, R. I. (1992). The human heat shock protein hsp70 interacts with HSF, the transcription factor that regulates heat shock gene expression. *Genes and Development*, *6*(7), 1153–1164. https://doi.org/10.1101/gad.6.7.1153

Ahn, S. G., Liu, P. C. C., Klyachko, K., Morimoto, R. I., & Thiele, D. J. (2001). The loop domain of heat shock transcription factor 1 dictates DNA-binding specificity and responses to heat stress. *Genes and Development*, *15*(16), 2134–2145. https://doi.org/10.1101/gad.894801

Ajami, M., Pazoki-Toroudi, H., Amani, H., Nabavi, S. F., Braidy, N., Vacca, R. A., … Nabavi, S. M. (2017). Therapeutic role of sirtuins in neurodegenerative disease and their modulation by polyphenols. *Neuroscience and Biobehavioral Reviews*, *73*, 39–47. https://doi.org/10.1016/j.neubiorev.2016.11.022

Åkerfelt, M., Morimoto, R. I., & Sistonen, L. (2010). Heat shock factors: Integrators of cell stress, development and lifespan. *Nature Reviews Molecular Cell Biology*, *11*(8), 545–555. https://doi.org/10.1038/nrm2938

Alasady, M. J., & Mendillo, M. L. (2020). The multifaceted role of HSF1 in tumorigenesis. *Advances in Experimental Medicine and Biology*, *1243*, 69–85. https://doi.org/10.1007/978-3-030-40204-4_5

Albani, D., Polito, L., Signorini, A., & Forloni, G. (2010). Neuroprotective properties of resveratrol in different neurodegenerative disorders. *BioFactors*, *36*(5), 370–376. https://doi.org/10.1002/biof.118

Amici, C., Sistonen, L., Santoro, M. G., & Morimoto, R. I. (1992). Antiproliferative prostaglandins activate heat shock transcription factor. *PNAS*, *89*(14), 6227–6231. https://doi.org/10.1073/pnas.89.14.6227

Anckar, J., & Sistonen, L. (2011). Regulation of HSF1 function in the heat stress response: implications in aging and disease. *Annual Review of Biochemistry*, *80*(1), 1089–1115. https://doi.org/10.1146/annurev-biochem-060809-095203

Arbez, N., Ratovitski, T., Roby, E., Chighladze, E., Stewart, J. C., Ren, M., … Ross, C. A. (2017). Post-translational modifications clustering within proteolytic domains decrease mutant huntingtin toxicity. *Journal of Biological Chemistry*, *292*(47), 19238–19254. https://doi.org/10.1074/jbc.M117.782300

Ardan, T., Baxa, M., Levinská, B., Sedlácková, M., Nguyen, T. D., Klíma, J., … Ellederová, Z. (2020). Transgenic minipig model of Huntington's disease exhibiting gradually progressing neurodegeneration. *DMM Disease Models and Mechanisms*, *13*(2), 1–12. https://doi.org/10.1242/dmm.041319

Aridon, P., Geraci, F., Turturici, G., D'amelio, M., Savettieri, G., & Sconzo, G. (2011). Protective role of heat shock proteins in Parkinson's disease. *Neurodegenerative Diseases*, *8*(4), 155–168. https://doi.org/10.1159/000321548

Arneaud, S. L. B., & Douglas, P. M. (2016). The stress response paradox: fighting degeneration at the cost of cancer. *FEBS Journal*, *283*(22), 4047–4055. https://doi.org/10.1111/febs.13764

Aron Badin, R. (2018). Nonhuman primate models of Huntington's disease and their application in translational research. In S. V. Precious, A. E. Rosser, & S. B. Dunnett (Eds.), *Huntington's Disease. Methods in Molecular Biology.* (Vol. 1780, pp. 267–284). Springer Nature. https://doi.org/10.1007/978-1-4939-7825-0_14

Aronin, N., Chase, K., Young, C., Sapp, E., Schwarz, C., Matta, N., … DiFiglia, M. (1995). CAG expansion affects the expression of mutant huntingtin in the Huntington's disease brain. *Neuron*, *15*(5), 1193–1201. https://doi.org/10.1016/0896-6273(95)90106-X

Arrasate, M., & Finkbeiner, S. (2012). Protein aggregates in Huntington's disease. *Experimental Neurology*, *238*(1), 1–11. https://doi.org/10.1016/j.expneurol.2011.12.013

Arrasate, M., Mitra, S., Schweitzer, E. S., Segal, M. R., & Finkbeiner, S. (2004). Inclusion body formation reduces levels of mutant huntingtin and the risk of neuronal death. *Nature*, *431*(7010), 805–810. https://doi.org/10.1038/nature02998

Auluck, P. K., Meulener, M. C., & Bonini, N. M. (2005). Mechanisms of suppression of α-synuclein neurotoxicity by geldanamycin in *Drosophila*. *Journal of Biological Chemistry*, *280*(4), 2873–2878. https://doi.org/10.1074/jbc.M412106200

Baldo, B., Weiss, A., Parker, C. N., Bibel, M., Paganetti, P., & Kaupmann, K. (2012). A screen for enhancers of clearance identifies huntingtin as a heat shock protein 90 (Hsp90) client protein. *Journal of Biological Chemistry*, *287*(2), 1406–1414. https://doi.org/10.1074/jbc.M111.294801

Baler, R., Dahl, G., & Voellmy, R. (1993). Activation of human heat shock genes is accompanied by oligomerization, modification, and rapid translocation of heat shock transcription factor HSF1. *Molecular and Cellular Biology*, *13*(4), 2486–2496. https://doi.org/10.1128/mcb.13.4.2486

Baler, R., Welch, W. J., & Voellmy, R. (1992). Heat shock gene regulation by nascent polypeptides and denatured proteins: hsp70 as a potential autoregulatory factor. *Journal of Cell Biology*, *117*(6), 1151–1159. https://doi.org/10.1083/jcb.117.6.1151

Bao, X., Wang, Y., Li, X., Li, X. M., Liu, Z., Yang, T., … Li, X. D. avi. (2014). Identification of "erasers" for lysine crotonylated histone marks using a chemical proteomics approach. *ELife*, *3*, 1–18. https://doi.org/10.7554/eLife.02999

Barker, R. A., Fujimaki, M., Rogers, P., & Rubinsztein, D. C. (2020). Huntingtin-lowering strategies for Huntington's disease. *Expert Opinion on Investigational Drugs*, *29*(10), 1125–1132. https://doi.org/10.1080/13543784.2020.1804552

Bates, G. (2003). Huntingtin aggregation and toxicity in Huntington's disease. *Lancet*, *361*(9369), 1642–1644. https://doi.org/10.1016/S0140-6736(03)13304-1

Bates, G. P., Dorsey, R., Gusella, J. F., Hayden, M. R., Kay, C., Leavitt, B. R., … Tabrizi, S. J. (2015). Huntington Disease. *Nature Reviews Disease Primers*, *1*. https://doi.org/https://doi:10.1038/nrdp.2015.5

Baxa, M., Hruska-Plochan, M., Juhas, S., Vodicka, P., Pavlok, A., Juhasova, J., … Motlik, J. (2013). A transgenic minipig model of huntington's disease. *Journal of Huntington's Disease*, *2*(1), 47–68. https://doi.org/10.3233/JHD-130001

Baxa, M., Levinska, B., Skrivankova, M., Pokorny, M., Juhasova, J., Klima, J., … Ellederova, Z. (2020). Longitudinal study revealing motor, cognitive and behavioral decline in a transgenic minipig model of Huntington's disease. *DMM Disease Models and Mechanisms*, *13*(2). https://doi.org/10.1242/dmm.041293

Bayram-Weston, Z., Jones, L., Dunnett, S. B., & Brooks, S. P. (2012). Light and electron microscopic characterization of the evolution of cellular pathology in YAC128 Huntington's disease transgenic mice. *Brain Research Bulletin*, *88*(2–3), 137–147. https://doi.org/10.1016/j.brainresbull.2011.05.005

Bayram-Weston, Z., Torres, E. M., Jones, L., Dunnett, S. B., & Brooks, S. P. (2012). Light and electron microscopic characterization of the evolution of cellular pathology in the *Hdh* (CAG)150 Huntington's disease knock-in mouse. *Brain Research Bulletin*, *88*(2–3), 189–198. https://doi.org/10.1016/j.brainresbull.2011.03.014

Ben-Zvi, A., Miller, E. A., & Morimoto, R. I. (2009). Collapse of proteostasis represents an early molecular event in *Caenorhabditis elegans* aging. *PNAS*, *106*(35), 14914–14919. https://doi.org/10.1017/S0022050700031454

Benn, C. L., Fox, H., & Bates, G. P. (2008). Optimisation of region-specific reference gene selection and relative gene expression analysis methods for pre-clinical trials of Huntington's disease. *Molecular Neurodegeneration*, *17*(3), 1–17. https://doi.org/10.1186/1750-1326-3-17

Bennett Frank, C., Krainer, A. R., & Cleveland, D. W. (2019). Antisense Oligonucleotide Therapies for Neurodegenerative Diseases. *Annual Review of Neuroscience*, *42*, 385–406. https://doi.org/10.1146/annurev-neuro-070918-050501

Bennett, E. J., Shaler, T. A., Woodman, B., Ryu, K. Y., Zaitseva, T. S., Becker, C. H., … Kopito, R. R. (2007). Global changes to the ubiquitin system in Huntington's disease. *Nature*, *448*(7154), 704–708. https://doi.org/10.1038/nature06022

Berger, Z., Ravikumar, B., Menzies, F. M., Oroz, L. G., Underwood, B. R., Pangalos, M. N., … Rubinsztein, D. C. (2006). Rapamycin alleviates toxicity of different aggregate-prone proteins. *Human Molecular Genetics*, *15*(3), 433–442. https://doi.org/10.1093/hmg/ddi458

Bersuker, K., Hipp, M. S., Calamini, B., Morimoto, R. I., & Kopito, R. R. (2013). Heat shock response activation exacerbates inclusion body formation in a cellular model of Huntington disease. *Journal of Biological Chemistry*, *288*(33), 23633–23638. https://doi.org/10.1074/jbc.C113.481945

Betsinger, C. N., & Cristea, I. M. (2019). Mitochondrial function, metabolic regulation, and human disease viewed through the prism of sirtuin 4 (SIRT4) functions. *Journal of Proteome Research*, *176*(12), 139–148. https://doi.org/10.1021/acs.jproteome.9b00086.

Bettencourt, C., Hensman-Moss, D., Flower, M., Wiethoff, S., Brice, A., Goizet, C., … Jones, L. (2016). DNA repair pathways underlie a common genetic mechanism modulating onset in polyglutamine diseases. *Annals of Neurology*, *79*(6), 983–990. https://doi.org/10.1002/ana.24656

Bianchi, M., Crinelli, R., Arbore, V., & Magnani, M. (2018). Induction of *ubiquitin C (UBC)* gene transcription is mediated by HSF1: role of proteotoxic and oxidative stress. *FEBS Open Bio*, *8*(9), 1471–1485. https://doi.org/10.1002/2211-5463.12484

Biebl, M. M., & Buchner, J. (2019). Structure, function, and regulation of the Hsp90 machinery. *Cold Spring Harbor Perspectives in Biology*, *11*(9). https://doi.org/10.1101/cshperspect.a034017

Bitterman, K. J., Anderson, R. M., Cohen, H. Y., Latorre-Esteves, M., & Sinclair, D. A. (2002). Inhibition of silencing and accelerated aging by nicotinamide, a putative negative regulator of yeast Sir2 and human SIRT1. *Journal of Biological Chemistry*, *277*(47), 45099–45107. https://doi.org/10.1074/jbc.M205670200

Bjørkøy, G., Lamark, T., Brech, A., Outzen, H., Perander, M., Øvervatn, A., … Johansen, T. (2005). p62/SQSTM1 forms protein aggregates degraded by autophagy and has a protective effect on huntingtin-induced cell death. *Journal of Cell Biology*, *171*(4), 603–614. https://doi.org/10.1083/jcb.200507002

Blank, M. F., & Grummt, I. (2017). The seven faces of SIRT7. *Transcription*, *8*(2), 67–74. https://doi.org/10.1080/21541264.2016.1276658

Boland, B., Yu, W. H., Corti, O., Mollereau, B., Henriques, A., Bezard, E., … Millan, M. J. (2018). Promoting the clearance of neurotoxic proteins in neurodegenerative disorders of ageing. *Nature Reviews Drug Discovery*, *17*(9), 660–688. https://doi.org/10.1038/nrd.2018.109

Bordone, L., Cohen, D., Robinson, A., Motta, M. C., Van Veen, E., Czopik, A., … Guarente, L. (2007). SIRT1 transgenic mice show phenotypes resembling calorie restriction. *Aging Cell*, *6*(6), 759–767. https://doi.org/10.1111/j.1474-9726.2007.00335.x

Bose, S., & Cho, J. (2017). Targeting chaperones, heat shock factor-1, and unfolded protein response: Promising therapeutic approaches for neurodegenerative

disorders. *Ageing Research Reviews*, *35*, 155–175. https://doi.org/10.1016/j.arr.2016.09.004

Bracher, A., & Verghese, J. (2015). The nucleotide exchange factors of Hsp70 molecular chaperones. *Frontiers in Molecular Biosciences*, *2*(APR), 1–9. https://doi.org/10.3389/fmolb.2015.00010

Brooks, S. P., Janghra, N., Higgs, G. V., Bayram-Weston, Z., Heuer, A., Jones, L., & Dunnett, S. B. (2012). Selective cognitive impairment in the YAC128 Huntington's disease mouse. *Brain Research Bulletin*, *88*(2–3), 121–129. https://doi.org/10.1016/j.brainresbull.2011.05.010

Brunet, A., Sweeney, L. B., Sturgill, J. F., Chua, K. F., Greer, P. L., Lin, Y., … Greenberg, M. E. (2004). Stress-dependent regulation of FOXO transcription factors by the SIRT1 deacetylase. *Science*, *303*(5666), 2011–2015. https://doi.org/10.1126/science.1094637

Bruni, A. C., Bernardi, L., & Gabelli, C. (2020). From beta amyloid to altered proteostasis in Alzheimer's disease. *Ageing Research Reviews*, *64*(May), 101126. https://doi.org/10.1016/j.arr.2020.101126

Bukau, B., & Horwich, A. L. (1998). The Hsp70 and Hsp60 chaperone machines. *Cell*, *92*(3), 351–366. https://doi.org/10.1016/S0092-8674(00)80928-9

Bustin, S. A. (2002). Quantification of mRNA using real-time reverse transcription PCR (RT-PCR): Trends and problems. *Journal of Molecular Endocrinology*, *29*(1), 23–39. https://doi.org/10.1677/jme.0.0290023

Butler, R., & Bates, G. P. (2006). Histone deacetylase inhibitors as therapeutics for polyglutamine disorders. *Nature Reviews Neuroscience*, *7*(10), 784–796. https://doi.org/10.1038/nrn1989

Byrne, L. M., Rodrigues, F. B., Blennow, K., Durr, A., Leavitt, B. R., Roos, R. A. C., … Wild, E. J. (2017). Neurofilament light protein in blood as a potential biomarker

of neurodegeneration in Huntington's disease: a retrospective cohort analysis. *The Lancet Neurology*, *16*(8), 601–609. https://doi.org/10.1016/S1474-4422(17)30124-2

Byrne, L. M., Rodrigues, F. B., Johnson, E. B., Wijeratne, P. A., De Vita, E., Alexander, D. C., … Wild, E. J. (2018). Evaluation of mutant huntingtin and neurofilament proteins as potential markers in Huntington's disease. *Science Translational Medicine*, *10*(458). https://doi.org/10.1126/scitranslmed.aat7108

Calamini, B., & Morimoto, R. I. (2012). Protein homeostasis as a therapeutic target for diseases of protein conformation. *Current Topics in Medicinal Chemistry*, *12*(22), 2623–2640. https://doi.org/10.2174/1568026611212220014

Calamini, B., Silva, M. C., Madoux, F., Hutt, D. M., Khanna, S., Chalfant, M. A., … Morimoto, R. I. (2012). Small-molecule proteostasis regulators for protein conformational diseases. *Nature Chemical Biology*, *8*(2), 185–196. https://doi.org/10.1038/nchembio.763

Calderwood, S. K., & Gong, J. (2016). Heat shock [roteins promote cancer: it's a protection racket. *Trends in Biochemical Sciences*, *41*(4), 311–323. https://doi.org/10.1016/j.tibs.2016.01.003

Canales, R. D., Luo, Y., Willey, J. C., Austermiller, B., Barbacioru, C. C., Boysen, C., … Goodsaid, F. M. (2006). Evaluation of DNA microarray results with quantitative gene expression platforms. *Nature Biotechnology*, *24*(9), 1115–1122. https://doi.org/10.1038/nbt1236

Carnemolla, A., Labbadia, J. P., Lazell, H., Neueder, A., Moussaoui, S., & Bates, G. P. (2014). Contesting the dogma of an age-related heat shock response impairment: Implications for cardiac-specific age-related disorders. *Human Molecular Genetics*, *23*(14), 3641–3656. https://doi.org/10.1093/hmg/ddu073

Carnemolla, A., Lazell, H., Moussaoui, S., & Bates, G. P. (2015). In vivo profiling reveals a competent heat shock response in adult neurons: Implications for

neurodegenerative disorders. *PLoS ONE*, *10*(7), 1–11. https://doi.org/10.1371/journal.pone.0131985

Carter, R. J., Lione, L. A., Humby, T., Mangiarini, L., Mahal, A., Bates, G. P., … Jennifer Morton, A. (1999). Characterization of progressive motor deficits in mice transgenic for the human Huntington's disease mutation. *Journal of Neuroscience*, *19*(8), 3248–3257. https://doi.org/10.1523/jneurosci.19-08-03248.1999

Carty, N., Berson, N., Tillack, K., Thiede, C., Scholz, D., Kottig, K., … Kwak, S. (2015). Characterization of HTT inclusion size, location, and timing in the zQ175 mouse model of Huntington's disease: An *in vivo* high-content imaging study. *PLoS ONE*, *10*(4), 1–18. https://doi.org/10.1371/journal.pone.0123527

Chafekar, S. M., Wisén, S., Thompson, A. D., Echeverria, A., Walter, G. M., Evans, C. G., … Duennwald, M. L. (2012). Pharmacological Tuning of Heat Shock Protein 70 Modulates Polyglutamine Toxicity and Aggregation. *ACS Chem Biol.*, *7*(9), 1556–1564. https://doi.org/10.1021/cb300166p

Chalkiadaki, A., & Guarente, L. (2015). The multifaceted functions of sirtuins in cancer. *Nature Reviews Cancer*, *15*(10), 608–624. https://doi.org/10.1038/nrc3985

Chang, A. R., Ferrer, C. M., & Mostoslavsky, R. (2020). SIRT6, a mammalian deacylase with multitasking abilities. *Physiological Reviews*, *100*(1), 145–169. https://doi.org/10.1152/physrev.00030.2018

Cheetham, M. E., & Caplan, A. J. (1998). Structure, function and evolution of DnaJ: Conservation and adaptation of chaperone function. *Cell Stress and Chaperones*. https://doi.org/10.1379/1466-1268(1998)003<0028:SFAEOD>2.3.CO;2

Chen, D., Bruno, J., Easlon, E., Lin, S. J., Cheng, H. L., Alt, F. W., & Guarente, L. (2008). Tissue-specific regulation of SIRT1 by calorie restriction. *Genes and Development*, *22*(13), 1753–1757. https://doi.org/10.1101/gad.1650608

Chen, H. J., Mitchell, J. C., Novoselov, S., Miller, J., Nishimura, A. L., Scotter, E. L., … Shaw, C. E. (2016). The heat shock response plays an important role in TDP-43 clearance: Evidence for dysfunction in amyotrophic lateral sclerosis. *Brain*, *139*(5), 1417–1432. https://doi.org/10.1093/brain/aww028

Chen, Z. J., Kren, B. T., Wong, P. Y. P., Low, W. C., & Steer, C. J. (2005). Sleeping Beauty-mediated down-regulation of huntingtin expression by RNA interference. *Biochemical and Biophysical Research Communications*, *329*(2), 646–652. https://doi.org/10.1016/j.bbrc.2005.02.024

Choi, S. E., Kwon, S., Seok, S., Xiao, Z., Lee, K.-W., Kang, Y., … Kemper, J. K. (2017). Obesity-linked phosphorylation of SIRT1 by casein kinase 2 inhibits its nuclear localization and [romotes fatty liver. *Molecular and Cellular Biology*, *37*(15), 1–14. https://doi.org/10.1128/mcb.00006-17

Chongtham, A., Barbaro, B., Filip, T., Syed, A., Huang, W., Smith, M. R., & Marsh, J. L. (2018). Nonmammalian models of Huntington's disease. In S. V. Precious, A. E. Rosser, & S. B. Dunnett (Eds.), *Huntington's Disease. Methods in Molecular Biology.* (Vol. 1780, pp. 75–96). Springer Nature. https://doi.org/10.1007/978-1-4939-7825-0_5

Chou, S. D., Prince, T., Gong, J., & Calderwood, S. K. (2012). mTOR is essential for the proteotoxic stress response, HSF1 activation and heat shock protein synthesis. *PloS One*, *7*(6), 1–9. https://doi.org/10.1371/journal.pone.0039679

Ciechanover, A., & Kwon, Y. T. a. (2015). Degradation of misfolded proteins in neurodegenerative diseases: therapeutic targets and strategies. *Experimental & Molecular Medicine*, *47*, e147. https://doi.org/10.1038/emm.2014.117

Cohen, H. Y., Miller, C., Bitterman, K. J., Wall, N. R., Hekking, B., Kessler, B., … Sinclair, D. A. (2004). Calorie restriction promotes mammalian cell survival by inducing the SIRT1 deacetylase. *Science*, *305*(5682), 390–392. https://doi.org/10.1126/science.1099196

Dabrowska, M., Juzwa, W., Krzyzosiak, W. J., & Olejniczak, M. (2018). Precise excision of the CAG tract from the huntingtin gene by Cas9 nickases. *Frontiers in Neuroscience*, *12*(February), 1–8. https://doi.org/10.3389/fnins.2018.00075

Dai, C., & Sampson, S. B. (2016). HSF1: Guardian of proteostasis in cancer. *Trends in Cell Biology*, *26*(1), 17–28. https://doi.org/10.1016/j.tcb.2015.10.011

Dai, C., Whitesell, L., Rogers, A. B., & Lindquist, S. (2007). Heat shock factor 1 is a powerful multifaceted modifier of carcinogenesis. *Cell*, *130*(6), 1005–1018. https://doi.org/10.1016/j.cell.2007.07.020

Dai, H., Sinclair, D. A., Ellis, J. L., & Steegborn, C. (2018). Sirtuin activators and inhibitors: Promises, achievements, and challenges. *Pharmacology and Therapeutics*, *188*,140–154. https://doi.org/10.1016/j.pharmthera.2018.03.004

Dai, S., Tang, Z., Cao, J., Zhou, W., Li, H., & Sampson, S. (2015). Suppression of the HSF1-mediated proteotoxic stress response by the metabolic stress sensor AMPK. *The EMBO Journal*, *34*(3), 275–293. https://doi.org/10.15252/embj.201489062

Davies, S., Turmaine, M., Cozens, B. A., DiFiglia, M., Sharp, A. H., Ross, C. A., … Bates, G. P. (1997). Formation of neuronal intranuclear inclusions underlies the neurological dysfunction in mice transgenic for the HD mutation. *Cell*, *90*(3), 537–548. https://doi.org/10.1016/s0092-8674(00)80513-9

DiFiglia, M., Sapp, E., Chase, K., Davies, S., & Bates, G. (1997). Aggregation of huntingtin in neuronal intranuclear inclusions and dystrophic neurites in brain. *Science*, *277*(5334), 1990–1993. https://doi.org/10.1126/science.277.5334.1990

DiFiglia, M., Sena-Esteves, M., & Chase, K. (2007). Therapeutic silencing of mutant huntingtin with siRNA attenuates striatal and cortical neuropathology and behavioral deficits. *PNAS*, *20*(8), 315–318.

Diguet, E., Petit, F., Escartin, C., Cambon, K., Bizat, N., Dufour, N., … Brouillet, E. (2009). Normal aging modulates the neurotoxicity of mutant huntingtin. *PLoS ONE*, *4*(2). https://doi.org/10.1371/journal.pone.0004637

Dikic, I. (2017). Proteasomal and autophagic degradation systems. *Annual Review of Biochemistry*, *86*, 193–224. https://doi.org/10.1146/annurev-biochem-061516-044908

Diller, K. R. (2006). Stress protein expression kinetics. *Annual Review of Biomedical Engineering*, *8*, 403–424. https://doi.org/10.1146/annurev.bioeng.7.060804.100449

Donmez, G., & Outeiro, T. F. (2013). SIRT1 and SIRT2: Emerging targets in neurodegeneration. *EMBO Molecular Medicine*, *5*(3), 344–352. https://doi.org/10.1002/emmm.201302451

Dragileva, E., Hendricks, A., Teed, A., Gillis, T., Lopez, E. T., Friedberg, E. C., … Wheeler, V. C. (2009). Intergenerational and striatal CAG repeat instability in Huntington's disease knock-in mice involve different DNA repair genes. *Neurobiology of Disease*, *33*(1), 37–47. https://doi.org/10.1016/j.nbd.2008.09.014

Du, J., Zhou, Y., Su, X., Yu, J. J., Khan, S., Jiang, H., … Lin, H. (2011). Sirt5 Is an NAD-dependent protein lysine demalonylase and desuccinylase. *Science*, *334*(6057), 806–809. https://doi.org/10.1126/science.1207861.Sirt5

Duan, W. (2013). Targeting Sirtuin-1 in Huntington's disease: Rationale and current status. *CNS Drugs*, *27*(5), 345–352. https://doi.org/10.1007/s40263-013-0055-0

Dues, D. J., Andrews, E. K., Schaar, C. E., Bergsma, A. L., Senchuk, M. M., & Van Raamsdonk, J. M. (2016). Aging causes decreased resistance to multiple stresses and a failure to activate specific stress response pathways. *Aging*, *8*(4), 777–795. https://doi.org/10.18632/aging.100939

Edwards, H. V., Cameron, R. T., & Baillie, G. S. (2011). The emerging role of HSP20 as a multifunctional protective agent. *Cellular Signalling*, *23*(9), 1447–1454. https://doi.org/10.1016/j.cellsig.2011.05.009

Ehrnhoefer, D. E., Martin, D. D. O., Schmidt, M. E., Qiu, X., Ladha, S., Caron, N. S., … Hayden, M. R. (2018). Preventing mutant huntingtin proteolysis and intermittent fasting promote autophagy in models of Huntington disease. *Acta Neuropathologica Communications*, *6*(1), 16. https://doi.org/10.1186/s40478-018-0518-0

Ehrnhoefer, D. E., Sutton, L., & Hayden, M. R. (2011). Small changes, big impact: Posttranslational modifications and function of huntingtin in Huntington disease. *Neuroscientist*, *17*(5), 475–492. https://doi.org/10.1177/1073858410390378

Escande, C., Chini, C. C. S., Nin, V., Dykhouse, K. M., Novak, C. M., Levine, J., … Chini, E. N. (2010). Deleted in breast cancer-1 regulates SIRT1 activity and contributes to high-fat diet-induced liver steatosis in mice. *Journal of Clinical Investigation*, *120*(2), 545–558. https://doi.org/10.1172/JCI39319

Evans, S. J. W., Douglas, I., Rawlins, M. D., Wexler, N. S., Tabrizi, S. J., & Smeeth, L. (2013). Prevalence of adult Huntington's disease in the UK based on diagnoses recorded in general practice records. *Journal of Neurology, Neurosurgery and Psychiatry*, *84*(10), 1156–1160. https://doi.org/10.1136/jnnp-2012-304636

Evers, M. M., Miniarikova, J., Juhas, S., Vallès, A., Bohuslavova, B., Juhasova, J., … Konstantinova, P. (2018). AAV5-miHTT gene therapy demonstrates broad distribution and strong human mutant huntingtin lowering in a Huntington's disease minipig model. *Molecular Therapy*, *26*(9), 2163–2177. https://doi.org/10.1016/j.ymthe.2018.06.021

Farshim, P. P., & Bates, G. P. (2018). Mouse models of Huntington's disease. In S. V. Precious, A. E. Rosser, & S. B. Dunnett (Eds.), *Huntington's Disease. Methods in*

Molecular Biology. (Vol. 1780, pp. 97–120). Springer Nature. https://doi.org/10.1007/978-1-4939-7825-0_6

Finka, A., Sharma, S. K., & Goloubinoff, P. (2015). Multi-layered molecular mechanisms of polypeptide holding, unfolding and disaggregation by HSP70/HSP110 chaperones. *Frontiers in Molecular Biosciences*, *2*(JUN), 1–12. https://doi.org/10.3389/fmolb.2015.00029

Flagella, M., Bui, S., Zheng, Z., Nguyen, C. T., Zhang, A., Pastor, L., … Luo, Y. (2006). A multiplex branched DNA assay for parallel quantitative gene expression profiling. *Analytical Biochemistry*, *352*(1), 50–60. https://doi.org/10.1016/j.ab.2006.02.013

Flower, M., Lomeikaite, V., Ciosi, M., Cumming, S., Morales, F., Lo, K., … Merkies, I. (2019). MSH3 modifies somatic instability and disease severity in Huntington's and myotonic dystrophy type 1. *Brain*, *142*(7), 1876–1886. https://doi.org/10.1093/brain/awz115

Ford, E., Voit, R., Liszt, G., Magin, C., Grummt, I., & Guarente, L. (2006). Mammalian Sir2 homolog SIRT7 is an activator of RNA polymerase I transcription. *Genes and Development*, *20*(9), 1075–1080. https://doi.org/10.1101/gad.1399706

Franco-Iborra, S., Plaza-Zabala, A., Montpeyo, M., Sebastian, D., Vila, M., & Martinez-Vicente, M. (2020). Mutant HTT (huntingtin) impairs mitophagy in a cellular model of Huntington disease. *Autophagy*, *17*(3), 672–689. https://doi.org/10.1080/15548627.2020.1728096

Franich, N. R., Hickey, M. A., Zhu, C., Osborne, G. F., Ali, N., Chu, T., … Chesselet, M. F. (2019). Phenotype onset in Huntington's disease knock-in mice is correlated with the incomplete splicing of the mutant huntingtin gene. *Journal of Neuroscience Research*, *97*(12), 1590–1605. https://doi.org/10.1002/jnr.24493

Frydman, J. (2001). Folding of newly translated proteins in vivo: The role of molecular chaperones. *Annual Review of Biochemistry*, *70*, 603–647. https://doi.org/0066-4154/01/0701-0603

Frye, R. A. (2000). Phylogenetic classification of prokaryotic and eukaryotic Sir2-like proteins. *Biochemical and Biophysical Research Communications*, *273*(2), 793–798. https://doi.org/10.1006/bbrc.2000.3000

Fujikake, N., Nagai, Y., Popiel, H. A., Okamoto, Y., Yamaguchi, M., & Toda, T. (2008). Heat shock transcription factor 1-activating compounds suppress polyglutamine-induced neurodegeneration through induction of multiple molecular chaperones. *Journal of Biological Chemistry*, *283*(38), 26188–26197. https://doi.org/10.1074/jbc.M710521200

Fujikake, N., Nagai, Y., Popiel, H. A., Okamoto, Y., Yamaguchi, M., & Toda, T. (2008). Heat shock transcription factor 1-activating compounds suppress polyglutamine-induced neurodegeneration through induction of multiple molecular chaperones. *Journal of Biological Chemistry*, *283*(38), 26188–26197. https://doi.org/10.1074/jbc.M710521200

Fujimoto, M., Takaki, E., Hayashi, T., Kitaura, Y., Tanaka, Y., Inouye, S., & Nakai, A. (2005). Active HSF1 significantly suppresses polyglutamine aggregate formation in cellular and mouse models. *Journal of Biological Chemistry*, *280*(41), 34908–34916. https://doi.org/10.1074/jbc.M506288200

Garriga-Canut, M., Agustín-Pavón, C., Herrmann, F., Sánchez, A., Dierssen, M., Fillat, C., & Isalan, M. (2012). Synthetic zinc finger repressors reduce mutant huntingtin expression in the brain of R6/2 mice. *PNAS*, *109*(45). https://doi.org/10.1073/pnas.1206506109

Gasset-Rosa, F., Chillon-Marinas, C., Goginashvili, A., Atwal, R. S., Artates, J. W., Tabet, R., … Lagier-Tourenne, C. (2017). Polyglutamine-expanded huntingtin exacerbates age-related disruption of nuclear integrity and nucleocytoplasmic

transport. *Neuron*, *94*(1), 48-57.e4. https://doi.org/10.1016/j.neuron.2017.03.027

Geater, C., Hernandez, S., Thompson, L., & Mattis, V. B. (2018). Cellular models: HD patient-derived pluripotent stem cells. In S. V. Precious, A. E. Rosser, & S. B. Dunnett (Eds.), *Huntington's Disease. Methods in Molecular Biology.* (Vol. 1780, pp. 41–74). Springer Nature. https://doi.org/10.1007/978-1-4939-7825-0_4

Genetic Modifiers of Huntington's Disease (GeM-HD) Consortium. (2015). Identification of genetic factors that modify clinical onset of Huntington's disease. *Cell*, *162*(3), 516–526. https://doi.org/10.1016/j.cell.2015.07.003

Genetic Modifiers of Huntington's Disease (GeM-HD) Consortium. (2019). CAG repeat not polyglutamine length determines timing of Huntington's disease onset. *Cell*, *178*(4), 887-900.e14. https://doi.org/10.1016/j.cell.2019.06.036

Ghosh, R., & Tabrizi, S. J. (2018). *Huntington disease*. *Handbook of Clinical Neurology* (1st ed., Vol. 147 (3rd s). Elsevier B.V. https://doi.org/10.1016/B978-0-444-63233-3.00017-8

Gidalevitz, T., Ben-zvi, A., Ho, K. H., Brignull, H. R., & Richard, I. (2006). Progressive disruption of cellular protein folding in models of polyglutamine diseases. *Science*, *311*(5766), 1471–1474. https://doi.org/10.1126/science.1124514

Gillis, J., Schipper-Krom, S., Juenemann, K., Gruber, A., Coolen, S., Van Den Nieuwendijk, R., … Reits, E. A. (2013). The DNAJB6 and DNAJB8 protein chaperones prevent intracellular aggregation of polyglutamine peptides. *Journal of Biological Chemistry*, *288*(24), 17225–17237. https://doi.org/10.1074/jbc.M112.421685

Gipson, T. A., Neueder, A., Wexler, N. S., Bates, G. P., & Housman, D. E. (2013). Aberrantly spliced HTT, a new player in Huntington's disease pathogenesis. *RNA Biology*, *10*(11), 1647–1652. https://doi.org/10.4161/rna.26706

Gomes, P., Fleming Outeiro, T., & Cavadas, C. (2015). Emerging role of sirtuin 2 in the regulation of mammalian metabolism. *Trends in Pharmacological Sciences*, *36*(11), 756–768. https://doi.org/10.1016/j.tips.2015.08.001

Gomez-Pastor, R., Burchfiel, E. T., Neef, D. W., Jaeger, A. M., Cabiscol, E., McKinstry, S. U., … Thiele, D. J. (2017). Abnormal degradation of the neuronal stress-protective transcription factor HSF1 in Huntington's disease. *Nature Communications*, *8*(May 2016), 1–17. https://doi.org/10.1038/ncomms14405

Gomez-Pastor, R., Burchfiel, E. T., & Thiele, D. J. (2018). Regulation of heat shock transcription factors and their roles in physiology and disease. *Nature Reviews Molecular Cell Biology*, *19*(1), 4–19. https://doi.org/10.1038/nrm.2017.73

Gong, J., Weng, D., Eguchi, T., Murshid, A., Sherman, M. Y., Song, B., & Calderwood, S. K. (2015). Targeting the *hsp70* gene delays mammary tumor initiation and inhibits tumor cell metastasis. *Oncogene*, *34*(43), 5460–5471. https://doi.org/10.1038/onc.2015.1

Gonitel, R., Moffitt, H., Sathasivam, K., Woodman, B., Detloff, P. J., Faull, R. L. M., & Bates, G. P. (2008). DNA instability in postmitotic neurons. *PNAS*, *105*(9), 3467–3472. https://doi.org/10.1073/pnas.0800048105

Goold, R., Hamilton, J., Menneteau, T., Flower, M., Bunting, E. L., Aldous, S. G., … Tabrizi, S. J. (2021). FAN1 controls mismatch repair complex assembly via MLH1 retention to stabilize CAG repeat expansion in Huntington's disease. *Cell Reports*, *36*(9), 109649. https://doi.org/10.1016/j.celrep.2021.109649

Gray, M., Shirasaki, D. I., Cepeda, C., André, V. M., Wilburn, B., Lu, X. H., … Yang, X. W. (2008). Full-length human mutant huntingtin with a stable polyglutamine repeat can elicit progressive and selective neuropathogenesis in BACHD mice. *Journal of Neuroscience*, *28*(24), 6182–6195. https://doi.org/10.1523/JNEUROSCI.0857-08.2008

Green, M., Schuetz, T. J., Sullivan, E. K., & Kingston, R. E. (1995). A heat shock-responsive domain of human HSF1 that regulates transcription activation domain function. *Molecular and Cellular Biology*, *15*(6), 3354–3362. https://doi.org/10.1128/mcb.15.6.3354

Gu, S., Cui, D., Chen, X., Xiong, X., & Zhao, Y. (2018). PROTACs: an emerging targeting technique for protein degradation in drug discovery. *BioEssays*, *40*(4). https://doi.org/10.1002/bies.201700247

Gu, X., Greiner, E. R., Mishra, R., Kodali, R., Osmand, A., Finkbeiner, S., … Yang, X. W. (2009). Serines 13 and 16 are critical determinants of full-length human mutant huntingtin induced disease pathogenesis in HD mice. *Neuron*, *64*(6), 828–840. https://doi.org/10.1016/j.neuron.2009.11.020

Guertin, M. J., & Lis, J. T. (2010). Chromatin landscape dictates HSF binding to target DNA elements. *PLoS Genetics*, *6*(9). https://doi.org/10.1371/journal.pgen.1001114

Guettouche, T., Boellmann, F., Lane, W. S., & Voellmy, R. (2005). Analysis of phosphorylation of human heat shock factor 1 in cells experiencing a stress. *BMC Biochemistry*, *6*, 1–14. https://doi.org/10.1186/1471-2091-6-4

Guisbert, E., Czyz, D. M., Richter, K., McMullen, P. D., & Morimoto, R. I. (2013). Identification of a tissue-selective heat shock response regulatory network. *PLoS Genetics*, *9*(4), 1–12. https://doi.org/10.1371/journal.pgen.1003466

Guo, Y., Pan, W., Liu, S., Shen, Z., Xu, Y., & Hu, L. (2020). ERK/MAPK signalling pathway and tumorigenesis (Review). *Experimental and Therapeutic Medicine*, 1997–2007. https://doi.org/10.3892/etm.2020.8454

Guo, Y., Guettouche, T., Fenna, M., Boellmann, F., Pratt, W. B., Toft, D. O., … Voellmy, R. (2001). Evidence for a mechanism of repression of heat shock factor 1 transcriptional activity by a multichaperone complex. *Journal of Biological Chemistry*, *276*(49), 45791–45799. https://doi.org/10.1074/jbc.M105931200

Guo, Q., Huang, B., Cheng, J., Seefelder, M., & Engler, T. (2018). The cryo-electron microscopy structure of huntingtin. *Nature*, *555*(7694), 117–120. https://doi.org/10.1038/nature25502

Gusella, J. F., Macdonald, M. E., & Lee, J. M. (2014). Genetic modifiers of Huntington's disease. *Movement Disorders*, *29*(11), 1359–1365. https://doi.org/10.1002/mds.26001

Gusella, J. F., Wexler, N. S., Conneally, P. M., Naylor, S. L., Anderson, M. A., Tanzi, R. E., … Martin, J. B. (1983). A polymorphic DNA marker genetically linked to Huntington's disease. *Nature*, *306*(5940), 234–238. https://doi.org/10.1038/306234a0

Gutekunst, C. A., Li, S. H., Yi, H., Mulroy, J. S., Kuemmerle, S., Jones, R., … Li, X. J. (1999). Nuclear and neuropil aggregates in Huntington's disease: Relationship to neuropathology. *Journal of Neuroscience*, *19*(7), 2522–2534. https://doi.org/10.1523/jneurosci.19-07-02522.1999

Guzhova, I. V., Lazarev, V. F., Kaznacheeva, A. V., Ippolitova, M. V., Muronetz, V. I., Kinev, A. V., & Margulis, B. A. (2011). Novel mechanism of Hsp70 chaperone-mediated prevention of polyglutamine aggregates in a cellular model of Huntington disease. *Human Molecular Genetics*, *20*(20), 3953–3963. https://doi.org/10.1093/hmg/ddr314

Hageman, J., Rujano, M. A., van Waarde, M. A. W. H., Kakkar, V., Dirks, R. P., Govorukhina, N., … Kampinga, H. H. (2010). A DNAJB chaperone subfamily with HDAC-dependent activities suppresses toxic protein aggregation. *Molecular Cell*, *37*(3), 355–369. https://doi.org/10.1016/j.molcel.2010.01.001

Haigis, M. C., Mostoslavsky, R., Haigis, K. M., Fahie, K., Christodoulou, D. C., Murphy, A. J. J., … Guarente, L. (2006). SIRT4 inhibits glutamate dehydrogenase and opposes the effects of calorie restriction in pancreatic β Cells. *Cell*, *126*(5), 941–954. https://doi.org/10.1016/j.cell.2006.06.057

Haigis, M. C., & Sinclair, D. A. (2010). Mammalian sirtuins: biological insights and disease relevance. *Annual Review of Pathology: Mechanisms of Disease*, *5*(1), 253–295. https://doi.org/10.1146/annurev.pathol.4.110807.092250

Handley, R. R., Reid, S. J., Patassini, S., Rudiger, S. R., Obolonkin, V., McLaughlan, C. J., … Snell, R. G. (2016). Metabolic disruption identified in the Huntington's disease transgenic sheep model. *Scientific Reports*, *6*(February), 1–11. https://doi.org/10.1038/srep20681

Hansson, O., Nylandsted, J., Castilho, R. F., Leist, M., Jaattela, M., & Brundin, P. (2003). Overexpression of heat shock protein 70 in R6/2 Huntington's disease mice has only modest effects on disease progression. *Brain Research*, *970*, 47–57. https://doi.org/10.1016/s0006-8993(02)04275-0

Harding, R. J., & Tong, Y. (2018). Proteostasis in Huntington's disease: disease mechanisms and therapeutic opportunities. *Acta Pharmacologica Sinica*, *3*, 1–16. https://doi.org/10.1038/aps.2018.11

Harper, S. Q., Staber, P. D., He, X., Eliason, S. L., Martins, I. H., Mao, Q., … Davidson, B. L. (2005). RNA interference improves motor and neuropathological abnormalities in a Huntington's disease mouse model. *PNAS*, *102*(16), 5820–5825. https://doi.org/10.1073/pnas.0501507102

Hay, D. G., Sathasivam, K., Tobaben, S., Stahl, B., Marber, M., Mestril, R., … Bates, G. P. (2004). Progressive decrease in chaperone protein levels in a mouse model of Huntington's disease and induction of stress proteins as a therapeutic approach. *Human Molecular Genetics*, *13*(13), 1389–1405. https://doi.org/10.1093/hmg/ddh144

Heikkinen, T., Lehtimäki, K., Vartiainen, N., Puoliväli, J., Hendricks, S. J., Glaser, J. R., … Park, L. C. (2012). Characterization of neurophysiological and behavioral changes, MRI brain volumetry and 1H MRS in zQ175 knock-in mouse model of

Huntington's Disease. *PLoS ONE*, *7*(12). https://doi.org/10.1371/journal.pone.0050717

Hensman-Moss, D. J., Tabrizi, S. J., Mead, S., Lo, K., Pardiñas, A. F., Holmans, P., … Tan, L. (2017). Identification of genetic variants associated with Huntington's disease progression: a genome-wide association study. *The Lancet Neurology*, *16*(9), 701–711. https://doi.org/10.1016/S1474-4422(17)30161-8

Herbst, M., & Wanker, E. E. (2007). Small molecule inducers of heat-shock response reduce polyQ-mediated huntingtin aggregation: A possible therapeutic strategy. *Neurodegenerative Diseases*, *4*(2–3), 254–260. https://doi.org/10.1159/000101849

Hershko, A., & Ciechanover, A. (1998). The ubiquitin system. *Annual Review of Biochemistry*, *458*(7237), 421. https://doi.org/10.1038/458421a

Herskovits, A. Z., & Guarente, L. (2014). SIRT1 in neurodevelopment and brain senescence. *Neuron*, *81*(3), 471–483. https://doi.org/10.1016/j.neuron.2014.01.028

Herskovits, A. Z., & Guarente, L. (2013). Sirtuin deacetylases in neurodegenerative diseases of aging. *Cell Research*, *23*(6), 746–758. https://doi.org/10.1038/cr.2013.70

Hietakangas, V., Ahlskog, J. K., Jakobsson, A. M., Hellesuo, M., Sahlberg, N. M., Holmberg, C. I., … Sistonen, L. (2003). Phosphorylation of serine 303 is a prerequisite for the stress-inducible SUMO modification of heat shock factor 1. *Molecular and Cellular Biology*, *23*(8), 2953–2968. https://doi.org/10.1128/mcb.23.8.2953-2968.2003

Hilger, R. A., Scheulen, M. E., & Strumberg, D. (2002). The Ras-Raf-MEK-ERK pathway in the treatment of cancer. *Onkologie*, *25*(6), 511–518. https://doi.org/10.1159/000068621

Hipp, M. S., Kasturi, P., & Hartl, F. U. (2019). The proteostasis network and its decline in ageing. *Nature Reviews Molecular Cell Biology*, *20*(7), 421–435. https://doi.org/10.1038/s41580-019-0101-y

Hipp, M. S., Park, S. H., & Hartl, U. U. (2014). Proteostasis impairment in protein-misfolding and -aggregation diseases. *Trends in Cell Biology*, *24*(9), 506–514. https://doi.org/10.1016/j.tcb.2014.05.003

Hipp, M. S., Patel, C. N., Bersuker, K., Riley, B. E., Kaiser, S. E., Shaler, T. A., … Kopito, R. R. (2012). Indirect inhibition of 26S proteasome activity in a cellular model of Huntington's disease. *Journal of Cell Biology*, *196*(5), 573–587. https://doi.org/10.1083/jcb.201110093

Hirakawa, T., Rokutan, K., Nikawa, T., & Kishi, K. (1996). Geranylgeranylacetone induces heat shock proteins in cultured guinea pig gastric mucosal cells and rat gastric mucosa. *Gastroenterology*, *111*(2), 345–357. https://doi.org/10.1053/gast.1996.v111.pm8690199

Ho, D. J., Calingasan, N. Y., Wille, E., Dumont, M., & Beal, M. F. (2010). Resveratrol protects against peripheral deficits in a mouse model of Huntington's disease. *Experimental Neurology*, *225*(1), 74–84. https://doi.org/10.1016/j.expneurol.2010.05.006

Hodges, A., Strand, A. D., Aragaki, A. K., Kuhn, A., Sengstag, T., Hughes, G., … Luthi-Carter, R. (2006). Regional and cellular gene expression changes in human Huntington's disease brain. *Human Molecular Genetics*, *15*(6), 965–977. https://doi.org/10.1093/hmg/ddl013

Holmans, P. A., Massey, T. H., & Jones, L. (2017). Genetic modifiers of Mendelian disease: Huntington's disease and the trinucleotide repeat disorders. *Human Molecular Genetics*, *26*(R2), R83–R90. https://doi.org/10.1093/hmg/ddx261

Holmberg, C. I., Hietakangas, V., Mikhailov, A., Rantanen, J. O., Kallio, M., Meinander, A., … Sistonen, L. (2001). Phosphorylation of serine 230 promotes inducible

transcriptional activity of heat shock factor 1. *EMBO Journal*, *20*(14), 3800–3810. https://doi.org/10.1093/emboj/20.14.3800

Hoogeveen, A. T., Willemsen, R., Meyer, N., Roolj, K. E. d., Roos, R. A. C., Ommen, G. J. B. va., & Galjaard, H. (1993). Characterization and localization of the Huntington disease gene product. *Human Molecular Genetics*, *2*(12), 2069–2073. https://doi.org/10.1093/hmg/2.12.2069

Horvath, S., Langfelder, P., Kwak, S., Aaronson, J., Rosinski, J., Vogt, T. F., … Yang, X. W. (2016). Huntington's disease accelerates epigenetic aging of human brain and disrupts DNA methylation levels. *Aging*, *8*(7), 1485–1512. https://doi.org/10.18632/aging.101005

Horwich, A. L., Fenton, W. A., Chapman, E., & Farr, G. W. (2007). Two families of chaperonin: Physiology and mechanism. *Annual Review of Cell and Developmental Biology*, *23*, 115–145. https://doi.org/10.1146/annurev.cellbio.23.090506.123555

Howitz, K. T., Bitterman, K. J., Cohen, H. Y., Lamming, D. W., Lavu, S., Wood, J. G., … Sinclair, D. A. (2003). Small molecule activators of sirtuins extend *Saccharomyces cerevisiae* lifespan. *Nature*, *425*(6954), 191–196. https://doi.org/10.1038/nature01960

Howland, D., Ellederova, Z., Aronin, N., Fernau, D., Gallagher, J., Taylor, A., … McBride, J. (2020). Large animal models of Huntington's disease: What we have learned and where we need to go next. *Journal of Huntington's Disease*, *9*(3), 201–216. https://doi.org/10.3233/JHD-200425

Hughes, A., & Jones, L. (2014). Pathogenic mechanisms. (G. Bates, S. Tabrizi, & L. Jones, Eds.), *Huntington's Disease* (4th edn). Oxford University Press. https://doi.org/10.1093/med/9780199929146.001.0001

Imai, S., Armstrong, C. M., Kaeberlein, M., & Guarente, L. (2000). Transcriptional silencing and longevity protein Sir2 is an NAD-dependent histone deacetylase. *Nature*, *403*, 795-800. https://doi.org/10.1038/35001622

Inoue, T., Hiratsuka, M., Osaki, M., Yamada, H., Kishimoto, I., Yamaguchi, S., … Oshimura, M. (2007). SIRT2, a tubulin deacetylase, acts to block the entry to chromosome condensation in response to mitotic stress. *Oncogene*, *26*(7), 945–957. https://doi.org/10.1038/sj.onc.1209857

Inoue, T., Hiratsuka, M., Osaki, M., & Oshimura, M. (2007). The molecular biology of mammalian SIRT proteins: SIRT2 in cell cycle regulation. *Cell Cycle*, *6*(9), 1011–1018. https://doi.org/10.4161/cc.6.9.4219

Jacobsen, J. C., Bawden, C. S., Rudiger, S. R., McLaughlan, C. J., Reid, S. J., Waldvogel, H. J., … Snell, R. G. (2010). An ovine transgenic Huntington's disease model. *Human Molecular Genetics*, *19*(10), 1873–1882. https://doi.org/10.1093/hmg/ddq063

Jana, N. R., Tanaka, M., Wang, G. H., & Nukina, N. (2000). Polyglutamine length-dependent interaction of Hsp40 and Hsp70 family chaperones with truncated N-terminal huntingtin: their role in suppression of aggregation and cellular toxicity. *Human Molecular Genetics*, *9*(13), 2009–2018. https://doi.org/10.1093/hmg/9.13.2009

Jana, N. R., & Nukina, N. (2005). BAG-1 associates with the polyglutamine-expanded huntingtin aggregates. *Neuroscience Letters*, *378*(3), 171–175. https://doi.org/10.1016/j.neulet.2004.12.031

Jana, N. R., Dikshit, P., Goswami, A., Kotliarova, S., Murata, S., Tanaka, K., & Nukina, N. (2005). Co-chaperone CHIP associates with expanded polyglutamine protein and promotes their degradation by proteasomes. *Journal of Biological Chemistry*, *280*(12), 11635–11640. https://doi.org/10.1074/jbc.M412042200

Janowska, M. K., Baughman, H. E. R., Woods, C. N., & Klevit, R. E. (2019). Mechanisms of small heat shock proteins. *Cold Spring Harbor Perspectives in Biology*, *11*(10). https://doi.org/10.1101/cshperspect.a034025

Jayaraj, G. G., Hipp, M. S., & Ulrich Hartl, F. (2019). Functional modules of the proteostasis network. *Cold Spring Harbor Perspectives in Biology*, *12*(1). https://doi.org/10.1101/cshperspect.a033951

Jeong, H., Cohen, D. E., Cui, L., Supinski, A., Savas, J. N., Mazzulli, J. R., … Krainc, D. (2012). Sirt1 mediates neuroprotection from mutant huntingtin by activation of the TORC1 and CREB transcriptional pathway. *Nature Medicine*, *18*(1), 159–165. https://doi.org/10.1038/nm.2559

Jeong, H., Then, F., Melia, T. J., Mazzulli, J. R., Cui, L., Savas, J. N., … Krainc, D. (2009). Acetylation targets mutant huntingtin to autophagosomes for degradation. *Cell*, *137*(1), 60–72. https://doi.org/10.1016/j.cell.2009.03.018

Jiang, M., Wang, J., Fu, J., Du, L., Jeong, H., West, T., … Duan, W. (2012). Neuroprotective role of Sirt1 in mammalian models of Huntington's disease through activation of multiple Sirt1 targets. *Nature Medicine*, *18*(1), 153–158. https://doi.org/10.1038/nm.2558

Johri, A., Chandra, A., & Beal, M. F. (2013). PGC-1α, mitochondrial dysfunction, and Huntington's disease. *Free Radical Biology and Medicine*, *62*, 37–46. https://doi.org/10.1016/j.freeradbiomed.2013.04.016

Joutsen, J., & Sistonen, L. (2019). Tailoring of proteostasis networks with heat shock factors. *Cold Spring Harbor Perspectives in Biology*, *11*(4). https://doi.org/10.1101/cshperspect.a034066

Juenemann, K., Schipper-Krom, S., Wiemhoefer, A., Kloss, A., Sanz, A. S., & Reits, E. A. J. (2013). Expanded polyglutamine-containing N-terminal huntingtin fragments are entirely degraded by mammalian proteasomes. *Journal of*

Biological Chemistry, *288*(38), 27068–27084. https://doi.org/10.1074/jbc.M113.486076

Juenemann, K., Weisse, C., Reichmann, D., Kaether, C., Calkhoven, C. F., & Schilling, G. (2011). Modulation of mutant huntingtin N-terminal cleavage and its effect on aggregation and cell death. *Neurotoxicity Research*, *20*(2), 120–133. https://doi.org/10.1007/s12640-010-9227-6

Juenemann, K., Wiemhoefer, A., & Reits, E. A. (2015). Detection of ubiquitinated huntingtin species in intracellular aggregates. *Frontiers in Molecular Neuroscience*, *8*(JAN), 1–8. https://doi.org/10.3389/fnmol.2015.00001

Jurivich, D. A., Sistonen, L., Kroes, R. A., & Morimoto, R. I. (1992). Effect of sodium salicylate on the human heat shock response. *Science*, *255*, 1243–1245. https://doi.org/10.1126/science.1546322

Kaeberlein, M., McDonagh, T., Heltweg, B., Hixon, J., Westman, E. A., Caldwell, S. D., … Kennedy, B. K. (2005). Substrate-specific activation of sirtuins by resveratrol. *Journal of Biological Chemistry*, *280*(17), 17038–17045. https://doi.org/10.1074/jbc.M500655200

Kaeberlein, M., McVey, M., & Guarente, L. (1999). The SIR2/3/4 complex and SIR2 alone promote longevity in *Saccharomyces cerevisiae* by two different mechanisms. *Genes and Development*, *13*(19), 2570–2580. https://doi.org/10.1101/gad.13.19.2570

Kakkar, V., Månsson, C., de Mattos, E. P., Bergink, S., van der Zwaag, M., van Waarde, M. A. W. H., … Kampinga, H. H. (2016). The S/T-Rich Motif in the DNAJB6 Chaperone Delays Polyglutamine Aggregation and the Onset of Disease in a Mouse Model. *Molecular Cell*, *62*(2), 272–283. https://doi.org/10.1016/j.molcel.2016.03.017

Kalmar, B., & Greensmith, L. (2017). Cellular chaperones as therapeutic targets in ALS to restore protein homeostasis and improve cellular function. *Frontiers in*

Molecular Neuroscience, *10*(September), 1–10. https://doi.org/10.3389/fnmol.2017.00251

Kalmar, B., Lu, C. H., & Greensmith, L. (2014). The role of heat shock proteins in Amyotrophic Lateral Sclerosis: The therapeutic potential of Arimoclomol. *Pharmacology and Therapeutics*, *141*(1), 40–54. https://doi.org/10.1016/j.pharmthera.2013.08.003

Kalmar, B., Novoselov, S., Gray, A., Cheetham, M. E., Margulis, B., & Greensmith, L. (2008). Late stage treatment with arimoclomol delays disease progression and prevents protein aggregation in the SOD1G93A mouse model of ALS. *Journal of Neurochemistry*, *107*(2), 339–350. https://doi.org/10.1111/j.1471-4159.2008.05595.x

Kaltenbach, L. S., Romero, E., Becklin, R. R., Chettier, R., Bell, R., Phansalkar, A., … Hughes, R. E. (2007). Huntingtin interacting proteins are genetic modifiers of neurodegeneration. *PLoS Genetics*, *3*(5), 689–708. https://doi.org/10.1371/journal.pgen.0030082

Kampinga, H. H., Andreasson, C., Barducci, A., Cheetham, M. E., & Cyr, D. (2019). Function, evolution, and structure of J-domain proteins. *Cell Stress and Chaperones*, *24*, 7–15. https://doi.org/https://doi.org/10.1007/s12192-018-0948-4

Kampinga, H. H., & Craig, E. A. (2010). The Hsp70 chaperone machinery: J-proteins as drivers of functional specificity. *Nat Rev Mol Cell Biol.*, *23*(1), 1–7. https://doi.org/10.1038/nrm2941.

Kampinga, H. H., Hageman, J., Vos, M. J., Kubota, H., Tanguay, R. M., Bruford, E. A., … Hightower, L. E. (2009). Guidelines for the nomenclature of the human heat shock proteins. *Cell Stress and Chaperones*, *14*(1), 105–111. https://doi.org/10.1007/s12192-008-0068-7

Karagöz, G. E., Acosta-Alvear, D., & Walter, P. (2019). The unfolded protein response: Detecting and responding to fluctuations in the protein-folding capacity of the endoplasmic reticulum. *Cold Spring Harbor Perspectives in Biology*, *11*(9). https://doi.org/10.1101/cshperspect.a033886

Karagöz, G. E., & Rüdiger, S. G. D. (2015). Hsp90 interaction with clients. *Trends in Biochemical Sciences*, *40*(2), 117–125. https://doi.org/10.1016/j.tibs.2014.12.002

Katsuno, M., Sang, C., Adachi, H., Minamiyama, M., Waza, M., Tanaka, F., … Sobue, G. (2005). Pharmacological induction of heat-shock proteins alleviates polyglutamine-mediated motor neuron disease. *PNAS*, *102*(46), 16801–16806. https://doi.org/10.1073/pnas.0506249102

Kaushik, S., & Cuervo, A. M. (2012). Chaperone-mediated autophagy: A unique way to enter the lysosome world. *Trends in Cell Biology*, *22*(8), 407–417. https://doi.org/10.1016/j.tcb.2012.05.006

Kay, C., Hayden, M. R., & Leavitt, B. R. (2017). Epidemiology of Huntington disease. *Handbook of Clinical Neurology*, *144* (3rd s, 31–46). https://doi.org/10.1016/B978-0-12-801893-4.00003-1

Kiffin, R., Christian, C., Knecht, E., & Cuervo, A. M. (2004). Activation of chaperone-mediated autophagy during oxidative stress. *Mol Biol Cell*, *15*(December), 5318–5328. https://doi.org/10.1091/mbc.E04

Kijima, T., Prince, T. L., Tigue, M. L., Yim, K. H., Schwartz, H., Beebe, K., … Neckers, L. (2018). HSP90 inhibitors disrupt a transient HSP90-HSF1 interaction and identify a noncanonical model of HSP90-mediated HSF1 regulation. *Scientific Reports*, *8*(1), 1–13. https://doi.org/10.1038/s41598-018-25404-w

Kim, H. W., Kim, S. A., & Ahn, S. G. (2016). Sirtuin inhibitors, EX527 and AGK2, suppress cell migration by inhibiting HSF1 protein stability. *Oncology Reports*, *35*(1), 235–242. https://doi.org/10.3892/or.2015.4381

Kim, E., Wang, B., Sastry, N., Masliah, E., Nelson, P. T., Cai, H., & Liao, F. F. (2016). NEDD4-mediated HSF1 degradation underlies α-synucleinopathy. *Human Molecular Genetics*, *25*(2), 211–222. https://doi.org/10.1093/hmg/ddv445

Kim, J. E., Chen, J., & Lou, Z. (2008). DBC1 is a negative regulator of SIRT1. *Nature*, *451*(7178), 583–586. https://doi.org/10.1038/nature06500

Kim, K. H., Hong, E. P., Shin, J. W., Chao, M. J., Loupe, J., Gillis, T., … Lee, J. M. (2020). Genetic and functional analyses point to FAN1 as the source of multiple Huntington disease modifier effects. *American Journal of Human Genetics*, *107*(1), 96–110. https://doi.org/10.1016/j.ajhg.2020.05.012

Kim, Y. E., Hipp, M. S., Bracher, A., Hayer-Hartl, M., & Ulrich Hartl, F. (2013). Molecular chaperone functions in protein folding and proteostasis. *Annual Review of Biochemistry* (Vol. 82). https://doi.org/10.1146/annurev-biochem-060208-092442

Kim, Y. E., Hosp, F., Frottin, F., Ge, H., Mann, M., Hayer-Hartl, M., & Hartl, F. U. (2016). Soluble oligomers of polyQ-expanded huntingtin target a multiplicity of key cellular factors. *Molecular Cell*, *63*(6), 950–964. https://doi.org/10.1016/j.molcel.2016.07.022

Kline, M. P., & Morimoto, R. I. (1997). Repression of the heat shock factor 1 transcriptional activation domain is modulated by constitutive phosphorylation. *Molecular and Cellular Biology*, *17*(4), 2107–2115. https://doi.org/10.1128/mcb.17.4.2107

Klug, A. (2010). The discovery of zinc fingers and their applications in gene regulation and genome manipulation. *Annual Review of Biochemistry*, *79*, 213–231. https://doi.org/10.1146/annurev-biochem-010909-095056

Kmiecik, S. W., Le Breton, L., & Mayer, M. P. (2020). Feedback regulation of heat shock factor 1 (Hsf1) activity by Hsp70-mediated trimer unzipping and

dissociation from DNA. *The EMBO Journal*, *39*(14), 1–22. https://doi.org/10.15252/embj.2019104096

Kmiecik, S. W., Drzewicka, K., Melchior, F., & Mayer, M. P. (2021). Heat shock transcription factor 1 is SUMOylated in the activated trimeric state. *Journal of Biological Chemistry*, *296*, 100324. https://doi.org/10.1016/j.jbc.2021.100324

Kordasiewicz, H. B., Stanek, L. M., Wancewicz, E. V., Mazur, C., McAlonis, M. M., Pytel, K. A., … Cleveland, D. W. (2012). Sustained therapeutic reversal of Huntington's disease by transient repression of huntingtin synthesis. *Neuron*, *74*(6), 1031–1044. https://doi.org/10.1016/j.neuron.2012.05.009

Kourtis, N., Moubarak, R. S., Aranda-Orgilles, B., Lui, K., Aydin, I. T., Trimarchi, T., … Aifantis, I. (2015). FBXW7 modulates cellular stress response and metastatic potential through HSF1 post-translational modification. *Nature Cell Biology*, *17*(3), 322–332. https://doi.org/10.1038/ncb3121

Kovalenko, M., Dragileva, E., St. Claire, J., Gillis, T., Guide, J. R., New, J., … Wheeler, V. C. (2012). *Msh2* acts in medium-spiny striatal neurons as an enhancer of CAG instability and mutant huntingtin phenotypes in Huntington's disease knock-in mice. *PLoS ONE*, *7*(9), 1–10. https://doi.org/10.1371/journal.pone.0044273

Kratter, I. H., Zahed, H., Lau, A., Tsvetkov, A. S., Daub, A. C., Weiberth, K. F., … Finkbeiner, S. (2016). Serine 421 regulates mutant huntingtin toxicity and clearance in mice. *Journal of Clinical Investigation*, *126*(9), 3585–3597. https://doi.org/10.1172/JCI80339

Kuemmerle, S., Gutekunst, C. A., Klein, A. M., Li, X. J., Li, S. H., Beal, M. F., … Ferrante, R. J. (1999). Huntingtin aggregates may not predict neuronal death in Huntington's disease. *Annals of Neurology*, *46*(6), 842–849. https://doi.org/10.1002/1531-8249(199912)46:6<842::AID-ANA6>3.0.CO;2-O

Kumar, S., & Lombard, D. B. (2018). Functions of the sirtuin deacylase SIRT5 in normal physiology and. *Crit Rev Biochem Mol Biol.*, *176*(5), 139–148. https://doi.org/10.1080/10409238.2018.1458071.

Kurosawa, M., Matsumoto, G., Kino, Y., Okuno, M., Kurosawa-Yamada, M., Washizu, C., … Nukina, N. (2015). Depletion of p62 reduces nuclear inclusions and paradoxically ameliorates disease phenotypes in Huntington's model mice. *Human Molecular Genetics*, *24*(4), 1092–1105. https://doi.org/10.1093/hmg/ddu522

Labbadia, J., Cunliffe, H., Weiss, A., Katsyuba, E., Sathasivam, K., Seredenina, T., … Bates, G. P. (2011). Altered chromatin architecture underlies progressive impairment of the heat shock response in mouse models of Huntington disease. *Journal of Clinical Investigation*, *121*(8), 3306–3319. https://doi.org/10.1172/JCI57413

Labbadia, J., & Morimoto, R. I. (2013). Huntington's disease: Underlying molecular mechanisms and emerging concepts. *Trends in Biochemical Sciences*, *38*(8), 378–385. https://doi.org/10.1016/j.tibs.2013.05.003

Labbadia, J., Novoselov, S. S., Bett, J. S., Weiss, A., Paganetti, P., Bates, G. P., & Cheetham, M. E. (2012). Suppression of protein aggregation by chaperone modification of high molecular weight complexes. *Brain*, *135*(4), 1180–1186. https://doi.org/10.1093/brain/aws022

Labbadia, J., & Morimoto, R. I. (2015). Repression of the heat shock Response is a programmed Event at the onset of reproduction. *Molecular Cell*, *59*(4), 639–650. https://doi.org/10.1016/j.molcel.2015.06.027

Labbadia, J., & Morimoto, R. I. (2015). The biology of proteostasis in aging and disease. *Annual Review of Biochemistry*, *84*, 435–464. https://doi.org/10.1146/annurev-biochem-060614-033955

Lakhani, V. V., Ding, F., & Dokholyan, N. V. (2010). Polyglutamine induced misfolding of Huntingtin Exon1 is modulated by the flanking sequences. *PLoS Computational Biology*, *6*(4), 39–41. https://doi.org/10.1371/journal.pcbi.1000772

Lakra, P., Aditi, K., & Agrawal, N. (2019). Peripheral expression of mutant huntingtin is a critical determinant of weight loss and metabolic disturbances in Huntington's disease. *Scientific Reports*, *9*(1), 1–15. https://doi.org/10.1038/s41598-019-46470-8

Lakshminarasimhan, M., Curth, U., Moniot, S., Mosalaganti, S., Raunser, S., & Steegborn, C. (2013). Molecular architecture of the human protein deacetylase Sirt1 and its regulation by AROS and resveratrol. *Bioscience Reports*, *33*(3), 395–404. https://doi.org/10.1042/BSR20120121

Landles, C., Milton, R. E., Ali, N., Flomen, R., Flower, M., Schindler, F., … Bates, G. P. (2020). Subcellular localization and formation of huntingtin aggregates correlates with symptom onset and progression in a Huntington's disease model. *Brain Communications*, *2*(2), 1–20. https://doi.org/10.1093/braincomms/fcaa066

Landles, C., Sathasivam, K., Weiss, A., Woodman, B., Moffitt, H., Finkbeiner, S., … Bates, G. P. (2010). Proteolysis of mutant huntingtin produces an exon 1 fragment that accumulates as an aggregated protein in neuronal nuclei in Huntington disease. *Journal of Biological Chemistry*, *285*(12), 8808–8823. https://doi.org/10.1074/jbc.M109.075028

Landwehrmeyer, G. B., Fitzer-Attas, C. J., Giuliano, J. D., Gonçalves, N., Anderson, K. E., Cardoso, F., … Sampaio, C. (2016). Data analytics from Enroll-HD, a global clinical research platform for Huntington's disease. *Movement Disorders Clinical Practice*, *4*(2), 212–224. https://doi.org/10.1002/mdc3.12388

Langbehn, D. R., Hayden, M. R., Paulsen, J. S., Johnson, H., Aylward, E., Biglan, K., … Stout, J. (2010). CAG-repeat length and the age of onset in Huntington Disease (HD): A review and validation study of statistical approaches. *American Journal of Medical Genetics, Part B: Neuropsychiatric Genetics*, *153*(2), 397–408. https://doi.org/10.1002/ajmg.b.30992

Langfelder, P., Cantle, J. P., Chatzopoulou, D., Wang, N., Gao, F., Al-Ramahi, I., … Yang, X. W. (2016). Integrated genomics and proteomics define huntingtin CAG length-dependent networks in mice. *Nature Neuroscience*, *19*(4), 623–633. https://doi.org/10.1038/nn.4256

Langley, B., & Sauve, A. (2013). Sirtuin deacetylases as therapeutic targets in the nervous system. *Neurotherapeutics*, *10*(4), 605–620. https://doi.org/10.1007/s13311-013-0214-5

Langley, E., Pearson, M., Faretta, M., Bauer, U. M., Frye, R. A., Minucci, S., … Kouzarides, T. (2002). Human SIR2 deacetylates p53 and antagonizes PML/p53-induced cellular senescence. *EMBO Journal*, *21*(10), 2383–2396. https://doi.org/10.1093/emboj/21.10.2383

Lanka, V., Wieland, S., Barber, J., & Cudkowicz, M. (2009). Arimoclomol: A potential therapy under development for ALS. *Expert Opinion on Investigational Drugs*, *18*(12), 1907–1918. https://doi.org/10.1517/13543780903357486

Lau, A. W., Liu, P., Inuzuka, H., & Gao, D. (2014). SIRT1 phosphorylation by AMP-activated protein kinase regulates p53 acetylation. *American Journal of Cancer Research*, *4*(3), 245–255.

Le Masson, F., Razak, Z., Kaigo, M., Audouard, C., Charry, C., Cooke, H., … Christians, E. S. (2011). Identification of heat shock factor 1 molecular and cellular targets during embryonic and adult female meiosis. *Molecular and Cellular Biology*, *31*(16), 3410–3423. https://doi.org/10.1128/mcb.05237-11

Lee, J. M., Ramos, E. M., Lee, J. H., Gillis, T., Mysore, J. S., Hayden, M. R., … Gusella, J. F. (2012). CAG repeat expansion in Huntington disease determines age at onset in a fully dominant fashion. *Neurology*, *78*(10), 690–695. https://doi.org/10.1212/WNL.0b013e318249f683

Lee, J. M., Pinto, R. M., Gillis, T., St. Claire, J. C., & Wheeler, V. C. (2011). Quantification of age-dependent somatic CAG repeat instability in *Hdh* CAG knock-in mice reveals different expansion dynamics in striatum and liver. *PLoS ONE*, *6*(8), 6–13. https://doi.org/10.1371/journal.pone.0023647

Li, F., Xiao, H., Zhou, F., Hu, Z., & Yang, B. (2017). Study of HSPB6: insights into the properties of the multifunctional protective agent. *Cellular Physiology and Biochemistry*, *44*(1), 314–332. https://doi.org/10.1159/000484889

Li, J., Chauve, L., Phelps, G., Brielmann, R. M., & Morimoto, R. I. (2016). E2F coregulates an essential HSF developmental program that is distinct from the heat-shock response. *Genes and Development*, *30*(18), 2062–2075. https://doi.org/10.1101/gad.283317.116

Li, J., Labbadia, J., & Morimoto, R. I. (2017). Rethinking HSF1 in stress, development, and organismal health. *Trends in Cell Biology*, *27*(12), 895–905. https://doi.org/10.1016/j.tcb.2017.08.002

Li, L., Shi, L., Yang, S., Yan, R., Zhang, D., Yang, J., … Yu, W. (2016). SIRT7 is a histone desuccinylase that functionally links to chromatin compaction and genome stability. *Nature Communications*, *7*. https://doi.org/10.1038/ncomms12235

Li, S. H., Schilling, G., Young, W. S., Li, X., Margolis, R. L., Stine, O. C., … Ross, C. A. (1993). Huntington's disease gene (IT15) is widely expressed in human and rat tissues. *Neuron*, *11*(5), 985–993. https://doi.org/10.1016/0896-6273(93)90127-D

Li, X., Zhang, S., Blander, G., Tse, J. G., Krieger, M., & Guarente, L. (2007). SIRT1 Deacetylates and positively regulates the nuclear receptor LXR. *Molecular Cell*, *28*(1), 91–106. https://doi.org/10.1016/j.molcel.2007.07.032

Li, Z., Wang, C., Wang, Z., Zhu, C., Li, J., Sha, T., … Lu, B. (2019). Allele-selective lowering of mutant HTT protein by HTT–LC3 linker compounds. *Nature*, *575*(7781), 203–209. https://doi.org/10.1038/s41586-019-1722-1

Lieberman, A. P., Shakkottai, V. G., & Albin, R. L. (2019). Polyglutamine repeats in neurodegenerative diseases. *Annual Review of Pathology: Mechanisms of Disease*, *14*, 1–27. https://doi.org/10.1146/annurev-pathmechdis-012418-012857

Lin, C. H., Tallaksen-Greene, S., Chien, W. M., Cearley, J. A., Jackson, W. S., Crouse, A. B., … Detloff, P. J. (2001). Neurological abnormalities in a knock-in mouse model of Huntington's disease. *Human Molecular Genetics*, *10*(2), 137–144. https://doi.org/10.1093/hmg/10.2.137

Lindquist, S. (1986). THE HEAT-SHOCK RESPONSE. *Annual Review of Biochemistry*, *55*, 1151–1191. https://doi.org/10.1146/annurev.bi.55.070186.005443

Lindquist, S. L., & Kelly, J. W. (2011). Chemical and biological approaches for adapting proteostasis to ameliorate protein misfolding and aggregation diseases-progress and prognosis. *Cold Spring Harbor Perspectives in Biology*, *3*(12). https://doi.org/10.1101/cshperspect.a004507

Liszt, G., Ford, E., Kurtev, M., & Guarente, L. (2005). Mouse Sir2 homolog SIRT6 is a nuclear ADP-ribosyltransferase. *Journal of Biological Chemistry*, *280*(22), 21313–21320. https://doi.org/10.1074/jbc.M413296200

Littlefield, O., & Nelson, H. C. M. (1999). A new use for the "wing" of the "winged" helix-turn-helix motif in the HSF-DNA cocrystal. *Nature Structural Biology*, *6*(5), 464–470. https://doi.org/10.1038/8269

Liu, D. J., Hammer, D., Komlos, D., Chen, K. Y., Firestein, B. L., & Liu, A. Y. C. (2014). SIRT1 knockdown promotes neural differentiation and attenuates the heat shock response. *Journal of Cellular Physiology*, *229*(9), 1224–1235. https://doi.org/10.1002/jcp.24556

Liu, J. P., & Zeitlin, S. O. (2017). Is huntingtin dispensable in the adult brain? *Journal of Huntington's Disease*, *6*(1), 1–17. https://doi.org/10.3233/JHD-170235

Liu, P. C. C., & Thiele, D. J. (1999). Modulation of human heat shock factor trimerization by the linker domain. *Journal of Biological Chemistry*, *274*(24), 17219–17225. https://doi.org/10.1074/jbc.274.24.17219

Livak, K. J., & Schmittgen, T. D. (2001). Analysis of relative gene expression data using real-time quantitative PCR and the 2-ΔΔCT method. *Methods*, *25*, 402–408. https://doi.org/10.1006/meth.2001.1262

Lotz, G. P., Legleiter, J., Aron, R., Mitchell, E. J., Huang, S. Y., Ng, C., … Muchowski, P. J. (2010). Hsp70 and Hsp40 functionally interact with soluble mutant huntingtin oligomers in a classic ATP-dependent reaction cycle. *Journal of Biological Chemistry*, *285*(49), 38183–38193. https://doi.org/10.1074/jbc.M110.160218

Lunkes, A., Lindenberg, K. S., Ben-Haem, L., Weber, C., Devys, D., Landwehrmeyer, G. B., … Trottier, Y. (2002). Proteases acting on mutant huntingtin generate cleaved products that differentially build up cytoplasmic and nuclear inclusions. *Molecular Cell*, *10*(2), 259–269. https://doi.org/10.1016/S1097-2765(02)00602-0

Luo, J., Nikolaev, A. Y., Imai, S. ichiro, Chen, D., Su, F., Shiloh, A., … Gu, W. (2001). Negative control of p53 by Sir2α promotes cell survival under stress. *Cell*, *107*(2), 137–148. https://doi.org/10.1016/S0092-8674(01)00524-4

Luo, W., Sun, W., Taldone, T., Rodina, A., & Chiosis, G. (2010). Heat shock protein 90 in neurodegenerative diseases. *Molecular Neurodegeneration*, *5*(24), 1–8. https://doi.org/10.1186/1750-1326-5-24

Luthi-Carter, R., Strand, A., Peters, N. L., Solano, S. M., Hollingsworth, Z. R., Menon, A. S., … Olson, J. M. (2000). Decreased expression of striatal signaling genes in a mouse model of Huntington's disease. *Human Molecular Genetics*, *9*(9), 1259–1271. https://doi.org/10.1093/hmg/9.9.1259

Mangiarini, L., Sathasivam, K., Mahatl, A., Mott, R., Seller, M., & Bates, G. P. (1997). Instability of highly expanded CAG repeats in mice transgenic for the Huntington's disease mutation. *Nature Genetics*, *15*(february), 197–200. https://doi.org/10.1038/ng0297-197

Mangiarini, L., Sathasivam, K., Seller, M., Cozens, B., Harper, A., Hetherington, C., … Bates, G. P. (1996). Exon 1 of the HD gene with an expanded CAG repeat is sufficient to cause a progressive neurological phenotype in transgenic mice. *Cell*, *87*(November 1, 1996), 493–506. https://doi.org/10.1016/s0092-8674(00)81369-0

Margulis, J., & Finkbeiner, S. (2014). Proteostasis in striatal cells and selective neurodegeneration in Huntington's disease. *Frontiers in Cellular Neuroscience*, *8*(AUG), 1–9. https://doi.org/10.3389/fncel.2014.00218

Martin, D. D. O., Ladha, S., Ehrnhoefer, D. E., & Hayden, M. R. (2014). Autophagy in Huntington disease and huntingtin in autophagy. *Trends in Neurosciences*, *38*(1), 26–35. https://doi.org/10.1016/j.tins.2014.09.003

Martinez-Vicente, M., Talloczy, Z., Wong, E., Tang, G., Koga, H., Kaushik, S., … Cuervo, A. M. (2010). Cargo recognition failure is responsible for inefficient autophagy in Huntington's disease. *Nature Neuroscience*, *13*(5), 567–576. https://doi.org/10.1038/nn.2528

Matsumoto, G., Wada, K., Okuno, M., Kurosawa, M., & Nukina, N. (2011). Serine 403 phosphorylation of p62/SQSTM1 regulates selective autophagic clearance of ubiquitinated proteins. *Molecular Cell*, *44*(2), 279–289. https://doi.org/10.1016/j.molcel.2011.07.039

Mayer, M. P., & Gierasch, L. M. (2019). Recent advances in the structural and mechanistic aspects of Hsp70 molecular chaperones. *Journal of Biological Chemistry*, *294*(6), 2085–2097. https://doi.org/10.1074/jbc.REV118.002810

McAllister, B., Gusella, J. F., Landwehrmeyer, G. B., Lee, J. M., MacDonald, M. E., Orth, M., … Massey, T. H. (2021). Timing and impact of psychiatric, cognitive, and motor abnormalities in Huntington disease. *Neurology*, *96*(19), e2395–e2406. https://doi.org/10.1212/WNL.0000000000011893

McBride, C. M., Levine, B., Xia, Y., & Bellamacina, C. (2014). Design, structure-activity relationship, and *in vivo* characterization of the development candidate NVP-HSP990. *Journal of Medicinal Chemistry*, (57), 9124–9129. https://doi.org/10.1021/jm501107q

McBride, J. L., Boudreau, R. L., Harper, S. Q., Staber, P. D., Monteys, A. M., Martins, I., … Davidson, B. L. (2008). Artificial miRNAs mitigate shRNA-mediated toxicity in the brain: Implications for the therapeutic development of RNAi. *PNAS*, *105*(15), 5868–5873. https://doi.org/10.1073/pnas.0801775105

McBride, J. L., Pitzer, M. R., Boudreau, R. L., Dufour, B., Hobbs, T., Ojeda, S. R., & Davidson, B. L. (2011). Preclinical safety of RNAi-mediated HTT suppression in the *rhesus macaque* as a potential therapy for Huntington's disease. *Molecular Therapy*, *19*(12), 2152–2162. https://doi.org/10.1038/mt.2011.219

McMillan, D., Xiao, X., Shao, L., Graves, K., & Benjamin, I. J. (1998). Targeted disruption of heat shock transcription factor 1 abolishes thermotolerance and protection against heat-inducible apoptosis. *J. Biol. Chem.*, *273*(13), 7523–7528. https://doi.org/10.1074/jbc.273.13.7523

Melber, A., & Haynes, C. M. (2018). UPR mt regulation and output: A stress response mediated by mitochondrial-nuclear communication. *Cell Research*, *28*(3), 281–295. https://doi.org/10.1038/cr.2018.16

Menalled, L. B., Kudwa, A. E., Miller, S., Fitzpatrick, J., Watson-Johnson, J., Keating, N., … Howland, D. (2012). Comprehensive behavioral and molecular characterization of a new knock-in mouse model of Huntington's disease: ZQ175. *PLoS ONE*, *7*(12). https://doi.org/10.1371/journal.pone.0049838

Menalled, L. B., Sison, J. D., Dragatsis, I., Zeitlin, S., & Chesselet, M. F. (2003). Time course of early motor and neuropathological anomalies in a knock-in mouse model of Huntington's disease with 140 CAG repeats. *Journal of Comparative Neurology*, *465*(1), 11–26. https://doi.org/10.1002/cne.10776

Mendillo, M. L., Santagata, S., Koeva, M., Bell, G. W., Hu, R., Tamimi, R. M., … Lindquist, S. (2012). HSF1 drives a transcriptional program distinct from heat shock to support highly malignant human cancers. *Cell*, *150*(3), 549–562. https://doi.org/10.1016/j.cell.2012.06.031

Menezes, D. L., Taverna, P., Jensen, M. R., Abrams, T., Stuart, D., Yu, G. K., … Gao, Z. (2012). The novel oral Hsp90 inhibitor NVP-HSP990 exhibits potent and broad-spectrum antitumor activities *in vitro* and *in vivo*. *Molecular Cancer Therapeutics*, *11*(3), 730–739. https://doi.org/10.1158/1535-7163.MCT-11-0667

Menzies, F. M., Fleming, A., Caricasole, A., Bento, C. F., Andrews, S. P., Ashkenazi, A., … Rubinsztein, D. C. (2017). Autophagy and neurodegeneration: pathogenic mechanisms and therapeutic opportunities. *Neuron*, *93*(5), 1015–1034. https://doi.org/10.1016/j.neuron.2017.01.022

Mercier, P. A., Winegarden, N. A., & Westwood, J. T. (1999). Human heat shock factor 1 is predominantly a nuclear protein before and after heat stress. *Journal of Cell Science*, *112*(16), 2765–2774. https://doi.org/10.1242/jcs.112.16.2765

Michishita, E., McCord, R. A., Berber, E., Kioi, M., Padilla-Nash, H., Damian, M., … Chua, K. F. (2008). SIRT6 is a histone H3 lysine 9 deacetylase that modulates

telomeric chromatin. *Nature*, *452*(7186), 492–496. https://doi.org/10.1038/nature06736

Milazzo, G., Mercatelli, D., Di Muzio, G., Triboli, L., De Rosa, P., Perini, G., & Giorgi, F. M. (2020). Histone deacetylases (HDACs): Evolution, specificity, role in transcriptional complexes, and pharmacological actionability. *Genes*, *11*(5). https://doi.org/10.3390/genes11050556

Miller, J., Arrasate, M., Brooks, E., Libeu, C. P., Legleiter, J., Hatters, D., … Finkbeiner, S. (2011). Identifying polyglutamine protein species *in situ* that best predict neurodegeneration. *Nature Chemical Biology*, *7*(12), 925–934. https://doi.org/10.1038/nchembio.694

Milnerwood, A. J., & Raymond, L. A. (2010). Early synaptic pathophysiology in neurodegeneration: Insights from Huntington's disease. *Trends in Neurosciences*, *33*(11), 513–523. https://doi.org/10.1016/j.tins.2010.08.002

Min, Z., Gao, J., & Yu, Y. (2019). The roles of mitochondrial SIRT4 in cellular metabolism. *Frontiers in Endocrinology*, *10*(JAN), 1–8. https://doi.org/10.3389/fendo.2018.00783

Moffitt, H., McPhail, G. D., Woodman, B., Hobbs, C., & Bates, G. P. (2009). Formation of polyglutamine inclusions in a wide range of non-CNS tissues in the *Hdh*Q150 knock-in mouse model of Huntington's disease. *PLoS ONE*, *4*(11). https://doi.org/10.1371/journal.pone.0008025

Mogk, A., Ruger-Herreros, C., & Bukau, B. (2019). Cellular functions and mechanisms of action of small heat shock proteins. *Annual Review of Microbiology*, *73*, 89–110. https://doi.org/10.1146/annurev-micro-020518-115515

Monsellier, E., Redeker, V., Ruiz-Arlandis, G., Bousset, L., & Melki, R. (2015). Molecular interaction between the chaperone Hsc70 and the N-terminal flank of huntingtin exon 1 modulates aggregation. *Journal of Biological Chemistry*, *290*(5), 2560–2576. https://doi.org/10.1074/jbc.M114.603332

Morimoto, R. I. (2020). Cell-nonautonomous regulation of proteostasis in aging and disease. *Cold Spring Harbor Perspectives in Biology*, *12*(4). https://doi.org/10.1101/cshperspect.a034074

Morimoto, R. I. (2011). The heat shock response: systems biology of proteotoxic stress in aging and disease. *Cold Spring Harbor Symposia on Quantitative Biology*, *LXXVI*. https://doi.org/10.1101/sqb.2012.76.010637

Morton, A. J., Glynn, D., Leavens, W., Zheng, Z., Faull, R. L. M., Skepper, J. N., & Wight, J. M. (2009). Paradoxical delay in the onset of disease caused by super-long CAG repeat expansions in R6/2 mice. *Neurobiology of Disease*, *33*(3), 331–341. https://doi.org/10.1016/j.nbd.2008.11.015

Morton, J. A., & Howland, D. S. (2013). Large genetic animal models of Huntington's disease. *Journal of Huntington's Disease*, *2*(1), 3–19. https://doi.org/10.3233/JHD-130050

Morton, J. A., Rudiger, S. R., Wood, N. I., Sawiak, S. J., Brown, G. C., Mclaughlan, C. J., … Simon Bawden, C. (2014). Early and progressive circadian abnormalities in Huntington's disease sheep are unmasked by social environment. *Human Molecular Genetics*, *23*(13), 3375–3383. https://doi.org/10.1093/hmg/ddu047

Muchowski, P. J., Schaffar, G., Sittler, A., Wanker, E. E., Hayer-Hartl, M. K., & Hartl, F. U. (2000). Hsp70 and Hsp40 chaperones can inhibit self-assembly of polyglutamine proteins into amyloid-like fibrils. *PNAS*, *97*(14), 7841–7846. https://doi.org/10.1073/pnas.140202897

Muchowski, P. J., & Wacker, J. L. (2005). Modulation of neurodegeneration by molecular chaperones. *Nature Reviews Neuroscience*, *6*(1), 11–22. https://doi.org/10.1038/nrn1587

Murphy, K. P. S. J., Carter, R. J., Lione, L. A., Mangiarini, L., Mahal, A., Bates, G. P., … Jennifer Morton, A. (2000). Abnormal synaptic plasticity and impaired spatial cognition in mice transgenic for exon 1 of the human Huntington's disease

mutation. *Journal of Neuroscience*, *20*(13), 5115–5123. https://doi.org/10.1523/jneurosci.20-13-05115.2000

Nadler, S. G., Tepper, M. A., Schacter, B., & Mazzucco, C. E. (1992). Interaction of the immunosuppressant deoxyspergualin with a member of the Hsp70 family of heat shock proteins. *Science*, *258*(5081), 484–486. https://doi.org/10.1126/science.1411548

Naia, L., & Rego, A. C. (2015). Sirtuins: Double players in Huntington's disease. *Biochimica et Biophysica Acta*, *1852*(10), 2183–2194. https://doi.org/10.1016/j.bbadis.2015.07.003

Nasir, J., Floresco, S. B., O'Kusky, J. R., Diewert, V. M., Richman, J. M., Zeisler, J., … Hayden, M. R. (1995). Targeted disruption of the Huntington's disease gene results in embryonic lethality and behavioral and morphological changes in heterozygotes. *Cell*, *81*(5), 811–823. https://doi.org/10.1016/0092-8674(95)90542-1

Nasrin, N., Kaushik, V. K., Fortier, E., Wall, D., Pearson, K. J., de Cabo, R., & Bordone, L. (2009). JNK1 phosphorylates SIRT1 and promotes its enzymatic activity. *PLoS ONE*, *4*(12). https://doi.org/10.1371/journal.pone.0008414

Naver, B., Stub, C., Møller, M., Fenger, K., Hansen, A. K., Hasholt, L., & Sørensen, S. A. (2003). Molecular and behavioral analysis of the R6/1 Huntington's disease transgenic mouse. *Neuroscience*, *122*(4), 1049–1057. https://doi.org/10.1016/j.neuroscience.2003.08.053

Neckers, L., Blagg, B., Haystead, T., Trepel, J. B., Whitesell, L., & Picard, D. (2018). Methods to validate Hsp90 inhibitor specificity, to identify off-target effects, and to rethink approaches for further clinical development. *Cell Stress and Chaperones*, *23*(4), 467–482. https://doi.org/10.1007/s12192-018-0877-2

Neckers, L., & Workman, P. (2012). Hsp90 molecular chaperone inhibitors: Are we there yet? *Clinical Cancer Research*, *18*(1), 64–76. https://doi.org/10.1158/1078-0432.CCR-11-1000

Neef, D. W., Jaeger, A. M., Gomez-Pastor, R., Willmund, F., Frydman, J., & Thiele, D. J. (2014). A direct regulatory interaction between chaperonin TRiC and stress-responsive transcription factor HSF1. *Cell Reports*, *9*(3), 955–966. https://doi.org/10.1016/j.celrep.2014.09.056

Neef, D. W., Jaeger, A. M., & Thiele, D. J. (2011). Heat shock transcription factor 1 as a therapeutic target in neurodegenerative diseases. *Nature Reviews Drug Discovery*, *10*(12), 930–944. https://doi.org/10.1038/nrd3453

Neef, D. W., Turski, M. L., & Thiele, D. J. (2010). Modulation of heat shock transcription factor 1 as a therapeutic target for small molecule intervention in neurodegenerative disease. *PLoS Biology*, *8*(1). https://doi.org/10.1371/journal.pbio.1000291

Neo, S. H., & Tang, B. L. (2018). Sirtuins as modifiers of Huntington's Disease (HD) pathology. *Progress in Molecular Biology and Translational Science*, *154*, 105–145. https://doi.org/10.1016/bs.pmbts.2017.11.013

Neudegger, T., Verghese, J., Hayer-Hartl, M., Hartl, F. U., & Bracher, A. (2016). Structure of human heat-shock transcription factor 1 in complex with DNA. *Nature Structural and Molecular Biology*, *23*(2), 140–146. https://doi.org/10.1038/nsmb.3149

Neueder, A., Achilli, F., Moussaoui, S., & Bates, G. P. (2014). Novel isoforms of heat shock transcription factor 1, HSF1γα and HSF1γβ, regulate chaperone protein gene transcription. *Journal of Biological Chemistry*, *289*(29), 19894–19906. https://doi.org/10.1074/jbc.M114.570739

Neueder, A., Gipson, T. A., Batterton, S., Lazell, H. J., Farshim, P. P., Paganetti, P., … Bates, G. P. (2017). HSF1-dependent and -independent regulation of the

mammalian *in vivo* heat shock response and its impairment in Huntington's disease mouse models. *Scientific Reports*, *7*(1), 12556. https://doi.org/10.1038/s41598-017-12897-0

Neueder, A., Landles, C., Ghosh, R., Howland, D., Myers, R. H., Faull, R. L. M., … Bates, G. P. (2017). The pathogenic exon 1 HTT protein is produced by incomplete splicing in Huntington's disease patients. *Scientific Reports*, *7*(1), 1–10. https://doi.org/10.1038/s41598-017-01510-z

Newton, E. M., Knauf, U., Green, M., & Kingston, R. E. (1996). The regulatory domain of human heat shock factor 1 is sufficient to sense heat stress. *Molecular and Cellular Biology*, *16*(3), 839–846. https://doi.org/10.1128/mcb.16.3.839

Nogueiras, R., Habegger, K. M., Chaudhary, N., Finan, B., Banks, A. S., Dietrich, M. O., … Tschöp, M. H. (2012). Sirtuin 1 and sirtuin 3: Physiological modulators of metabolism. *Physiological Reviews*, *92*(3), 1479–1514. https://doi.org/10.1152/physrev.00022.2011

Nollen, E. A. A., Garcia, S. M., Van Haaften, G., Kim, S., Chavez, A., Morimoto, R. I., & Plasterk, R. H. A. (2004). Genome-wide RNA interference screen identifies previously undescribed regulators of polyglutamine aggregation. *PNAS*, *101*(17), 6403–6408. https://doi.org/10.1073/pnas.0307697101

North, B. J., Rosenberg, M. A., Jeganathan, K. B., Hafner, A. V, Michan, S., Dai, J., … Sinclair, D. A. (2014). SIRT2 induces the checkpoint kinase BubR1 to increase lifespan. *The EMBO Journal*, *33*(13), 1438–1453. https://doi.org/10.15252/embj.201386907

North, B. J., Marshall, B. L., Borra, M. T., Denu, J. M., & Verdin, E. (2003). The human Sir2 ortholog, SIRT2, is an NAD+-dependent tubulin deacetylase. *Molecular Cell*, *11*(2), 437–444. https://doi.org/10.1016/S1097-2765(03)00038-8

North, B. J., & Verdin, E. (2007). Interphase nucleo-cytoplasmic shuttling and localization of SIRT2 during mitosis. *PLoS ONE*, *2*(8). https://doi.org/10.1371/journal.pone.0000784

Novoselov, S. S., Mustill, W. J., Gray, A. L., Dick, J. R., Kanuga, N., Kalmar, B., … Cheetham, M. E. (2013). Molecular chaperone mediated late-stage neuroprotection in the SOD1G93A mouse model of amyotrophic lateral sclerosis. *PLoS ONE*, *8*(8), e73944. https://doi.org/10.1371/journal.pone.0073944

Olzscha, H., Schermann, S. M., Woerner, A. C., Pinkert, S., Hecht, M. H., Tartaglia, G. G., … Vabulas, R. M. (2011). Amyloid-like aggregates sequester numerous metastable proteins with essential cellular functions. *Cell*, *144*(1), 67–78. https://doi.org/10.1016/j.cell.2010.11.050

Orr, A. L., Li, S., Wang, C. E., Li, H., Wang, J., Rong, J., … Li, X. J. (2008). N-terminal mutant huntingtin associates with mitochondria and impairs mitochondrial trafficking. *Journal of Neuroscience*, *28*(11), 2783–2792. https://doi.org/10.1523/JNEUROSCI.0106-08.2008

Orr, A. L., Huang, S., Roberts, M. A., Reed, J. C., Li, S., & Li, X. J. (2008). Sex-dependent effect of BAG1 in ameliorating motor deficits of Huntington disease transgenic mice. *Journal of Biological Chemistry*, *283*(23), 16027–16036. https://doi.org/10.1074/jbc.M710606200

Ortega, Z., & Lucas, J. J. (2014). Ubiquitin-proteasome system involvement in Huntington's disease. *Frontiers in Molecular Neuroscience*, *7*(SEP), 1–11. https://doi.org/10.3389/fnmol.2014.00077

Palfi, S., Brouillet, E., Jarraya, B., Bloch, J., Jan, C., Shin, M., … Déglon, N. (2007). Expression of mutated huntingtin fragment in the putamen is sufficient to produce abnormal movement in non-human primates. *Molecular Therapy*, *15*(8), 1444–1451. https://doi.org/10.1038/sj.mt.6300185

Pallos, J., Bodai, L., Lukacsovich, T., Purcell, J. M., Steffan, J. S., Thompson, L. M., & Marsh, J. L. (2008). Inhibition of specific HDACs and sirtuins suppresses pathogenesis in a Drosophila model of Huntington's disease. *Human Molecular Genetics*, *17*(23), 3767–3775. https://doi.org/10.1093/hmg/ddn273

Palpagama, T. H., Waldvogel, H. J., Faull, R. L. M., & Kwakowsky, A. (2019). The role of microglia and astrocytes in Huntington's disease. *Frontiers in Molecular Neuroscience*, *12*(October), 1–15. https://doi.org/10.3389/fnmol.2019.00258

Parker, J. A., Arango, M., Abderrahmane, S., Lambert, E., Tourette, C., Catoire, H., & Néri, C. (2005). Resveratrol rescues mutant polyglutamine cytotoxicity in nematode and mammalian neurons. *Nature Genetics*, *37*(4), 349–350. https://doi.org/10.1038/ng1534

Paulsen, J. S., Ph, D., Long, J. D., Ph, D., Ross, C. A., Harrington, L., … Ph, D. (2014). Prediction of manifest Huntington disease with clinical and imaging measures: A 12-year prospective observational study. *Lancet Neurology*, *13*(12), 1193–1201. https://doi.org/10.1016/S1474-4422(14)70238-8.

Peng, Q., Wu, B., Jiang, M., Jin, J., Hou, Z., Zheng, J., … Duan, W. (2016). Characterization of behavioral, neuropathological, brain metabolic and key molecular changes in zQ175 knock-in mouse model of Huntington's disease. *PLoS ONE*, *11*(2). https://doi.org/10.1371/journal.pone.0148839

Perrin, V., Régulier, E., Abbas-Terki, T., Hassig, R., Brouillet, E., Aebischer, P., … Déglon, N. (2007). Neuroprotection by Hsp104 and Hsp27 in lentiviral-based rat models of Huntington's disease. *Molecular Therapy*, *15*(5), 903–911. https://doi.org/10.1038/mt.sj.6300141

Peterson, L. B., & Blagg, B. S. (2009). To fold or not to fold: Modulation and consequences of Hsp90 inhibition. *Future Medicinal Chemistry*, *1*(2), 267–283. https://doi.org/10.4155/fmc.09.17

Picard, F., Kurtev, M., & Chung, N. (2004). Sirt1 promotes fat mobilization in white adipocytes by repressing PPAR-γ. *Nature*, *23*(1), 1–7. https://doi.org/10.1038/nature02583.Sirt1

Pinho, B. R., Almeida, L. M., Duchen, M. R., & Oliveira, J. M. A. (2021). Allosteric activation of Hsp70 reduces mutant huntingtin levels, the clustering of N-terminal fragments, and their nuclear accumulation. *Life Sciences*, *285*. https://doi.org/10.1016/j.lfs.2021.120009

Pinto, R. M., Arning, L., Giordano, J. V., Razghandi, P., Andrew, M. A., Gillis, T., … Wheeler, V. C. (2020). Patterns of CAG repeat instability in the central nervous system and periphery in Huntington's disease and in spinocerebellar ataxia type 1. *Human Molecular Genetics*, *29*(15), 2551–2567. https://doi.org/10.1093/hmg/ddaa139

Pinto, R. M., Dragileva, E., Kirby, A., Lloret, A., Lopez, E., St. Claire, J., … Wheeler, V. C. (2013). Mismatch repair genes *Mlh1* and *Mlh3* modify CAG instability in Huntington's disease mice: genome-wide and candidate approaches. *PLoS Genetics*, *9*(10). https://doi.org/10.1371/journal.pgen.1003930

Pouladi, M. A., Morton, A. J., & Hayden, M. R. (2013). Choosing an animal model for the study of Huntington's disease. *Nature Reviews Neuroscience*, *14*(10), 708–721. https://doi.org/10.1038/nrn3570

Pouladi, M. A., Stanek, L. M., Xie, Y., Franciosi, S., Southwell, A. L., Deng, Y., … Hayden, M. R. (2012). Marked differences in neurochemistry and aggregates despite similar behavioural and neuropathological features of Huntington disease in the full-length BACHD and YAC128 mice. *Human Molecular Genetics*, *21*(10), 2219–2232. https://doi.org/10.1093/hmg/dds037

Powers, E. T., Morimoto, R. I., Dillin, A., Kelly, J. W., & Balch, W. E. (2009). Biological and chemical approaches to diseases of proteostasis deficiency. *Annual Review*

of Biochemistry, *78*(1), 959–991. https://doi.org/10.1146/annurev.biochem.052308.114844

Prahlad, V., Cornelius, T., & Morimoto, R. I. (2008). Regulation of the cellular heat shock response in *Caenorhabditis elegans* by thermosensory neurons. *Science*, *320*(5877), 811–814. https://doi.org/10.1126/science.1156093

Prakash, S., & Matouschek, A. (2004). Protein unfolding in the cell. *Trends in Biochemical Sciences*, *29*(11), 593–600. https://doi.org/10.1016/j.tibs.2004.09.011

Pratt, W. B., Gestwicki, J. E., Osawa, Y., & Lieberman, A. P. (2015). Targeting Hsp90/Hsp70-based protein quality control for treatment of adult onset neurodegenerative diseases. *Annual Review of Pharmacology and Toxicology*, *55*(1), 353–371. https://doi.org/10.1146/annurev-pharmtox-010814-124332

Putcha, P., Danzer, K. M., Kranich, L. R., Scott, A., Silinski, M., Mabbett, S., … McLean, P. J. (2010). Brain-permeable small-molecule inhibitors of Hsp90 prevent alpha-synuclein oligomer formation and rescue alpha-synuclein-induced toxicity. *Journal of Pharmacology and Experimental Therapeutics*, *332*(3), 849–857. https://doi.org/10.1124/jpet.109.158436

Qi, L., Zhang, X. D., Wu, J. C., Lin, F., Wang, J., DiFiglia, M., & Qin, Z. H. (2012). The role of chaperone-mediated autophagy in huntingtin degradation. *PLoS ONE*, *7*(10), 1–16. https://doi.org/10.1371/journal.pone.0046834

Qin, Z. H., Wang, Y., Kegel, K. B., Kazantsev, A., Apostol, B. L., Thompson, L. M., … DiFiglia, M. (2003). Autophagy regulates the processing of amino terminal huntingtin fragments. *Human Molecular Genetics*, *12*(24), 3231–3244. https://doi.org/10.1093/hmg/ddg346

Rabindran, S. K., Haroun, R. I., Clos, J., Wisniewski, J., Rabindran, S. K., Haroun, R., … Wut, C. (1993). Regulation of heat shock factor trimer formation: role of a

conserved leucine zipper. *Science*, *259*(5092), 230–234. Retrieved from https://www.jstor.org/stable/2880574

Ramdzan, Y. M., Trubetskov, M. M., Ormsby, A. R., Newcombe, E. A., Sui, X., Tobin, M. J., … Hatters, D. M. (2017). Huntingtin inclusions trigger cellular quiescence, deactivate apoptosis, and lead to delayed necrosis. *Cell Reports*, *19*(5), 919–927. https://doi.org/10.1016/j.celrep.2017.04.029

Ratovitski, T., O'Meally, R. N., Jiang, M., & Chaerkady, R. (2017). Post-translational modifications (PTMs), identified on endogenous huntingtin, cluster within proteolytic domains between HEAT repeats. *Journal or Proteome Research* (Vol. 176). https://doi.org/10.1021/acs.jproteome.6b00991.Supplementary

Rattray, I., Smith, E. J., Crum, W. R., Walker, T. A., Gale, R., Bates, G. P., & Modo, M. (2017). Correlations of behavioral deficits with brain pathology assessed through longitudinal MRI and histopathology in the *Hdh*Q150/Q150 mouse model of Huntington's disease. *PLoS ONE* (Vol. 12). https://doi.org/10.1371/journal.pone.0168556

Rattray, I., Smith, E., Gale, R., Matsumoto, K., Bates, G. P., & Modo, M. (2013). Correlations of Behavioral deficits with brain pathology assessed through longitudinal MRI and histopathology in the R6/2 mouse model of HD. *PLoS ONE*, *8*(4). https://doi.org/10.1371/journal.pone.0060012

Ravikumar, B., Duden, R., & Rubinsztein, D. C. (2002). Aggregate-prone proteins with polyglutamine and polyalanine expansions are degraded by autophagy. *Human Molecular Genetics*, *11*(9), 1107–1117. https://doi.org/10.1093/hmg/11.9.1107

Ravikumar, B., Vacher, C., Berger, Z., Davies, J. E., Luo, S., Oroz, L. G., … Rubinsztein, D. C. (2004). Inhibition of mTOR induces autophagy and reduces toxicity of polyglutamine expansions in fly and mouse models of Huntington disease. *Nature Genetics*, *36*(6), 585–595. https://doi.org/10.1038/ng1362

Raychaudhuri, S., Loew, C., Körner, R., Pinkert, S., Theis, M., Hayer-Hartl, M., … Hartl, F. U. (2014). Interplay of acetyltransferase EP300 and the proteasome system in regulating heat shock transcription factor 1. *Cell*, *156*(5), 975–985. https://doi.org/10.1016/j.cell.2014.01.055

Raynes, R., Pombier, K. M., Nguyen, K., Brunquell, J., Mendez, J. E., & Westerheide, S. D. (2013). The SIRT1 modulators AROS and DBC1 regulate HSF1 activity and the heat shock response. *PLoS ONE*, *8*(1). https://doi.org/10.1371/journal.pone.0054364

Reid, S. J., Patassini, S., Handley, R. R., Rudiger, S. R., McLaughlan, C. J., Osmand, A., … Snell, R. G. (2013). Further molecular characterisation of the OVT73 transgenic sheep model of huntington's disease identifies cortical aggregates. *Journal of Huntington's Disease*, *2*(3), 279–295. https://doi.org/10.3233/JHD-130067

Reis, S. D., Pinho, B. R., & Oliveira, J. M. A. (2017). Modulation of molecular chaperones in Huntington's disease and other polyglutamine disorders. *Molecular Neurobiology*, *54*(8), 5829–5854. https://doi.org/10.1007/s12035-016-0120-z

Ribchester, R. R., Thomson, D., Wood, N. I., Hinks, T., Gillingwater, T. H., Wishart, T. M., … Morton, A. J. (2004). Progressive abnormalities in skeletal muscle and neuromuscular junctions of transgenic mice expressing the Huntington's disease mutation. *European Journal of Neuroscience*, *20*(11), 3092–3114. https://doi.org/10.1111/j.1460-9568.2004.03783.x

Rimoldi, M., Servadio, A., & Zimarino, V. (2001). Analysis of heat shock transcription factor for suppression of polyglutamine toxicity. *Brain Research Bulletin*, *56*(3–4), 353–362. https://doi.org/10.1016/S0361-9230(01)00602-5

Riva, L., Koeva, M., Yildirim, F., Pirhaji, L., Dinesh, D., Mazor, T., … Fraenkel, E. (2012). Polyglutamine expanded huntingtin dramatically alters the genome-wide

binding of HSF1. *Journal of Huntington's Disease*, *1*(1), 33–45. https://doi.org/10.3233/JHD-2012-120020

Rodgers, J. T., Lerin, C., Haas, W., Gygi, S. P., Spiegelman, B. M., & Puigserver, P. (2005). Nutrient control of glucose homeostasis through a complex of PGC-1α and SIRT1. *Nature*, *434*(7029), 113–118. https://doi.org/10.1038/nature03354

Rodgers, J. T., & Puigserver, P. (2007). Fasting-dependent glucose and lipid metabolic response through hepatic sirtuin 1. *PNAS*, *104*(31), 12861–12866. https://doi.org/10.1073/pnas.0702509104

Rodrigues, F. B., & Wild, E. J. (2020). Huntington's Disease Clinical Trials Corner: April 2020. *Journal of Huntington's Disease*, *9*(2), 185–197. https://doi.org/10.3233/JHD-200002

Rodrigues, F. B., Byrne, L., McColgan, P., Robertson, N., Tabrizi, S. J., Leavitt, B. R., … Wild, E. J. (2016). Cerebrospinal fluid total tau concentration predicts clinical phenotype in Huntington's disease. *Journal of Neurochemistry*, *139*(1), 22–25. https://doi.org/10.1111/jnc.13719

Rodríguez-González, C., Lin, S., Arkan, S., & Hansen, C. (2020). Co-chaperones DNAJA1 and DNAJB6 are critical for regulation of polyglutamine aggregation. *Scientific Reports*, *10*(1), 1–9. https://doi.org/10.1038/s41598-020-65046-5

Rogov, V., Dötsch, V., Johansen, T., & Kirkin, V. (2014). Interactions between autophagy receptors and ubiquitin-like proteins form the molecular basis for selective autophagy. *Molecular Cell*, *53*(2), 167–178. https://doi.org/10.1016/j.molcel.2013.12.014

Rosenzweig, R., Nillegoda, N. B., Mayer, M. P., & Bukau, B. (2019). The Hsp70 chaperone network. *Nature Reviews Molecular Cell Biology*, *20*(11), 665–680. https://doi.org/10.1038/s41580-019-0133-3

Rothgiesser, K. M., Erener, S., Waibel, S., Lüscher, B., & Hottiger, M. O. (2010). SIRT2 regulates NF-κB-dependent gene expression through deacetylation of p65 Lys310. *Journal of Cell Science*, *123*(24), 4251–4258. https://doi.org/doi:10.1242/jcs.073783

Rujano, M. A., Kampinga, H. H., & Salomons, F. A. (2007). Modulation of polyglutamine inclusion formation by the Hsp70 chaperone machine. *Experimental Cell Research*, *313*(16), 3568–3578. https://doi.org/10.1016/j.yexcr.2007.07.034

Saitoh, Y., Fujikake, N., Okamoto, Y., Akiko Popiel, H., Hatanaka, Y., Ueyama, M., … Nagai, Y. (2015). P62 Plays a protective role in the autophagic degradation of polyglutamine protein oligomers in polyglutamine disease model flies. *Journal of Biological Chemistry*, *290*(3), 1442–1453. https://doi.org/10.1074/jbc.M114.590281

Sala, A. J., Bott, L. C., & Morimoto, R. I. (2017). Shaping proteostasis at the cellular, tissue, and organismal level. *Journal of Cell Biology*, *216*(5), 1231–1241. https://doi.org/10.1083/jcb.201612111

Santagata, S., Hu, R., Lin, N. U., Mendillo, M. L., Collins, L. C., Hankinson, S. E., … Ince, T. A. (2011). High levels of nuclear heat-shock factor 1 (HSF1) are associated with poor prognosis in breast cancer. *PNAS*, *108*(45), 18378–18383. https://doi.org/10.1073/pnas.1115031108

Sarkar, S., Ravikumar, B., Floto, R. A., & Rubinsztein, D. C. (2009). Rapamycin and mTOR-independent autophagy inducers ameliorate toxicity of polyglutamine-expanded huntingtin and related proteinopathies. *Cell Death and Differentiation*, *16*(1), 46–56. https://doi.org/10.1038/cdd.2008.110

Sasaki, T., Maier, B., Koclega, K. D., Chruszcz, M., Gluba, W., Stukenberg, P. T., … Scrable, H. (2008). Phosphorylation regulates SIRT1 function. *PLoS ONE*, *3*(12). https://doi.org/10.1371/journal.pone.0004020

Sasi, B. K., Sonawane, P. J., Gupta, V., Sahu, B. S., & Mahapatra, N. R. (2014). Coordinated transcriptional regulation of *Hspa1a* gene by multiple transcription factors: Crucial roles for HSF-1, NF-Y, NF-κB, and CREB. *Journal of Molecular Biology*, *426*(1), 116–135. https://doi.org/10.1016/j.jmb.2013.09.008

Sathasivam, K., Neueder, A., Gipson, T. A., Landles, C., Benjamin, A. C., Bondulich, M. K., … Bates, G. P. (2013). Aberrant splicing of HTT generates the pathogenic exon 1 protein in Huntington disease. *PNAS*, *110*(6), 2366–2370. https://doi.org/10.1073/pnas.1221891110

Sathasivam, K., Hobbs, C., Turmaine, M., Mangiarini, L., Mahal, A., Bertaux, F., … Bates, G. P. (1999). Formation of polyglutamine inclusions in non-CNS tissue. *Human Molecular Genetics*, *8*(5), 813–822. https://doi.org/10.1093/hmg/8.5.813

Sathasivam, K., Lane, A., Legleiter, J., Warley, A., Woodman, B., Finkbeiner, S., … Bates, G. P. (2010). Identical oligomeric and fibrillar structures captured from the brains of R6/2 and knock-in mouse models of Huntington's disease. *Human Molecular Genetics*, *19*(1), 65–78. https://doi.org/10.1093/hmg/ddp467

Satoh, A., Brace, C. S., Ben-Josef, G., West, T., Wozniak, D. F., Holtzman, D. M., … Imai, S. -i. (2010). SIRT1 promotes the central adaptive response to diet restriction through activation of the dorsomedial and lateral nuclei of the hypothalamus. *Journal of Neuroscience*, *30*(30), 10220–10232. https://doi.org/10.1523/JNEUROSCI.1385-10.2010

Saudou, F., & Humbert, S. (2016). The biology of huntingtin. *Neuron*, *89*(5), 910–926. https://doi.org/10.1016/j.neuron.2016.02.003

Sauve, A. A., Moir, R. D., Schramm, V. L., & Willis, I. M. (2005). Chemical activation of Sir2-dependent silencing by relief of nicotinamide inhibition. *Molecular Cell*, *17*(4), 595–601. https://doi.org/10.1016/j.molcel.2004.12.032

Sauve, A. A., Wolberger, C., Schramm, V. L., & Boeke, J. D. (2006). The biochemistry of sirtuins. *Annual Review of Biochemistry*, *75*, 435–465. https://doi.org/10.1146/annurev.biochem.74.082803.133500

Scher, M. B., Vaquero, A., & Reinberg, D. (2007). SirT3 is a nuclear NAD+-dependent histone deacetylase that translocates to the mitochondria upon cellular stress. *Genes and Development*, *21*(8), 920–928. https://doi.org/10.1101/gad.1527307

Scherz-Shouval, R., Santagata, S., Mendillo, M. L., Sholl, L. M., Ben-Aharon, I., Beck, A. H., … Lindquist, S. (2014). The reprogramming of tumor stroma by HSF1 is a potent enabler of malignancy. *Cell*, *158*(3), 564–578. https://doi.org/10.1016/j.cell.2014.05.045

Scherzinger, E., Lurz, R., Turmaine, M., Mangiarini, L., Hollenbach, B., Hasenbank, R., … Wanker, E. E. (1997). Huntingtin-encoded polyglutamine expansions form amyloid-like protein aggregates *in vitro* and *in vivo*. *Cell*, *90*(3), 549–558. https://doi.org/10.1016/S0092-8674(00)80514-0

Scherzinger, E., Sittler, A., Schweiger, K., Heiser, V., Lurz, R., Hasenbank, R., … Wanker, E. E. (1999). Self-assembly of polyglutamine-containing huntingtin fragments into amyloid-like fibrils: Implications for Huntington's disease pathology. *PNAS*, *96*(8), 4604–4609. https://doi.org/10.1073/pnas.96.8.4604

Schilling, G., Becher, M. W., Sharp, A. H., Jinnah, H. A., Duan, K., Kotzuk, J. A., … Borchelt, D. R. (1999). Intranuclear inclusions and neuritic aggregates in transgenic mice expressing a mutant N-terminal fragment of huntingtin. *Human Molecular Genetics*, *8*(3), 397–407. https://doi.org/10.1093/hmg/8.3.397

Schultz, J. L., Moser, A. D., & Nopoulos, P. C. (2020). The association between CAG repeat length and age of onset of juvenile-onset Huntington's disease. *Brain Sciences*, *10*(9), 1–7. https://doi.org/10.3390/brainsci10090575

Scior, A., Buntru, A., Arnsburg, K., Ast, A., Iburg, M., Juenemann, K., … Kirstein, J. (2018). Complete suppression of Htt fibrilization and disaggregation of Htt fibrils

by a trimeric chaperone complex. *The EMBO Journal*, *37*(2), 282–299. https://doi.org/10.15252/embj.201797212

Serwetnyk, M. A., & Blagg, B. S. J. (2021). The disruption of protein−protein interactions with co-chaperones and client substrates as a strategy towards Hsp90 inhibition. *Acta Pharmaceutica Sinica B*, *11*(6), 1446–1468. https://doi.org/10.1016/j.apsb.2020.11.015

Shahmoradian, S. H., Galaz-Montoya, J. G., Schmid, M. F., Cong, Y., Ma, B., Spiess, C., … Chiu, W. (2013). TRiC's tricks inhibit huntingtin aggregation. *ELife*, *2013*(2), 1–17. https://doi.org/10.7554/eLife.00710

Shen, K., Calamini, B., Fauerbach, J. A., Ma, B., Shahmoradian, S. H., Serrano Lachapel, I. L., … Frydman, J. (2016). Control of the structural landscape and neuronal proteotoxicity of mutant Huntingtin by domains flanking the polyQ tract. *ELife*, *5*(OCTOBER2016), 1–29. https://doi.org/10.7554/eLife.18065

Shi, T., Wang, F., Stieren, E., & Tong, Q. (2005). SIRT3, a mitochondrial sirtuin deacetylase, regulates mitochondrial function and thermogenesis in brown adipocytes. *Journal of Biological Chemistry*, *280*(14), 13560–13567. https://doi.org/10.1074/jbc.M414670200

Shi, Y., Mosser, D. D., & Morimoto, R. I. (1998). Molecular chaperones as HSF1-specific transcriptional repressors. *Genes and Development*, *12*(5), 654–666. https://doi.org/10.1101/gad.12.5.654

Shibata, M., Lu, T., Furuya, T., Degterev, A., Mizushima, N., Yoshimori, T., … Yuan, J. (2006). Regulation of intracellular accumulation of mutant huntingtin by beclin 1. *Journal of Biological Chemistry*, *281*(20), 14474–14485. https://doi.org/10.1074/jbc.M600364200

Shin, J. W., Kim, K. H., Chao, M. J., Atwal, R. S., Gillis, T., MacDonald, M. E., … Lee, J. M. (2016). Permanent inactivation of Huntington's disease mutation by

personalized allele-specific CRISPR/Cas9. *Human Molecular Genetics*, *25*(20), 4566–4576. https://doi.org/10.1093/hmg/ddw286

Shirasaki, D. I., Greiner, E. R., Al-Ramahi, I., Gray, M., Boontheung, P., Geschwind, D. H., … Yang, X. W. (2012). Network organization of the huntingtin proteomic interactome in mammalian brain. *Neuron*, *75*(1), 41–57. https://doi.org/10.1016/j.neuron.2012.05.024

Shorter, J. (2011). The mammalian disaggregase machinery: Hsp110 synergizes with Hsp70 and Hsp40 to catalyze protein disaggregation and reactivation in a cell-free system. *PLoS ONE*, *6*(10). https://doi.org/10.1371/journal.pone.0026319

Sieradzan, K. A., Mechan, A. O., Jones, L., Wanker, E. E., Nukina, N., & Mann, D. M. A. (1999). Huntington's disease intranuclear inclusions contain truncated, ubiquitinated huntingtin protein. *Experimental Neurology*, *156*(1), 92–99. https://doi.org/10.1006/exnr.1998.7005

Sinnige, T., Yu, A., & Morimoto, R. I. (2020). Challenging proteostasis: role of the chaperone network to control aggregation-prone proteins in human disease. *Advances in Experimental Medicine and Biology*, *1243*, 53–68. https://doi.org/10.1007/978-3-030-40204-4_4.

Sittler, A., Lurz, R., Lueder, G., Priller, J., Hayer-Hartl, M. K., Hartl, F. U., … Wanker, E. E. (2001). Geldanamycin activates a heat shock response and inhibits huntingtin aggregation in a cell culture model of Huntington's disease. *Human Molecular Genetics*, *10*(12), 1307–1315. https://doi.org/10.1093/hmg/10.12.1307

Slow, E. J., van Raamsdonk, J., Rogers, D., Coleman, S. H., Graham, R. K., Deng, Y., … Hayden, M. R. (2003). Selective striatal neuronal loss in a YAC128 mouse model of Huntington disease. *Human Molecular Genetics*, *12*(13), 1555–1567. https://doi.org/10.1093/hmg/ddg169

Smith, G. A., Rocha, E. M., McLean, J. R., Hayes, M. A., Izen, S. C., Isacson, O., & Hallett, P. J. (2014). Progressive axonal transport and synaptic protein changes correlate

with behavioral and neuropathological abnormalities in the heterozygous Q175 KI mouse model of Huntington's disease. *Human Molecular Genetics*, *23*(17), 4510–4527. https://doi.org/10.1093/hmg/ddu166

Smith, H. L., Li, W., & Cheetham, M. E. (2015). Molecular chaperones and neuronal proteostasis. *Seminars in Cell and Developmental Biology*, *40*, 142–152. https://doi.org/10.1016/j.semcdb.2015.03.003

Smith, M. R., Syed, A., Lukacsovich, T., Purcell, J., Barbaro, B. A., Worthge, S. A., … Marsh, J. L. (2014). A potent and selective sirtuin 1 inhibitor alleviates pathology in multiple animal and cell models of huntington's disease. *Human Molecular Genetics*, *23*(11), 2995–3007. https://doi.org/10.1093/hmg/ddu010

Soares, T. R., Reis, S. D., Pinho, B. R., Duchen, M. R., & Oliveira, J. M. A. (2019). Targeting the proteostasis network in Huntington's disease. *Ageing Research Reviews*, *49*(July 2018), 92–103. https://doi.org/10.1016/j.arr.2018.11.006

Southwell, A. L., Kordasiewicz, H. B., Langbehn, D., Skotte, N. H., Parsons, M. P., Villanueva, E. B., … Hayden, M. R. (2018). Huntingtin suppression restores cognitive function in a mouse model of Huntington's disease. *Science Translational Medicine*, *10*(461), 1–13. https://doi.org/10.1126/scitranslmed.aar3959

Spreafico, A., Delord, J. P., De Mattos-Arruda, L., Berge, Y., Rodon, J., Cottura, E., … Cortes, J. (2015). A first-in-human phase I, dose-escalation, multicentre study of HSP990 administered orally in adult patients with advanced solid malignancies. *British Journal of Cancer*, *112*(4), 650–659. https://doi.org/10.1038/bjc.2014.653

Stanek, L. M., Yang, W., Angus, S., Sardi, P. S., Hayden, M. R., Hung, G. H., … Shihabuddin, L. S. (2013). Antisense oligonucleotide-mediated correction of transcriptional dysregulation is correlated with behavioral benefits in the

YAC128 mouse model of huntington's disease. *Journal of Huntington's Disease*, *2*(2), 217–228. https://doi.org/10.3233/JHD-130057

Steffan, J. S., Agrawal, N., Pallos, J., Rockabrand, E., Trotman, L. C., Slepko, N., … Marsh, J. L. (2004). SUMO modification of huntingtin and Huntington's disease pathology. *Science*, *304*(5667), 100–104. https://doi.org/10.1126/science.1092194

Steffan, J. S., Kazantsev, A., Spasic-Boskovic, O., Greenwald, M., Zhu, Y. Z., Gohler, H., … Thompson, L. M. (2000). The Huntington's disease protein interacts with p53 and CREB-binding protein and represses transcription. *PNAS*, *97*(12), 6763–6768. https://doi.org/10.1073/pnas.100110097

Stünkel, W., & Campbell, R. M. (2011). Sirtuin 1 (SIRT1): The misunderstood HDAC. *Journal of Biomolecular Screening*, *16*(10), 1153–1169. https://doi.org/10.1177/1087057111422103

Su, K. H., Dai, S., Tang, Z., Xu, M., & Dai, C. (2019). Heat shock factor 1 is a direct antagonist of AMP-Activated protein kinase. *Molecular Cell*, *76*(4), 546-561.e8. https://doi.org/10.1016/j.molcel.2019.08.021

Swami, M., Hendricks, A. E., Gillis, T., Massood, T., Mysore, J., Myers, R. H., & Wheeler, V. C. (2009). Somatic expansion of the Huntington's disease CAG repeat in the brain is associated with an earlier age of disease onset. *Human Molecular Genetics*, *18*(16), 3039–3047. https://doi.org/10.1093/hmg/ddp242

Tabrizi, S. J., Flower, M. D., Ross, C. A., & Wild, E. J. (2020). Huntington disease: new insights into molecular pathogenesis and therapeutic opportunities. *Nature Reviews Neurology*, *16*(10), 529–546. https://doi.org/10.1038/s41582-020-0389-4

Tabrizi, S. J., Ghosh, R., & Leavitt, B. R. (2019). Huntingtin lowering strategies for disease modification in Huntington's disease. *Neuron*, *101*(5), 801–819. https://doi.org/10.1016/j.neuron.2019.01.039

Tabrizi, S. J., Leavitt, B. R., Landwehrmeyer, G. B., Wild, E. J., Saft, C., Barker, R. A., … Lane, R. M. (2019). Targeting huntingtin expression in patients with Huntington's disease. *New England Journal of Medicine*, *380*(24), 2307–2316. https://doi.org/10.1056/nejmoa1900907

Tabrizi, S. J., Scahill, R. I., Owen, G., Durr, A., Leavitt, B. R., Roos, R. A., … Langbehn, D. R. (2013). Predictors of phenotypic progression and disease onset in premanifest and early-stage Huntington's disease in the TRACK-HD study: Analysis of 36-month observational data. *The Lancet Neurology*, *12*(7), 637–649. https://doi.org/10.1016/S1474-4422(13)70088-7

Taipale, M., Krykbaeva, I., Koeva, M., Kayatekin, C., Westover, K. D., Karras, G. I., & Lindquist, S. (2012). Quantitative analysis of Hsp90-client interactions reveals principles of substrate recognition. *Cell*, *150*(5), 987–1001. https://doi.org/10.1016/j.cell.2012.06.047

Takahashi, T., Kikuchi, S., Katada, S., Nagai, Y., Nishizawa, M., & Onodera, O. (2008). Soluble polyglutamine oligomers formed prior to inclusion body formation are cytotoxic. *Human Molecular Genetics*, *17*(3), 345–356. https://doi.org/10.1093/hmg/ddm311

Tam, S., Geller, R., Spiess, C., & Frydman, J. (2006). The chaperonin TRiC controls polyglutamine aggregation and toxicity through subunit-specific interactions. *Nat Cell Biol.*, *8*(10), 1155–1162. https://doi.org/10.1038/ncb1477

Tang, Z., Dai, S., He, Y., Doty, R. A., Shultz, L. D., Sampson, S. B., & Dai, C. (2015). MEK guards proteome stability and inhibits tumor-suppressive amyloidogenesis via HSF1. *Cell*, *160*(4), 729–744. https://doi.org/10.1016/j.cell.2015.01.028

Tanner, K. G., Landry, J., Sternglanz, R., & Denu, J. M. (2000). Silent information regulator 2 family of NAD-dependent histone/protein deacetylases generates a unique product, 1-O-acetyl-ADP-ribose. *PNAS*, *97*(26), 14178–14182. https://doi.org/10.1073/pnas.250422697

Tanno, M., Sakamoto, J., Miura, T., Shimamoto, K., & Horio, Y. (2007). Nucleocytoplasmic shuttling of the NAD+-dependent histone deacetylase SIRT1. *Journal of Biological Chemistry*, *282*(9), 6823–6832. https://doi.org/10.1074/jbc.M609554200

Telenius, H., Kremer, H. P. H., Thellmann, J., Andrew, S. E., Almqvist, E., Anvret, M., … Hayden, M. R. (1993). Molecular analysis of juvenile Huntington disease: The major influence on (CAG)n repeat length is the sex of the affected parent. *Human Molecular Genetics*, *2*(10), 1535–1540. https://doi.org/10.1093/hmg/2.10.1535

Thakur, A. K., Jayaraman, M., Mishra, R., Thakur, M., Chellgren, V. M., L Byeon, I. J., … Wetzel, R. (2009). Polyglutamine disruption of the huntingtin exon 1 N terminus triggers a complex aggregation mechanism. *Nature Structural and Molecular Biology*, *16*(4), 380–389. https://doi.org/10.1038/nsmb.1570

The Huntington's disease collaborative research group. (1993). A novel gene containing a trinucleotide repeat that is expanded and unstable on Huntington's disease chromosomes. *Cell*, *72*(6), 971–983. https://doi.org/10.1016/0092-8674(93)90585-E

Tomé, S., Manley, K., Simard, J. P., Clark, G. W., Slean, M. M., Swami, M., … Pearson, C. E. (2013). MSH3 polymorphisms and protein levels affect CAG repeat instability in Huntington's disease mice. *PLoS Genetics*, *9*(2). https://doi.org/10.1371/journal.pgen.1003280

Tomita, T., Hamazaki, J., Hirayama, S., McBurney, M. W., Yashiroda, H., & Murata, S. (2015). Sirt1-deficiency causes defective protein quality control. *Scientific Reports*, *5*, 1–9. https://doi.org/10.1038/srep12613

Tomoshige, S., Nomura, S., Ohgane, K., Hashimoto, Y., & Ishikawa, M. (2017). Discovery of small molecules that induce the degradation of huntingtin.

Angewandte Chemie - International Edition, *56*(38), 11530–11533. https://doi.org/10.1002/anie.201706529

Trepel, J., Mollapour, M., Giaccone, G., & Neckers, L. (2010). Targeting the dynamic HSP90 complex in cancer. *Nature Reviews Cancer*, *10*(8), 537–549. https://doi.org/10.1038/nrc2887

Truant, R., Atwal, R. S., & Burtnik, A. (2007). Nucleocytoplasmic trafficking and transcription effects of huntingtin in Huntington's disease. *Progress in Neurobiology*, *83*(4), 211–227. https://doi.org/10.1016/j.pneurobio.2006.11.004

Trushina, E., Dyer, R. B., Badger, J. D., Ure, D., Eide, L., Tran, D. D., … McMurray, C. T. (2004). Mutant huntingtin impairs axonal trafficking in mammalian neurons *in vivo* and *in vitro*. *Molecular and Cellular Biology*, *24*(18), 8195–8209. https://doi.org/10.1128/mcb.24.18.8195-8209.2004

Tulino, R., Benjamin, A. C., Jolinon, N., Smith, D. L., Chini, E. N., Carnemolla, A., & Bates, G. P. (2016). SIRT1 activity is linked to its brain region-specific phosphorylation and is impaired in Huntington's disease mice. *PLoS ONE*, *11*(1), 1–25. https://doi.org/10.1371/journal.pone.0145425

Vacher, C., Garcia-Oroz, L., & Rubinsztein, D. C. (2005). Overexpression of yeast hsp104 reduces polyglutamine aggregation and prolongs survival of a transgenic mouse model of Huntington's disease. *Human Molecular Genetics*, *14*(22), 3425–3433. https://doi.org/10.1093/hmg/ddi372

Vachey, G., & Déglon, N. (2018). CRISPR/Cas9-mediated genome editing for Huntington's disease. In S. V. Precious, A. E. Rosser, & S. B. Dunnett (Eds.), *Huntington's Disease. Methods in Molecular Biology.* (Vol. 1780, pp. 463–482). Springer Nature. https://doi.org/10.1007/978-1-4939-7825-0_21

Van Raamsdonk, J. M., Murphy, Z., Slow, E. J., Leavitt, B. R., & Hayden, M. R. (2005). Selective degeneration and nuclear localization of mutant huntingtin in the

YAC128 mouse model of Huntington disease. *Human Molecular Genetics*, *14*(24), 3823–3835. https://doi.org/10.1093/hmg/ddi407

Van Raamsdonk, J. M., Pearson, J., Slow, E. J., Hossain, S. M., Leavitt, B. R., & Hayden, M. R. (2005). Cognitive dysfunction precedes neuropathology and motor abnormalities in the YAC128 mouse model of Huntington's disease. *Journal of Neuroscience*, *25*(16), 4169–4180. https://doi.org/10.1523/JNEUROSCI.0590-05.2005

Vaquero, A., Scher, M., Lee, D., Erdjument-Bromage, H., Tempst, P., & Reinberg, D. (2004). Human SirT1 interacts with histone H1 and promotes formation of facultative heterochromatin. *Molecular Cell*, *16*(1), 93–105. https://doi.org/10.1016/j.molcel.2004.08.031

Vaziri, H., Dessain, S. K., Eaton, E. N., Imai, S.-I., Frye, R. A., Pandita, T. K., … Weinberg, R. A. (2001). hSIR2 SIRT1 functions as an NAD-dependent p53 deacetylase. *Cell*, *107*, 149–159.

Verhoef, L. G. G., Lindsten, K., Masucci, M. G., & Dantuma, N. P. (2002). Aggregate formation inhibits proteasomal degradation of polyglutamine proteins. *Human Molecular Genetics*, *11*(22), 2689–2700. https://doi.org/10.1093/hmg/11.22.2689

Vieweg, S., Mahul-Mellier, A.-L., Ruggeri, F. S., Riguet, N., DeGuire, S. M., Chiki, A., … Lashuel, H. A. (2021). The Nt17 domain and its helical conformation regulate the aggregation, cellular properties and neurotoxicity of mutant huntingtin exon 1. *Journal of Molecular Biology*, 167222. https://doi.org/https://doi.org/10.1016/j.jmb.2021.167222

Vihervaara, A., & Sistonen, L. (2014). HSF1 at a glance. *Journal of Cell Science*, *127*(2), 261–266. https://doi.org/10.1242/jcs.132605

Vihervaara, A., Sergelius, C., Vasara, J., Blom, M. A. H., Elsing, A. N., Roos-Mattjus, P., & Sistonen, L. (2013). Transcriptional response to stress in the dynamic

chromatin environment of cycling and mitotic cells. *Proceedings of the National Academy of Sciences of the United States of America*, *110*(36). https://doi.org/10.1073/pnas.1305275110

von Hörsten, S., Schmitt, I., Nguyen, H. P., Holzmann, C., Schmidt, T., Walther, T., … Riess, O. (2003). Transgenic rat model of Huntington's disease. *Human Molecular Genetics*, *12*(6), 617–624. https://doi.org/10.1093/hmg/ddg075

Vonsattel, J. P. G., & DiFiglia, M. (1998). Huntington Disease. *Journal of Neuropathology and Experimental Neurology*, *57*(5), 148–162.

Vos, M. J., Zijlstra, M. P., Kanon, B., van Waarde-Verhagen, M. A. W. H., Brunt, E. R. P., Oosterveld-Hut, H. M. J., … Kampinga, H. H. (2010). HSPB7 is the most potent polyQ aggregation suppressor within the HSPB family of molecular chaperones. *Human Molecular Genetics*, *19*(23), 4677–4693. https://doi.org/10.1093/hmg/ddq398

Vujanac, M., Fenaroli, A., & Zimarino, V. (2005). Constitutive nuclear import and stress-regulated nucleocytoplasmic shuttling of mammalian heat-shock factor 1. *Traffic*, *6*(3), 214–229. https://doi.org/10.1111/j.1600-0854.2005.00266.x

Wacker, J. L., Huang, S.-Y., Steele, A. D., Aron, R., Lotz, G. P., Nguyen, Q., … Muchowski, P. J. (2009). Loss of Hsp70 Exacerbates Pathogenesis But Not Levels of Fibrillar Aggregates in a Mouse Model of Huntington's Disease. *Journal of Neuroscience*, *29*(28), 9104–9114. https://doi.org/10.1523/JNEUROSCI.2250-09.2009

Waelter, S., Boeddrich, A., Lurz, R., Scherzinger, E., Lueder, G., Lehrach, H., & Wanker, E. E. (2001). Accumulation of mutant huntingtin fragments in aggresome-like inclusion bodies as a result of insufficient protein degradation. *Molecular Biology of the Cell*, *12*(5), 1393–1407. https://doi.org/10.1091/mbc.12.5.1393

Wang, A. M., Miyata, Y., Klinedinst, S., Peng, H. M., Chua, J. P., Komiyama, T., … Lieberman, A. P. (2013). Activation of Hsp70 reduces neurotoxicity by promoting

polyglutamine protein degradation. *Nature Chemical Biology*, *9*(2), 112–118. https://doi.org/10.1038/nchembio.1140

Wang, A. M., Morishima, Y., Clapp, K. M., Peng, H. M., Pratt, W. B., Gestwicki, J. E., … Lieberman, A. P. (2010). Inhibition of Hsp70 by methylene blue affects signaling protein function and ubiquitination and modulates polyglutamine protein degradation. *Journal of Biological Chemistry*, *285*(21), 15714–15723. https://doi.org/10.1074/jbc.M109.098806

Wang, G., Liu, X., Gaertig, M. A., Li, S., & Li, X. J. (2016). Ablation of huntingtin in adult neurons is nondeleterious but its depletion in young mice causes acute pancreatitis. *PNAS*, *113*(12), 3359–3364. https://doi.org/10.1073/pnas.1524575113

Wang, Y. L., Liu, W., Wada, E., Murata, M., Wada, K., & Kanazawa, I. (2005). Clinico-pathological rescue of a model mouse of Huntington's disease by siRNA. *Neuroscience Research*, *53*(3), 241–249. https://doi.org/10.1016/j.neures.2005.06.021

Wang, Z., Inuzuka, H., Zhong, J., Wan, L., Fukushima, H., Sarkar, F. H., & Wei, W. (2012). Tumor suppressor functions of FBW7 in cancer development and progression. *FEBS Letters*, *586*(10), 1409–1418. https://doi.org/10.1016/j.febslet.2012.03.017

Wanker, E. E., Ast, A., Schindler, F., Trepte, P., & Schnoegl, S. (2019). The pathobiology of perturbed mutant huntingtin protein–protein interactions in Huntington's disease. *Journal of Neurochemistry*, *151*(4), 507–519. https://doi.org/10.1111/jnc.14853

Watanabe, S., Ageta-Ishihara, N., Nagatsu, S., Takao, K., Komine, O., Endo, F., … Yamanaka, K. (2014). SIRT1 overexpression ameliorates a mouse model of SOD1-linked amyotrophic lateral sclerosis via HSF1/HSP70i chaperone system. *Molecular Brain*, *7*(1), 1–11. https://doi.org/10.1186/s13041-014-0062-1

Waza, M., Adachi, H., Katsuno, M., Minamiyama, M., Sang, C., Tanaka, F., … Sobue, G. (2005). 17-AAG, an Hsp90 inhibitor, ameliorates polyglutamine-mediated motor neuron degeneration. *Nature Medicine*, *11*(10), 1088–1095. https://doi.org/10.1038/nm1298

Wei, Y., Zhao, X., Kariya, Y., Teshigawara, K., & Uchida, A. (1995). Inhibition of proliferation and induction of apoptosis by abrogation of heat-shock protein (HSP) 70 expression in tumor cells. *Cancer Immunology Immunotherapy*, *40*(2), 73–78. https://doi.org/10.1007/BF01520287

Westerheide, S. D., Anckar, J., Stevens, S. M., Sistonen, L., & Morimoto, R. I. (2009). Stress-inducible regulation of heat shock factor 1 by the deacetylase SIRT1. *Science*, *323*(February), 1063–1067. https://doi.org/10.1017/S0967199409990190

Westerheide, S. D., Bosman, J. D., Mbadugha, B. N. A., Kawahara, T. L. A., Matsumoto, G., Kim, S., … Morimoto, R. I. (2004). Celastrols as inducers of the heat shock response and cytoprotection. *Journal of Biological Chemistry*, *279*(53), 56053–56060. https://doi.org/10.1074/jbc.M409267200

Westerheide, S. D., & Morimoto, R. I. (2005). Heat shock response modulators as therapeutic tools for diseases of protein conformation. *Journal of Biological Chemistry*, *280*(39), 33097–33100. https://doi.org/10.1074/jbc.R500010200

Wexler, N. (2004). Venezuelan kindreds reveal that genetic and enviromental factors modulate huntington disease. *PNAS*, *101*(10), 3498–3503. https://doi.org/doi/10.1073/pnas.0308679101

Wheeler, V. C., Auerbach, W., White, J. K., Srinidhi, J., Auerbach, A., Ryan, A., … MacDonald, M. E. (1999). Length-dependent gametic CAG repeat instability in the Huntington's disease knock-in mouse. *Human Molecular Genetics*, *8*(1), 115–122. https://doi.org/10.1093/hmg/8.1.115

Wheeler, V. C., & Dion, V. (2021). Modifiers of CAG/CTG repeat instability: insights from mammalian models. *Journal of Huntington's Disease*, *10*(1), 123–148. https://doi.org/10.3233/JHD-200426

Wheeler, V. C., Lebel, L. A., Vrbanac, V., Teed, A., te Riele, H. T., & MacDonald, M. E. (2003). Mismatch repair gene *Msh2* modifies the timing of early disease in *Hdh*Q111 striatum. *Human Molecular Genetics*, *12*(3), 273–281. https://doi.org/10.1093/hmg/ddg056

Wheeler, V. C., White, J. K., Gutekunst, C. A., Vrbanac, V., Weaver, M., Li, X. J., … MacDonald, M. E. (2000). Long glutamine tracts cause nuclear localization of a novel form of huntingtin in medium spiny striatal neurons in *Hdh*(Q92) and *Hdh*(Q111) knock-in mice. *Human Molecular Genetics*, *9*(4), 503–513. https://doi.org/10.1093/hmg/9.4.503

Wild, E. J., Boggio, R., Langbehn, D., Robertson, N., Haider, S., Miller, J. R. C., … Weiss, A. (2015). Quantification of mutant huntingtin protein in cerebrospinal fluid from Huntington's disease patients. *Journal of Clinical Investigation*, *125*(5), 1979–1986. https://doi.org/10.1172/JCI80743

Wild, E. J., & Tabrizi, S. J. (2017). Therapies targeting DNA and RNA in Huntington's disease. *The Lancet Neurology*, *16*(10), 837–847. https://doi.org/10.1016/S1474-4422(17)30280-6

Woerner, A. C., Frottin, F., Hornburg, D., Feng, L. R., Meissner, F., Patra, M., … Hipp, M. S. (2016). Cytoplasmic protein aggregates interfere with nucleocytoplasmic transport of protein and RNA. *Science*, *351*(6269), 173–176. https://doi.org/10.1126/science.aad2033

Woodman, B., Butler, R., Landles, C., Lupton, M. K., Tse, J., Hockly, E., … Bates, G. P. (2007). The *Hdh*Q150/Q150 knock-in mouse model of HD and the R6/2 exon 1 model develop comparable and widespread molecular phenotypes. *Brain*

Research Bulletin, *72*(2-3 SPEC. ISS.), 83–97. https://doi.org/10.1016/j.brainresbull.2006.11.004

Wu, D., Vonk, J. J., Salles, F., Vonk, D., Haslbeck, M., Melki, R., … Kampinga, H. H. (2019). The N terminus of the small heat shock protein HSPB7 drives its polyQ aggregation-suppressing activity. *Journal of Biological Chemistry*, *294*(25), 9985–9994. https://doi.org/10.1074/jbc.RA118.007117

Wu, J., Liu, T., Rios, Z., Mei, Q., Lin, X., & Cao, S. (2017). Heat shock proteins and cancer. *Trends in Pharmacological Sciences*, *38*(3), 226–256. https://doi.org/10.1016/j.tips.2016.11.009

Wyttenbach, A., Carmichael, J., Swartz, J., Furlong, R. A., Narain, Y., Rankin, J., & Rubinsztein, D. C. (2000). Effects of heat shock, heat shock protein 40 (HDJ-2), and proteasome inhibition on protein aggregation in cellular models of Huntington's disease. *PNAS*, *97*(6), 2898–2903. https://doi.org/10.1073/pnas.97.6.2898

Wyttenbach, A., Sauvageot, O., Carmichael, J., Diaz-Latoud, C., Arrigo, A. P., & Rubinsztein, D. C. (2002). Heat shock protein 27 prevents cellular polyglutamine toxicity and suppresses the increase of reactive oxygen species caused by huntingtin. *Human Molecular Genetics*, *11*(9), 1137–1151. https://doi.org/10.1093/hmg/11.9.1137

Xia, N., Tenzer, S., Lunov, O., Karl, M., Simmet, T., Daiber, A., … Li, H. (2021). Regulation of NADPH oxidase-mediated superoxide production by acetylation and deacetylation. *Frontiers in Physiology*, *12*(August). https://doi.org/10.3389/fphys.2021.693702

Xiao, X. Z., Zuo, X. X., Davis, A. A., McMillan, D. R., Curry, B. B., Richardson, J. A., & Benjamin, I. J. (1999). HSF1 is required for extra-embryonic development,

postnatal growth and protection during inflammatory responses in mice. *EMBO Journal*, *18*(21), 5943–5952. https://doi.org/10.1093/emboj/18.21.5943

Yamanaka, T., Miyazaki, H., Oyama, F., Kurosawa, M., Washizu, C., Doi, H., & Nukina, N. (2008). Mutant Huntingtin reduces HSP70 expression through the sequestration of NF-Y transcription factor. *EMBO Journal*, *27*(6), 827–839. https://doi.org/10.1038/emboj.2008.23

Yan, S., Tu, Z., Liu, Z., Fan, N., Yang, H., Yang, S., … Li, X. J. (2018). A Huntingtin knockin pig model recapitulates features of selective neurodegeneration in Huntington's disease. *Cell*, *173*(4), 989-1002.e13. https://doi.org/10.1016/j.cell.2018.03.005

Yang, H., & Hu, H. Y. (2016). Sequestration of cellular interacting partners by protein aggregates: implication in a loss-of-function pathology. *FEBS Journal*, *283*(20), 3705–3717. https://doi.org/10.1111/febs.13722

Yang, J., Bridges, K., Chen, K. Y., & Liu, A. Y. C. (2008). Riluzole increases the amount of latent HSF1 for an amplified heat shock response and cytoprotection. *PLoS ONE*, *3*(8). https://doi.org/10.1371/journal.pone.0002864

Yang, S., Cheng, P., Banta, H., Piotrowska-, K., Yang, J., Cheng, E. C. H., … Chan, A. W. S. (2008). Towards a transgenic model of Huntington's disease in a non- human primate. *Nature*, *453*(7197), 921–924. https://doi.org/10.1038/nature06975.

Yang, S., Chang, R., Yang, H., Zhao, T., Hong, Y., Kong, H. E., … Li, X. J. (2017). CRISPR/Cas9-mediated gene editing ameliorates neurotoxicity in mouse model of Huntington's disease. *Journal of Clinical Investigation*, *127*(7), 2719–2724. https://doi.org/10.1172/JCI92087

Yu-Taeger, L., Petrasch-Parwez, E., Osmand, A. P., Redensek, A., Metzger, S., Clemens, L. E., … Nguyen, H. P. (2012). A novel BACHD transgenic rat exhibits characteristic neuropathological features of Huntington disease. *Journal of Neuroscience*, *32*(44), 15426–15438. https://doi.org/10.1523/JNEUROSCI.1148-12.2012

Zarouchlioti, C., Parfitt, D. A., Li, W., Gittings, L. M., & Cheetham, M. E. (2017). DNAJ Proteins in neurodegeneration: Essential and protective factors. *Philosophical Transactions of the Royal Society B: Biological Sciences*, *373*(1738). https://doi.org/10.1098/rstb.2016.0534

Zeitler, B., Froelich, S., Marlen, K., Shivak, D. A., Yu, Q., Li, D., … Zhang, H. S. (2019). Allele-selective transcriptional repression of mutant HTT for the treatment of Huntington's disease. *Nature Medicine*, *25*(7), 1131–1142. https://doi.org/10.1038/s41591-019-0478-3

Zeitlin, S., Liu, J., Chapman, D. L., & Papaioannou, V. E. (1995). Increased apoptosis and early embyonic lethality in mice nullizygous for the Huntington's disease gene homologue. *Nature*, *11*(october), 155–163.

Zelin, E., & Freeman, B. C. (2015). Lysine deacetylases regulate the heat shock response including the age-associated impairment of HSF1. *Journal of Molecular Biology*, *427*(7), 1644–1654. https://doi.org/10.1016/j.jmb.2015.02.010

Zhang, S., Binari, R., Zhou, R., & Perrimon, N. (2010). A genome-wide RNA interference screen for modifiers of aggregates formation by mutant huntingtin in *Drosophila*. *Genetics*, *184*(4), 1165–1179. https://doi.org/10.1534/genetics.109.112516

Zhao, X., Chen, X. Q., Han, E., Hu, Y., Paik, P., Ding, Z., … Mobley, W. C. (2016). TRiC subunits enhance BDNF axonal transport and rescue striatal atrophy in Huntington's disease. *PNAS*, *113*(38), E5655–E5664. https://doi.org/10.1073/pnas.1603020113

Zhou, Y., Peskett, T. R., Landles, C., Warner, J. B., Sathasivam, K., Smith, E. J., … Saibil, H. R. (2021). Correlative light and electron microscopy suggests that mutant huntingtin dysregulates the endolysosomal pathway in presymptomatic Huntington's disease. *Acta Neuropathologica Communications*, *9*(1), 1–21. https://doi.org/10.1186/s40478-021-01172-z

Zielonka, D., Piotrowska, I., Marcinkowski, J. T., & Mielcarek, M. (2014). Skeletal muscle pathology in Huntington's disease. *Frontiers in Physiology*, *5*(OCT), 1–5. https://doi.org/10.3389/fphys.2014.00380

Zou, J., Guo, Y., Guettouche, T., Smith, D. F., & Voellmy, R. (1998). Repression of heat shock transcription factor HSF1 activation by HSP90 (HSP90 complex) that forms a stress-sensitive complex with HSF1. *Cell*, *94*(4), 471–480. https://doi.org/10.1016/S0092-8674(00)81588-3

Zourlidou, A., Gidalevitz, T., Kristiansen, M., Landles, C., Woodman, B., Wells, D. J., … Bates, G. P. (2007). Hsp27 overexpression in the R6/2 mouse model of Huntington's disease: Chronic neurodegeneration does not induce Hsp27 activation. *Human Molecular Genetics*, *16*(9), 1078–1090. https://doi.org/10.1093/hmg/ddm057

Zuccato, C., & Cattaneo, E. (2007). Role of brain-derived neurotrophic factor in Huntington's disease. *Progress in Neurobiology*, *81*(5–6), 294–330. https://doi.org/10.1016/j.pneurobio.2007.01.003

Zühlke, C., Rless, O., Bockel, B., Lange, H., & Thies, U. (1993). Mitotic stability and meiotic variability of the (CAG)n repeat in the huntington disease gene. *Human Molecular Genetics*, *2*(12), 2063–2067. https://doi.org/10.1093/hmg/2.12.2063